

INFORMATION TO USERS

This manuscript has been reproduced from the microfilm master. UMI films the text directly from the original or copy submitted. Thus, some thesis and dissertation copies are in typewriter face, while others may be from any type of computer printer.

The quality of this reproduction is dependent upon the quality of the copy submitted. Broken or indistinct print, colored or poor quality illustrations and photographs, print bleedthrough, substandard margins, and improper alignment can adversely affect reproduction.

In the unlikely event that the author did not send UMI a complete manuscript and there are missing pages, these will be noted. Also, if unauthorized copyright material had to be removed, a note will indicate the deletion.

Oversize materials (e.g., maps, drawings, charts) are reproduced by sectioning the original, beginning at the upper left-hand corner and continuing from left to right in equal sections with small overlaps.

ProQuest Information and Learning
300 North Zeeb Road, Ann Arbor, MI 48106-1346 USA
800-521-0600

UMI[®]

University of Alberta

Visualization of Polymer Blending and Drop Breakup

by



Bin Lin

A thesis submitted to the Faculty of Graduate Studies and Research in
partial fulfillment of the requirements for the degree of
Doctor of Philosophy

in

Chemical Engineering

Department of Chemical & Materials Engineering

Edmonton, Alberta

Spring 2005



Library and
Archives Canada

Bibliothèque et
Archives Canada

0-494-08265-8

Published Heritage
Branch

Direction du
Patrimoine de l'édition

395 Wellington Street
Ottawa ON K1A 0N4
Canada

395, rue Wellington
Ottawa ON K1A 0N4
Canada

Your file *Votre référence*

ISBN:

Our file *Notre référence*

ISBN:

NOTICE:

The author has granted a non-exclusive license allowing Library and Archives Canada to reproduce, publish, archive, preserve, conserve, communicate to the public by telecommunication or on the Internet, loan, distribute and sell theses worldwide, for commercial or non-commercial purposes, in microform, paper, electronic and/or any other formats.

The author retains copyright ownership and moral rights in this thesis. Neither the thesis nor substantial extracts from it may be printed or otherwise reproduced without the author's permission.

AVIS:

L'auteur a accordé une licence non exclusive permettant à la Bibliothèque et Archives Canada de reproduire, publier, archiver, sauvegarder, conserver, transmettre au public par télécommunication ou par l'Internet, prêter, distribuer et vendre des thèses partout dans le monde, à des fins commerciales ou autres, sur support microforme, papier, électronique et/ou autres formats.

L'auteur conserve la propriété du droit d'auteur et des droits moraux qui protègent cette thèse. Ni la thèse ni des extraits substantiels de celle-ci ne doivent être imprimés ou autrement reproduits sans son autorisation.

In compliance with the Canadian Privacy Act some supporting forms may have been removed from this thesis.

Conformément à la loi canadienne sur la protection de la vie privée, quelques formulaires secondaires ont été enlevés de cette thèse.

While these forms may be included in the document page count, their removal does not represent any loss of content from the thesis.

Bien que ces formulaires aient inclus dans la pagination, il n'y aura aucun contenu manquant.


Canada

ABSTRACT

Polymer blends are attractive because they provide improved performance and enhanced properties over homopolymers. The final blend properties depend on morphology, and the morphology, in turn, is controlled by the blending process. Therefore, it is vital to understand how one polymer drop incorporates into a second kind of polymer and how the final particle distribution is obtained. Accordingly, this thesis focuses on visualization of one polymer drop melting, deforming and breaking up inside another polymer melt under shear flow.

Two kinds of visualization geometries were used: parallel plate and Couette. It was found that drop breakup in polymer systems can occur at all viscosity ratios even when the viscosity ratio is greater than 3.5. This has been proven to be impossible for Newtonian systems in simple shear flows. At least four kinds of distinct drop breakup mechanisms were observed in uncompatibilized polymer systems subject to simple shear: “erosion”, “parallel breakup”, “vorticity alignment and breakup” and “tip streaming”. The first three mechanisms are unique to viscoelastic systems.

In Newtonian systems, drop breakup can be well described with Capillary number and viscosity ratio. For polymer systems, besides interfacial tension, viscosity ratio and shear rate, there are other important governing factors, such as shear history, normal stresses and relaxation time. The stress ratio and the drop Deborah number are two important dimensionless parameters that were used to describe drop breakup in polymer systems.

In compatibilized systems, the copolymer may promote drop breakup if the copolymer is saturated and distributes homogeneously across the interface; conversely, it

may stabilize the drop if there is a concentration gradient and insufficient coverage at the interface in which case a tiny tip develops. Fast in-situ reaction assists drop breakup by stretching the drop into a thin sheet, whereas slow reaction delays drop breakup since newly formed copolymer product accumulates at the drop tips.

Finally, this thesis shows that deformation, melting and mixing mechanisms affect the morphology of compatibilized polymers blends. By controlling melting and mixing sequences, it is possible to control the final mean particle size and particle size distribution and thereby influence final properties.

ACKNOWLEDGEMENT

First, I would like to express my sincere gratitude to my supervisor, Professor Uttandaraman Sundararaj, for his guidance, encouragement and help throughout the course of this thesis. Without his supervision and friendship, this thesis would be impossible.

I would also like to thank the Department of Chemical and Materials Engineering, University of Alberta for providing an excellent environment for research. Many people in the department provide me with help during my study. My special thanks are going to Ms. Tina Barker, who performed SEM sample coating and analysis presented in Chapter 1 and Chapter 5; Mr. Hongbing Chen, who provided the stress distribution results from computational flow dynamics simulation presented in Chapter 3; Ms. Yun Bai, who provided shear rate distribution data of the miniature mixer (APAM) presented in Chapter 5; Mr. Baoliang Shi, who helped with TEM analysis presented in Chapter 5; Mr. Walter Boddez, Mr. Richard Cooper and Mr. Les Dean, who assisted me in electronics connections and equipment examinations; Mr. Bob Smith, Mr. Bob Scott, Mr. James Mckinnon, Mr. Clark Bicknell and Mr. Dave Parlin, who helped me in constructing Couette mixer in our lab and many other machine jobs.

My thanks also go to many people outside University of Alberta who helped with the project. I am grateful to IMI-NRC (Industrial Materials Institute, National Research Council of Canada) for providing me the opportunity to use the specially designed Couette cell. I enjoyed my collaboration work with Dr. Frej Mighri and Dr. Michel A. Huneault. I would like to thank them for their critical discussions and suggestions.

During various times working at IMI-NRC, I really appreciated Dr. Frej Mighri and Mr. Robert Lemieux, for help with the experiments.

I am grateful to the generous donation of polymers by GE Plastics, Dow chemicals, Petromont and DuPont. I am also grateful to Professor Christopher W. Macosko and Professor Frank S. Bates at University of Minnesota for providing the block copolymer presented in Chapter 4 and Chapter 5.

The Natural Sciences and Engineering Research Council of Canada (NSERC) is highly acknowledged for financial support of this research. Graduate students award from Department of Chemical and Materials Engineering, Dissertation Fellowship from University of Alberta, Andrew Stewart Memorial Graduate Prize, Province Alberta Graduate Fellowship and Mary Louise Graduate Student Award are also highly acknowledged.

Finally, I would like to thank my family and friends who provide me with unfailing encouragement, support and understanding during these past years.

TABLE OF CONTENTS

Chapter 1	Introduction	1
1.1	Polymer and Polymer Blends	1
1.2	Polymer Blend Morphology Development	4
1.3	Drop Breakup	7
1.4	Visualization	11
1.5	Motivation of the Thesis	14
1.6	References	15
Chapter 2	Deformation and Breakup of a Polymer Drop Sheared between Parallel Plates — Sheet Formation of a Polycarbonate Drop inside a Polyethylene Matrix	19
2.1	Introduction	19
2.2	Experiment	22
	2.2.1 Materials	22
	2.2.2 Experimental Setup	26
	2.2.3 Experimental Procedure	27
2.3	Results	28
2.4	Discussion	32
2.5	Conclusions	43
2.6	References	44
Chapter 3	Polymer Drop Deformation and Breakup Mechanisms in Couette Cell	47
3.1	Introduction	47
3.2	Experiment	52
	3.2.1 Materials and Preparation	52
	3.2.2 Experimental Setup	56
	3.2.3 Experimental Procedure	57
3.3	Results and Discussion	61
	3.3.1 Erosion	61
	3.3.1.1 Visualization	61
	3.3.1.2 Erosion Mechanism	68
	3.3.1.3 Erosion Kinetics	73
	3.3.2 Parallel Breakup	78
	3.3.2.1 Visualization	78
	3.3.2.2 Parallel Breakup Mechanism	79
	3.3.2.3 Stress Analysis	83
	3.3.3 Vorticity Alignment and Breakup	87
	3.3.3.1 Visualization	87
	3.3.3.2 Discussion	89
	3.3.4 Tip Streaming	92

	3.3.4.1 Visualization	92
	3.3.4.2 Discussion	94
	3.3.5 Summary on Drop Deformation and Breakup Mechanisms	96
3.4	Conclusions	101
3.5	References	103
Chapter 4	Effect of Pre-made Compatibilizer and in-situ Compatibilization on Polymer Drop Deformation and Breakup Mechanisms in Couette Cell	107
4.1	Introduction	107
4.2	Experiment	110
	4.2.1 Materials and Preparation	110
	4.2.2 Experimental Setup	112
	4.2.3 Experimental Procedure	113
4.3	Results and Discussion	115
	4.3.1 Effect of Pre-made Compatibilizer	115
	4.3.2 Effect of Reactive Compatibilization	126
	4.3.2.1 Cross-Link Reaction	126
	4.3.2.2 Graft Reaction	131
4.4	Conclusions	133
4.5	References	136
Chapter 5	Morphology Development of Polymer Blends in a Miniature Mixer	139
5.1	Introduction	139
5.2	Experiment	142
	5.2.1 Materials	142
	5.2.2 Experimental Setup	145
	5.2.3 Experimental Procedure	146
	5.2.4 Scanning Electron Microscopy (SEM) and Image Analysis	147
	5.2.5 Transmission Electron Microscopy (TEM)	149
5.3	Results	149
	5.3.1 Visualization	149
	5.3.2 Polymer Blends	153
	5.3.2.1 Blends from Batch Mixer and APAM	153
	5.3.2.2 Pre-made Copolymer	155
	5.3.2.2.1 Copolymer Composition	155
	5.3.2.2.2 Copolymer Molecular Weight	157
	5.3.2.2.3 Blending Sequences	159
	5.3.2.3 In-situ Reactive Compatibilization	165
	5.3.2.3.1 Blend Composition	165
	5.3.2.3.2 Premelting	168
5.4	Discussion	170
5.5	Conclusions	174

5.6	References	175
Chapter 6	Conclusions and Future Work	178
6.1	General Discussion and Conclusions	178
6.2	Future Work	185
6.2.1	Couette Cell	185
6.2.1.1	Effect of Interfacial Modifier on Drop Breakup	185
6.2.1.2	Effect of Drop Phase Concentration	187
6.2.1.3	Three Dimension Visualization on Drop Deformation and Breakup	187
6.2.2	Parallel Plates	188
6.2.2.1	Radial and End/Wall Effects	188
6.2.2.2	Cone-and-Plate Device	189
6.3	References	189
Appendix		
Appendix I	New Mixing Device Design and Construction	191
Appendix II	Average Shear Rate in Couette Cell	199
Appendix III	Diffusivity Calculation	204
Appendix III	Saturation Concentration	206
Appendix V	Movies on Drop Deformation and Breakup	208

List of Tables:

Table 2.1	Properties of polymers used.	24
Table 2.2	Critical conditions for sheet formation at 220°C.	36
Table 3.1	Properties of polymers used.	53
Table 3.2	Interfacial tension of polymer systems studied.	56
Table 3.3	Critical conditions for erosion experiments.	72
Table 3.4	Experimental conditions for calculation of PE2/PC5 erosion rate.	76
Table 3.5	Kinetic constants for PE2/PC5 erosion at 230°C.	77
Table 3.6	Critical conditions for parallel breakup experiments.	85
Table 3.7	Critical conditions for vorticity breakup experiments.	90
Table 3.8	Critical conditions for tip streaming experiments.	95
Table 4.1	Properties of homopolymers used.	112
Table 4.2	Summary on PS drop deformation and breakup in PE matrix without and with block copolymer P(S-b-E).	125
Table 4.3	Summary on PSOX drop deformation and breakup in PE matrix without and with cross-link reaction.	130
Table 5.1	Properties of corn syrup and silicone oil used.	142

Table 5.2	Properties of homopolymers used.	144
Table 5.3	Properties of copolymers used.	144
Table 5.4	Effect of blending sequences on particle size. Blend: PS/PE (90/10) with 10% P(S-b-E).	160
Table 5.5	Effect of blending sequences on particle size. Blend: PS/PMMA (90/10) with 10% P(S-b-MMA) (25,000-25,000 g/mol).	162
Table 5.6	Effect of blending sequences on particle size. Blend: PS/PMMA (90/10) with 10% P(S-b-MMA) (50,000-50,000 g/mol).	163
Table 5.7	Effect of blending sequences on particle size. Blend: PS/PMMA (90/10) with 10% P(S-b-MMA) (80,000-80,000 g/mol).	163
Table 5.8	Effect of blend composition on particle size.	167

List of Figures:

- Figure 1.1** The morphology of an immiscible blend A/B changes as the relative amount of polymer B increases. The white color stands for phase A and the black color, for phase B. (a) dispersed B droplets in phase A; (b) co-continuous morphology; (c) dispersed A droplets in phase B. 2
- Figure 1.2** Polymer blending process, morphology and properties relationship. Extruder figure from Tadmor and Gogos, 1979. Ductility plot adapted from Wu, 1985. 3
- Figure 1.3** Initial morphology development of solid feed PE/PC (polyethylene/polycarbonate 80:20wt%) in Haake batch mixer at 220°C and 50 rpm for 1 min. Solid pellet feed also used. (a) PC phase extracted with methylene chloride — the PC phase consists of sheets/ribbons, cylinders and droplets in the PE matrix; (b) PE phase extracted with dodecane — PC sheets/ribbons and cylinders remain; (c) PE phase extracted with dodecane — PC cylinders and droplets remain. Note scale bars. 6
- Figure 1.4** Initial morphology development of premelted PE/PC (polyethylene/polycarbonate 80:20wt%) in Haake batch mixer at 220°C and 50 rpm. The blend was premelted first at 220°C and then mixed for 20 s. (a) PC phase extracted with methylene chloride — sample shows holes where PC ribbons, cylinders and droplets once were; (b) a PC sheet after the PE phase was extracted, the dotted circled in the lower left corresponds to the area enlarged in (c); (c) the thickness of the PC sheet is 1-10 μm. Note scale bars. 7
- Figure 1.5** A Newtonian drop in Newtonian matrix under simple shear. 8
- Figure 1.6** Critical Capillary number versus viscosity ratio for Newtonian systems (Grace, 1982). 9
- Figure 1.7** PEI/PC (80:20 wt%) blending at 340°C, 10 rpm. PEI added first. Note the scale bar. (a) Aggregate PEI pellets ($t=38s$); (b) Stretching and sheeting out of the deformed PEI pellets ($t=48s$); (c) Stretching of PEI melt ($t=117s$); (d) Deformation and stretching

	of PC pellets ($t=148s$). From Lin and Sundararaj, 2004.	13
Figure 2.1	(a) Complex viscosity of PC and PE at 220°C and (b) Elastic modulus of PC and PE at 220°C.	25
Figure 2.2	Illustration of the parallel plates setup.	27
Figure 2.3	Deformation and breakup of a PC1 drop inside PE2 matrix at 220°C and $1s^{-1}$. The drop has an initial size (D_0) 0.79 mm. The drop deforms to a flat sheet first, then to a long thread. (a) Spherical drop at $t=0s$; (b) Flat elliptical drop at $t=7s$; (c) Drop stretched to a sheet at $t=22s$; (d) Drop continuing stretching to a sheet at $t=33s$; (e) A long thread developed at $t=101s$; (f) Entangled threads and small droplets at $t=699s$; (g) Breakup of a thread at $t=960s$. Note scale bars.	29
Figure 2.4	Deformation and breakup of a PC4 drop inside PE2 matrix at 220°C and $1s^{-1}$. The drop has an initial size (D_0) 0.48 mm. The drop deforms to a flat sheet first, then, a long thread tip develops. (a) Spherical drop at $t=0s$; (b) Deformed and twisted drop at $t=381s$; (c) Flattened drop at $t=858s$; (d) Drop stretched to a sheet at $t=887s$; (e) Drop elongated in the flow direction and a tiny thin tip developed at $t=924s$; (f)-(h) One daughter droplet after breakup: (f) Threads entangled with the daughter droplet at $t=1070s$; (g) the flattened droplet at $t=1187s$; and (g) A ribbon or sheet pulling out of the droplet at $t=1208s$. Note scale bars.	31
Figure 2.5	Reduced dimensions of the drop change with time at a shear rate of $1s^{-1}$. (a) Reduced length in the flow direction and (b) Reduced length in the velocity gradient direction, calculated by assuming the drop volume conserves. Note there is an abrupt increase in R_1 or an abrupt decrease in R_2 .	34
Figure 2.6	Illustration of two modes of sheet breakup.	36

Figure 2.7	Critical strain versus viscosity ratio when the drop becomes a sheet. The solid circles are data for the drop when it breaks up via Type A, and the open circles are data for the drop when it breaks up via Type B. The lines are guides to the eyes.	37
Figure 2.8	Critical strain versus stress ratio when the drop becomes a sheet. The solid circles are data for the drop when it breaks up via Type A, and the open circles are data for the drop when it breaks up via Type B. The lines are guides to the eyes.	38
Figure 2.9	Deborah number versus stress ratio. The solid circles are data for the drop when it breaks up via Type A, and the open circles are data for the drop when it breaks up via Type B. The lines are guides to the eyes.	39
Figure 2.10	Definition of the inner and outer edges of a PC drop.	42
Figure 3.1	Critical Capillary number versus viscosity ratio for Newtonian systems (Grace, 1982).	48
Figure 3.2	(a) Viscosity ratio of PE/PC systems at 220°C; (b) Viscosity ratio of PE2/PC5 at 220°C and 230°C; (c) Complex viscosity and elastic modulus of PS, PSOX, PE1 and PE2 at 190°C; (d) Complex viscosity and elastic modulus of PBT, PA6, PE1 and PE2 at 230°C.	54
Figure 3.3	Couette flow cell setup (Mighri and Huneault, 2001a).	57
Figure 3.4	Experiment Type 1 — Stepwise shear rate increase at constant temperature. (a) Temperature profile of PE melt; (b) Average shear rate applied. The solid circles shown are the experimental conditions corresponding to Figure 3.6.	59
Figure 3.5	Experiment Type 2 — Stepwise temperature increase at constant shear rate. (a) Temperature profile of PE melt; (b) Average shear rate applied. The solid circles shown are the experimental conditions corresponding to Figure 3.7.	60

Figure 3.6 Drop deformation and erosion of a PC4 drop ($D_0=0.75\text{mm}$) in a PE1 matrix at 220°C with stepwise shear rate increase shown in Figure 3.4. Time and conditions for each figure: (a) $t=0\text{s}$, $\dot{\gamma}=1.2\text{s}^{-1}$, $\eta_r=15.1$; (b) $t=315\text{s}$, $\dot{\gamma}=7.7\text{s}^{-1}$, $\eta_r=15.5$; (c) $t=1030\text{s}$, $\dot{\gamma}=22.6\text{s}^{-1}$, $\eta_r=14.8$; (d) $t=1326\text{s}$, $\dot{\gamma}=26.8\text{s}^{-1}$, $\eta_r=14.7$; (e) $t=1425\text{s}$, $\dot{\gamma}=27.8\text{s}^{-1}$, $\eta_r=14.7$; (f) $t=1456\text{s}$, $\dot{\gamma}=28.9\text{s}^{-1}$, $\eta_r=14.6$. Note scale bar. For the micrographs, the flow direction is horizontal and the vorticity direction is vertical.

62

Figure 3.7 Drop deformation and erosion of a PC5 drop ($D_0=0.83\text{mm}$) in a PE2 matrix with stepwise temperature increase shown in Figure 3.6. Time and conditions for each figure: (a) $t=0\text{s}$, $T=163^\circ\text{C}$, $\dot{\gamma}=1.2\text{s}^{-1}$, $\eta_r=1194$; (b) $t=586\text{s}$, $T=186^\circ\text{C}$, $\dot{\gamma}=16.8\text{s}^{-1}$, $\eta_r=151$; (c) $t=1019\text{s}$, $T=210^\circ\text{C}$, $\dot{\gamma}=17.0\text{s}^{-1}$, $\eta_r=30$; (d) $t=1351\text{s}$, $T=223^\circ\text{C}$, $\dot{\gamma}=17.4\text{s}^{-1}$, $\eta_r=17.8$; (e) $t=1550\text{s}$, $T=233^\circ\text{C}$, $\dot{\gamma}=16.8\text{s}^{-1}$, $\eta_r=8.8$; (f) $t=1632\text{s}$, $T=233^\circ\text{C}$, $\dot{\gamma}=16.6\text{s}^{-1}$, $\eta_r=8.8$; (g) $t=1747\text{s}$, $T=233^\circ\text{C}$, $\dot{\gamma}=16.8\text{s}^{-1}$, $\eta_r=8.8$; (h) $t=2075\text{s}$, $T=233^\circ\text{C}$, $\dot{\gamma}=16.5\text{s}^{-1}$, $\eta_r=8.8$; (i) $t=2238\text{s}$, $T=233^\circ\text{C}$, $\dot{\gamma}=17.2\text{s}^{-1}$, $\eta_r=8.8$; (j) $t=2356\text{s}$, $T=233^\circ\text{C}$, $\dot{\gamma}=17.4\text{s}^{-1}$, $\eta_r=8.8$. Note scale bar. For the micrographs, the flow direction is horizontal and the vorticity direction is vertical.

64

Figure 3.8 Drop deformation and erosion of a PC5 ($D_0=1.10\text{mm}$) in a PE2 matrix at 230°C with stepwise shear rate increase. Time and conditions for each figure: (a) $t=714\text{s}$, $\dot{\gamma}=12.9\text{s}^{-1}$, $\eta_r=8.8$; (b) $t=753\text{s}$, $\dot{\gamma}=12.8\text{s}^{-1}$, $\eta_r=8.8$; (c) $t=1006\text{s}$, $\dot{\gamma}=13.7\text{s}^{-1}$, $\eta_r=8.8$; (d) $t=1834\text{s}$, $\dot{\gamma}=18.0\text{s}^{-1}$, $\eta_r=8.8$; Note scale bar. For the micrographs, the flow direction is horizontal and the vorticity direction is vertical.

66

Figure 3.9 A PC5 drop ($D_0=1.05\text{mm}$) in a PE1 matrix at 220°C with stepwise shear rate increase. (a) $t=2412\text{s}$, $\dot{\gamma}=36.5\text{s}^{-1}$, $\eta_r=35.5$. Small droplets aligned along vorticity axis; circles drawn around a few extended droplets; (b) Schematic illustration of small droplets in (a); (c) Schematic illustration of small threads around the upper part of mother drop. Note scale bars. For the micrographs, the flow direction is horizontal and the vorticity direction is vertical.

67

- Figure 3.10** Shear stress versus distance along axis. Two-dimensional simulation geometry and axis shown in inset. The shear stress at the surface of the PC drop is clearly one order of magnitude larger than inside the drop. From Chen *et al.* (2004b). 70
- Figure 3.11** Critical shear rate for polymer drop erosion at different viscosity ratios. 73
- Figure 3.12** PE2/PC5 erosion profile – Volume remaining versus time. 75
- Figure 3.13** PE2/PC5 erosion profile – Semilogarithmic plot of volume remaining versus time for determination of the erosion rate. 77
- Figure 3.14** Drop deformation and breakup of a PC4 drop ($D_0=0.68\text{mm}$) in a PE2 matrix at 220°C subject to stepwise shear rate increase. Time and conditions for each figure: (a) initial drop: $t=0\text{s}$, $\dot{\gamma}=1.2\text{s}^{-1}$, $\eta_r=5.8$; (b) erosion of small droplets from the surface of mother drop: $t=421\text{s}$, $\dot{\gamma}=16.1\text{s}^{-1}$, $\eta_r=6.5$; (c) drop stretches into a sheet: $t=882\text{s}$, $\dot{\gamma}=32.4\text{s}^{-1}$, $\eta_r=6.4$; (d) breakup of the sheet: $t=883\text{s}$, $\dot{\gamma}=32.3\text{s}^{-1}$, $\eta_r=6.4$. Note scale bar. For the micrographs, the flow direction is horizontal and the vorticity direction is vertical. 78
- Figure 3.15** Deformation and breakup of a PC5 drop (initial diameter 0.51mm) in a PE2 matrix at 230°C subject to stepwise shear rate increase. Time and conditions for each figure: (a) initial drop: $t=50\text{s}$, $\dot{\gamma}=7.2\text{s}^{-1}$, $\eta_r=8.7$; (b) elliptical drop: $t=t_0=2348\text{s}$, $\dot{\gamma}=30.3\text{s}^{-1}$, $\eta_r=8.6$; (c) drop stretches into a sheet: $t=2368\text{s}$, $\dot{\gamma}=30.3\text{s}^{-1}$, $\eta_r=8.6$; (d) continues stretching: $t=2370\text{s}$, $\dot{\gamma}=30.5\text{s}^{-1}$, $\eta_r=8.6$; (e) drop rupture begins: $t=2370\text{s}$, $\dot{\gamma}=30.5\text{s}^{-1}$, $\eta_r=8.6$; (f) drop has ruptured: $t=2371\text{s}$, $\dot{\gamma}=30.2\text{s}^{-1}$, $\eta_r=8.6$; (g) daughter droplet that results from breakup: $t=2375\text{s}$, $\dot{\gamma}=30.6\text{s}^{-1}$, $\eta_r=8.6$. Note scale bar. For the micrographs, the flow direction is horizontal and the vorticity direction is vertical. 81
- Figure 3.16** Drop volume changes with time if the drop keeps an elliptical shape or elliptical/cylindrical shape. The time, t_0 , corresponding to the time indicated in Figure 3.15b. 82

- Figure 3.17** Reduced lengths a , b and c plotted versus time for a PC5 drop from Figure 3.15. The drop has an equivalent diameter $D_0 = 0.48\text{mm}$ at time t_0 , corresponding to the time indicated in Figure 3.15b. 82
- Figure 3.18** Capillary number versus viscosity ratio when parallel breakup occurs. No relationship emerges. 85
- Figure 3.19** Stress ratio versus Deborah number when parallel breakup occurs. 86
- Figure 3.20** Deformation and breakup of a PC3 drop ($D_0 = 0.60\text{ mm}$) in a PE1 matrix at 220°C subject to a stepwise shear rate increase. Time and conditions for each figure: (a) $t=72\text{s}$, $\dot{\gamma}=5.4\text{s}^{-1}$, $\eta_r=7.4$; (b) $t=461\text{s}$, $\dot{\gamma}=7.9\text{s}^{-1}$, $\eta_r=7.6$; (c) $t=653\text{s}$, $\dot{\gamma}=7.8\text{s}^{-1}$, $\eta_r=7.6$; (d) $t=874\text{s}$, $\dot{\gamma}=8.6\text{s}^{-1}$, $\eta_r=7.6$; (e) $t=941\text{s}$, $\dot{\gamma}=8.3\text{s}^{-1}$, $\eta_r=7.6$; (f) $t=950\text{s}$, $\dot{\gamma}=8.3\text{s}^{-1}$, $\eta_r=7.6$. Note scale bar. For the micrographs, the flow direction is horizontal and the vorticity direction is vertical. 87
- Figure 3.21** Deformation and breakup of a PS drop ($D_0 = 0.59\text{ mm}$) in a PE1 matrix at 190°C subject to a stepwise shear rate increase. Time and conditions for each figure: (a) $t=1270\text{s}$, $\dot{\gamma}=6.2\text{s}^{-1}$, $\eta_r=7.8$; (b) $t=1458\text{s}$, $\dot{\gamma}=6.4\text{s}^{-1}$, $\eta_r=7.7$. 89
- Figure 3.22** Stress growth of PC3 at 220°C and a shear rate of (a) 1s^{-1} and (b) 3s^{-1} . 91
- Figure 3.23** Deformation and breakup of a PC1 drop ($D_0 = 0.58\text{ mm}$) in a PE2 matrix at 220°C subject to a stepwise shear rate increase. Time and conditions for each figure: (a) $t=13\text{s}$, $\dot{\gamma}=1.8\text{s}^{-1}$, $\eta_r=2.4$; (b) $t=139\text{s}$, $\dot{\gamma}=1.8\text{s}^{-1}$, $\eta_r=2.4$; (c) $t=191\text{s}$, $\dot{\gamma}=1.8\text{s}^{-1}$, $\eta_r=2.4$; (d) $t=376\text{s}$, $\dot{\gamma}=1.8\text{s}^{-1}$, $\eta_r=2.4$; (e) $t=444\text{s}$, $\dot{\gamma}=5.5\text{s}^{-1}$, $\eta_r=2.6$; (f) $t=456\text{s}$, $\dot{\gamma}=5.6\text{s}^{-1}$, $\eta_r=2.6$. Note scale bar. For the micrographs, the flow direction is horizontal and the vorticity direction is vertical. 93

Figure 3.24	Stress ratio versus Deborah number when tip streaming occurs.	96
Figure 3.25	Polymer drop breakup mechanisms subject to simple shear flow.	97
Figure 3.26	Capillary number versus viscosity ratio for drop breakup subject to simple shear flow. The solid lines are experimental correlations from Grace (1982) for Newtonian drops and the data points correspond to polymer drop breakup.	97
Figure 3.27	Critical shear rate for polymer drop breakups at different viscosity ratios subject to simple shear flow. The lines are guides to the eyes: parallel breakup —, erosion — —, vorticity breakup ·····, tip streaming - · · .	99
Figure 3.28	Stress ratio versus Deborah number for polymer drop breakup subject to simple shear flow. The lines drawn are the trends of breakups: parallel breakup —, erosion — —, vorticity breakup ·····, tip streaming - · · .	100
Figure 4.1	(a) Cross-link reaction between PSOX and PEMA; (b) Graft reaction between PA6 and PEMA.	111
Figure 4.2	Complex viscosity and elastic modulus for PS, PS+1%P(S-b-E) and PS+5%P(S-b-E) at 190°C.	114
Figure 4.3	Deformation and breakup of a PS drop ($D_0=0.52\text{mm}$) in a PEI matrix at 190°C subject to a stepwise shear rate increase. Time and conditions for each figure: (a) $t=5\text{s}$, $\dot{\gamma}=0.3\text{s}^{-1}$, $\eta_r=15.0$; (b) $t=535\text{s}$, $\dot{\gamma}=4.4\text{s}^{-1}$, $\eta_r=8.7$; (c) $t=541\text{s}$, $\dot{\gamma}=4.0\text{s}^{-1}$, $\eta_r=9.0$; (d) $t=1547\text{s}$, $\dot{\gamma}=8.4\text{s}^{-1}$, $\eta_r=7.0$. Note scale bar. For the micrographs, the flow direction is horizontal and the vorticity direction is vertical.	116
Figure 4.4	Pre-made copolymer. Deformation and breakup of a PS+5%P(S-b-E) drop ($D_0=0.58\text{mm}$) in a PEI matrix at 190°C subject to a stepwise shear rate increase. Time and conditions	

for each figure: (a) $t=0s$, $\dot{\gamma}=3.0s^{-1}$, $\eta_r=5.3$; (b) $t=126s$, $\dot{\gamma}=3.6s^{-1}$, $\eta_r=5.2$; (c) $t=480s$, $\dot{\gamma}=3.8s^{-1}$, $\eta_r=5.2$; (d) $t=669s$, $\dot{\gamma}=6.6s^{-1}$, $\eta_r=4.7$. Note scale bar. For the micrographs, the flow direction is horizontal and the vorticity direction is vertical.

117

Figure 4.5 Pre-made copolymer. Deformation and breakup of a PS drop ($D_0=0.53mm$) coated with P(S-b-E) in a PE1 matrix at $190^\circ C$ subject to a stepwise shear rate increase. Time and conditions for each figure: (a) $t=114s$, $\dot{\gamma}=2.3s^{-1}$, $\eta_r \approx 10.5$; (b) $t=801s$, $\dot{\gamma}=2.3s^{-1}$, $\eta_r \approx 10.5$; (c) $t=1124s$, $\dot{\gamma}=2.3s^{-1}$, $\eta_r \approx 10.5$; (d) $t=1158s$, $\dot{\gamma}=3.4s^{-1}$, $\eta_r \approx 9.3$; (e) $t=1291s$, $\dot{\gamma}=6.0s^{-1}$, $\eta_r \approx 7.8$; (f) $t=1665s$, $\dot{\gamma}=7.4s^{-1}$, $\eta_r \approx 7.4$. Note scale bar. The viscosity ratio is obtained by using PS data for drop phase viscosity. For the micrographs, the flow direction is horizontal and the vorticity direction is vertical.

120

Figure 4.6 Deformation and breakup of a PSOX chunk ($D_0 \approx 0.67mm$) in a PE2 matrix at $190^\circ C$ subject to a stepwise shear rate increase. Time and conditions for each figure: (a) $t=0s$, $\dot{\gamma}=2.3s^{-1}$, $\eta_r=5.0$; (c) $t=358s$, $\dot{\gamma}=3.8s^{-1}$, $\eta_r=4.4$; (e) $t=378s$, $\dot{\gamma}=3.6s^{-1}$, $\eta_r=4.5$; (g) $t=723s$, $\dot{\gamma}=6.0s^{-1}$, $\eta_r=3.9$. Figures (b), (d), (f) and (h) are schematics for (a), (c), (e) and (g). Note scale bar. For the micrographs, the flow direction is horizontal and the vorticity direction is vertical.

127

Figure 4.7 Reactive system. Deformation and breakup of a PSOX chunk ($D_0 \approx 0.60mm$) inserted inside a PEMA pellet then in a PE2 matrix at $190^\circ C$ subject to a stepwise shear rate increase. Time and conditions for each figure: (a) $t=0s$, $\dot{\gamma}=0.6s^{-1}$, $\eta_r \approx 6.4$; (b) $t=145s$, $\dot{\gamma}=1.9s^{-1}$, $\eta_r \approx 5.2$; (c) $t=734s$, $\dot{\gamma}=4.1s^{-1}$, $\eta_r \approx 4.3$; (d) $t=1159s$, $\dot{\gamma}=8.9s^{-1}$, $\eta_r \approx 3.4$; (e) $t=1445s$, $\dot{\gamma}=9.7s^{-1}$, $\eta_r \approx 3.3$. Note scale bar. The viscosity ratio is obtained by using PSOX data for drop phase viscosity. For the micrographs, the flow direction is horizontal and the vorticity direction is vertical.

129

Figure 4.8 Deformation and breakup of a PA6 drop ($D_0=0.58mm$) in a PE1 matrix at $230^\circ C$ subject to a stepwise shear rate increase. Time and conditions for each figure: (a) $t=17s$, $\dot{\gamma}=1.3s^{-1}$, $\eta_r=0.46$; (b) $t=169s$, $\dot{\gamma}=2.2s^{-1}$, $\eta_r=0.48$; (c) $t=961s$, $\dot{\gamma}=13.3s^{-1}$, $\eta_r=0.56$.

Note scale bar. For the micrographs, the flow direction is horizontal and the vorticity direction is vertical.

131

- Figure 4.9** Reactive system. Deformation and breakup of a PA6 ($D_0=0.48\text{mm}$) inserted inside a PEMA pellet then in a PE1 matrix at 230°C subject to a stepwise shear rate increase. Time and conditions for each figure: (a) $t=13\text{s}$, $\dot{\gamma}=1.9\text{s}^{-1}$, $\eta_r \approx 0.48$; (b) $t=40\text{s}$, $\dot{\gamma}=1.8\text{s}^{-1}$, $\eta_r \approx 0.48$; (c) $t=55\text{s}$, $\dot{\gamma}=1.9\text{s}^{-1}$, $\eta_r \approx 0.48$; (d) $t=80\text{s}$, $\dot{\gamma}=1.9\text{s}^{-1}$, $\eta_r \approx 0.48$. Two lines are drawn in (d) to show the width of the sheet. Note scale bar. The viscosity ratio is obtained by using PA6 data for drop phase viscosity. For the micrographs, the flow direction is horizontal and the vorticity direction is vertical. 132
- Figure 4.10** Schematics of effect of copolymer and in-situ reaction on polymer drop breakup. (a) Copolymer is dry coated evenly at the drop surface and the drop surface is saturated with block copolymer; (b) Copolymer is premixed with the drop phase and the drop interfacial concentration is lower than the saturation coverage; (c) Fast graft reaction occurs at the interface; (d) Cross-linking reaction takes place gradually and small amount of cross-linked product forms at the interface. For all schematics, the flow direction is horizontal and the vorticity direction is vertical. 134
- Figure 5.1** Photograph of APAM setup. The diameter of the stainless chamber is 13 mm. For more details, refer to Breuer *et al.* (2004). 146
- Figure 5.2** Batch mixer cross-section view. 146
- Figure 5.3** Deformation and breakup of a corn syrup drop ($D_0=0.84\text{ mm}$) in silicone oil at room temperature subject to a stepwise shear rate increase generated by a Couette apparatus. The viscosity ratio is 1.08. Time and conditions for each figure: (a) $t=153\text{s}=t_0$, $\dot{\gamma}=3.4\text{s}^{-1}$; (b) $t=t_0+39\text{s}$, $\dot{\gamma}=7.8\text{s}^{-1}$; (c) $t=t_0+45\text{s}$, $\dot{\gamma}=7.8\text{s}^{-1}$; (d) $t=t_0+48\text{s}$, $\dot{\gamma}=7.9\text{s}^{-1}$; (e) $t=t_0+49\text{s}$, $\dot{\gamma}=7.9\text{s}^{-1}$. Note scale bar. 150
- Figure 5.4** Deformation and breakup of a corn syrup drop ($D_0=0.89\text{ mm}$) in silicone oil at room temperature and 10 rpm in the APAM. The viscosity ratio is 1.08. Time and conditions for each figure:

	(a) $t=100s=t_0$; (b) $t=t_0+2s$; (c) $t=t_0+3s$; (d) $t=t_0+8s$. Note scale bar.	151
Figure 5.5	Coalescence of two corn syrup drops ($D_{0,L}=1.04$ mm; $D_{0,R}=0.94$ mm) in silicone oil at room temperature and 10 rpm in the APAM. The viscosity ratio is 1.08. Time and conditions for each figure: (a) $t=1277s=t_0$; (b) $t=1286s=t_0+9s$; (c) $t=1291=t_0+14s$; (d) $t=1292=t_0+15s$; (e) $t=1294=t_0+17s$. Note scale bar.	152
Figure 5.6	(a) Number average diameter and (b) Polydispersity of dispersed particle size obtained from batch mixer and the APAM. The block copolymer P(S-b-MMA) used has a molecular weight of 80,000-80,000 g/mol.	154
Figure 5.7	Dependence of the dispersed phase size for PS/PE (90/10) blend as a function of the weight percentage of P(S-b-E). The amount of copolymer is 10% of PMMA.	156
Figure 5.8	Dependence of the dispersed phase size for PS/PMMA (90/10) blend as a function of copolymer P(S-b-MMA) molecular weight. The amount of copolymer is 10% of PMMA.	158
Figure 5.9	TEM micrographs of PS/PMMA/P(S-b-MMA) (89.0/9.9/1.1 wt%) blends. PS and P(S-b-MMA) was first mixed at 190°C for 10 min, and PMMA were then added and mixed for 10 min. The molecular weight of P(S-b-MMA) for each figure: (a) 25,000-25,000 g/mol, (b) 80,000-80,000 g/mol. Note scale bars.	164
Figure 5.10	TEM micrographs of PS/PMMA/P(S-b-MMA) (89.0/9.9/1.1 wt%) blends. PS and P(S-b-MMA) were first mixed at 190°C for 10 min in a master batch and then mixed with PMMA in a new batch for 10 min. The molecular weight of P(S-b-MMA) for each figure: (a) 25,000-25,000 g/mol; (b) and (c) 80,000-80,000 g/mol. Note scale bars.	165
Figure 5.11	SEM micrographs of PSOX/PE/PEMA blends with a composition of (a) 90/10/0; (b) 90/0/10. Note scale bars.	166

- Figure 5.12** SEM micrographs of PSOX/PE/PEMA blends with a composition of (a) 10/90/0; (b) 10/85/5; (c) 10/80/10; (d) 10/75/15. Note scale bars. 167
- Figure 5.13** Dependence of the dispersed phase (a) number average diameter and (b) volume average diameter for PSOX/PE/PEMA blend as a function of premelting time. All polymers are added together. For the 10/80/10 blend, premelt 5 min, few particles are discernable, and spherical domains are averaged. 169
- Figure I.1** Couette apparatus cross-sectional illustration. 194
- Figure I.2** Cross-sectional illustration of (a) Outer quartz cylinder; (b) Inner quartz cylinder; (c) Assembly of cylinders; (d) Inner quartz plate; (e) Inner quartz cone. 195
- Figure V.1** Pre-made copolymer. Deformation and breakup of a PS+1%P(S-b-E) drop ($D_0=0.51\text{mm}$) in a PE1 matrix at 190°C subject to a stepwise shear rate increase. Time and conditions for each figure: (a) $t=2\text{s}$, $\dot{\gamma}=0.2\text{s}^{-1}$, $\eta_r=21$; (b) $t=396\text{s}$, $\dot{\gamma}=4.4\text{s}^{-1}$, $\eta_r=11$; (c) $t=505\text{s}$, $\dot{\gamma}=4.4\text{s}^{-1}$, $\eta_r=11$; (d) $t=719\text{s}$, $\dot{\gamma}=6.3\text{s}^{-1}$, $\eta_r=9$; (e) $t=814\text{s}$, $\dot{\gamma}=6.3\text{s}^{-1}$, $\eta_r=9$; (f) $t=816\text{s}$, $\dot{\gamma}=6.5\text{s}^{-1}$, $\eta_r=9$. The scale bar for each figure is same as shown in figure (a). For the micrographs, the flow direction is horizontal and the vorticity direction is vertical. 210

Nomenclature:

a	Constant in equation (III.3)
A	Area in equations (5.3) and (IV.1), μm^2
C	Constant in equation (II.14)
Ca	Capillary number
d	Constant in equation (III.3)
D	Diameter, mm
D_{eq}	Equivalent diameter in equation (5.3), μm
D_n	Number average diameter in equation (5.4), μm
D_v	Volume average diameter in equation (5.5), μm
D_v/D_n	Polydispersity
D_s	Surface diffusivity, cm^2/s
De	Deborah number
E_{coh}	Cohesive energy, J/mol
ΔG_m	Free energy of mixing
G'	Elastic modulus, Pa
H, h	Height shown in Figure I.2, mm
ΔH_m	Enthalpy of mixing
k_{app}	Rate constant in equations (3.4)-(3.7)
k_d	Constant in equations (III.2)
m	Power law constant in equation (II.1)
m_r	Remaining mass in equation (3.6), g

m_t	Mass at time t , g
M	Molecular weight, g/mol
M_n	Number average molecular weight, g/mol
M_w	Weight average molecular weight, g/mol
n	Number of particles in Chapter 5
n	Power law constant in equation (II.1)
N	Number of molecules in equation (IV.3)
N_{Avo}	Avogadro number, 6.023×10^{23} /mol
N_{II}	First normal stress difference, Pa
P	Drop perimeter
Pe_s	Surface Peclet number
r	r -axis in cylindrical coordinate
R	Radius, mm
SD	Standard deviation
S_r	Stress ratio defined in equation (2.3)
t	Time, s
t	Thickness shown in Figure (I.2), mm
t_{on}	Onset time in equations (3.6) and (3.7), s
T	Temperature, °C
T_{II}	Normal stress, Pa
v	Velocity, m/s
V	Molar volume in equation (III.4), cm^3/mol
V_r	Remaining volume in equation (3.7), mm^3

V_t	Drop volume at time t , mm ³
x	x -axis
z	z -axis in cylindrical coordinate

Greek Letters

$\dot{\gamma}$	Shear rate, s ⁻¹
Γ	Interfacial tension, mN/m
Γ'	Dynamic interfacial tension, mN/m
δ	Solubility parameter, J ^{1/2} /cm ^{3/2}
η	Viscosity, Pa·s
η^*	Complex viscosity, Pa·s
η_r	Viscosity ratio
λ	Relaxation time, s
θ	θ -axis in cylindrical coordinate
τ	Shear stress, Pa
ϕ	Volume fraction
Φ	Diameter shown in Figure (I.2)
ω	Frequency, s ⁻¹
Ω	Rotation speed, s ⁻¹

Subscripts

c	Critical
d	Drop phase, dispersed phase or minor phase

<i>i</i>	Inner cylinder or inner surface
<i>L</i>	Left
<i>m</i>	Matrix phase or major phase
<i>o</i>	Outer cylinder
<i>R</i>	Right
<i>t</i>	Time <i>t</i>
0	Initially or zero time
1	Flow direction
2	Velocity gradient direction
3	Vorticity direction

Abbreviations for Polymers:

EVAc	Ethylene-co-vinyl acetate
HDPE	High-density polyethylene
LDPE	Low-density polyethylene
NR	Natural rubber
PA	Polyamide, Nylon
PA6	Nylon 6
PBT	Polybutylene terephthalate
PC	Polycarbonate
PDMS	Polydimethylsiloxane, Silicone oil
PE	Polyethylene
PEI	Poly(ether imide)
PEMA	Polyethylene maleic anhydride
PIB	Polyisobutylene
PMMA	Poly(methyl methacrylate)
PP	Polypropylene
PS	Polystyrene
PSOX	Polystyrene oxazoline
P(S-b-E)	Polystyrene-block-polyethylene
P(S-b-MMA)	Polystyrene-block-poly(methyl methacrylate)

Chapter 1

Introduction

1.1 POLYMER AND POLYMER BLENDS

Polymers are found everywhere in today's society, from food packaging, clothing, home furnishings, transportation, medical devices, to information technology. Some of them are natural polymers, such as protein, cellulose and silk; but most of them are synthetic, such as polystyrene (PS), polyethylene (PE) and polyamide or nylon (PA). Polymers are giant molecules made up of many simple repeating units.

Polymers are the fastest growing structural materials. In 1992, the world production of polymers was more than two times that of steel. Polymeric materials are widely used due to their high strength, lightweight and relatively low cost compared to metals and other materials. However, they also exhibit unique properties, for example, high viscosity and rubber-like elasticity. Almost all polymers that exist today need to be processed at high temperature, typically in the range 200°C to 380°C.

Polymer blends are composed of at least two polymers. The blends can be classified as either miscible or immiscible. Miscible blends show unlimited solubility and a zero interfacial tension. They are homogeneous down to molecular level and have a negative value of the free energy of mixing: $\Delta G_m \approx \Delta H_m \leq 0$ and a positive value of the second derivative: $\partial^2 \Delta G_m / \partial \phi^2 > 0$ (Utracki, 1989). Immiscible blends show a limited mutual solubility, a finite interfacial tension and have a positive value of the free energy of mixing: $\Delta G_m \approx \Delta H_m > 0$.

The first polymer blend was introduced in 1846 (Parkes, 1846), consisting of natural rubber (NR) and gutta-percha (GP). Today, the world production of polymer blends is around 51 million tons a year and worth over US\$ 200 billion (Utracki, 2002). There were approximately 2500 US patents and 2000 technical papers published on polymer blends in 2003. Polymer blend production increases at a rate about three times higher than that of the overall polymer industry (Utracki, 2002). Polymer blends are very attractive because they provide enhanced properties such as better low-temperature impact performance, higher strength and reduced flammability, and cost less than developing a new kind of polymer (Utracki and Shi, 1992).

The blend morphology is characterized by the shape, size and distribution of the constituting domains (Janssen, 1993). For immiscible blends, the morphology can be classified as dispersed droplets or co-continuous depending on the relative blend compositions. Figure 1.1 shows that the morphology of an immiscible blend changes from dispersed droplet to co-continuous, and to dispersed droplet again as the concentration of one of its component, B, increases. This thesis only focuses on the drop dispersion morphology.

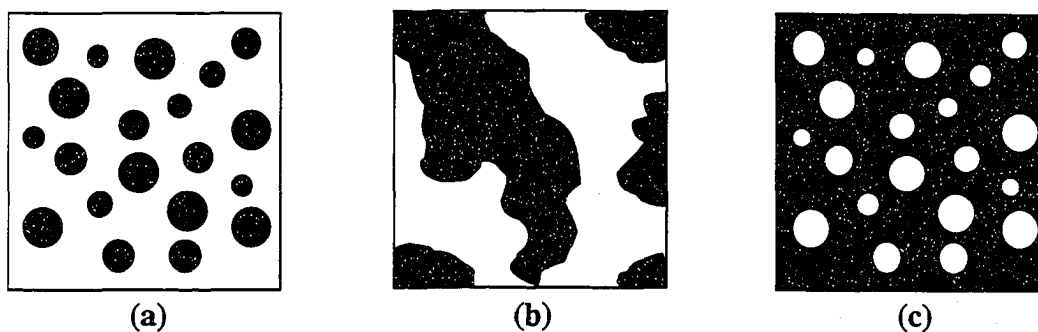


Figure 1.1 The morphology of an immiscible blend A/B changes as the relative amount of polymer B increases. The white color stands for phase A and the black color, for phase B. (a) dispersed B droplets in phase A; (b) co-continuous morphology; (c) dispersed A droplets in phase B.

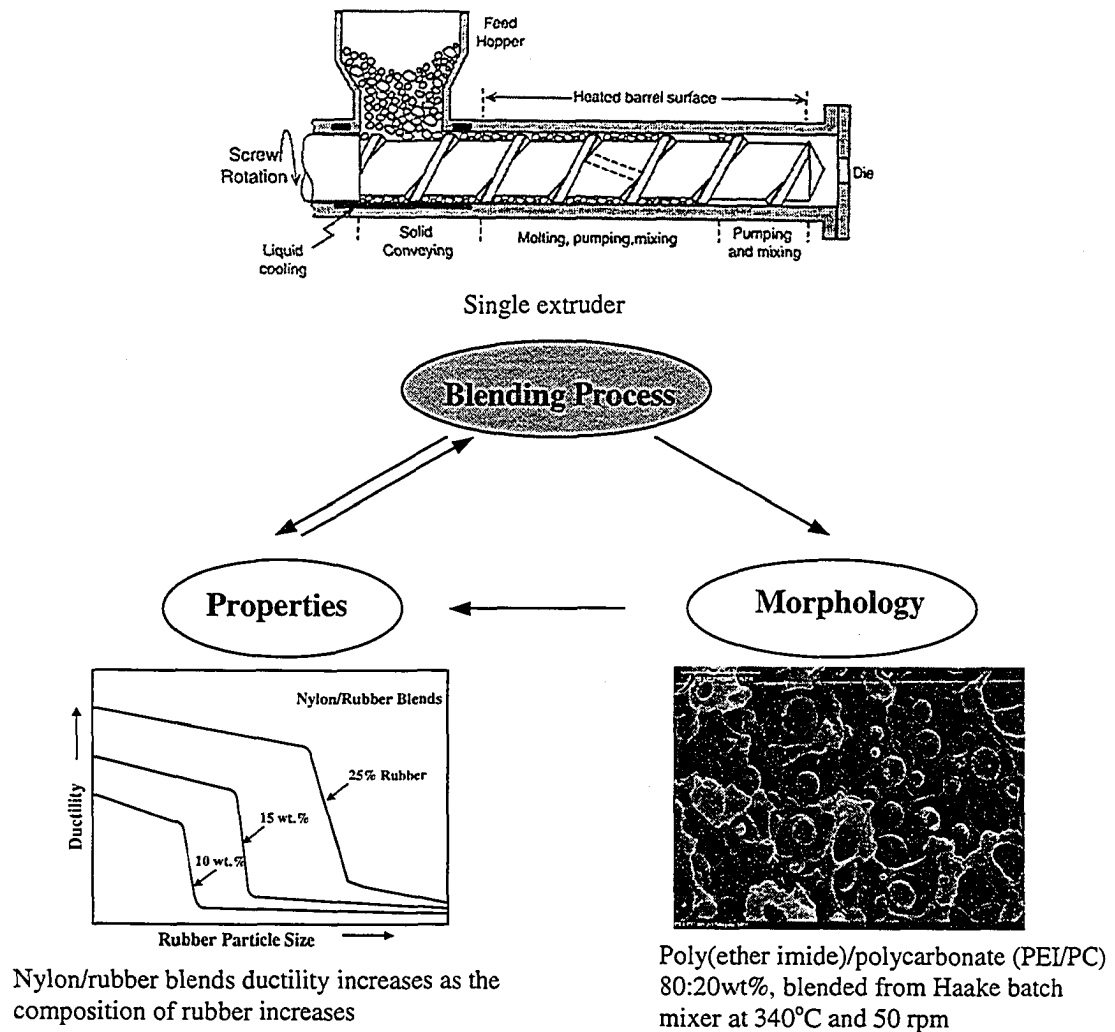


Figure 1.2 Polymer blending process, morphology and properties relationship. Extruder figure from Tadmor and Gogos, 1979. Ductility plot adapted from Wu, 1985.

Figure 1.2 illustrates the relationship among polymer processing, morphology and properties. Generally, the properties of a blend depend on how one polymer disperses or incorporates into another kind of polymer, i.e., the morphology. The morphology, in turn, is determined by the processing. Figure 1.2 gives an example showing that the ductility of nylon/rubber blends depends on the dispersed rubber particle size. When the particle size

is below a critical value, the ductility can be improved greatly. Since the blending process is crucial in determining the final dispersion morphology and controlling the blend properties, it is important to understand the fundamental governing factors during the blending process.

1.2 POLYMER BLEND MORPHOLOGY DEVELOPMENT

Both batch mixers and extruders are commonly used in polymer processing. Batch mixers were first developed for mixing fine carbon black particles into rubber in 1916 (Tadmor and Gogos, 1979). The high intensity batch mixers are now widely used for blending of dissimilar polymers, dispersing fillers, and incorporating dyes or other additives into a polymer matrix or into a polymer blend. However, an extruder is used more frequently in industry because it can be operated continuously.

A typical extrusion operation includes many steps (Tadmor and Gogos, 1979) such as: handling of solid polymer pellets; melting; pressurizing and pumping; mixing; and devolatilization. All of these steps occur continuously and within a few minutes. It is difficult to understand such complicated processes without determining the fundamentals of each process step. Among all these single processes, melting and mixing are the most important and basic processing steps because melting affects the process rate and mixing determines the morphology (Gulke, 1994). During the melting and mixing processes, the solid polymer pellets experience melting or softening, deformation and breakup. In later stages of mixing, a balance between breakup and coalescence leads to the final morphology.

It has been shown that the final morphology of polymer blends develops rapidly during the blending process (Scott and Macosko, 1991, 1995; Sundararaj *et al.* 1992, 1995; Lindt and Ghosh, 1992). Scott and Macosko (1991, 1995) studied the initial polymer blends morphology development in a batch mixer and found that a large number of sheets or ribbons of the dispersed phase form in the matrix in the first minute of the mixing. Sundararaj *et al.* (1992) showed that in the initial stage of polymer blending in a twin-screw extruder, long, thin ribbons and sheets occurred during the melting and softening stage. Lindt and Ghosh (1992) also observed that the lamellar structures were formed during the early stages of morphology development in a single screw extruder. The sheets and lamellar structures are unstable because of interfacial forces, and they subsequently break up to smaller droplets. Bourry and Favis (1998) indicated that the morphology of the dispersed phase could be modified very rapidly under the dynamic conditions in the melt state, and that the drop size changes dramatically during the melting and softening stage. Therefore, the initial morphology development of blends is crucial in understanding the final morphology.

Figures 1.3 and 1.4 show scanning electron microscopy (SEM) micrographs of the initial morphology of a polyethylene (PE) and polycarbonate (PC) blend (80:20 wt%) prepared in a Haake 600 series batch mixer (Paramus, NJ) at 220°C and 50 rpm (rotation per minute). In Figure 1.3, the PE/PC sample was blended for 1 min. In Figure 1.4, the PE/PC sample was first melted and then blended for 20 s. Both samples were quenched in liquid nitrogen immediately after the runs. For some micrographs, the PC phase was extracted with methylene chloride at room temperature overnight (Figure 1.3a, Figure 1.4a). For other micrographs, the PE phase was extracted with dodecane at 90°C for 1 h

(Figures 1.3b-c, Figures 1.4b-c). Both Figure 1.3 and Figure 1.4 show that the PC phase forms sheets, ribbons, cylinders and droplets during the initial morphology development. Figure 1.4c gives the cross sectional view of a PC sheet. The thickness of the PC sheets is in the order of 1-10 μm , which is also observed by many other researchers (e.g., Sundararaj *et al.* 1995; Willemse *et al.* 1999).

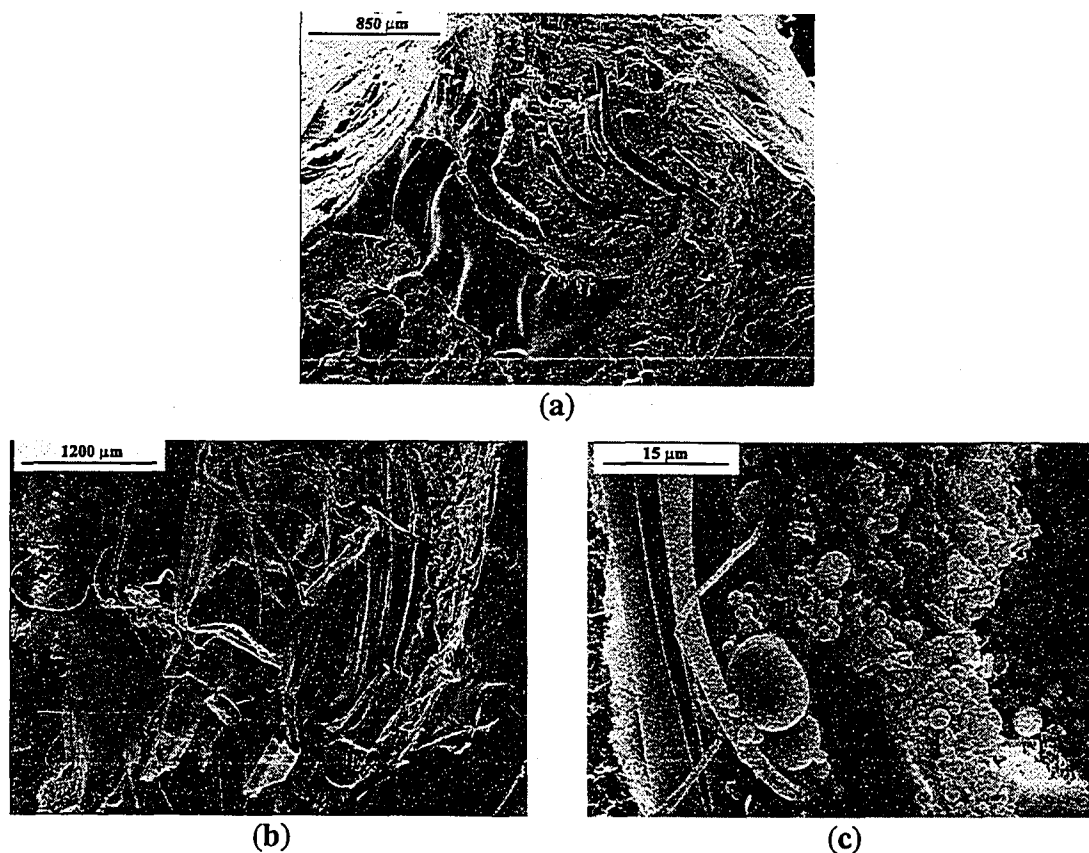


Figure 1.3 Initial morphology development of solid feed PE/PC (polyethylene/polycarbonate 80:20wt%) in Haake batch mixer at 220°C and 50 rpm for 1 min. Solid pellet feed was used. (a) PC phase extracted with methylene chloride — the PC phase consists of sheets/ribbons, cylinders and droplets in the PE matrix; (b) PE phase extracted with dodecane — PC sheets/ribbons and cylinders remain; (c) PE phase extracted with dodecane — PC cylinders and droplets remain. Note scale bars.

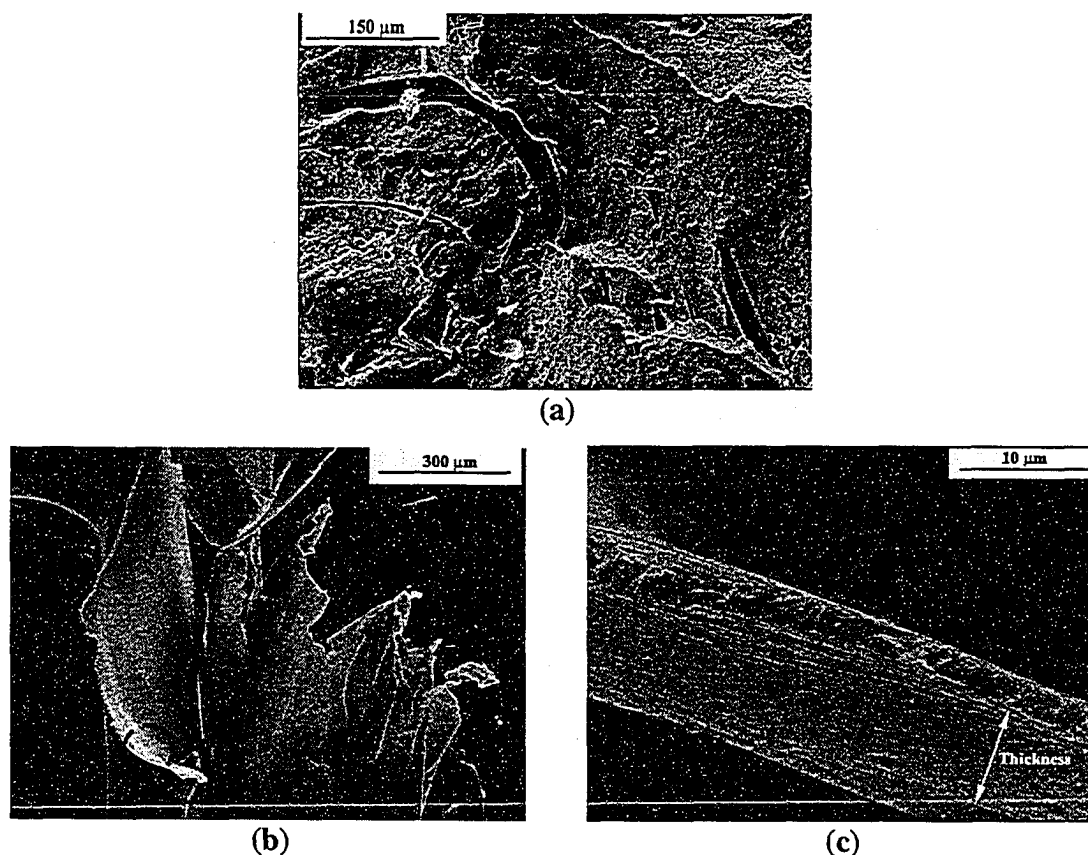


Figure 1.4 Initial morphology development of PE/PC (polyethylene/polycarbonate 80:20wt%) in Haake batch mixer at 220°C and 50 rpm. The blend was premelted first at 220°C and then mixed for 20 s. (a) PC phase extracted with methylene chloride — sample shows holes where PC ribbons, cylinders and droplets once were; (b) a PC sheet after the PE phase was extracted, the dotted circled in the lower left corresponds to the area enlarged in (c); (c) the thickness of the PC sheet is 1-10 μm. Note scale bars.

1.3 DROP BREAKUP

During the initial blending process, the millimeter sized polymer pellets are deformed and broken up into sub-micron sized droplets rapidly. In the literature, the deformation and breakup of millimeter drop in well-defined flow fields under quasi-equilibrium conditions have been studied extensively, though most studies are confined to Newtonian systems.

One of the first researchers in the area of drop deformation and breakup was Taylor. He established a small deformation theory based on Einstein's theory for small solid spheres suspended in a Newtonian fluid (Taylor, 1932). By balancing the interfacial stress and the shear stress (Figure 1.5), he predicted the maximum drop size that would be stable for small deformations in Newtonian fluids. He also predicted that no drop breakup would occur when the viscosity ratio, the ratio of drop phase viscosity to matrix phase viscosity ($\eta_r = \eta_d / \eta_m$), is greater than 2.5. He later published his experimental study (Taylor, 1934) on a Newtonian drop in Newtonian fluids subject to a planar simple shear in a parallel band shear flow device.

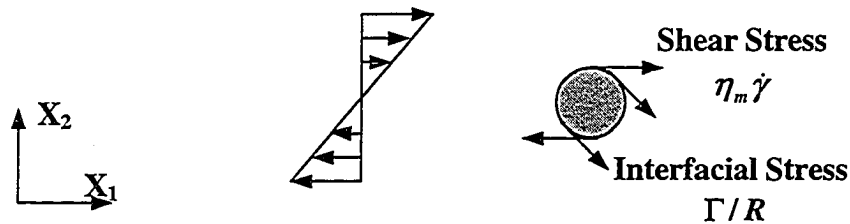


Figure 1.5 A Newtonian drop in Newtonian matrix under simple shear.

Subsequent to Taylor's work, special attention was given to the drop configuration and orientation during breakup and to the relationship between the viscosity ratio and the critical Capillary number (e.g., Rumscheidt and Mason, 1961; Karam and Bellinger, 1968; Torza *et al.*, 1972; Grace, 1982). The Capillary number is a ratio of shear stress to interfacial stress ($Ca = \eta_m \dot{\gamma} R / \Gamma$, where $\dot{\gamma}$ is shear rate, R is drop radius and Γ is interfacial tension). For Newtonian systems, the critical Capillary number, the flow condition where the drop breaks up, has been found to correlate with the viscosity ratio of the two phases. One of the most comprehensive studies was done by

Grace (1982), who studied Newtonian fluid systems with a wide viscosity ratio range from 10^{-6} to 950 in both a simple shear flow field using a Couette device and an extensional flow field using a four-roll device. He correlated critical Capillary number with viscosity ratio (Figure 1.6). Figure 1.6 showed that a drop breaks up over the full range of viscosity ratio studied in extensional flow for Newtonian systems and at a lower critical Capillary number than that needed for drop breakup in simple shear. However, in simple shear flow field, a Newtonian drop will not break in a Newtonian matrix if the viscosity ratio is greater than 3.5, where the drop keeps an elliptical shape and spins inside the matrix. The flow field in either a batch mixer or an extruder is a combination of shear and extensional flow. In this thesis, only shear flow field is studied.

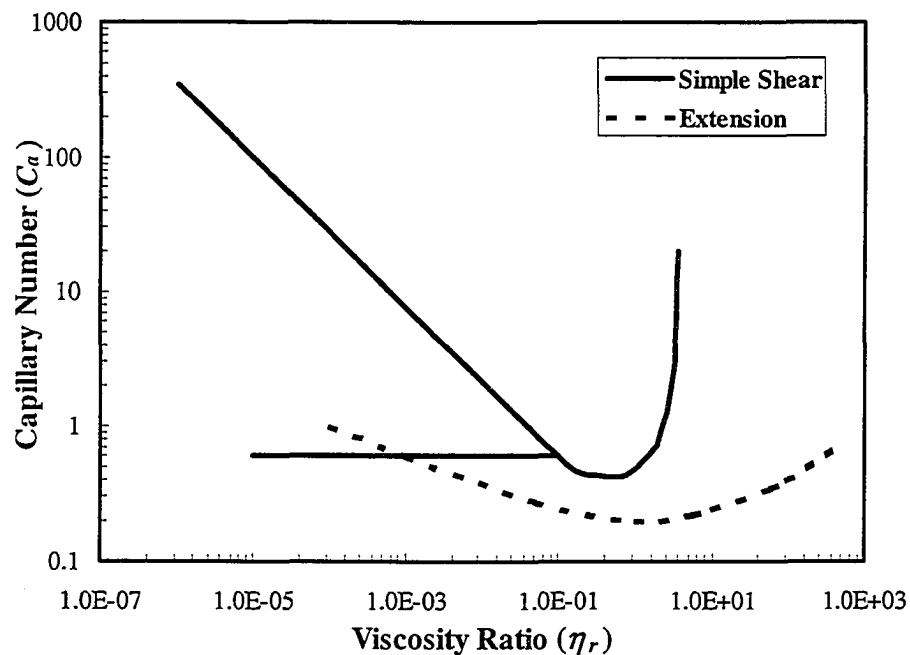


Figure 1.6 Critical Capillary number versus viscosity ratio for Newtonian systems (Grace, 1982).

Studies on drop deformation and breakup under transient conditions are few. It was found that the Newtonian drop was initially extended affinely with the flow into a thin liquid thread (or cylinder) during extension (Elemans *et al.*, 1993; Janssen and Meijer, 1993). The thread was later broken into many small droplets when interfacial tension driven instabilities, or capillary instability, grew at the interface. Drop breakup through transient conditions is most likely to occur in real mixing process, however, for polymer systems, due to the complexity properties of the materials and the flow fields, studies on polymer drop deformation and breakup are few even in quasi-equilibrium flow conditions.

Polymers, unlike Newtonian fluids, are viscoelastic and shear-thinning materials. It has been shown that viscoelastic properties affect drop deformation and breakup. Vanoene (1972) used thermodynamic analysis of droplet formation and obtained the interfacial tension for viscoelastic fluids in flow, or dynamic interfacial tension (Γ'), by accounting the difference of the first normal stress (N_1) between the drop phase and the matrix phase to the interfacial tension in the absence of flow (Γ):

$$\Gamma' = \Gamma + \frac{1}{6}R[N_{1,d} - N_{1,m}]$$
, where the subscripts d and m stand for drop phase and matrix phase, respectively. Therefore, he predicted that elasticity of the drop phase would stabilize the droplet, but that the elasticity of the matrix phase would destabilize the droplet. Elemendorp and Maalcke (1985) studied the effects of elasticity on viscoelastic systems in a Couette device. They found that normal forces from the drop phase tend to resist drop deformation, while normal forces from the matrix phase tend to assist drop deformation. Elemendorp and Maalcke (1985) also found that it was inappropriate to use the dynamic interfacial tension proposed by Vanoene (1972) since at higher shear rates,

the dynamic interfacial tension values went to zero or negative. However, the study of Vanoene (1972) has shed some light on polymer drop deformation and breakup, and later studies have shown that normal stress does indeed play an important role in polymer-polymer systems (Sundararaj *et al.*, 1995; Levitt *et al.*, 1996; Hobbie and Migler, 1999; Migler *et al.*, 1999; Migler 2000; Mighri and Huneault, 2001b). So far, polymer drop deformation and breakup mechanisms in shear flow under quasi-equilibrium conditions are still not known.

1.4 VISUALIZATION

The basic research approach used in this thesis is visualization. “A picture is worth a thousand words”, or in this study, a picture is worth at least a thousand numerical data points. Visualization is an excellent method to understand polymer pellet deformation, melting, flow and dispersion.

Visualization of drop deformation has been performed successfully on model viscoelastic fluids and polymers in different flow fields. A number of researchers have focused on polymer systems using model fluids. Han and Funatsu (1978) studied glycerin drop deformation in a pressure driven shear flow and found that the viscoelastic drops require more shear stress for breakup compared with Newtonian drops. Peuvrel and Navard (1990) obtained the velocity profile of a hydroxypropylcellulose drop in a cone and plate device, and showed that the profile was linear and laminar. Shih *et al.* (1995) observed glass fiber dispersion in corn syrup solution in a batch mixer and a twin-screw extruder (TSE) and determined the effects of mixing parameters, such as mixing time, rotation speed and degree of fill, on the dispersion of glass fiber. Bigio and Wang (1996)

studied the distributive mixing by flow visualization of dyed silicone oil in a TSE and developed scale-up rules. Mighri *et al.* (1998) used transparent parallel plates to observe the deformation and breakup of Boger fluid drops. They found that the matrix elasticity helped drop deformation and drop elasticity resisted drop deformation. Gauri and Koelling (1999) visualized the flow field in the vicinity of a bubble front and suggested that the extensional rheology was important in determining the wall thickness in gas-assisted injection molding. Mighri and Huneault (2001a) studied drop deformation and breakup using model fluids in a transparent Couette cell. They observed that an elastic drop was easily aligned and elongated in the vorticity direction.

Polymer flow visualization has been applied to observe polymer pellets melting and mixing process in both batch mixer and extruder. Some important aspects of the mixing process have been established by visualization through a transparent glass window in the front of a batch mixer (Min and White, 1985; Shih *et al.*, 1991; Shih, 1995, Sundararaj, 1996; Sundararaj *et al.*, 1996; Lin and Sundararaj, 2001, 2004). Min and White (1985) studied the flow behavior of elastomers and molten plastics in a Banbury type mixer. They observed the stretching, tearing, “sheeting out”, and bending in elastomers, and “sheeting out” in plastics. The “sheeting out” phenomenon was observed as the colored sample sheet was sheared as a thin film layer on the chamber wall. Lin and Sundararaj (2001, 2004) visualized the blending process of poly(ether imide)/polycarbonate (PEI/PC) in a batch mixer at 340°C. Distinct pellet deforming, softening, aggregation, stretching, bending, sheeting and dispersing were seen during the blending process (Figure 1.7).

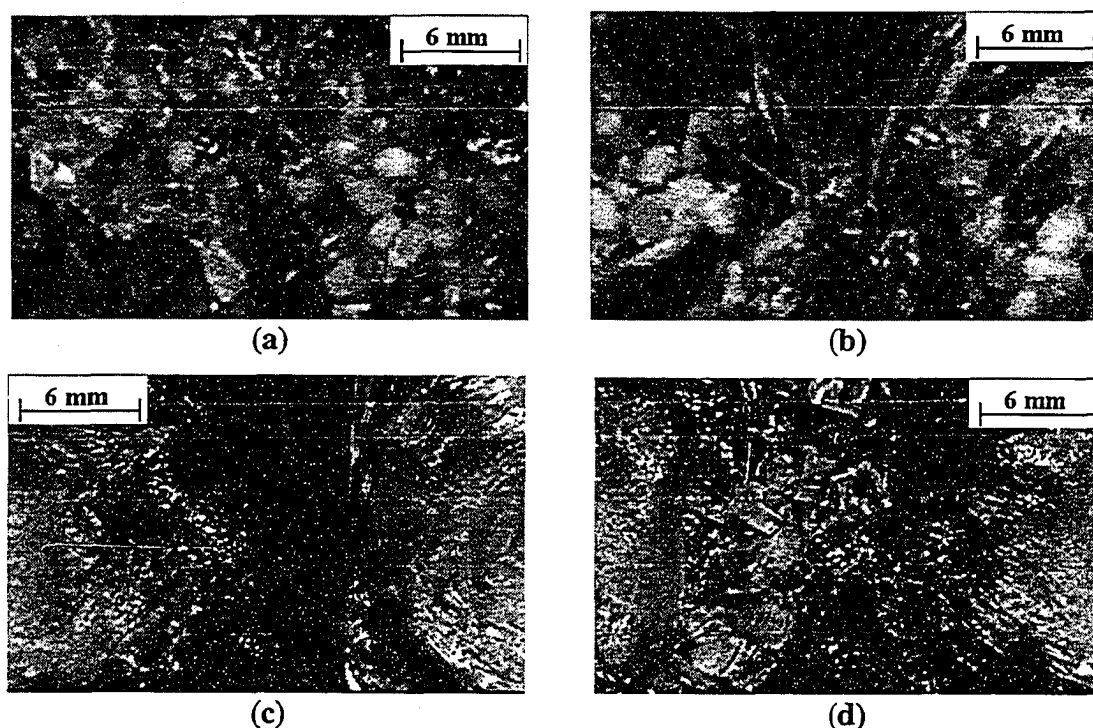


Figure 1.7 PEI/PC (80:20 wt%) blending at 340°C, 10 rpm. PEI was added first. (a) Aggregate PEI pellets ($t=38s$); (b) Stretching and sheeting out of the deformed PEI pellets ($t=48s$); (c) Stretching of PEI melt ($t=117s$); (d) Deformation and stretching of PC pellets ($t=148s$). Note scale bars. From Lin and Sundararaj, 2004.

Polymer melting process of polymers in extruders has also been successfully observed (Kim and White, 1994; Sakai, 1995; Zhu and Geng, 1999; Chen *et al.*, 2003). The visualization experiments were accomplished by using some glass windows on the barrel or one glass barrel. Kim and White (1994) studied the fluid motions of aluminum flakes in EVAc (ethylene-co-vinyl acetate) through four glass windows and determined the residence time distributions in TSE. Sakai (1995) observed HDPE (high-density polyethylene) and PP melting via a side glass window on the barrel. Gogos *et al.* (1996) visualized the dispersive mixing of PS/LDPE (major phase/minor phase, LDPE: low-density polyethylene) and LDPE/PS (major phase/minor phase) blends in a model mixer (twin screw mixing element evaluator). Zhu and Geng viewed HDPE pellets melting

through a transparent barrel. More recently, Chen *et al.* (2004) studied the melting mechanism of PS/PP blend using a sliding barrel along a TSE.

Visualization studies on polymer drop deformation are few. Sundararaj *et al.* (1994) and Levitt *et al.* (1996) investigated the initial breakup mechanisms of polymer blends by observing polymer pellet deformation between two parallel plates and found that sheets formed easily during initial shear. Migler *et al.* (1999) viewed PS drop deformation in PE (polyethylene) in channel flow at the die of the extruder. They observed that the micron-sized PS drops aligned in the vorticity direction and subsequently broke up, which was ascribed to the difference of shear stress at varying depth from the wall.

1.5 MOTIVATION OF THE THESIS

It is now well known that the final morphology is developed in the first two minutes of mixing in a batch mixer (Favis, 1990; Scott and Macosko, 1991, 1995) or even in the first few seconds (Sundararaj *et al.*, 1995), and in the first few seconds of residence time in an extruder (Sundararaj *et al.*, 1992; Lindt and Ghosh, 1992). To visualize the initial morphology development on-line is difficult because: (1) polymers usually melt well above room temperature; (2) the flow field is a combination of elongation and shear; (3) the size scale is extremely small, on the order of microns; and (4) the time scale to observe the breakup process is short.

The objective of this thesis is to study how polymer pellets are melted and mixed during the initial polymer blending processes. The technique used in this thesis is visualization, i.e., to visualize how a single polymer drop melts, deforms and breaks up

inside a second polymer melt under shear flow in quasi-equilibrium conditions. The drop diameter used for visualization studies is around 0.5 mm to 1.0 mm, a size scale similar to that of polymer pellets.

The organization of the thesis is as follows: Chapter 2 presents visualization results on drop deformation and breakup subject to shear flow in parallel plates; Chapter 3 shows drop deformation and breakup mechanisms under simple shear flow generated by Couette cell; Chapter 4 studies the effect of compatibilizer on drop deformation and breakup in simple shear; Chapter 5 provides results of drop visualization in a mini-Mixer (APAM) and the effect of compatibilization in polymer blending; Chapter 6 summarizes this thesis work and discusses future work.

1.5 REFERENCES

- Bigio, D.; Wang, K. *Polym. Eng. Sci.* **1996**, *36*, 2832-2839.
- Bourry, D.; Favis, B.D. *Polymer* **1998**, *39*, 1851-1856.
- Chen, H.; Sundararaj, U.; Nandakumar, K.; Wetzel, M.D. *Ind. Eng. Chem. Res.* **2004**, *43*, 6822-6831.
- Elemans, P.H.M; Bos, H.L.; Janssen, J.M.H.; Meijer, H.E.H. *Chem. Eng. Sci.* **1993**, *48*, 267-276.
- Elemendorp, J.J.; Maalcke, R.J. *Polym. Eng. Sci.* **1985**, *25*, 1041-1047.
- Favis, B.D. *J. Appl. Polym. Sci.* **1990**, *39*, 285-300.
- Gauri, V.; Koelling, K.W. *SPE ANTEC Tech. Papers* **1999**, *59*, 1291-1295.
- Gogos, C.G.; Essenghir, M.; Todd, D.B.; Yu, D.W. *Macromol. Symp.* **1996**, *101*, 185-198.

- Grace, H.P. *Chem. Eng. Commun.* **1982**, *14*, 225-277.
- Grulke, E.A. *Polymer Processing Engineering*; Prentice-Hall: New Jersey, 1994.
- Han, C.D.; Funatsu, K. *J. Rheol.* **1978**, *22*, 113-133.
- Hobbie, E.K.; Migler, K.B. *Phys. Rev. Lett.* **1999**, *82*, 5393-5396.
- Janssen, J.M.H. *PhD Thesis*; Eindhoven University of Technology, 1993.
- Janssen, J.M.H.; Meijer, H.E.H. *J. Rheol.* **1993**, *37*, 597-608.
- Karam, H.J.; Bellinger, J.C. *I & EC Fundam.* **1968**, *7*, 576-581.
- Levitt, L.; Macosko, C.W.; Pearson, S.D. *Polym. Eng. Sci.* **1996**, *36*, 1647-1655.
- Lin, B.; Sundararaj, U. *SPE ANTEC Tech. Papers* **2001**, *59*, 3056-3060.
- Lin, B.; Sundararaj, U. *J. Appl. Polym. Sci.* **2004**, *92*, 1165-1175.
- Lindt, J.T.; Ghosh, A.K. *Polym. Eng. Sci.* **1992**, *32*, 1802-1813.
- Mighri, F.; Carreau, P.J.; Ajji, A. *J. Rheol.* **1998**, *42*, 1477-1490.
- Mighri, F.; Huneault, M.A. *J. Rheol.* **2001a**, *45*, 783-797.
- Mighri, F.; Huneault, M.A. *3rd Pacific Rim Conference on Rheology*, Paper No. 005, 2001b.
- Migler, K.B.; Hobbie, E.K.; Qiao, F. *Polym. Eng. Sci.* **1999**, *39*, 2282-2291.
- Migler, K.B. *J. Rheol.* **2000**, *44*, 277-290.
- Min, K.; White, J.L. *Rubber Chem. Technol.* **1985**, *58*, 1024-1037.
- Parkes, A. *Brit. Pat.*, **1846**, 1147.
- Peuvrel, E.; Navard, P. *Macromolecules* **1990**, *23*, 4874-4875.
- Rumscheidt, F.D.; Mason, S.G. *J. Colloid Interface Sci.* **1961**, *16*, 238-261.
- Ratnagiri, R.; Scott, C.E. *Polym. Eng. Sci.* **2001**, *41*, 1310-1321.
- Sakai, T. *Adv. Polym. Tech.* **1995**, *14*, 277-290.

- Scott, C.E.; Macosko, C.W. *Polym. Bull.* **1991**, *26*, 341-348.
- Scott, C.E.; Macosko, C.W. *Polymer* **1995**, *36*, 461-470.
- Shih, C.-K.; Tynan, D.G.; Denelsbeck, D.A. *Polym. Eng. Sci.* **1991**, *31*, 1670-1673.
- Shih, C.-K.; Royer, D.J.; Tynan, D.G. *SPE ANTEC Tech. Papers* **1995**, *53*, 2413-2418.
- Shih, C.-K. *Polym. Eng. Sci.* **1995**, *35*, 1688-1694.
- Sundararaj, U.; Macosko, C.W.; Rolando, R.J.; Chan, H.T. *Polym. Eng. Sci.* **1992**, *32*, 1814-1823.
- Sundararaj, U.; Dori, Y.; Macosko, C.W. *SPE ANTEC Tech. Papers* **1994**, *52*, 2448-2451.
- Sundararaj, U.; Dori, Y.; Macosko, C.W. *Polymer* **1995**, *36*, 1957-1968.
- Sundararaj, U. *Macromol. Symp.* **1996**, *112*, 85-89.
- Sundararaj, U.; Macosko, C.W.; Shih, C.K. *Polym. Eng. Sci.* **1996**, *36*, 1769-1781.
- Tadmor, Z.; Gogos, C.G. *Principles of Polymer Processing*; Wiley-Interscience: New York, 1979.
- Taylor, G.I. *Proc. R. Soc. London, Ser. A* **1932**, *138*, 41-48.
- Taylor, G.I. *Proc. R. Soc. London, Ser. A* **1934**, *146*, 501-523.
- Torza, S.; Cox, R.G.; Mason, S.G. *J. Colloid Interface Sci.* **1972**, *38*, 395-411.
- Utracki, L.A. *Polymer Alloys and Blends: Thermodynamics and Rheology*; Hanser Publisher: Munich, 1989.
- Utracki, L.A.; Shi, Z.H. *Polym. Eng. Sci.* **1992**, *32*, 1824-1833.
- Utracki, L.A. *Polymer Blends Handbook*; Kluwer Academic Publishers: Dordrecht, 2002; Vol.1.
- Vanoene, H. *J. Colloid Interface Sci.* **1972**, *40*, 448-467.

Willemse, R.C.; Ramaker, E.J.U.; van Dam, J.; de Boer, A.P. *Polymer* **1999**, *40*, 6651-6659.

Wu, S.H. *Polymer* **1985**, *26*, 1855-1863.

Zhu, L.; Geng, X. *SPE ANTEC Tech. Papers* **1999**, *57*, 370-374.

Chapter 2

Deformation and Breakup of a Polymer Drop

Sheared between Parallel Plates —

Sheet Formation of a Polycarbonate Drop inside a Polyethylene Matrix

2.1 INTRODUCTION

Polymer blends are attractive because they provide better performance than homopolymers and are of much lower development costs than synthesizing new polymers (Elmendorp and Van der Vegt, 1991; Utracki and Shi, 1992). The polymer blending process is crucial because it determines the final morphology and this in turn affects the properties of blends. Blending is performed mostly in batch mixers or extruders. Therefore, it is important to understand the flow and deformation processes in these mixers. However, the flow field in either a batch mixer or an extruder is complicated, consisting of a combination of extensional and shear flow. In addition, the final morphology is developed in the first two minutes of mixing in a batch mixer (Favis, 1990; Scott and Macosko, 1991, 1995) and in the first few seconds of residence time in an extruder (Lindt and Ghosh, 1992; Sundararaj *et al.*, 1992), which is too fast to observe the drop breakup process. Therefore, drop breakup was visualized in a model shear flow field under quasi-equilibrium conditions for polymer-polymer systems in order to understand the morphology development in the initial blending stages.

The deformation and breakup of an isolated drop in a matrix has been studied extensively for the last seven decades (Taylor, 1932, 1934; Rumscheidt and Mason, 1961; Karam and Bellinger, 1968; Torza *et al.*, 1972; Grace, 1982; Elmendorp and Van

der Vegt, 1991; Utracki and Shi, 1992; Rallison, 1984; Stone, 1994; Briscoe *et al.*, 1999). Work in drop breakup experiments and numerical simulations can be found in review papers of Rallison (1984), Elmendorp and Van der Vegt (1991), Stone (1994), Utracki and Shi (1992), Briscoe *et al.* (1999) and Ottino *et al.* (2000).

It is now well accepted that Capillary number and viscosity ratio are the important parameters for Newtonian drop breakup. The Capillary number, Ca , is a ratio of shear stress to interfacial stress ($Ca = \eta_m \dot{\gamma} R / \Gamma$, where $\dot{\gamma}$ is shear rate, R is drop radius and Γ is interfacial tension). The viscosity ratio is a ratio of drop phase viscosity to matrix phase viscosity ($\eta_r = \eta_d / \eta_m$). The correlation between the Capillary number and viscosity ratio can be well described in Figure 1.6 (Grace, 1982). However, drop breakup in polymer-polymer systems is not well understood.

Wu (1987) found that, for polymer systems in an extruder, drop breakup occurs even when the viscosity ratio is higher than 3.5. He also correlated Capillary number with viscosity ratio: $Ca = 4\eta_r^{\pm 0.84}$, where the plus (+) sign in the exponent applies for $\eta_r > 1$ and the minor (-) sign applies for $\eta_r < 1$. There are some problems associated with Wu's study: (1) the dispersed phase has a concentration of 15%; (2) the drop size used is the final extruded drop size; (3) the flow field inside the extruder is a combination of shear and extension; and (4) there is not much data presented for $\eta_r < 1$. However, Wu's study provides a good first attempt to find important forces for polymer drop breakup and drop size prediction. Favis and Chalfoux (1987) also found that polymer drops in a batch mixer can break up even when the viscosity ratio is as high as 17. Though these studies were obtained either from a twin-screw extruder or a batch mixer, where the flow field is

no longer pure shear, it at least suggests that polymer systems are different from Newtonian systems because polymers are shear-thinning and viscoelastic materials.

Two devices are commonly used in generating a shear flow field: one is a Couette cell and the other is a parallel plate device. The Couette cell is the most popular device used for generating simple shear flow. A drop of one phase is placed in the gap between two concentric cylinders filled with another fluid (Trevelyan and Mason, 1951; Rumscheidt and Mason, 1961; Karam and Bellinger, 1968; Tavgac, 1972; Grace, 1982; de Bruijn, 1989, 1993; Tjahjadi *et al.*, 1992; Cormas-Cordona, 2000; Cormas-Cordona and Tucker, 2001; Mighri and Huneault, 2001; Lin *et al.*, 2003a, 2003b). The two cylinders can be either counter-rotating or only one of them may rotate. The gap between the two cylinders should be small compared to the diameters of the cylinders so that the shear rate across the gap is constant and independent of the drop's radial position. Parallel plates (Sundararaj *et al.*, 1994, 1995; Levitt *et al.*, 1995; Varanasi *et al.*, 1994; Tsakalos *et al.*, 1998; Mighri *et al.*, 1998; Guido and Villone, 1998; Yamane *et al.*, 1998) normally use rotating transparent plates or may consist of cone-and-plate. Unlike the Couette cell, the flow field generated by parallel plates is not homogenous. However, very viscous polymers can be studied with a parallel plate device. Moreover, it is easier to load samples into a parallel plate device than into a Couette cell.

Due to the difficulty in viewing drop breakup at a high processing temperature, only a few reports have been published on visualization of drop deformation and breakup in polymer systems in the literature. Sundararaj *et al.* (1994, 1995) studied initial blend morphology and showed that sheets could easily be formed in a shear flow. Levitt *et al.* (1996) traced polypropylene (PP) drops in a polystyrene (PS) matrix with transparent

counter-rotating parallel plates and observed widening of the drop along the vorticity direction. They attributed the widening to the difference of elasticity between major and minor phases, which overcame the contraction caused by interfacial tension. Hobbie and Migler (1999) and Migler *et al.* (1999) viewed PS drop inside polyethylene (PE) matrix by a pressure-driven optical flow cell situated at the exit, or die region, of a twin-screw extruder. They observed that PS drops are elongated perpendicularly to the flow field in PE matrix. The vorticity elongation was ascribed to the normal stress existing in polymers.

In this Chapter, softening, deforming and then breaking up of a polycarbonate (PC) drop (drop diameter: 0.5 ~ 1 mm) in a PE matrix will be described. The system was subjected to a shear flow generated by a rotating parallel plate. The drop deformation and breakup was viewed at a temperature of 220°C through a transparent plate.

2.2 EXPERIMENT

2.2.1 Materials

The polymer systems studied comprised PC drops inside a PE matrix. All polymers were obtained in pellet form. Six grades of polycarbonate (PC1-PC6), generously denoted by GE Plastics, were used as the drop phase and two grades of polyethylene (PE1 and PE2), generously denoted by Petromont, were used as the matrix phase. The refractive index is 1.58 for PC and 1.49 for PE (van Krevelen, 1976). Since the difference between the two indices is large, it is easy to see a PC drop inside a PE matrix directly.

Table 2.1 lists the molecular weight (M_n and M_w), complex viscosity (η^*) and elastic modulus (G') at a shear rate of 1 s^{-1} , and the relaxation time (λ) of the polymers used. The glass transition temperature (T_g) for PC is 150°C (Lin and Sundararaj, 2004a). The experiments were run at 220°C , which was around $30\text{-}50^\circ\text{C}$ lower than the processing temperature. The lower temperature was used in the experiments (also in Chapter 3) since this thesis is focused on the initial morphology development. That is, during processing, initial melting may occur before the material reaches the final processing temperature. Dynamic rheological characterizations were performed using a Rheometrics RMS800 Rheometer with a 25 mm parallel plate fixture at 10% strain. Figure 2.1a shows the complex viscosity of PC and PE at 220°C . Figure 2.1b gives the elastic modulus of PC and PE at 220°C . The relaxation time, λ , was obtained from the complex viscosity versus frequency data. The intersection of the line representing the zero shear viscosity limit at low frequency and the line representing the power law viscosity at high frequency was determined to be the critical frequency, ω_c , and $\lambda = 1/\omega_c$.

The PC spherical drops were specially prepared in Dow Corning 550 silicone oil at 210°C . Initially, one PC pellet was cut into about 200 small pieces with a razor. A small PC piece was heated for 30 min in 100 mL of silicone oil. The PC softened and became spherical due to interfacial tension. The temperature was then slowly reduced below 100°C over a period of 20 minutes. During the heating and cooling processes, a stirrer was used to suspend the PC particle in the fluid. The PC drop was rinsed with heptane five times to remove the silicone oil on the surface. The dimensions of the spheres were measured through imaging using an Olympus BHSM optical microscope.

Table 2.1 Properties of polymers used.

Polymer Commercial Name (Abbreviation)	Source	Molecular Weight ^a (g/mol)		Viscosity at $\dot{\gamma} = 1s^{-1}$ & 220°C (η^* , Pa's)	Elastic Modulus at $\dot{\gamma} = 1s^{-1}$ & 220°C (G' , Pa)	Relaxation Time (λ , s)
		<i>Mn</i>	<i>Mw</i>			
Polycarbonate: Lexan OQ1030 (PC1)	GE Plastics	7,660	17,200	1,800	33	0.05
Polycarbonate: Lexan OQ1050 (PC2)	GE Plastics	8,500	17,430	2,000	45	0.05
Polycarbonate: Lexan OQ1020 (PC3)	GE Plastics	7,220	17,880	2,600	75	0.05
Polycarbonate: Lexan AP1300 (PC4)	GE Plastics	8,840	22,710	5,600	220	0.10
Polycarbonate: Lexan 140 (PC5)	GE Plastics	10,780	27,100	20,200	2200	0.17
Polycarbonate: Lexan 104 (PC6)	GE Plastics	12,610	28,860	35,900	5000	0.22
Polyethylene: DMDA-8920 (PE1)	Petromont	14,400	53,400	370	25	0.10
Polyethylene: DMDB-8907 (PE2)	Petromont	19,800	68,900	980	110	0.15

a. Provided by supplier.

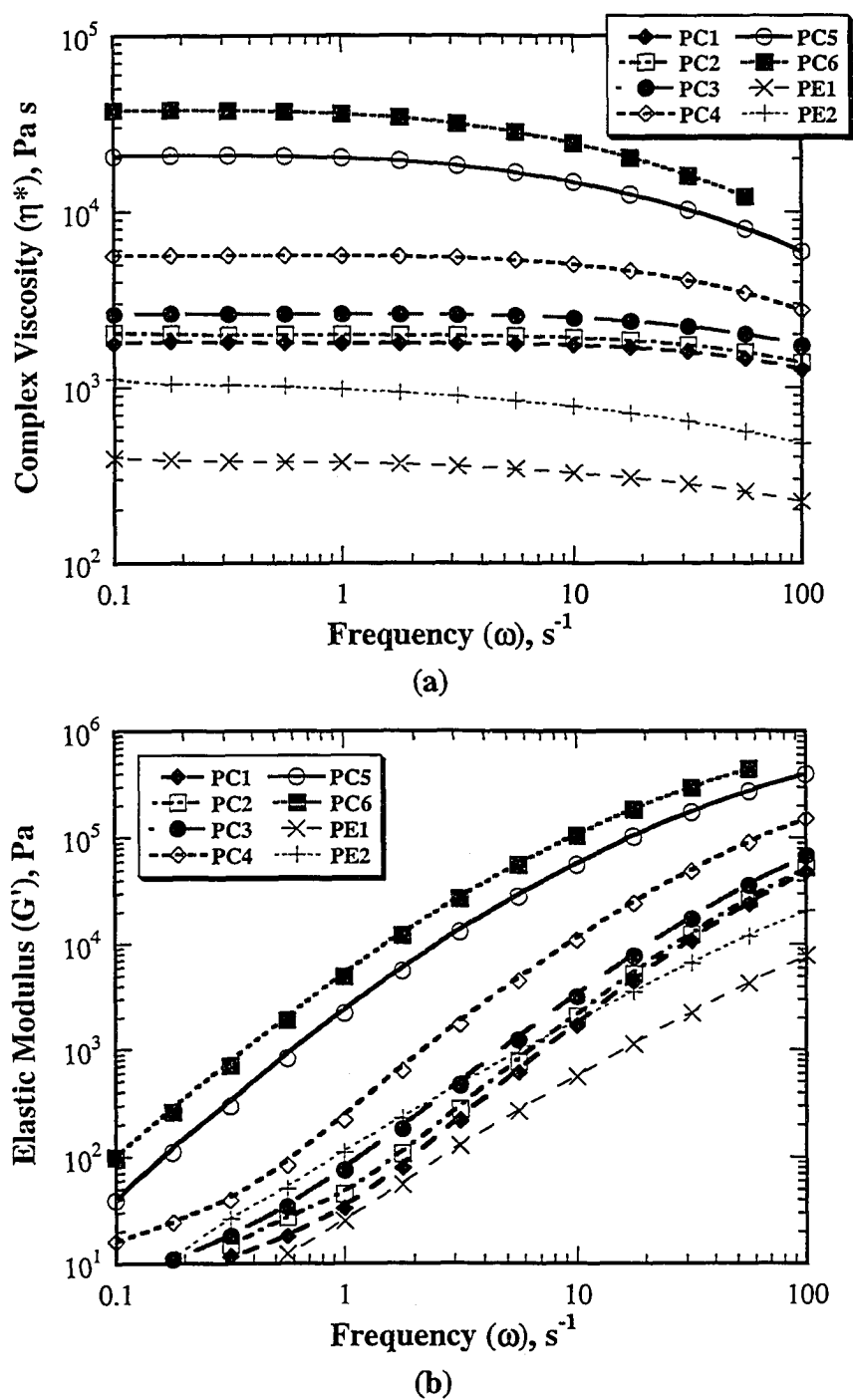


Figure 2.1 (a) Complex viscosity of PC and PE at 220°C and (b) Elastic modulus of PC and PE at 220°C.

The PE disks (25 mm in diameter and 2 mm in thickness) were prepared using a heated compression plate press (Carver #2086) with an internal water cooling system. The PE pellets were dry mixed with 0.05 wt% Irgafos 168, an antioxidant from Ciba-Geigy, before being heated in the press. The samples were then made by sandwiching a PC drop between two PE disks (see Figure 2.2). Before each run, the sandwiched sample was annealed in a vacuum oven at 135°C and -25 inHg overnight. The PC drop was in a position 6.25 mm from the disk edge when the sample was placed into the parallel plate setup. The interfacial tension between PC and PE is 17.2 mN/m at 220°C based on the breaking thread measurement on PC/PP by Chapleau *et al.* (2000).

2.2.2 Experimental Setup

The transparent parallel plates setup used consisted of a stationary lower disk plate and a rotating upper disk plate (Sundararaj *et al.*, 1994) ($D = 25 \text{ mm}$, see Figure 2.2). Both plates were made of quartz. The entire mixer assembly was heated with a band heater. The rotation speed of the upper disk was controlled by a DC motor (NSH-11D5, Bodine Electric Company). The drop deformation and breakup processes were recorded with a Pulnix CCD camera [TMC-7] with a zoom attachment. The camera was mounted onto a rotary base plate with an x-axis stage so that the camera was able to travel in the radial direction and rotate to track the drop during the experiment. As the drop rotated and translated in the matrix, the camera was moved around to track the drop. The visualization plane through the transparent quartz cylinder is the plane containing the flow axis ($x_1: \theta$) and the vorticity axis ($x_3: r$).

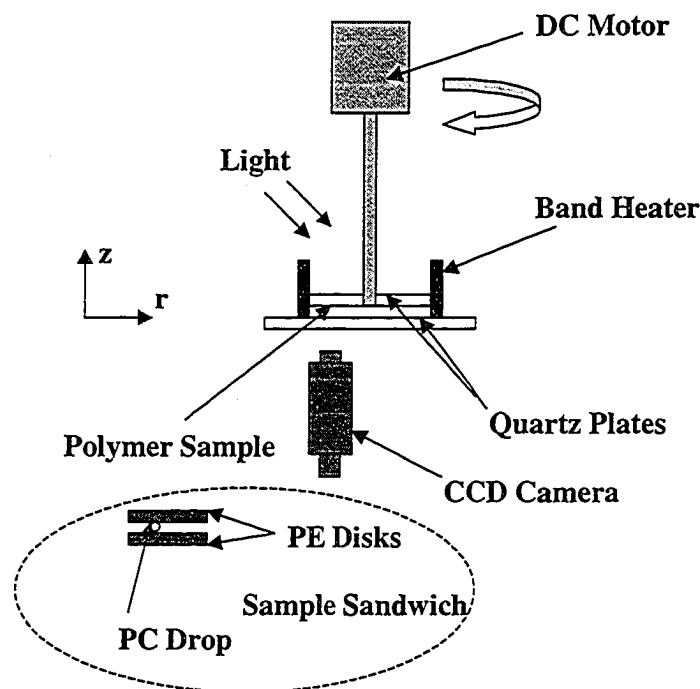


Figure 2.2 Illustration of the parallel plates setup.

2.2.3 Experimental Procedure

The parallel plates were preheated to 135°C, and the sample was added between the quartz disks. The temperature was then increased to 190°C to completely melt the PE. The upper quartz plate was pushed down and the bubbles between the sample and the plates were squeezed out. The gap between the two quartz plates was 2 mm. The run was started when the temperature reached 220°C and the DC motor was then turned on. The rotation speed was set at 1.3 rpm, and therefore, the shear rate ($\dot{\gamma}_x$ or $\dot{\gamma}_{12}$) of the drop was around 1s⁻¹. For PE2/PC3 system, experiments were performed at two other shear rates, 0.5s⁻¹ and 2s⁻¹. The PC drop deformation was recorded using the CCD camera and video setup. The video footage was later analyzed with Matrox Marvel G400-TV (Matrox Graphics Inc.) and the drop size was measured with SigmaScan Pro (version 4.01, SPSS Inc.) software.

2.3 RESULTS

Figure 2.3 shows micrographs of a PC1 drop as it deforms and breaks up in a PE2 matrix at a shear rate of 1s^{-1} . The viscosity ratio of the system is 1.8. The spherical drop (Figure 2.3a, $D_0 = 0.79$ mm or $R_0 = 0.39$ mm) deforms to a elliptical drop after it is sheared at 1s^{-1} for 7 s (Figure 2.3b). It continues to stretch in the flow direction (x_1 : θ). The half-length of the drop in x_1 direction is designated as R_1 , the half-length in x_2 direction is R_2 , and the half-length in x_3 direction is R_3 . R_1 and R_3 can be measured from the image and R_2 can be calculated by assuming that the drop volume is conserved:

$$R_2 = \frac{R_0^3}{R_1 R_3} \quad (2.1)$$

where R_0 is the initial spherical drop radius. In Figure 2.3c ($t=22\text{s}$), R_1 has increased to 2.6 times of R_0 , R_3 has decreased to 88% of R_0 . R_2 via eqn. (2.1) is calculated to have decreased to 44% of R_0 . The drop continues to be stretched into a flattened shape as shown in Figure 2.3d ($t=33\text{s}$), where R_1 is 2.2 times larger than R_0 , R_3 remains 88% of R_0 , and R_2 is decreased to 36% of R_0 . Therefore, the drop is much flatter in the x_2 (velocity gradient) direction and assumes the shape of a “sheet”.

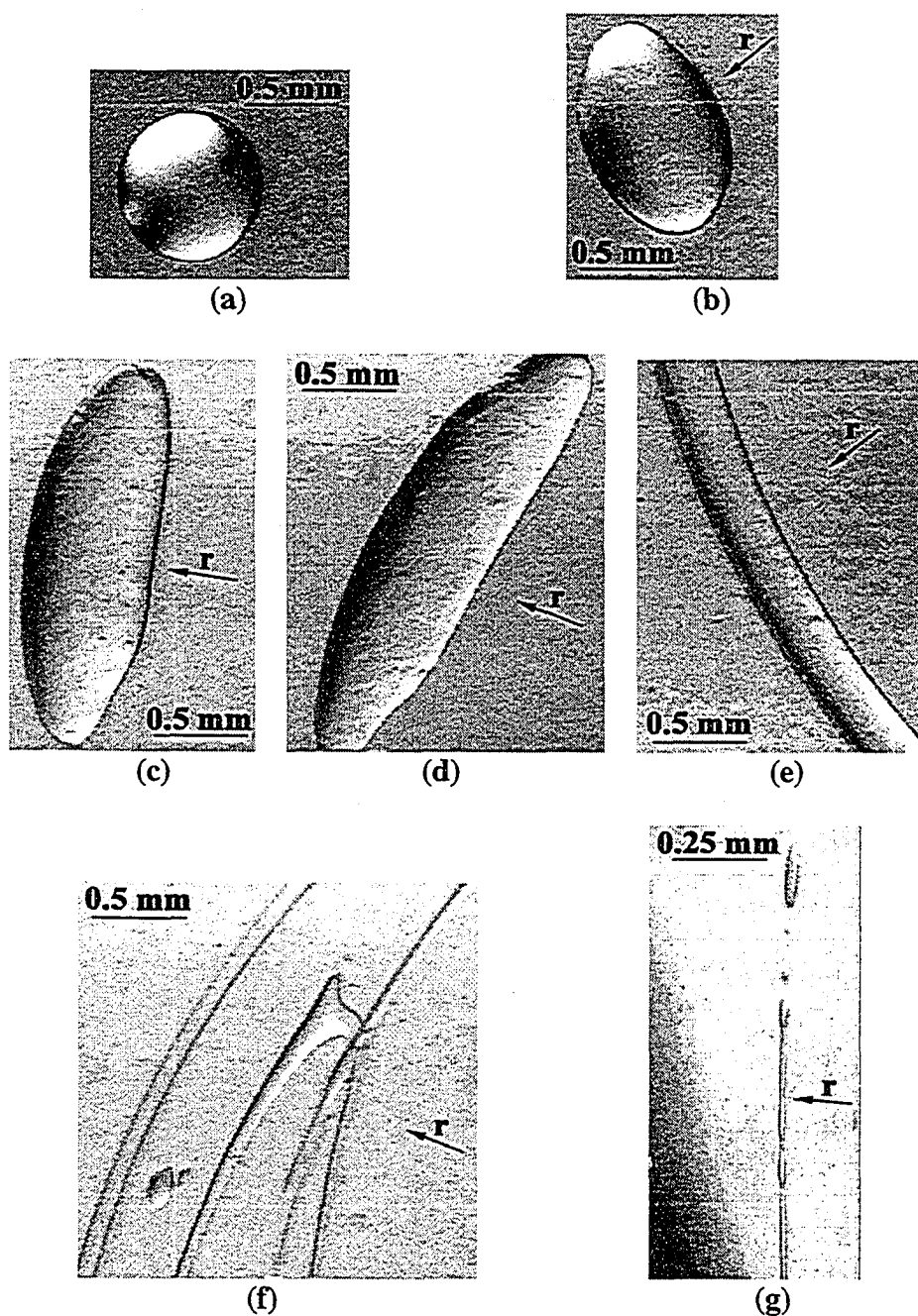


Figure 2.3 Deformation and breakup of a PC1 drop inside PE2 matrix at 220°C and 1s⁻¹. The drop has an initial size (D_0) 0.79 mm. The drop deforms to a flat sheet first, then to a long thread. (a) Spherical drop at $t=0$ s; (b) Flat elliptical drop at $t=7$ s; (c) Drop stretched to a sheet at $t=22$ s; (d) Drop continuing stretching to a sheet at $t=33$ s; (e) A long thread developed at $t=101$ s; (f) Entangled threads and small droplets at $t=699$ s; (g) Breakup of a thread at $t=960$ s. Note scale bars.

It should also be emphasized that the drop in Figures 2.3c and 2.3d appears to be stretched more at the outer edge of the drop (left side of images), than at the center of the disk. The asymmetric deformation suggests that the shear rate across the drop is inhomogeneous, and the shear rate is greater at the outer radius than at the inner radius. The sheet then elongates in x_1 and narrows in x_3 . Figure 2.3e shows that the drop's shape is between a sheet and thread. As time goes on, a thread appears, and it becomes thinner and thinner, and then twists and entangles in the matrix (Figure 2.3f). Figure 2.3g shows a typical thread breakup. The thread has broken into many smaller droplets as shown in Figure 2.3g.

Figure 2.4 shows a PC4 drop deforming and breaking up inside a PE2 matrix ($\eta_r = 5.8$ at $\dot{\gamma} = 1s^{-1}$). The drop has an initial diameter of 0.48 mm, or $R_0 = 0.24$ mm (Figure 2.4a). The drop spins around x_3 axis, or r direction, and then it tumbles, deforms and folds as shown in Figure 2.4b. In Figure 2.4c, the drop unfolds and flattens to a sheet, where $R_1/R_0 = 1.5$, $R_3/R_0 = 1.0$ and $R_2/R_0 = 0.6$. The sheet continues to elongate in the x_1 axis, or θ direction. Figure 2.4d shows that the drop becomes asymmetric with a thinner tip with a width of 0.03 mm, and thicker body. The length of R_1 has increased to 2.3 times of R_0 , R_3 decreased by 10% and the average R_2 decreased by 50%. As the drop elongates in θ direction, it contracts in the other two axes, with the length in x_2 axis (velocity gradient direction) decreasing faster. Figure 2.4e shows that a thin tip develops projecting out of the drop. Both the drop body and its tip elongate in θ direction and therefore, it is not able to capture the full image, but the initial drop breaks up into smaller droplets.

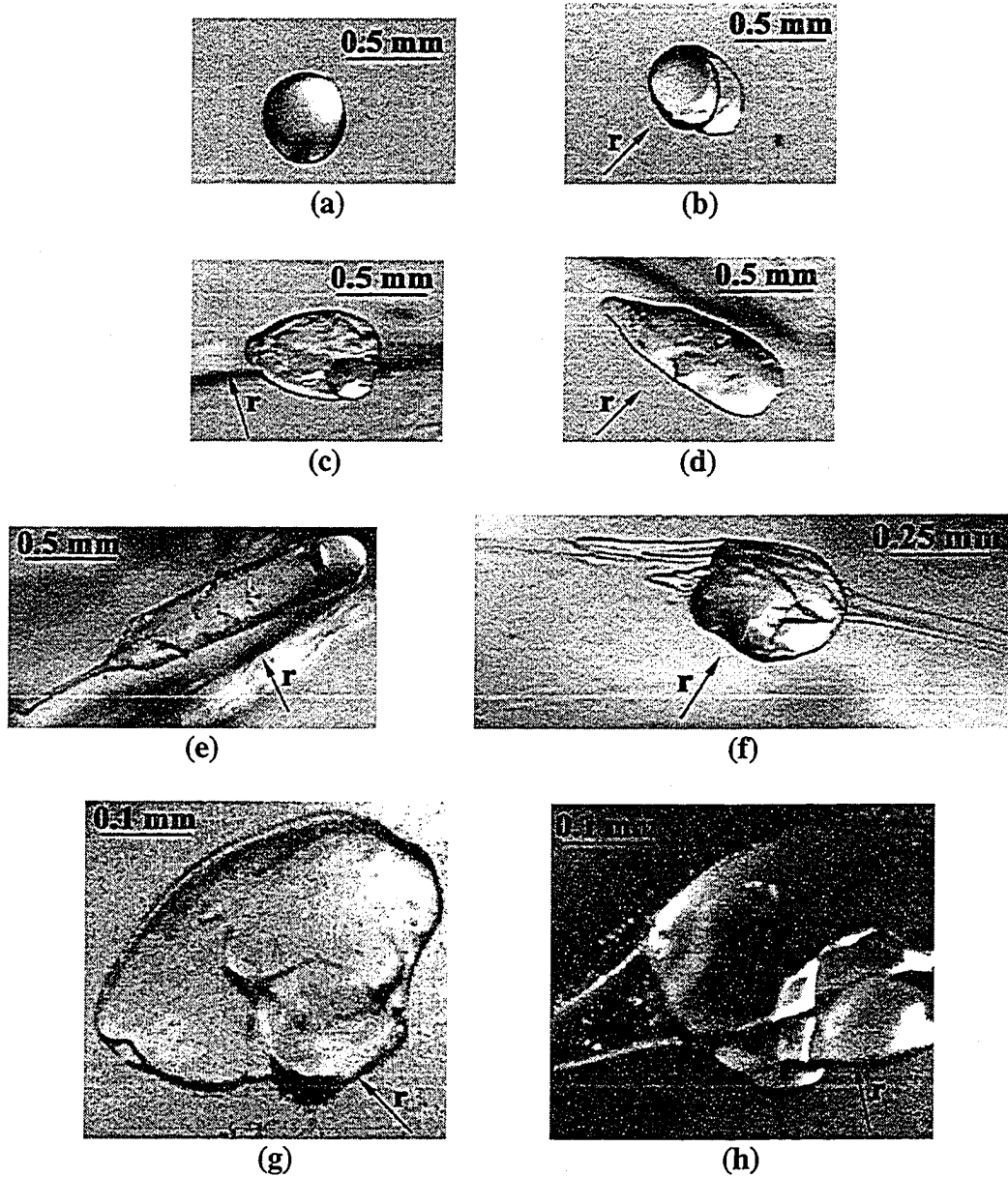


Figure 2.4 Deformation and breakup of a PC4 drop inside PE2 matrix at 220°C and 1s^{-1} . The drop has an initial size (D_0) 0.48 mm. The drop deforms to a flat sheet first, then, a long thread tip develops. (a) Spherical drop at $t=0\text{s}$; (b) Deformed and twisted drop at $t=381\text{s}$; (c) Flattened drop at $t=858\text{s}$; (d) Drop stretched to a sheet at $t=887\text{s}$; (e) Drop elongated in the flow direction and a tiny thin tip developed at $t=924\text{s}$; (f)-(h) One daughter droplet after breakup: (f) Threads entangled with the daughter droplet at $t=1070\text{s}$; (g) the flattened droplet at $t=1187\text{s}$; and (h) A ribbon or sheet pulling out of the droplet at $t=1208\text{s}$. Note scale bars.

Figures 2.4f-2.4h are images of one of the daughter droplets at higher magnifications. Figure 2.4f shows the deformed twisted droplet with small threads entangled around it. Figure 2.4g is an image of the folded daughter droplet, and Figure 2.4h shows a thin sheet pulling off from the droplet, and even small droplets breaking off. These small droplets have radius on the order of 2-5 μm .

2.4 DISCUSSION

Previous results have shown that a PC drop initially deforms to a sheet before it breaks up. The sheets formed in polymer drop breakup experiments are different from the cylinders observed in Newtonian systems. The interfacial tension between PC and PE is 17.2 mN/m at 220°C (Chapleau *et al.*, 2000). Therefore, the interfacial stress (Γ/R) is in the order of 10 N/m² when the drop has a diameter of 1 mm. The viscous stress is $\tau = \eta_m \dot{\gamma}$. The normal stress, $T_{11}(\dot{\gamma})$, can be approximated with the first normal stress difference, $N_1(\dot{\gamma}) = T_{11}(\dot{\gamma}) - T_{22}(\dot{\gamma})$, since $T_{22}(\dot{\gamma})$ is normally much smaller than $T_{11}(\dot{\gamma})$ (Macosko, 1993). At low shear rate or frequency, the first normal stress difference $N_1(\dot{\gamma})$ can be approximated as two times as the elastic modulus, $G'(\dot{\gamma})$. The interfacial stress ($\sim 10 \text{ N/m}^2$) is small compared with the viscous stress, τ , and the normal stress, $T_{11}(\dot{\gamma})$, since both τ and $T_{11}(\dot{\gamma})$ are in the order of 100 N/m². Consequently, in polymers, the interfacial stress is not strong enough to pull in an extended drop into a cylindrical shape; instead, a sheet is formed. It has been found that during the initial stages of polymer blending, lamellar structures or sheets are formed (Scott and Macosko, 1991, 1995; Lindt and Ghosh, 1992; Sundararaj *et al.*, 1992, 1995) and morphology development via sheet break up is an effective way to achieve quick reduction in particle dimension (Sundararaj

et al., 1995; Willemse *et al.*, 1999; Potente *et al.*, 2001). The dimensions of the drop decrease faster in the velocity gradient direction (R_2) than in the vorticity direction (R_3). The normal stress retards the contraction of the drop in the vorticity direction (Mighri and Huneault, 2001).

Figure 2.5 shows the changes in dimensions R_1 and R_2 of a PC drop inside a PE matrix with time at 1s^{-1} . The dimensions are recorded from the start of the experiment until the time that a full drop cannot be seen on the screen, i.e., before the major dimension of the drop exceeds the viewing screen dimensions. There is a critical point where there is an abrupt increase in R_1 , or decrease in R_2 . When a horizontal line is drawn through the data of the initial plateau zone, and a second line through the data obtained from the abrupt increase (or decrease for R_2), the intersection of those two lines corresponds to a critical “incubation” time (t_c) before the drop begins to stretch into sheet.

Figure 2.6 illustrates the sheet breakup types. In Type A, the drop is stretched into a sheet first and the sheet is then transformed to a thin thread, which is broken up into small droplets. In Type B, the drop breaks up as an extended sheet with a tiny thin thread tip and the cylindrical tip breaks into many small droplets. Table 2.2 lists the critical conditions for sheet formation: shear rate, critical time, initial drop size, viscosity ratio, Capillary number, Deborah number and stress ratio. Deborah number, De , is a ratio of the material relaxation time (λ) to the processing time (t). In this case, the processing time is chosen as the critical time, t_c , when the drop deforms to a sheet, and therefore,

$$De = \frac{\lambda}{t_c} \quad (2.2)$$

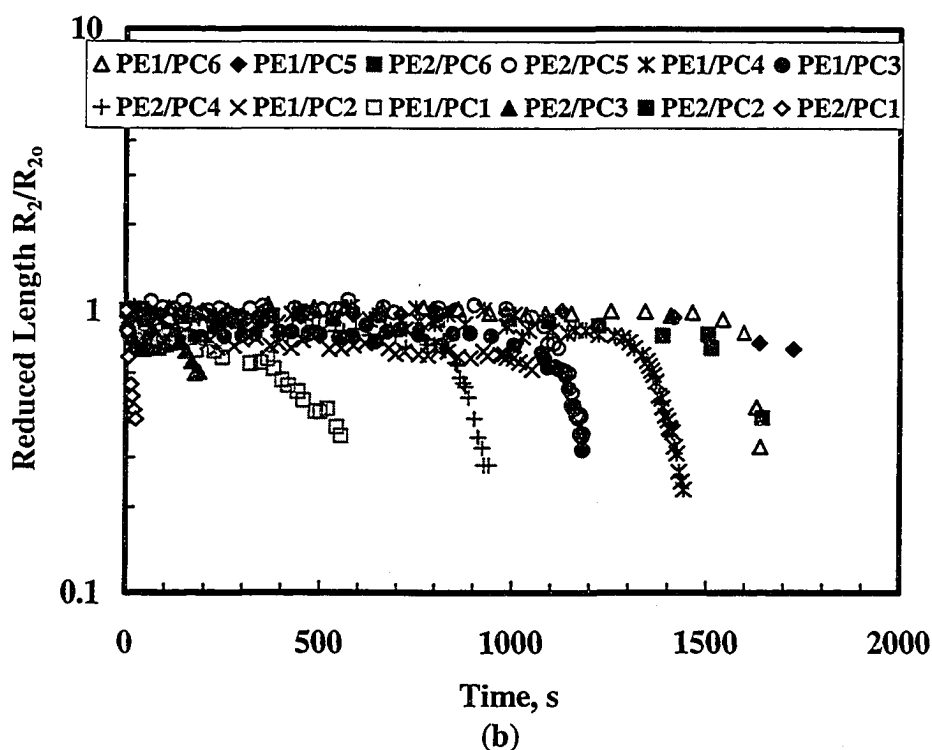
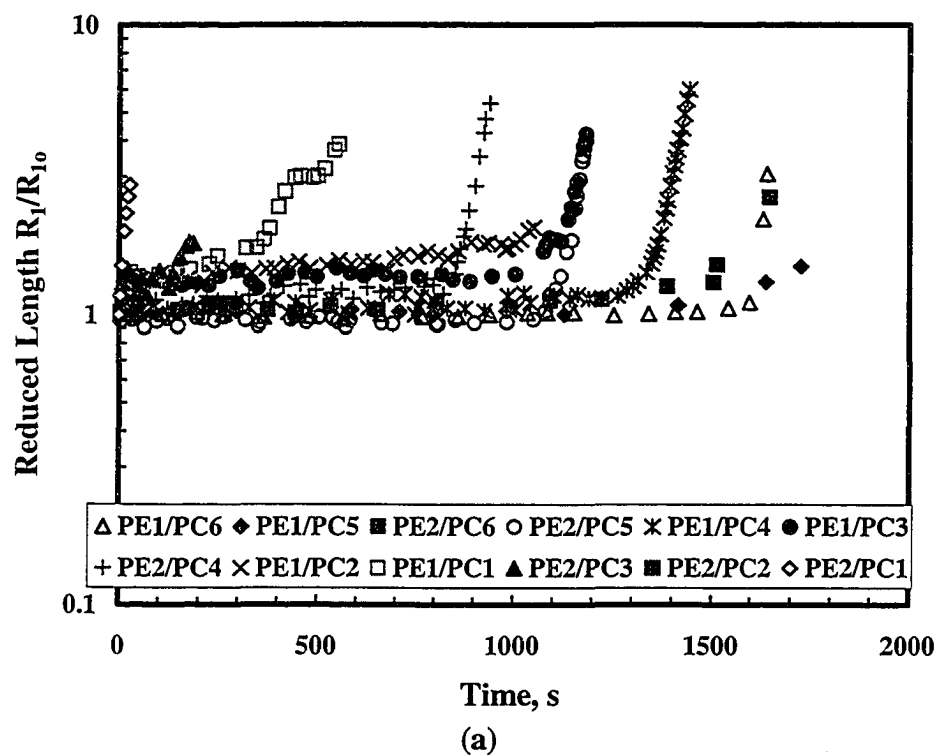


Figure 2.5 Reduced dimensions of the drop change with time at a shear rate of 1s^{-1} . (a) Reduced length in the flow direction and (b) Reduced length in the velocity gradient direction, calculated by assuming the drop volume conserves. Note there is an abrupt increase in R_1 or an abrupt decrease in R_2 .

When the drop is pulled into a sheet, the normal stresses in polymers play an important role. Thus, normal stresses are included in the analysis. The stresses acting on the drop are: the breakup stresses including the viscous stress and normal stress from the matrix phase and the restoring stresses including interfacial stress and normal stress in the drop. Therefore, one can define a ratio of the breakup stresses to the restoring stresses (Sundararaj *et al.*, 1995; Ghodgaonkar and Sundararaj, 1996; Lin *et al.*, 2003a; Lin and Sundararaj, 2004b) as stress ratio:

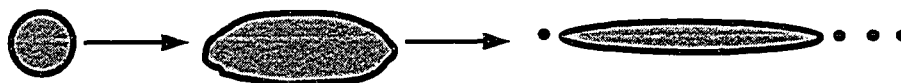
$$S_r = \frac{\text{Breakup Stress}}{\text{Restoring Stress}} = \frac{\eta_m \dot{\gamma} + N_{1m}}{\Gamma/R + N_{1d}} \quad (2.3)$$

where the subscripts d stands for the drop phase and m for the matrix phase. At low shear rate or frequency, $N_1(\dot{\gamma}) = 2G'(\dot{\gamma})$ (Macosko, 1993). Thus the stress ratio can be further simplified to:

$$S_r = \frac{\eta_m \dot{\gamma} + 2G'_m}{\Gamma/R + 2G'_d} \quad (2.4)$$

Viscosity ratio (η_r) is often used as a critical parameter for drop deformation and breakup (Taylor, 1932, 1934; Grace, 1982). It was found that stress ratio (S_r), instead of viscosity ratio (η_r), is more relevant for describing polymer drop deformation and breakup (Lin *et al.*, 2003a). However, both η_r and S_r can be used to describe the sheet

Type A:



Type B:



Figure 2.6 Illustration of two modes of sheet breakup.

Table 2.2 Critical conditions for sheet formation at 220°C.

System: Matrix/ Drop	Shear Rate ($\dot{\gamma}$, s^{-1})	Critical Time (t_c , s)	Initial Drop Diameter (D_0 , mm)	Viscosity Ratio (η_r)	Capillary Number (Ca)	Deborah Number ($De \times 10^5$)	Stress Ratio (S_r)	Sheet Break- up Type
PE2/PC1	1	2.4	0.79	1.82	22.48	2080	10.92	A
PE2/PC2	1	12	0.67	2.03	19.07	417	10.20	A
PE2/PC3	0.5	38	0.63	2.57	9.34	132	5.21	A
PE2/PC3	1	108	0.54	2.67	15.37	46.3	5.60	A
PE2/PC3	2	78	0.63	2.80	34.15	32.1	4.68	A
PE1/PC1	1	300	0.64	4.79	6.93	16.7	3.53	A
PE1/PC2	1	860	0.52	5.34	5.63	5.8	2.71	A
PE2/PC4	1	830	0.48	5.75	13.66	12.0	2.33	B
PE1/PC3	1	920	0.65	7.03	7.04	5.4	2.08	B
PE1/PC4	1	1,250	0.57	15.11	6.17	8.0	0.84	B
PE2/PC5	1	1,090	0.90	20.58	25.61	15.6	0.27	B
PE2/PC6	1	1,390	0.68	36.63	19.35	15.8	0.12	B
PE1/PC5	1	1,560	0.69	54.09	7.47	10.9	0.09	B
PE1/PC6	1	1,590	0.48	96.27	5.20	13.8	0.04	B

breakup phenomena, probably due to a low shear rate ($\leq 2s^{-1}$) applied on the systems. At this low shear rate, the drop and the matrix are linear viscoelastic materials (Macosko, 1993).

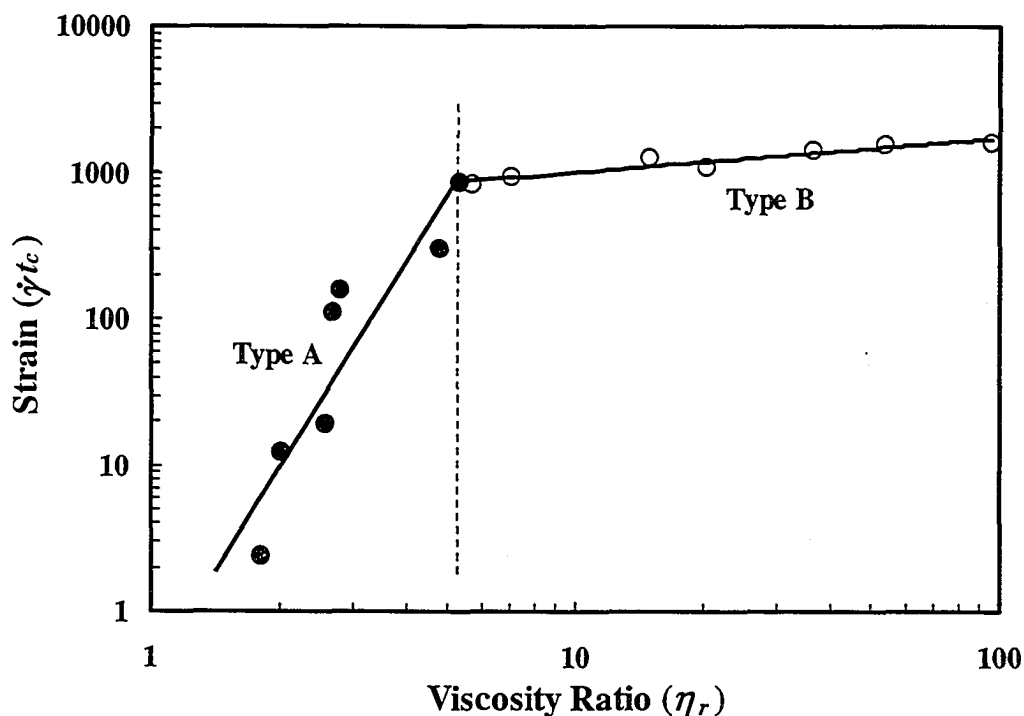


Figure 2.7 Critical strain versus viscosity ratio when the drop becomes a sheet. The solid circles are data for the drop when it breaks up via Type A, and the open circles are data for the drop when it breaks up via Type B. The lines are guides to the eyes.

Figure 2.7 shows that the critical strain, a dimensionless time obtained from $\dot{\gamma}t_c$, increases with η_r . When $1 < \eta_r \leq 5$, the rate of increase of the critical strain or time is much higher than when $5 < \eta_r \leq 100$. At lower viscosity ratios, the drop breaks up through Type A. At higher viscosity ratios, the drop breaks up via Type B. Therefore, breakup occurs easier and quicker when the viscosity ratio is ~ 1 (Grace, 1982; Wu,

1987). It should be pointed out that the transition from Type A breakup to Type B breakup is not clear and distinct when plotting strain versus η_r .

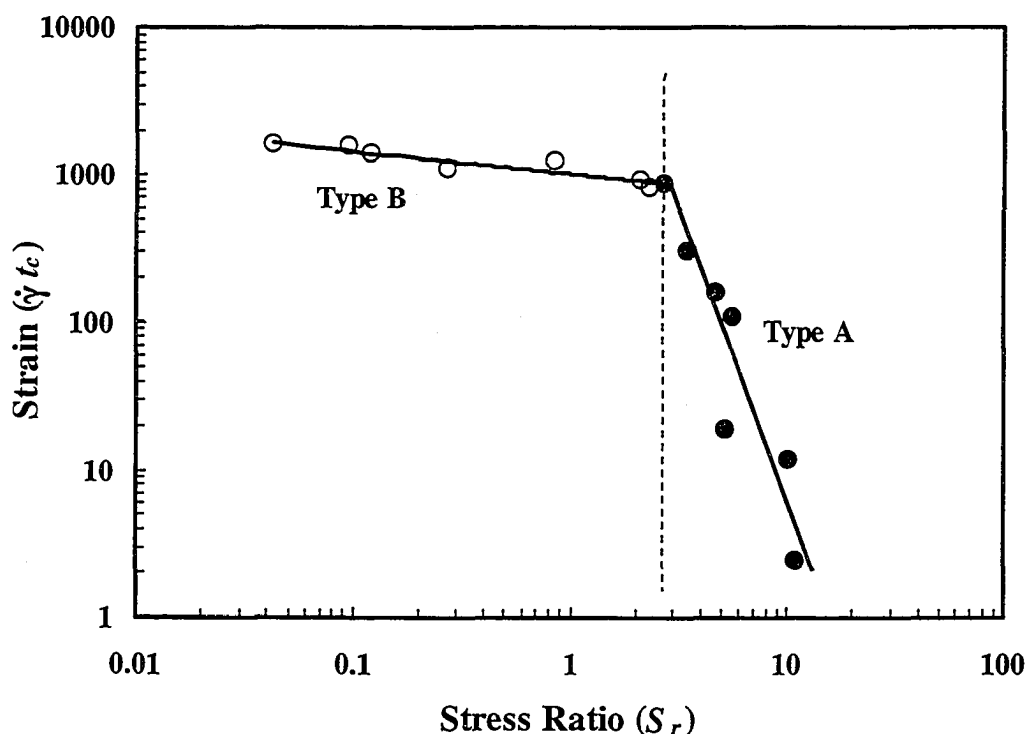


Figure 2.8 Critical strain versus stress ratio when the drop becomes a sheet. The solid circles are data for the drop when it breaks up via Type A, and the open circles are data for the drop when it breaks up via Type B. The lines are guides to the eyes.

Figure 2.8 shows that the critical strain decreases with S_r . As the stress ratio increases, the strain or time needed to deform and break up the drop decreases. An increase in the stress ratio means that the drop breaking stress is much higher than the restoring stress, and it is easier to break up the drop. However, there are two different trends, depending on the stress ratio. If S_r is greater than 3, the drop experiences Type A breakup, and the critical strain decreases sharply with S_r . If S_r is less than 3, the drop

experiences Type B breakup, and the critical strain decreases much more slowly with increasing S_r . In this plot, the separation between the two types of breakup is clear.

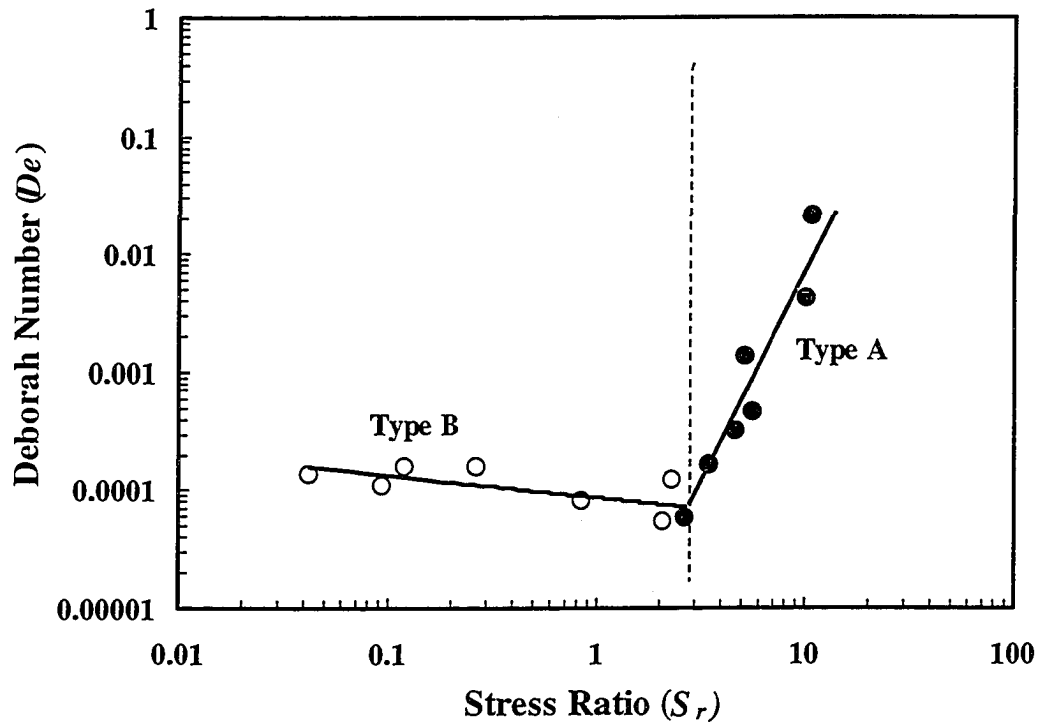


Figure 2.9 Deborah number versus stress ratio. The solid circles are data for the drop when it breaks up via Type A, and the open circles are data for the drop when it breaks up via Type B. The lines are guides to the eyes.

Figure 2.9 shows a plot of drop Deborah number versus stress ratio. A plot of Deborah number versus viscosity ratio shows similar trend, however, the separation between the two types of breakup is not as clear as that shown in the Deborah number versus stress ratio plot (Figure 2.9). The Deborah number is a ratio of the material relaxation time to the processing time. It can be used to normalize different systems and operating parameters since it incorporates the drop properties and processing conditions. A minimum De occurs at $S_r \approx 3$. At lower S_r , De is relatively constant but decreases

slightly with increasing S_r . At higher S_r , De increases quickly with increasing S_r . A relatively constant De with increasing S_r when $S_r < 3$ suggests that the critical time for a drop to break increases proportionally when the drop relaxation time increases. Similarly, for $S_r > 3$, as S_r increases, the matrix properties dominate drop breakup. Consequently, a sharp increase in De or increased normalized critical breakup time can be observed.

The observations in the parallel plates device on the deformation and breakup of a PC drop inside PE are somewhat different from those observed in the Couette cell (see Chapter 3, Lin *et al.*, 2003a, 2003b). Possible reasons may be that (1) the shear field in the parallel plate device is not homogeneous; (2) the drop size (0.5 ~ 0.9 mm) is relatively large (25 ~ 50%) compared to the gap (2 mm) between the two plates; (3) the shear rate used in parallel plates is low and (4) the temperature gradient across the radius is 5°C, which may affect the drop physical properties.

For reason (1), since the shear rate is dependent on the drop position in both r and z axes, the shear rate across the drop is not a constant. In addition, a shift of the drop to the edge or to the lower plate will affect the shear rate. For reason (2), the gap in the Couette cell is 4 mm but for the parallel plates, the gap is 2 mm, and thus, the end or wall effects (Uijtewaal *et al.*, 1993; Shapira and Haber, 1990) for the parallel plates may not be negligible. For reason (3), experiments done in the parallel plates at a shear rate $\leq 2s^{-1}$, which is lower than that used in Couetter cell. At low shear rates, it has been also observed by other researchers that sheets formed in parallel plates (Sundararaj *et al.* 1994; Levitt *et al.*, 1996). For reason (4), experiments in the parallel plates device were started when a drop was in a position half of the rotating disk radius. Experiments were stopped when a drop shifted to the edge. It is conceivable that temperature gradient was

present along the radius direction of the parallel plates. As a result, properties of the drop inside the device might have small fluctuations over the experiment period.

Both parallel plates (Chapter 2) and Couette cell (Chapters 3 and 4) were used in this thesis to visualize drop deformation and breakup. First of all, these equipments are frequently used shear devices. Second, in parallel plates, the shear rate varies in different locations, which is likely to occur in real polymer blending process; whereas, the flow field in Couette is homogeneous and the flow field is more rigorous, which is useful for studying the pure shear effects. Third, both devices are good starts for studying polymer drops since the temperature and shear rate can be easily controlled.

In parallel plates, the shear rate across the whole width of a drop can be approximated by using radial position and gap size. For example, the PC1 drop in Figure 2.3d has a length of 0.68 mm along the r direction (Figure 2.10). If one takes the shear rate in the mid-plane as 1 s^{-1} , the shear rate difference between the inner and outer edge of the drop is 0.1 s^{-1} , that is, a shear rate of 0.95 s^{-1} ($\dot{\gamma}_i$) and 1.05 s^{-1} ($\dot{\gamma}_o$) will be for the inner and outer edge of the drop, respectively. The stress ratio is 10.7 for the inner drop edge ($S_{r,i}$) and 10.9 for the outer edge ($S_{r,o}$). The difference between inner and outer stress ratios is 0.2 and the corresponding difference in critical time for each part to become a sheet is 0.4 s (3.5 s for the inner edge and 3.1 s for the outer edge). The drop's outer side is therefore easier to deform than the inner side. Since it begins to form a sheet first, the outer edge is also thinner (Sundararaj *et al.*, 1995).

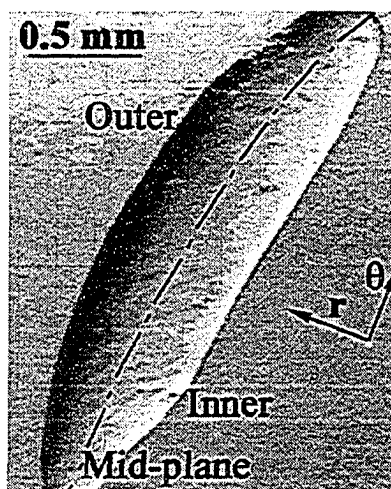


Figure 2.10 Definition of the inner and outer edges of a PC drop.

The subsequent transformation of a sheet to a thread may be due to the asymmetric drop shape, which results in interfacial stress gradient across different drop surfaces. In Figure 2.10, the dimensions of the drop are $R_1 = 1.29$ mm, $R_2 = 0.13$ mm and $R_3 = 0.34$ mm. The local curvatures across the drop surfaces: x_1x_3 (θr), x_1x_2 (θz) and x_2x_3 (zr) are different, and the smallest curvature is across the x_2x_3 (zr) surface. Therefore, the stress due to interfacial tension is the largest in the x_2x_3 (zr) plane. The interfacial stress gradient requires a contraction of the drop in x_3 . This is accomplished since the maximum interfacial stress may be equivalent to or greater than the drop normal stress, $2G' = 66$ N/m², which initially prevented the drop from reducing in x_3 direction so that it formed a sheet. As a result of the interfacial stress exceeding normal stress, the drop contracts in x_3 , or the r direction, and the drop looks more like a thread than a sheet. In this way, a drop with lower normal stress, or lower elastic modulus, will more easily form a thread. In contrast, a drop with higher normal stress, or higher elastic modulus, will more likely form a thin cylindrical tip. Due to a high curvature in the cylindrical tip

region, the local interfacial stress is huge. This may explain why there are two kinds of deformation and breakup modes after the drop is stretched into a sheet.

2.5 CONCLUSIONS

The deformation and breakup of a polycarbonate drop sheared inside a polyethylene matrix was studied in a transparent rotating parallel plate device at 220°C and low shear rates. Sheet formation was observed during the initial shearing of the drop. The drop then broke up via two different modes: either stretching into a thin thread (Type A) or extending into a sheet with a thin cylindrical tip (Type B). Drop breakup occurs when the viscosity ratio is greater than 3.5, which is impossible for Newtonian systems.

The formation of the sheet was characterized by a critical strain ($\dot{\gamma}t_c$) or a critical time (t_c) when the drop stretched in the flow direction (θ) and contracted a little bit in the vorticity direction (r), and contracted significantly in the velocity gradient direction (z). The critical strain, $\dot{\gamma}t_c$, was related to the viscosity ratio (η_r), stress ratio (S_r) and drop Deborah number (De). For the systems studied, the drop was easier to break up at lower η_r and higher S_r . When the stress ratio was less than 3, the drop Deborah number decreased with increased S_r . The normalized critical time for the drop to form a sheet was fairly constant as S_r increased and the drop was broken up through Type B breakup. When the stress ratio was higher than 3, the drop Deborah number increased with increasing S_r , resulting in a delay in sheet formation and the drop was broken up via Type A.

2.6 REFERENCES

- Briscoe, B.J.; Lawrence, C.J.; Mietus, W.G.P. *Adv. Colloid Interface Sci.* **1999**, *81*, 1-17.
- Chapleau, N.; Favis, B.D.; Carreau, P.J. *Polymer* **2000**, *41*, 6695-6698.
- Comas-Cardona, S. *MSc Thesis*; University of Illinois at Urbana-Champaign, 2000.
- Comas-Cardona, S.; Tucker, C.L. *J. Rheol.* **2001**, *45*, 259-273.
- de Bruijn, R.A. *PhD thesis*; Eindhoven University of Technology, The Netherlands, 1989.
- de Bruijn, R.A. *Chem. Eng. Sci.* **1993**, *48*, 277-284.
- Elmendorp, J.J.; Van der Vegt A.K. In *Two Phase Polymer Systems*; Utracki, L.A. Ed.; Hanser Publishers: New York, 1991, p.166-184.
- Favis, B.D.; Chalifoux, J.P. *Polym. Eng. Sci.* **1987**, *27*, 1591-1600.
- Favis, B.D. *J. Appl. Polym. Sci.* **1990**, *39*, 285-300.
- Flumerfelt, R.W. *Ind. Eng. Chem. Fundam.* **1972**, *11*, 312-318.
- Ghodgaonkar, P.G.; Sundararaj, U. *Polym. Eng. Sci.* **1996**, *36*, 1656-1665.
- Grace, H.P. *Chem. Eng. Commun.* **1982**, *14*, 225-277.
- Guido, S.; Villone, M. *J. Rheol.* **1998**, *42*, 395-415.
- Hobbie, E.K.; Migler, K.B. *Phys. Rev. Lett.* **1999**, *82*, 5393-5396.
- Karam, H.J.; Bellinger, J.C. *I & EC Fundam.* **1968**, *7*, 576-581.
- Levitt, L.; Macosko, C.W.; Pearson, S.D. *Polym. Eng. Sci.* **1996**, *36*, 1647-1655.
- Lin, B.; Mighri, F.; Huneault, M.A.; Sundararaj, U. *Macromol. Rapid Commun.* **2003a**, *24*, 783-788.

- Lin, B.; Sundararaj, U.; Mighri, F.; Huneault, M.A. *Polym. Eng. Sci.* **2003b**, *43*, 891-904.
- Lin, B.; Sundararaj, U. *J. Appl. Polym. Sci.* **2004a**, *92*, 1165-1175.
- Lin, B.; Sundararaj, U. *Polymer* **2004b**, *45*, 7605-7613.
- Lindt, J.T.; Ghosh, A.K. *Polym. Eng. Sci.* **1992**, *32*, 1802-1813.
- Macosko, C.W. *Rheology: Principles, Measurements, and Applications*; Wiley: New York, 1993; p141.
- Mighri, F.; Carreau, P.J.; Ajji, A. *J. Rheol.* **1998**, *42*, 1477-1490.
- Mighri, F.; Huneault, M.A. *J. Rheol.* **2001**, *45*, 783-797.
- Migler, K.B.; Hobbie, E.K.; Qiao, F. *Polym. Eng. Sci.* **1999**, *39*, 2282-2291.
- Ottino, J.M.; DeRoussel, P.; Hansen, S.; Khakhar, D.V. *Adv. Chem. Eng.* **2000**, *25*, 105-204.
- Potente, H.; Bastian, M.; Bergemann, K.; Senge, M.; Scheel, G.; Winkelmann, Th. *Polym. Eng. Sci.* **2001**, *41*, 222-231.
- Rallison, J.M. *Annu. Rev. Fluid Mech.* **1984**, *16*, 45-66.
- Rumscheidt, F.D.; Mason, S.G. *J. Colloid Interface Sci.* **1961**, *16*, 238-261.
- Scott, C.E.; Macosko, C.W. *Polym. Bull.* **1991**, *26*, 341-348.
- Scott, C.E.; Macosko, C.W. *Polymer* **1995**, *36*, 461-470.
- Shapira, M.; Haber, S. *Int. J. Multiphase Flow* **1990**, *16*, 305-321.
- Stone, H.A. *Annu. Rev. Fluid Mech.* **1994**, *26*, 65-102.
- Sundararaj, U.; Macosko, C.W.; Rolando, R.J.; Chan, H.T. *Polym. Eng. Sci.* **1992**, *32*, 1814-1823.

- Sundararaj, U.; Dori, Y.; Macosko, C.W. *SPE ANTEC Tech. Papers* **1994**, *52*, 2448-2451.
- Sundararaj, U.; Dori, Y.; Macosko, C.W. *Polymer* **1995**, *36*, 1957-1968.
- Tavgac, T. *PhD thesis*; University of Houston, 1972.
- Taylor, G.I. *Proc. R. Soc. London, Ser. A* **1932**, *138*, 41-48.
- Taylor, G.I. *Proc. R. Soc. London, Ser. A* **1934**, *146*, 501-523.
- Tjahjadi, M.; Stone, H.A.; Ottino, J.M. *J. Fluid. Mech.* **1992**, *243*, 297-317.
- Torza, S.; Cox, R.G.; Mason, S.G. *J. Colloid Interface Sci.* **1972**, *38*, 395-411.
- Trevelyan, B.J.; Mason, S.G. *J. Colloid Interface Sci.* **1951**, *6*, 354-361.
- Tsakalos, V.T.; Navard, P.; Peuvrel-Disdier, E. *J. Rheol.* **1998**, *42*, 1403-1417.
- Uijtewaal, W.S.J.; Nijhof, E.J.; Heethaar, R.M. *Phys. Fluids A* **1993**, *5*, 819-825.
- Utracki, L.A.; Shi, Z.H. *Polym. Eng. Sci.* **1992**, *32*, 1824-1833.
- van Krevelen, D.W. *Properties of Polymers*, 2nd ed.; Elsevier Scientific Company: Amsterdam, 1976 (chapter 10).
- Vanoene, H. *J. Colloid Interface Sci.* **1972**, *40*, 448-467.
- Varanasi, P.P.; Ryan, M.E.; Stroeve, P. *Ind. Eng. Chem. Res.* **1994**, *33*, 1858-1866.
- Willemse, R.C.; Ramaker, E.J.U.; van Dam, J.; de Boer, A.P. *Polymer* **1999**, *40*, 6651-6659.
- Wu, S.H. *Polym. Eng. Sci.* **1987**, *27*, 335-343.
- Yamane, H.; Takahashi, M.; Hayashi, R.; Okamoto, K.; Kashihara, H.; Masuda, T. *J. Rheol.* **1998**, *42*, 567-580.

Chapter 3

Polymer Drop Deformation and Breakup Mechanisms in Couette Cell

3.1 INTRODUCTION

The study of deformation and breakup of an isolated drop in a matrix is important to understand some fundamental problems, such as mixing and dispersing. Though it has been investigated extensively since Taylor's pioneering work (1932, 1934), most research has concentrated on Newtonian systems. Drop breakup in polymer-polymer systems is not well understood. To study the deformation and breakup of a polymer drop in a second polymer melt will help to understand how one polymer disperses into another, and will give valuable insight into how the final drop distribution is obtained in immiscible polymer blends.

In Newtonian systems, the critical Capillary number (the flow condition where the drop breaks up) has been found to correlate with the viscosity ratio of the two phases. The Capillary number is a ratio of shear stress to interfacial stress ($Ca = \eta_m \dot{\gamma} R / \Gamma$, where $\dot{\gamma}$ is shear rate, R is drop radius and Γ is interfacial tension) and the viscosity ratio is a ratio of the drop phase viscosity to the matrix phase viscosity ($\eta_r = \eta_d / \eta_m$). Figure 3.1 shows the critical Capillary number versus viscosity ratio (Grace, 1982) for Newtonian systems both in simple shear and extensional flow fields. Drop breakup occurs at all viscosity ratios when it is subjected to extensional flow. However, a Newtonian drop will not breakup in simple shear when the viscosity ratio is greater than 3.5 (Taylor, 1932, 1934; Rumscheidt and Mason, 1961; Karam and Bellinger, 1968; Torza *et al.*, 1972; Grace, 1982). At viscosity ratio less than 3.5, a Newtonian drop breaks up in a Newtonian

matrix under simple shear via either drop fracture or tip streaming (Figure 3.1). Drop fracture is the main drop breakup mode: the drop breaks up into two daughter droplets with one or several satellite droplets in between. Drop fracture occurs for $10^{-6} < \eta_r < 3.5$. In tip streaming, streams of small droplets are released from the tips of a pointed drop in the flow direction (see Figure 3.1). Tip streaming occurs at $\eta_r < 0.1$ and at a lower Capillary number than drop fracture. It has been postulated that tip streaming is due to surfactants (de Bruijn, 1993; Milliken *et al.*, 1993; Milliken and Leal, 1991, 1992, 1994; Tretheway and Leal, 1999).

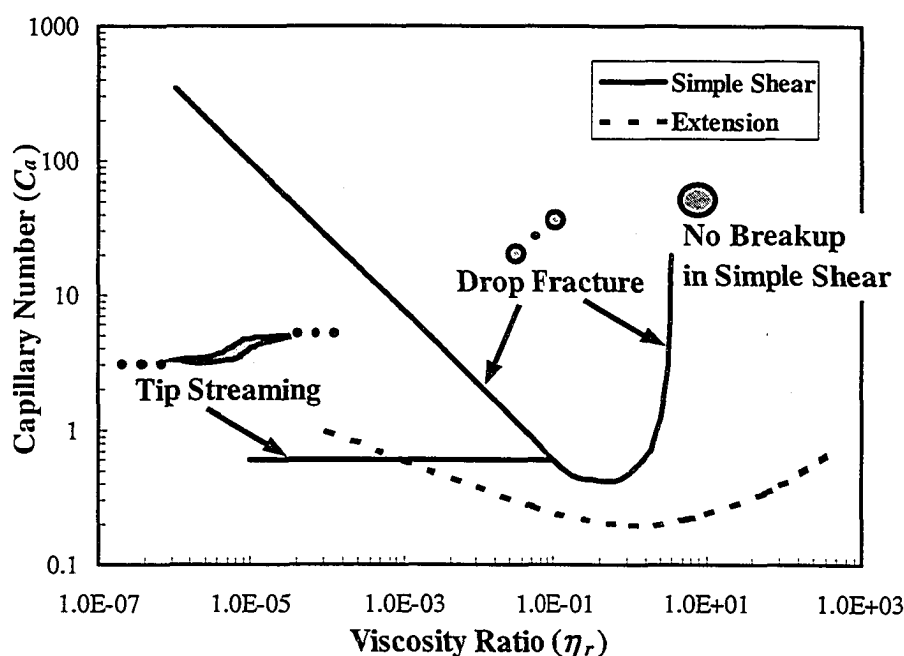


Figure 3.1 Critical Capillary number versus viscosity ratio for Newtonian systems (Grace, 1982).

Polymers are shear thinning and viscoelastic materials, which are quite different from Newtonian materials. Polymer drops may break up differently from Newtonian drops as suggested by Wu (1987) and Favis and Chalifoux (1987). In the literature, it is

found that even the viscoelasticity alone affects drop breakup greatly, though the effects of elasticity on drop breakup are in controversy. Flumerfelt (1972) used parallel belts to generate a simple shear field to study the breakup condition for a Newtonian drop in a viscoelastic matrix. He found that the critical shear rate for breakup would be decreased by increasing the viscosity of the matrix, decreasing the elasticity of the matrix, or decreasing the interfacial tension.

Vanoene (1972) studied the dispersion of one polymer phase inside another polymer matrix. The polymer samples were premixed in a Kenics mixer and then extruded from a capillary rheometer. There were three important parameters: particle size, interfacial tension and viscoelasticity differences between the two phases, which were shown to be responsible for blend morphology. Using thermodynamic analysis of droplet formation, Vanoene (1972) introduced a dynamic interfacial tension (Γ'), which could be expressed in the form of $\Gamma' = \Gamma + \frac{1}{6}R[N_{1,d} - N_{1,m}]$, where Γ is the interfacial tension in the absence of flow and N_1 is the first normal stress. Therefore, drop elasticity would stabilize the droplet and matrix elasticity would destabilize the droplet. However, the dynamic interfacial tension may go to zero or negative if the matrix normal stress is much greater than the drop normal stress and the absolute value of $\frac{1}{6}R[N_{1,d} - N_{1,m}]$ exceeds Γ .

Elmendorp and Maalcke (1985) conducted an experimental study on a Separan (polyacrylamide solution, viscoelastic) drop deformation inside a silicone (Newtonian) matrix and a silicone drop in a Separan matrix subject to simple shear flow generated by a Couette device. The Couette was composed of an inner cylinder mounted on the torsion

head of a Weissenberg rheogoniometer and a rotating outer cylinder having a pyrex bottom plate mounted on the drive shaft of the rheogoniometer. Therefore, the drop behavior could be visualized from the bottom of the cylinders and rheological properties of the matrix could be measured simultaneously. It was found the normal forces exhibited by the drop phase tend to stabilize the drop, while normal forces exhibited by the matrix tend to destabilize the drop.

Milliken and Leal (1991) observed shape deformation of viscoelastic drops in viscous Newtonian oil under an extensional flow field via a computer controlled four-roll mill (Bentley, 1985; Bentley and Leal, 1986). They found that drop elasticity inhibited drop deformation. They observed two modes of breakup, normal tip streaming and tip streaming with stretch. Their observations were later verified with numerical solutions by Ramaswamy and Leal (1999).

Varanasi *et al.* (1994) compared breakup of viscoelastic and Newtonian drops suspended in a highly viscous Newtonian fluid under simple shear in a transparent counterrotating cone-and-plate device. They found that the first normal stress difference, N_1 , in a viscoelastic drop suppressed drop breakup.

Mighri *et al.* (1998) studied the elastic effects on drop deformation using Boger fluids in transparent parallel disks and found that matrix elasticity helped to deform the drops, whereas the drop elasticity resisted drop deformation. More recently, Mighri and Huneault (2001a) visualized dispersion of elastic (Boger fluid) drops in a PDMS matrix through a transparent Couette flow cell and found that the drops were elongated perpendicular to flow direction, i.e., in the vorticity direction. They suggested that this

kind of elongation is due to the normal stresses acting along the streamlines inside the drop.

It should be emphasized that most of the research work on viscoelastic systems was performed at room temperature. One of the main difficulties in studying a polymer drop in a polymer matrix has been viewing breakup at the high processing temperatures for most polymers. Additionally, real polymer materials are different from purely elastic materials like Boger fluids because the viscosity of real polymers decreases with increasing shear rate. Visualization studies on drop breakup in polymer systems suggest that the normal stress plays an important role for polymer-polymer systems (Sundararaj *et al.*, 1995; Levitt *et al.*, 1996; Hobbie and Migler, 1999; Migler *et al.*, 1999; Migler 2000; Mighri and Huneault, 2001b; Lin and Sundararaj, 2004). The normal stress also contributes to phenomena such as sheet formation (Sundararaj *et al.*, 1995), widening of drops (Levitt *et al.*, 1996) or elongation (Hobbie and Migler, 1999; Migler *et al.*, 1999; Migler 2000; Mighri and Huneault, 2001b) in the vorticity direction. It is now known that the final morphology of polymer blends develops rapidly during the blending process. During the initial stages of polymer blending, lamellar structures or sheets are formed (Lindt and Ghosh, 1992; Scott and Macosko, 1991, 1995; Sundararaj *et al.*, 1992, 1994, 1995) and morphology development via sheet break up is an effective way to achieve quick reduction in particle dimension (Sundararaj *et al.*, 1995; Willemsse *et al.*, 1999; Potente *et al.*, 2001).

In Chapter 2, the deformation and breakup of a polycarbonate (PC) drop in polyethylene (PE) matrix were presented for shear flow generated by parallel plates. In this chapter, studies on how a polymer drop (drop diameter: 0.5 ~ 1 mm) is softened,

deformed and then broken up in PE matrix subject to simple shear flow generated by a heated transparent counter-rotating Couette cell are presented. Through the visualization, at least four distinctly different breakup mechanisms are observed for polymer-polymer systems under simple shear in quasi-equilibrium conditions.

3.2 EXPERIMENT

3.2.1 Materials and Preparation

The polymer systems used were composed of drops of PC, PS (polystyrene), PSOX (polystyrene oxazoline), PBT (polybutylene terephthalate) and PA6 (Nylon 6) inside a matrix of PE. The source, commercial name, abbreviation, average molecular weight, specific heat and density are given in Table 3.1. Differential Scanning Calorimetry (DSC) was performed using a DSC 2910 calorimeter from TA Instruments to obtain the specific heat capacity for PC5 and PE at high temperatures. The refractive index difference between the drop and the matrix for the systems studied are greater than 0.04, which is sufficient for visualizing a drop in a matrix.

Dynamic rheological characterizations were performed on a Rheometrics RMS800 Rheometer with a 25 mm parallel plate fixture at 10% strain (Chapter 2). Figure 3.2a shows the viscosity ratio of PE/PC systems at 220°C. Figure 3.2b gives the viscosity ratio for PC5/PE2 system at 220°C and 230°C. Figure 3.2c plots the viscosity and elastic modulus for PS, PSOX and PE at 190°C. Figure 3.2d presents the viscosity and elastic modulus for PBT, PA6 and PE at 230°C. For all the systems studied, the

Table 3.1 Properties of polymers used.

Polymer (Abbreviation)	Source	Molecular Weight ^a (M _w , g/mol)	Specific Heat (C _p , kJ/kg·K)	Density ^a (ρ, kg/m ³)	Refractive Index ^b
Polycarbonate: Lexan OQ1030 (PC1)	GE Plastics	17,200	1.59 ^b (25°C)	1,200 (25°C)	1.58
Polycarbonate: Lexan OQ1020 (PC3)	GE Plastics	17,880	1.59 ^b (25°C)	1,200 (25°C)	1.58
Polycarbonate: Lexan AP1300 (PC4)	GE Plastics	22,710	1.59 ^b (25°C)	1,200 (25°C)	1.58
Polycarbonate: Lexan 140 (PC5)	GE Plastics	27,100	1.78 (220°C) 1.80 (230°C)	1,200 (25°C)	1.58
Polycarbonate: Lexan 104 (PC6)	GE Plastics	28,860	1.59 ^b (25°C)	1,200 (25°C)	1.58
Polybutylene Terephthalate: Valox 195 (PBT)	GE Plastics		1.55 ^b (25°C)	1,310 (25°C)	1.64
Polystyrene: PS666D (PS)	Dow	160,000	1.72 ^b (25°C)	1,040 (25°C)	1.59
Polystyrene Oxazoline (PSOX, 1% Oxazoline)	Dow	160,000			1.66
Nylon 6 (PA6)	Scientific Polymer Products	10,000	2.14 ^b (25°C)	1,140 (23°C)	1.53
Polyethylene: DMDA-8920 (PE1)	Petromont	14,400	2.11 (190°C)	950 (25°C)	1.49
Polyethylene: DMDB-8907 (PE2)	Petromont	19,800	2.56 (190°C)	950 (25°C)	1.49

a. Provided by supplier.

b. van Krevelen (1976).

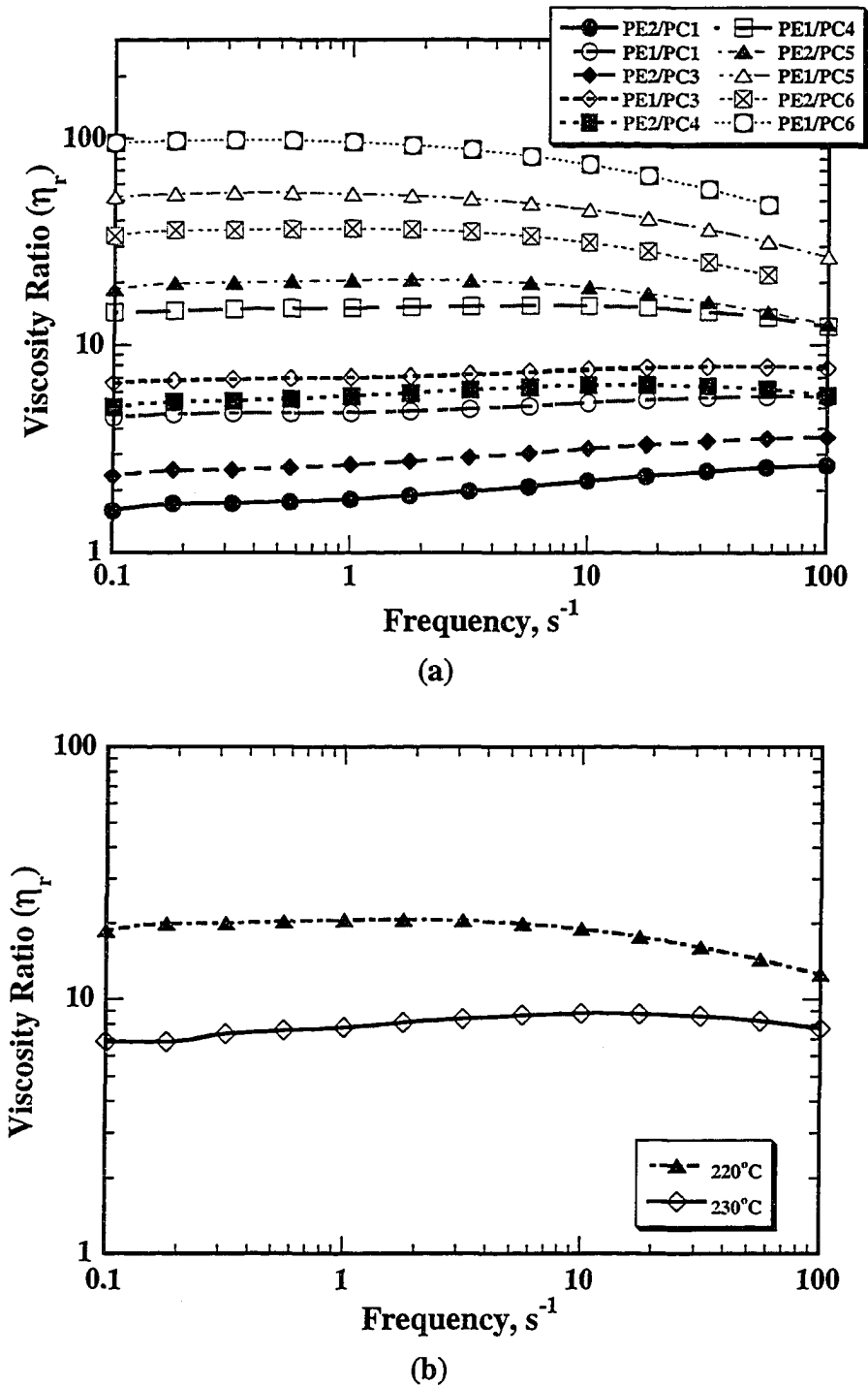
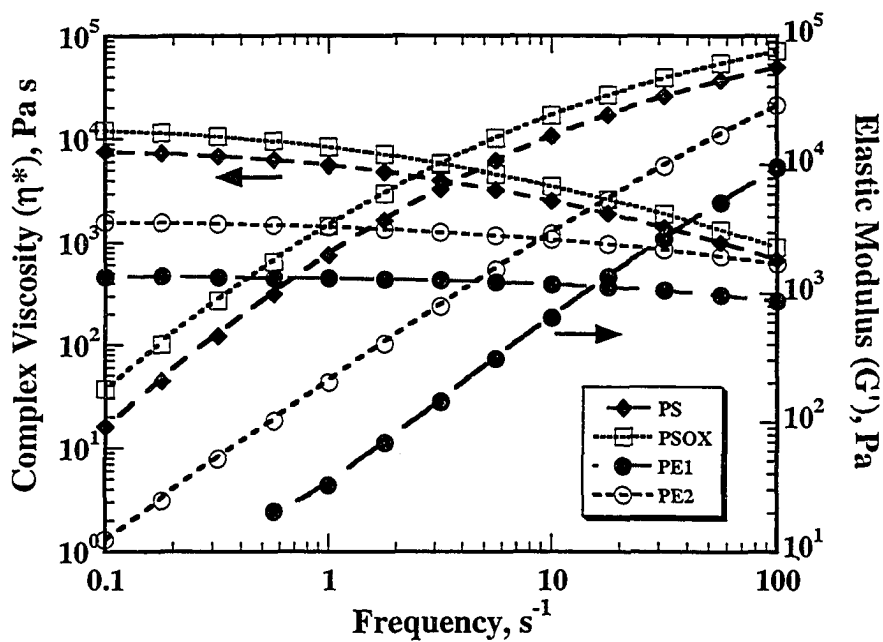
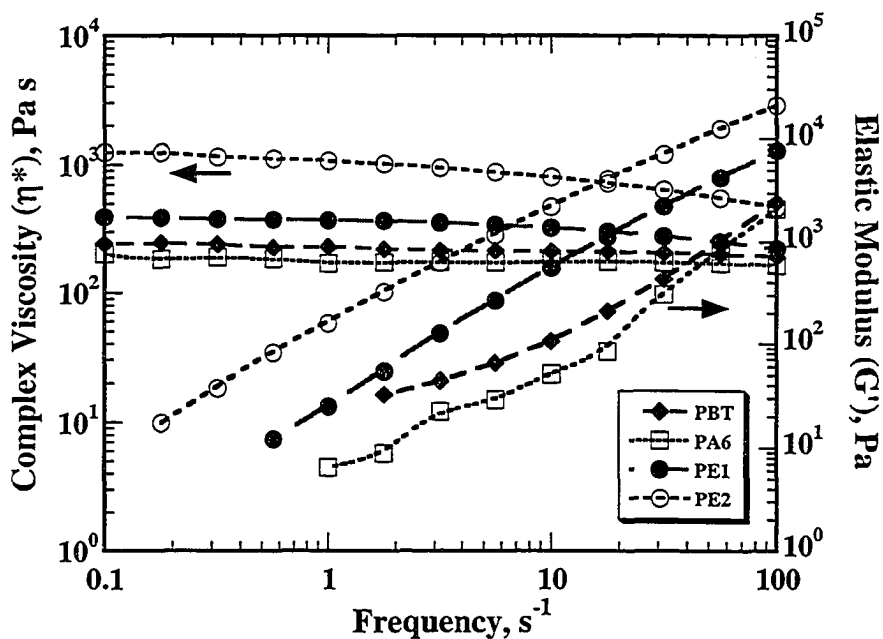


Figure 3.2 (a) Viscosity ratio of PE/PC systems at 220°C; (b) Viscosity ratio of PE2/PC5 at 220°C and 230°C; (c) Complex viscosity and elastic modulus of PS, PSOX, PE1 and PE2 at 190°C; (d) Complex viscosity and elastic modulus of PBT, PA6, PE1 and PE2 at 230°C.



(c)



(d)

Figure 3.2 (Continued).

viscosity ratio ranged from 0.5 to 100. Figure 3.2a shows that the viscosity ratio of PE/PC systems varies slightly with frequency (or shear rate) and Figure 3.2b shows that the viscosity ratio decreases with increasing temperature.

Table 3.2 lists the interfacial tension data for the systems studied. The PC, PS, PA6 and PBT spheres were specially prepared (Chapter 2, Lin *et al.*, 2003b). The PSOX chunks were added to the Couette directly after cutting the pellets in order to avoid reaction of the oxazoline group during the heating process of drop preparation. The dimensions of the spheres were measured after imaging the spheres using an Olympus BHSM optical microscope.

Table 3.2 Interfacial tension of polymer systems studied.

Polymer Systems	Interfacial Tension (mN/m)	Reference	Method
PE/PC	17.2 (220°C) 16.3 (230°C)	Chapleau <i>et al.</i> , 2000	Breaking thread
PE/PS	4.9 (190°C)	Elemans <i>et al.</i> , 1990	Breaking thread
PE/PSOX	4.9 (190°C)	PE/PS data	
PE/PA6	15.2 (230°C)	Chapleau <i>et al.</i> , 2000	Breaking thread
PE/PBT	10.6 (230°C)	Wu, 1989	Harmonic mean equation

3.2.2 Experimental Setup

The transparent Couette flow cell used consists of two counter-rotating concentric cylinders (Figure 3.3). The outer transparent cylinder is made of quartz (I.D. = 117 mm) and is heated by infrared heaters. The inner cylinder is made of steel (O.D. = 109 mm) and is heated by six cartridge heaters uniformly distributed inside the cylinder. The Couette cell has a gap 4 mm in width and 50 mm in height. A detailed description of the setup can be found elsewhere (Mighri and Huneault, 2001a).

The drop deformation and breakup processes were recorded using two video camera systems: a high-resolution digital camcorder [3 CCD XL1, from Canon] with a magnification macrolens and a digital chronometer; and a Pulnix CCD camera [TMC-7]. In the Couette setup, the visualization plane through the transparent quartz cylinder is the plane containing the flow direction and the vorticity axis. The observations were made close to the gap center and at the mid portion of the transparent cell in order to minimize the wall and end effects.

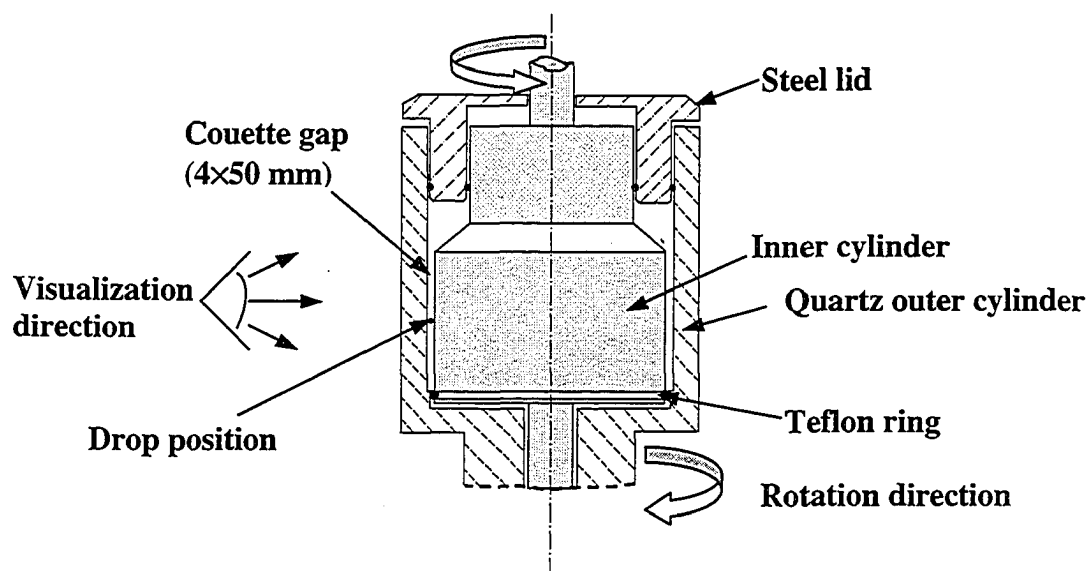


Figure 3.3 Couette flow cell setup (Mighri and Huneault, 2001a).

3.2.3 Experimental Procedure

All polymers were dried under vacuum at 80°C (for PE, PC, PS and PSOX) or at 120°C (for PBT and PA6) overnight before the experiments. At the beginning of each run, the Couette cell was preheated up to 125°C. The 4 mm gap was then filled with PE pellets premixed with a small amount of thermal stabilizer, Irganox 1076 [octadecyl-3-(3,5-di-tert-butyl-4-hydroxy-phenyl)-propionate], from Ciba chemicals, and 4-6 drops

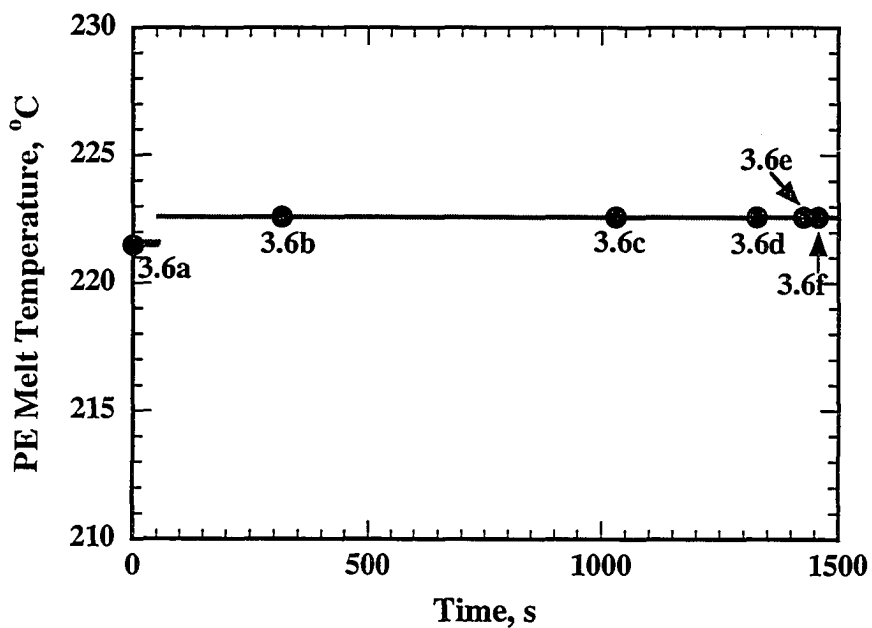
were inserted carefully into the PE matrix. A vacuum pump was used to remove air from the polymer system. The temperature of the Couette device was then increased to the desired starting temperature and the matrix was allowed to melt at low shear rates for temperature uniformity. The drop deformation and breakup processes were then recorded at a well-controlled shear rate and temperature. Finally, the digital recording was analyzed using Adobe Photoshop software. Drop images at a given deformation time were grabbed, and their dimensions were measured based on prior calibration.

Experiments were performed by either increasing shear rate stepwise at a constant temperature (Experiment Type 1) or increasing temperature stepwise at a constant shear rate (Experiment Type 2). Figures 3.4 and 3.5 illustrate the typical PE melt temperature and average shear rate profiles for each type of the experiments. The average shear rate, $\dot{\gamma}$, is calculated for a power law fluid according to the following equations (Macosko, 1993; see Appendix II for details in obtaining the equations):

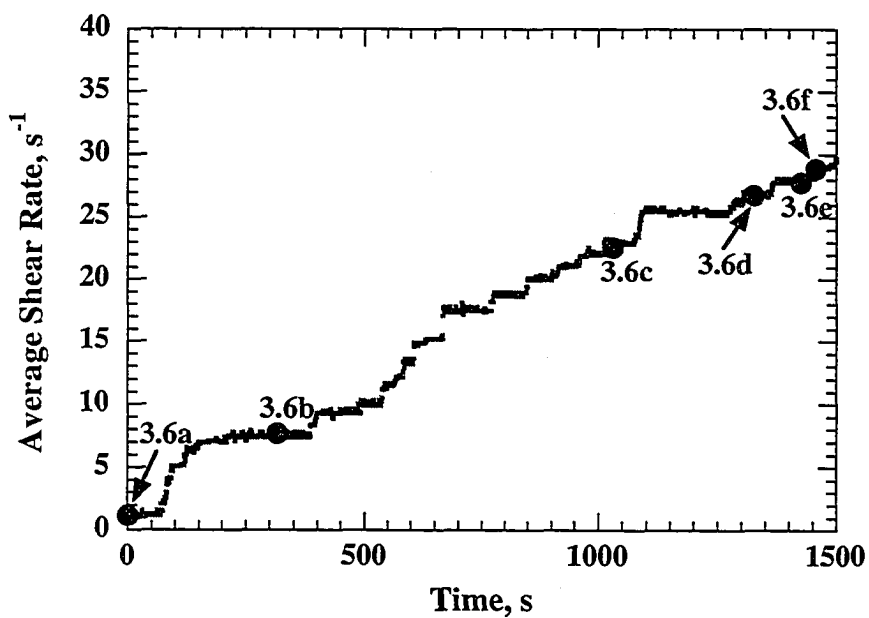
$$\dot{\gamma}_i = \frac{2}{n} \left(\frac{R_i^{\frac{2}{n}}}{R_i^{\frac{2}{n}} - R_o^{\frac{2}{n}}} \right) \cdot \Omega(t) \quad (3.1a)$$

$$\dot{\gamma}_o = \dot{\gamma}_i \left(\frac{R_i}{R_o} \right)^{\frac{2}{n}} \quad (3.1b)$$

$$\dot{\gamma} = \frac{\dot{\gamma}_i + \dot{\gamma}_o}{2} \quad (3.1c)$$

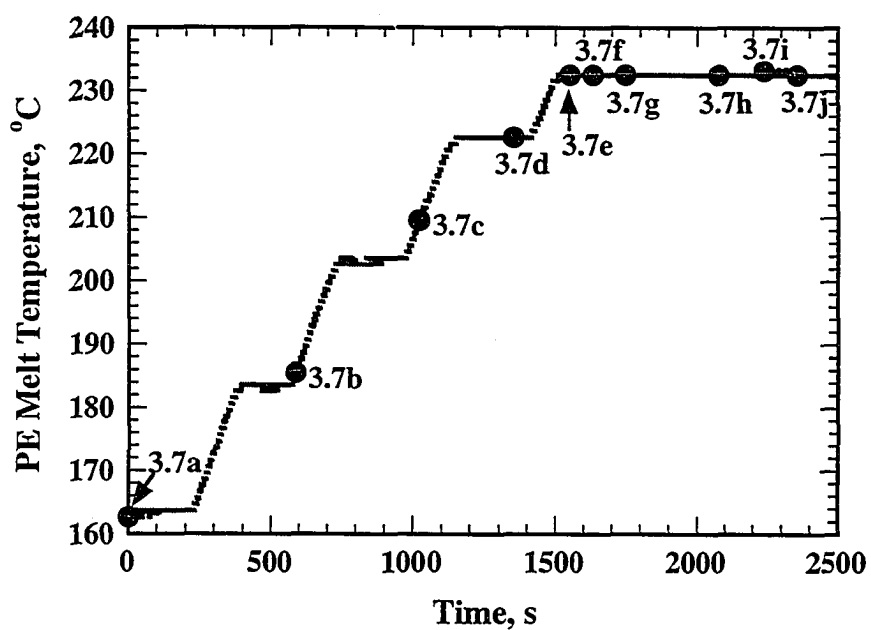


(a)

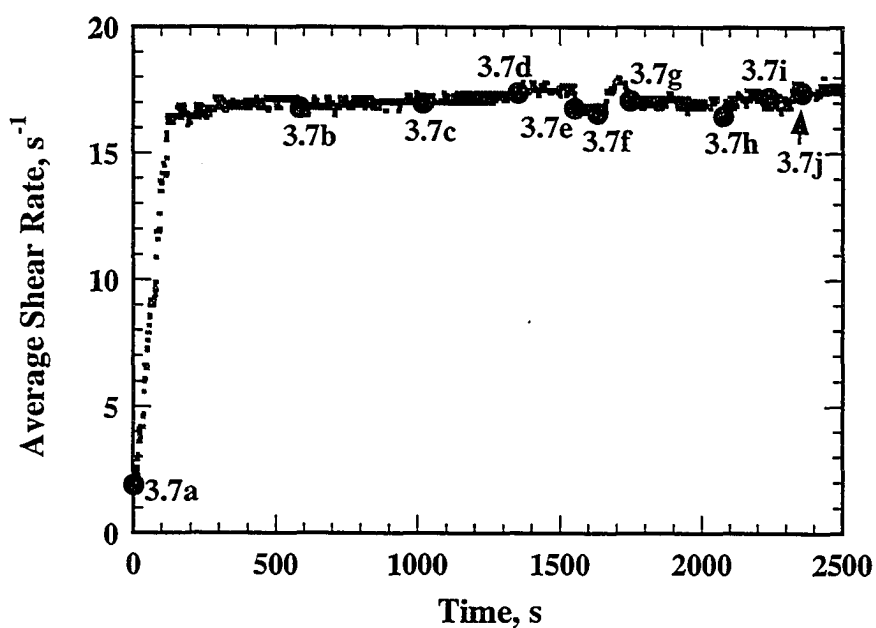


(b)

Figure 3.4 Experiment Type 1 — Stepwise shear rate increase at constant temperature. (a) Temperature profile of PE melt; (b) Average shear rate applied. The solid circles shown are the experimental conditions corresponding to Figure 3.6.



(a)



(b)

Figure 3.5 Experiment Type 2 — Stepwise temperature increase at constant shear rate. (a) Temperature profile of PE melt; (b) Average shear rate applied. The solid circles shown are the experimental conditions corresponding to Figure 3.7.

where n is the power-law index in the high frequency range; the subscript i and o are the inner cylinder and outer cylinder, respectively; R is the radius of the cylinders; $\Omega(t) = \Omega_o(t) - \Omega_i(t)$ is the relative rotation speed between the outer and inner cylinders. The solid circles in Figures 3.4 and 3.5 correspond to the images shown in the relevant micrographs in Figures 3.6 and 3.7, respectively.

3.3 RESULTS AND DISCUSSION

3.3.1 Erosion

3.3.1.1 Visualization

Figure 3.6 shows typical images of a PC4 drop deforming in a PE1 matrix at 220°C for different shear rates. The corresponding viscosity ratio, η_r , is approximately constant around 15. Initially at a shear rate of 1.2s^{-1} , the drop looks fairly spherical (Figure 3.6a), however, it is slightly deformed to an oval shape even at this low shear rate. It is then deformed into a diamond-like cross-section when the shear rate is increased to approximately 8s^{-1} (Figure 3.6b). The drop is in the shape of old-fashioned top and spins in the matrix. The drop maintains the diamond shape even at a shear rate of 23s^{-1} (Figure 3.6c). Streams of daughter droplets, cylinders and sheets are seen coming off the mother drop when the shear rate is increased to 27s^{-1} (Figure 3.6d). The drop then becomes irregular in shape with small daughter droplets and ribbons peeling off the mother drop (Figure 3.6e). When the drop softens, a cloud of daughter droplets envelop the main drop, and the main drop looks like a burning sun, releasing thin ribbons and

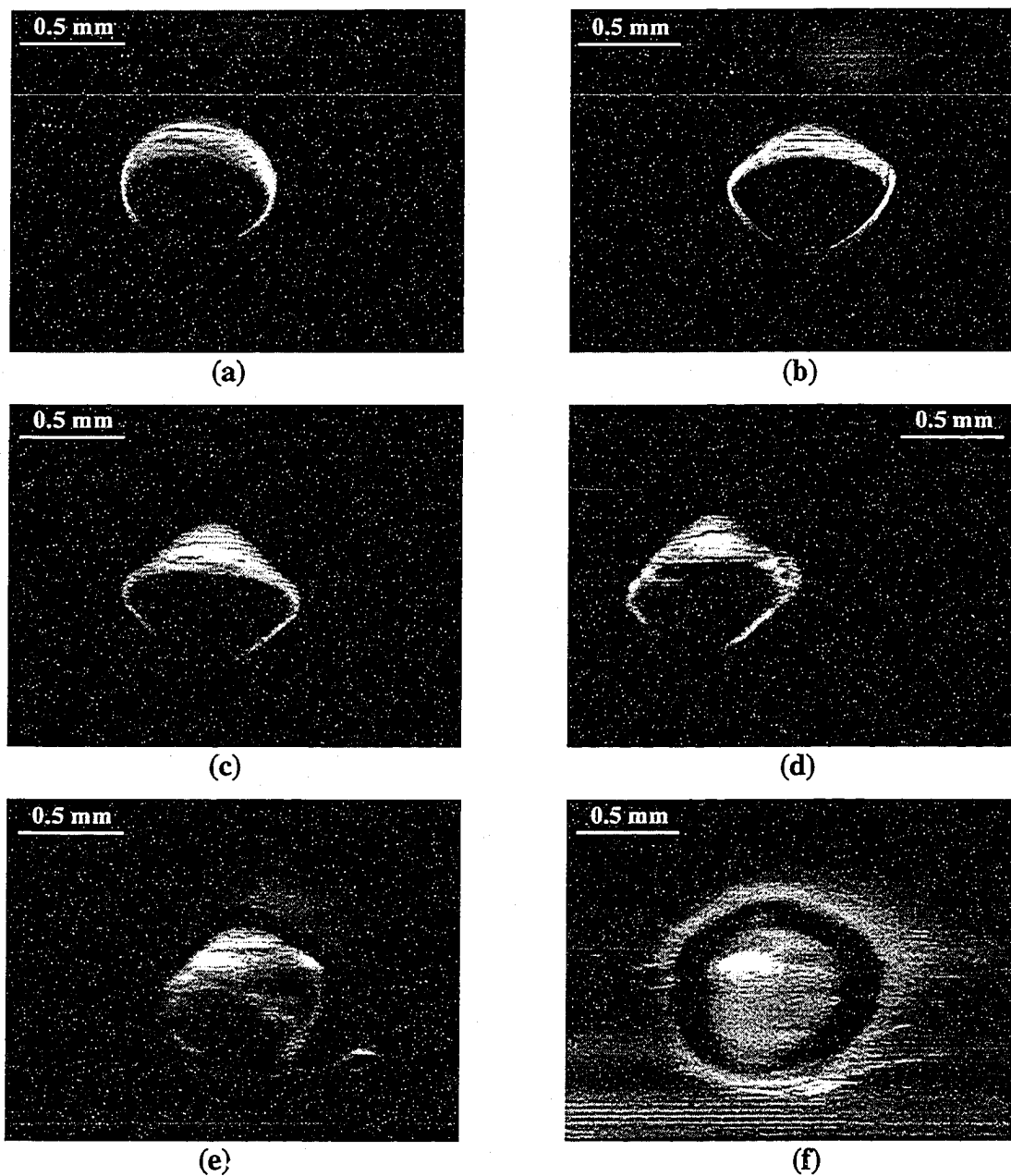


Figure 3.6 Drop deformation and erosion of a PC4 drop ($D_0=0.75\text{mm}$) in a PE1 matrix at 220°C with stepwise shear rate increase shown in Figure 3.4. Time and conditions for each figure: (a) $t=0\text{s}$, $\dot{\gamma}=1.2\text{s}^{-1}$, $\eta_r=15.1$; (b) $t=315\text{s}$, $\dot{\gamma}=7.7\text{s}^{-1}$, $\eta_r=15.5$; (c) $t=1030\text{s}$, $\dot{\gamma}=22.6\text{s}^{-1}$, $\eta_r=14.8$; (d) $t=1326\text{s}$, $\dot{\gamma}=26.8\text{s}^{-1}$, $\eta_r=14.7$; (e) $t=1425\text{s}$, $\dot{\gamma}=27.8\text{s}^{-1}$, $\eta_r=14.7$; (f) $t=1456\text{s}$, $\dot{\gamma}=28.9\text{s}^{-1}$, $\eta_r=14.6$. Note scale bar. For the micrographs, the flow direction is horizontal and the vorticity direction is vertical.

small streams of droplets into PE melt (Figure 3.6f). This phenomenon is described as “erosion”. This is the first time the erosion phenomenon has been visualized for polymer systems.

Is erosion a kind of drop breakup? Tests performed with stepwise increase of temperature clarified this question. Figure 3.7 shows a PC5 drop of 0.83 mm in diameter (Figure 3.7a) that deformed and eroded in a PE2 matrix. Temperature was stepwise increased from 160°C to 230°C, while the shear rate was maintained at around 17s^{-1} . As temperature reached 200°C (Figure 3.7b), the drop remained rigid with little change in its shape because of the high viscosity ratio of the system ($\eta_r = 151$ at 186°C) at these temperatures. Essentially, the drop behaved like a solid sphere in a fluid. Figure 3.7c shows the drop shape after temperature is increased to 210°C (at this temperature, $\eta_r = 30$). Here, the drop started to deform into a diamond-like shape. After another 13°C increase in temperature to 223°C, the viscosity ratio decreased to 18 and the drop became more diamond-like in shape, as shown in Figure 3.7d, with little streams of droplets, sheets and cylinders coming off the mother drop. When the temperature was raised to 233°C (at this temperature, η_r decreased to 8.8), ribbons formed and encircled the mother drop (Figure 3.7e), and the entire drop began to soften. Figure 3.7f shows the presence of a cloud of daughter droplets and cylinders around the mother drop, with thin ribbons stretching out from the mother drop.

Figure 3.7g shows the completely softened drop with thin ribbons and streams of daughter droplets being pulled away in the melt flow stream. The drop size is larger in Figure 3.7g than in Figure 3.7a. This is due to flattening of the drop in the velocity

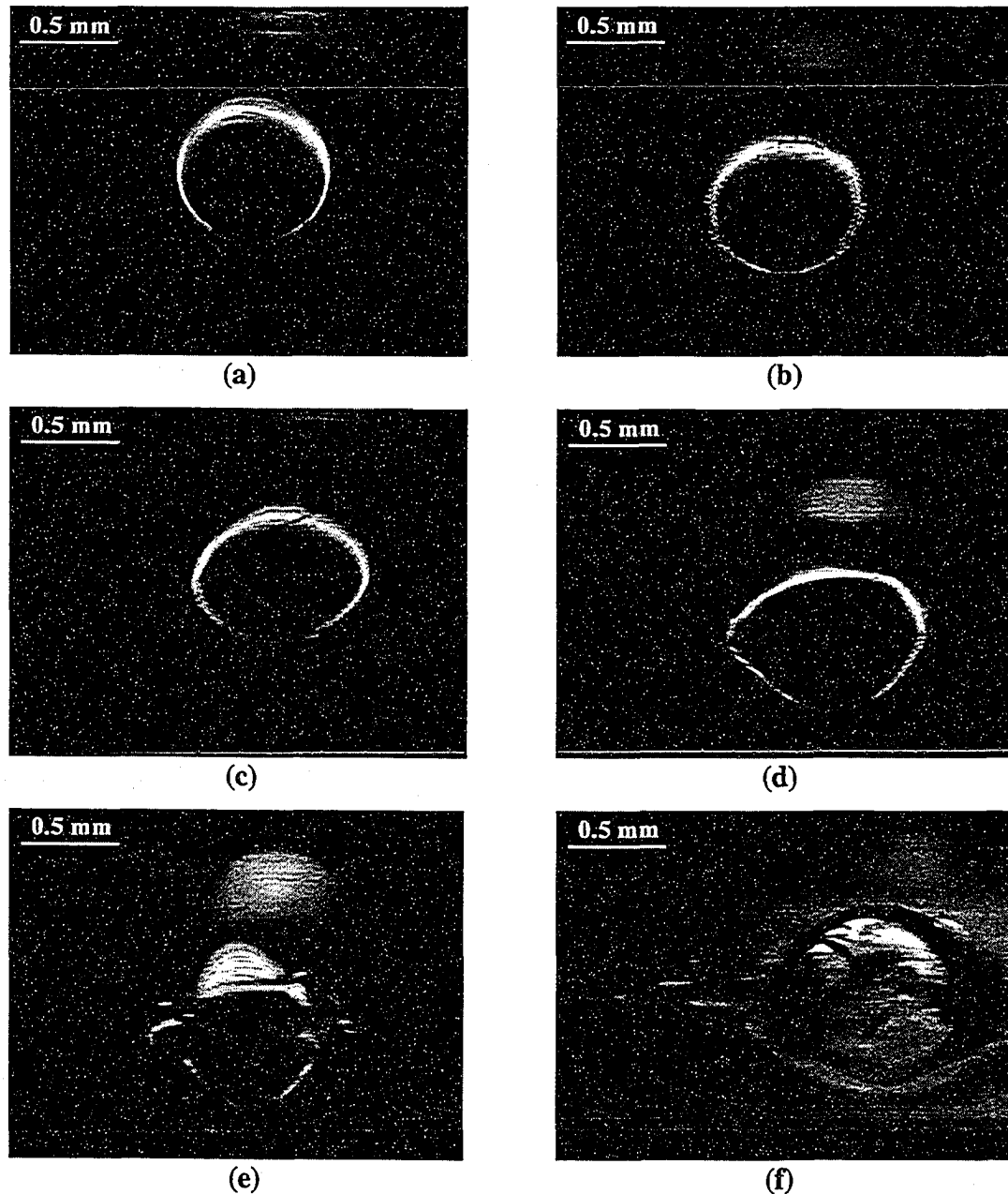


Figure 3.7 Drop deformation and erosion of a PC5 drop ($D_0=0.83\text{mm}$) in a PE2 matrix with stepwise temperature increase shown in Figure 3.6. Time and conditions for each figure: (a) $t=0\text{s}$, $T=163^\circ\text{C}$, $\dot{\gamma}=1.2\text{s}^{-1}$, $\eta_r=1194$; (b) $t=586\text{s}$, $T=186^\circ\text{C}$, $\dot{\gamma}=16.8\text{s}^{-1}$, $\eta_r=151$; (c) $t=1019\text{s}$, $T=210^\circ\text{C}$, $\dot{\gamma}=17.0\text{s}^{-1}$, $\eta_r=30$; (d) $t=1351\text{s}$, $T=223^\circ\text{C}$, $\dot{\gamma}=17.4\text{s}^{-1}$, $\eta_r=17.8$; (e) $t=1550\text{s}$, $T=233^\circ\text{C}$, $\dot{\gamma}=16.8\text{s}^{-1}$, $\eta_r=8.8$; (f) $t=1632\text{s}$, $T=233^\circ\text{C}$, $\dot{\gamma}=16.6\text{s}^{-1}$, $\eta_r=8.8$; (g) $t=1747\text{s}$, $T=233^\circ\text{C}$, $\dot{\gamma}=16.8\text{s}^{-1}$, $\eta_r=8.8$; (h) $t=2075\text{s}$, $T=233^\circ\text{C}$, $\dot{\gamma}=16.5\text{s}^{-1}$, $\eta_r=8.8$; (i) $t=2238\text{s}$, $T=233^\circ\text{C}$, $\dot{\gamma}=17.2\text{s}^{-1}$, $\eta_r=8.8$; (j) $t=2356\text{s}$, $T=233^\circ\text{C}$, $\dot{\gamma}=17.4\text{s}^{-1}$, $\eta_r=8.8$. Note scale bar. For the micrographs, the flow direction is horizontal and the vorticity direction is vertical.

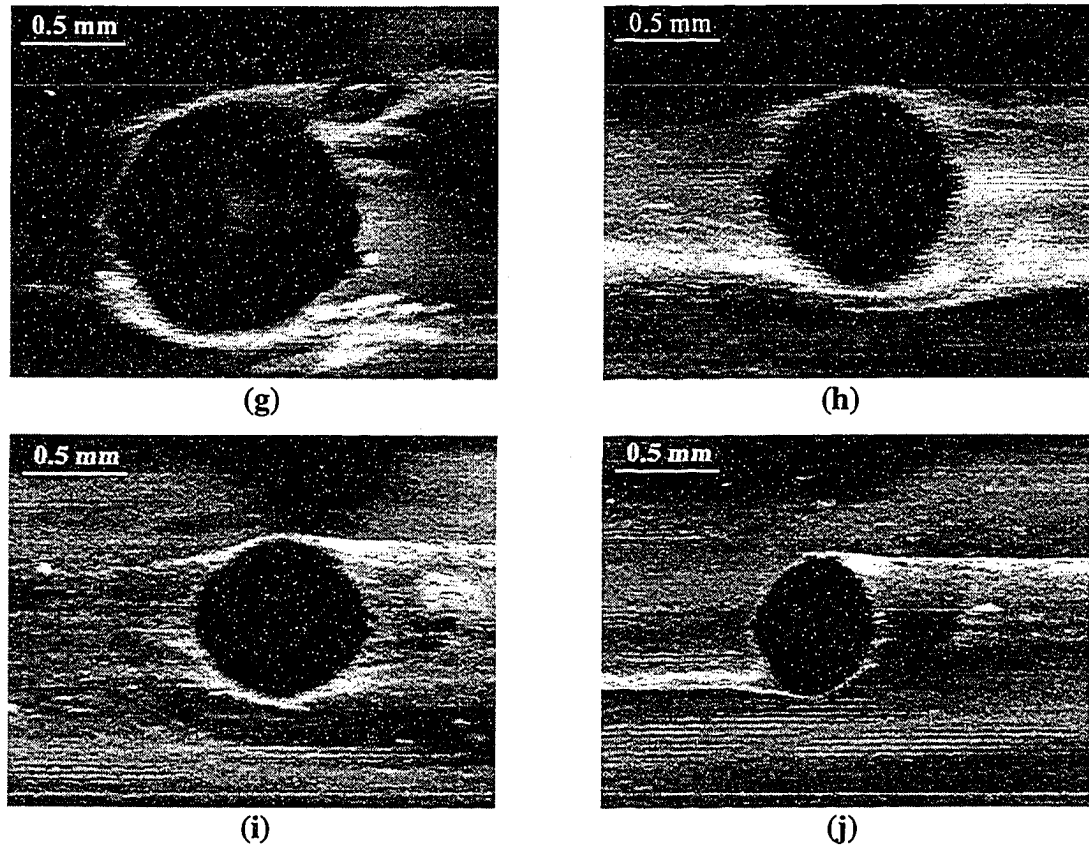


Figure 3.7 (Continued).

gradient direction, thermal expansion and the cloud of droplets around the mother drop. The flattening of the drop in the velocity gradient direction was verified using 3D computational flow dynamics simulation results by Chen *et al.* (2004a). A flattened drop may be due to the presence of normal stresses in both matrix and drop. The size of the mother drop becomes smaller and smaller because of the loss of mass as thin ribbons and streams are eroded from the surface of the mother drop (Figures 3.7h–j). Figure 3.7j shows that almost 90% of the initial drop volume has been eroded as the drop breaks up by this mechanism. This new mechanism describes how a polymer drop can be deformed and dispersed into a polymer melt during polymer blending.

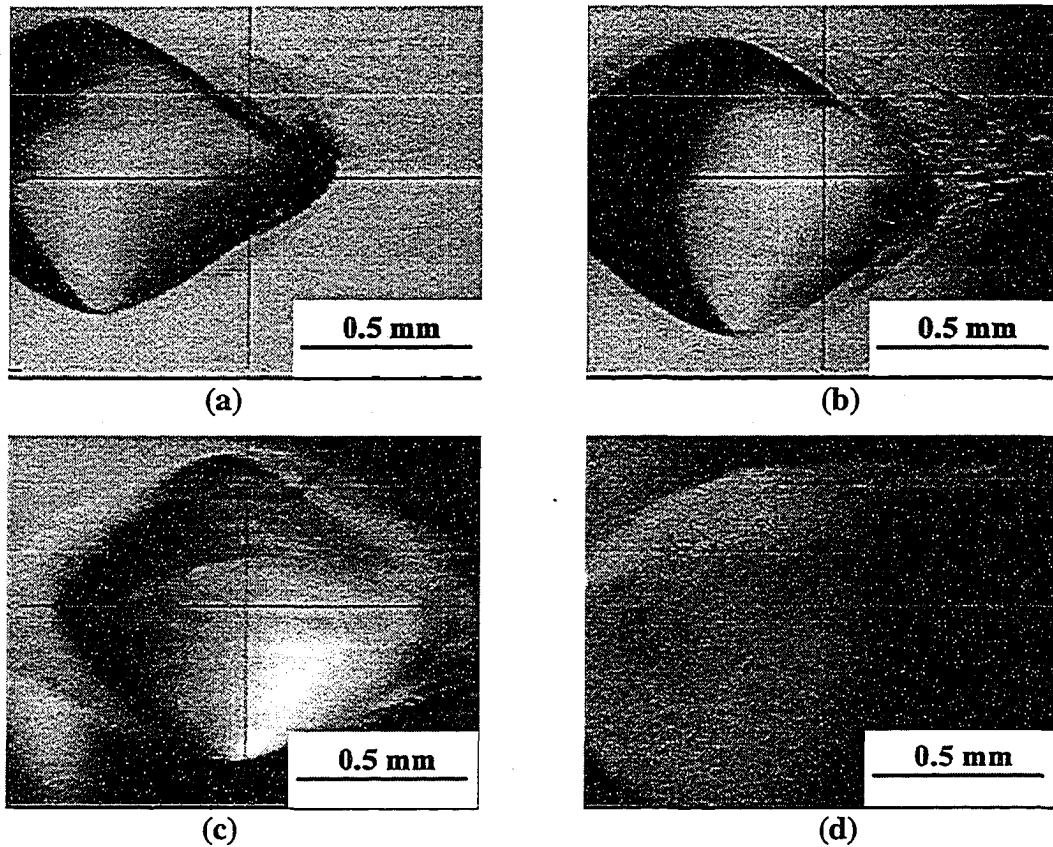


Figure 3.8 Drop deformation and erosion of a PC5 ($D_0=1.10\text{mm}$) in a PE2 matrix at 230°C with stepwise shear rate increase. Time and conditions for each figure: (a) $t=714\text{s}$, $\dot{\gamma}=12.9\text{s}^{-1}$, $\eta_r=8.8$; (b) $t=753\text{s}$, $\dot{\gamma}=12.8\text{s}^{-1}$, $\eta_r=8.8$; (c) $t=1006\text{s}$, $\dot{\gamma}=13.7\text{s}^{-1}$, $\eta_r=8.8$; (d) $t=1834\text{s}$, $\dot{\gamma}=18.0\text{s}^{-1}$, $\eta_r=8.8$; Note scale bar. For the micrographs, the flow direction is horizontal and the vorticity direction is vertical.

In order to visualize more details on surface erosion, a high magnification Pulnix CCD camera was used to follow a PC5 drop deformation and erosion in a PE2 matrix for a stepwise increasing shear rate at 230°C . Typical pictures showing the kinetics of drop erosion are shown in Figure 3.8. At a shear rate of 13s^{-1} , thin layers or sheets peeling off the diamond shaped mother drop are observed, as shown in Figure 3.8a. These sheets are broken into small droplets within a minute after their formation (Figure 3.8b). Clouds of small droplets and ribbons are formed around the mother drop 5 min later at a slightly

higher shear rate of around 14s^{-1} (Figure 3.8c). These droplets and ribbons continue to peel off the mother drop as the mother drop is continuously sheared. In Figure 3.8d, the entire surface of the mother drop is seen to erode as thin ribbons of PC are released into the surrounding PE matrix. In fact, it is difficult to discern the edges of the mother drop through the cloud of ribbons and small droplets.

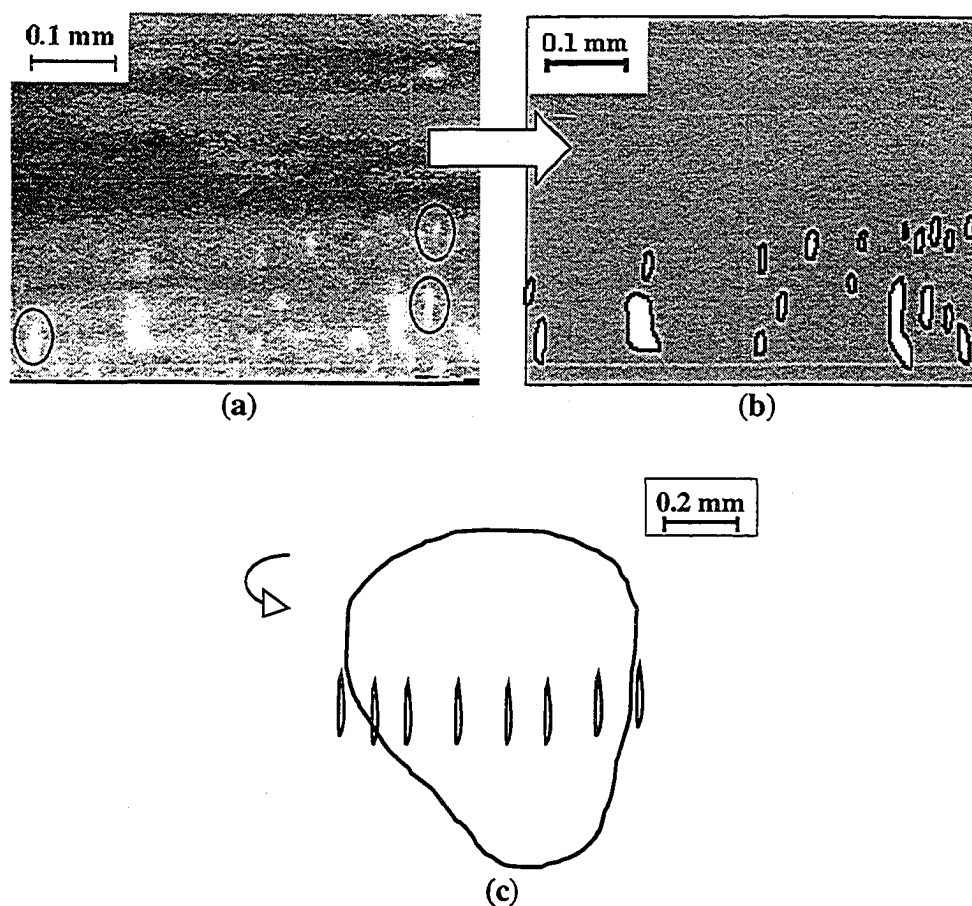


Figure 3.9 A PC5 drop ($D_0=1.05\text{mm}$) in a PE1 matrix at 220°C with stepwise shear rate increase. (a) $t=2412\text{s}$, $\dot{\gamma}=36.5\text{s}^{-1}$, $\eta_r=35.5$. Small droplets aligned along vorticity axis; circles drawn around a few extended droplets; (b) Schematic illustration of small droplets in (a); (c) Schematic illustration of small threads around the upper part of mother drop. Note scale bars. For the micrographs, the flow direction is horizontal and the vorticity direction is vertical.

Images of the drop breakup at even higher magnification are displayed in Figure 3.9 for a PC5 drop in a PE1 matrix. Figure 3.9a shows that many droplets elongated in the vorticity direction (white sausage shapes) are suspended in the PE melt. The sizes of these small droplets are in the range of 5–20 μm . These droplets are much smaller than those leaving the mother drop and are the result of the subsequent breakup of the daughter droplets. Figure 3.9b shows schematic representations of the drops in Figure 3.9a. Figure 3.9c illustrates the small threads surrounding the mother drop schematically. The schematics are shown because though the image (i.e. the threads surrounding the drop) could be seen clearly in the analog video recording, it was difficult to obtain clear still pictures via digital frame grabbing. The micron level particles are aligned perpendicularly to the flow direction, suggesting that this breakup is along the vorticity axis and results from normal stress development inside the PC droplets (Hobbie and Migler, 1999; Migler *et al.*, 1999; Mighri and Huneault, 2001b). Vorticity alignment and breakup is another kind of breakup mechanism for polymer systems and will be discussed in more detail in Section 3.3.3.

3.3.1.2 Erosion Mechanism

Erosion, in the form of thin ribbons and streams of small droplets peeling off the mother drop, is a new kind of drop deformation and breakup mode. It mainly occurs in PE/PC systems and is also observed in PE1/PBT system. Contrary to empirical correlations and theoretical predictions of drop breakup in Newtonian systems (Taylor, 1932, 1934; Grace, 1982) that drop will not breakup when $\eta_r > 3.5$, drop breakup via

erosion occurs over a viscosity range from 0.6 to 60. This may be due to the shear-thinning and viscoelastic properties of polymers.

In polymer systems, at low shear rates, the shear stress stretches the drop in the flow direction and the normal stress elongates the drop in the direction perpendicular to the flow, i.e., vorticity axis. As a result, the spherical drop is deformed into a diamond-like shape and resembles an old-fashioned spinning top. When the shear rate is increased further, both shear and normal stresses are increased because shear stress is proportional to $\dot{\gamma}$ and normal stress is proportional to $\dot{\gamma}^2$. A new competition between the forces results in more irregular drop shape.

According to recent numerical simulation work on PC5 drop breakup in a PE2 melt, the shear stress acting on the surface of the drop is one time larger than that inside the drop (Chen *et al.*, 2004b). From the simulation, it was found that the maximum shear stress of the drop surface could reach 5 times (Figure 3.10) of that in the matrix phase. If the shear stress at the surface is larger than that inside the drop and the surface of the drop is less viscous than in the center of the drop (due to shear thinning), it is reasonable that the surface can be easily peeled off. Therefore, when the shear rate reaches a critical value, the drop can no longer sustain the material at the surface, and surface erosion begins as the drop releases ribbons and droplets into the matrix.

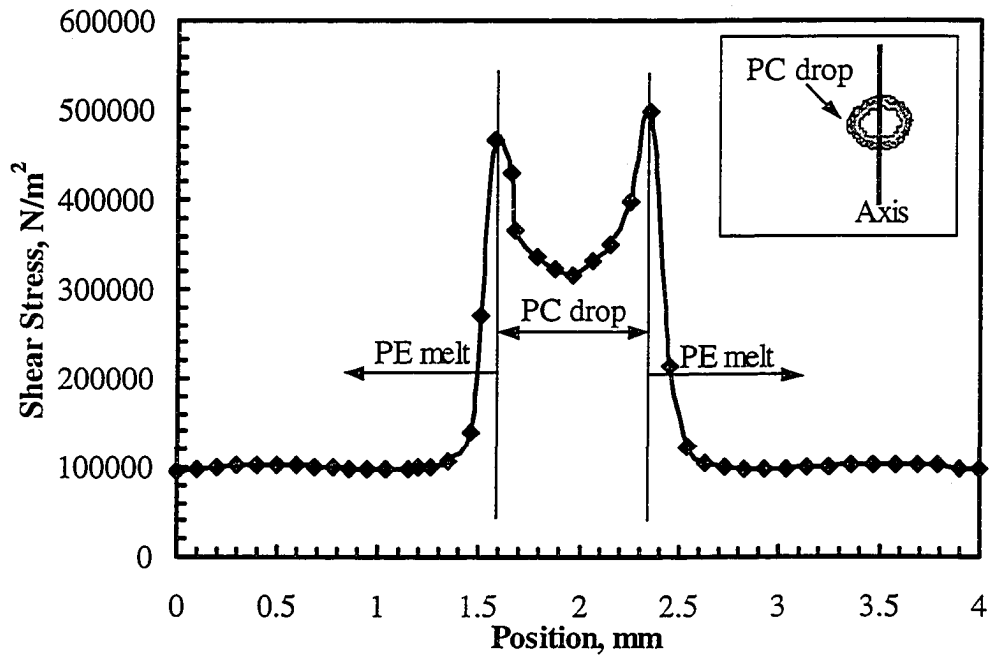


Figure 3.10 Shear stress versus distance along axis. Two-dimensional simulation geometry and axis shown in inset. The shear stress at the surface of the PC drop is clearly one order of magnitude larger than inside the drop. From Chen *et al.* (2004b).

It is observed that the Capillary number decreases when the drop size decreases as the drop continuously releases streams of droplets and ribbons into the matrix via erosion. It is also found that the critical shear rate does not change much with the drop size. For example, when the diameter of a PC5 drop is varied from 0.51 mm to 1.69 mm, the critical shear rate for the drop erosion in PE2 matrix at 230°C is almost unchanged (see Table 3.3, $\sim 17\text{s}^{-1}$). Therefore, the Capillary number may not be the critical parameter to characterize erosion, rather a critical shear rate may be more relevant.

Table 3.3 lists the critical conditions when erosion occurred. Deborah number, De , is a ratio of the characteristic material relaxation time to the characteristic process time. It is related to the rate of relaxation of the drop and the rate of deformation of the drop:

$$De = \lambda \dot{\gamma} \quad (3.2)$$

where $\dot{\gamma}$ is the critical shear rate; λ is the characteristic relaxation time of the drop phase and is obtained from the complex viscosity versus frequency data:

$$\lambda = 1/\omega_c \quad (3.3)$$

where ω_c is the critical frequency determined from the intersection of the line representing the Newtonian viscosity limit at low frequency and the line representing the power law viscosity at high frequency.

Figure 3.11 shows a plot of the critical shear rate for the onset of polymer drop erosion in a PE matrix as a function of viscosity ratio. The critical shear rate increases with viscosity ratio when viscosity ratio is less than 24, but is almost constant at higher viscosity ratios. An increase of shear rate with viscosity ratio is expected at lower viscosity ratios because a critical shear force is required to deform a fluid-like drop. However, when the viscosity ratio is high, the drop behaves like a solid particle inside the matrix. The ratio of the surface shear stress to the stress inside the drop may be larger than 2. Therefore, the shear force needed to peel off the droplets may not increase significantly at a higher viscosity ratio.

Table 3.3 Critical conditions for erosion experiments.

System: Matrix/ Drop	Test Temp. (°C)	Initial Drop Diam. (mm)	Critical Shear Rate ($\dot{\gamma}$, s ⁻¹)	Viscosity Ratio (η_r)	Elastic Modulus (G', Pa)		Capillary Number (Ca)	Deborah Number (De)
					Drop	Matrix		
PE1/PBT	230	0.65	4.7	0.6	60	210	50	0.05
PE2/PC3	230	0.57	4.7	1.5	250	670	65	0.15
PE2/PC3	220	0.60	6.7	3.1	1,720	1,300	91	0.32
PE2/PC4	230	0.66	9.6	3.7	3,520	1,560	140	0.49
PE2/PC4	220	0.68	11.3	6.5	15,860	2,260	164	1.10
PE2/PC4	220	0.67	14.2	6.5	20,340	2,870	198	1.38
PE2/PC4	220	0.68	16.1	6.5	23,270	3,270	224	1.56
PE2/PC5	230	1.69	16.0	9.8	33,390	2,800	557	1.56
PE2/PC5	230	0.55	16.2	9.8	33,810	2,840	183	1.57
PE2/PC5	230	0.54	16.9	9.8	35,300	2,980	186	1.64
PE2/PC5	230	0.51	16.9	9.8	35,300	2,980	176	1.64
PE2/PC5	230	0.83	17.1	9.8	35,730	3,020	289	1.66
PE2/PC5	230	1.10	17.5	9.8	36,580	3,100	390	1.70
PE2/PC5	230	0.72	18.4	9.7	38,500	3,280	266	1.79
PE1/PC4	220	0.75	28.9	14.8	43,040	2,160	175	2.81
PE1/PC4	220	0.86	25.6	14.8	37,950	1,900	182	2.49
PE2/PC5	220	0.95	31.9	16.1	178,500	6,580	566	5.49
PE2/PC6	220	0.71	38.8	24.1	326,300	8,030	501	8.42
PE1/PC5	220	0.86	36.7	35.5	205,670	2,770	246	6.31
PE1/PC5	220	1.05	33.8	36.1	189,240	2,540	280	5.81
PE1/PC6	220	0.79	33.3	57.0	280,850	2,500	208	7.23

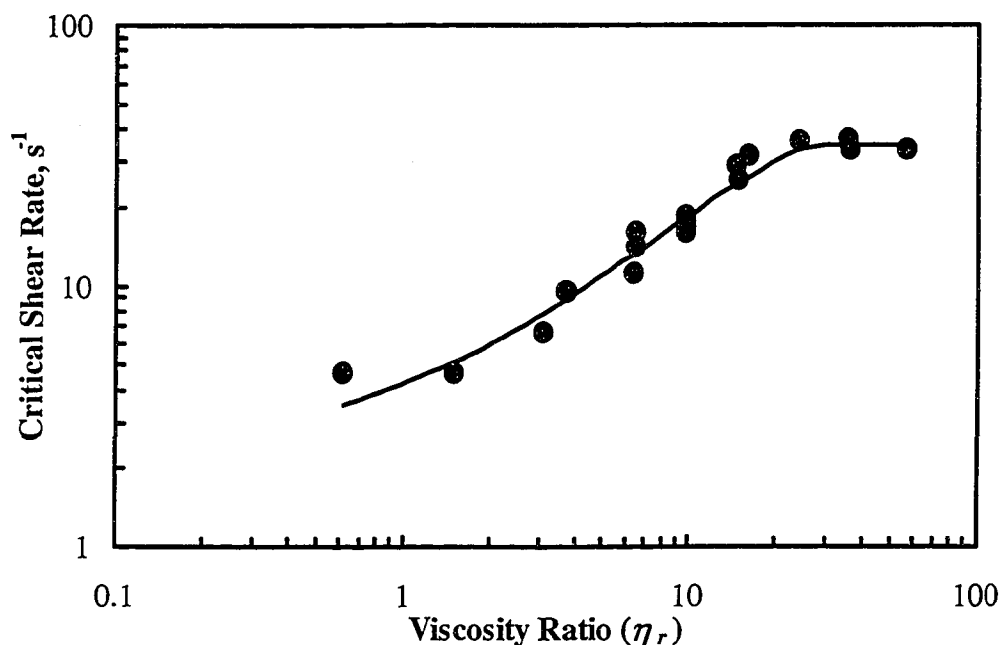


Figure 3.11 Critical shear rate for polymer drop erosion at different viscosity ratios.

Sheets are formed at the beginning of surface erosion of the mother drop. Breakup via sheets and subsequent sheet breakup are effective ways to achieve quick reduction in particle dimension (Sundararaj *et al.*, 1995; Willemsse *et al.*, 1999). Ribbons and daughter droplets leave the mother drop within a minute or so after the sheets are stretched along the flow direction. These ribbons and small droplets break up further to micron-size domains.

3.3.1.3 Erosion Kinetics

The erosion breakup phenomenon is new for polymer drops in a polymer matrix, but it has already been studied in many other fields, such as agglomerate dispersion (Rwei *et al.*, 1990, 1991), drug delivery (Kenley *et al.*, 1987), and rock erosion. There are a few studies on modeling the erosion process. Kao and Mason (1975) proposed that the

number of spherical particles pulled off the periphery of an agglomerate was proportional to the shear stress generated by the matrix at a given point on the surface of the agglomerate:

$$R_0^3 - R_t^3 = k\dot{\gamma}t \quad (3.4)$$

where R_0 is the initial agglomerate radius, R_t is the agglomerate radius at time t , k is a rate constant and $\dot{\gamma}$ is the shear rate. Powell and Mason (1982) presented a second dispersion rate model for agglomerates without surface tension in the form of:

$$R_0 - R_t = k\dot{\gamma}t \quad (3.5)$$

Both models are considered at short times of agglomerate breakup, i.e., the strain, $\dot{\gamma}t$, is small — less than 1,000. A third model, a pseudo-first order kinetic model, is proposed by Kenley *et al.* (1987), based on the degradation rate of copolymer (*d,l*-latide/glycolide) in drug delivery.

$$\ln(m_r) = -k_{app} \times (t - t_{on}) \quad (3.6)$$

where m_r ($= m_t / m_0$) is the remaining mass of the copolymer, m_0 is the initial mass, m_t is the mass at time t , t_{on} is the onset time and k_{app} is a rate constant.

In the case of erosion of a polymer drop, the erosion is slow at the beginning and some softening time is needed before a distinct “peeling off” occurs. Once the erosion starts, it lasts for a long period of time (20 – 30 min). After this time, it is unable to visualize the drop any more because it is too small. Figure 3.12 plots the erosion profile of PE2/PC5 system at 230°C. The remaining volume, which is roughly equivalent to the remaining mass, is used in the plot. Zero time corresponds to the time when the temperature of the matrix phase is 230°C and the average shear rate is 17s⁻¹. Pictures taken when the drop began to soften were analyzed and the volume at that point was set as the initial volume. Each data point in Figure 3.12 was obtained from the average size of 30 images (1 second of video). The procedure for volume determination is as follows:

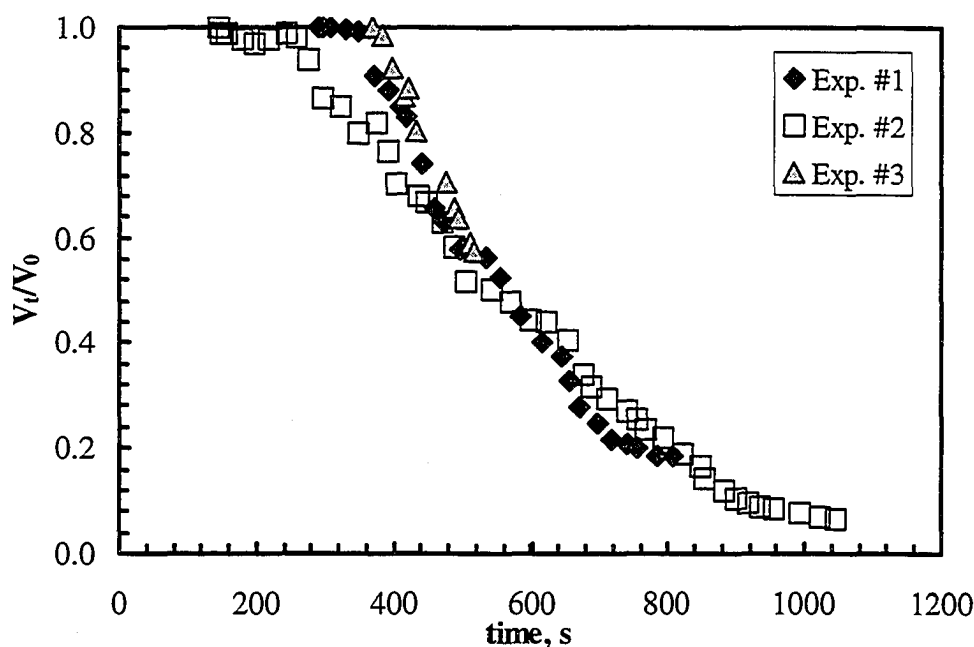


Figure 3.12 PE2/PC5 erosion profile – Volume remaining versus time.

(1) measure the drop area using image analysis; (2) calculate the equivalent diameter of a circle with the same area; and (3) calculate the remaining volume of the drop by assuming the drop is spherical. Three sets of experimental data (Exp. #1, #2 and #3) are presented and the experimental conditions are shown in Table 3.4.

Table 3.4 Experimental conditions for calculation of PE2/PC5 erosion rate.

Exp. No.	Stepwise temperature increase at $\dot{\gamma} \approx 17s^{-1}$					Stepwise shear rate increase at $T = 230^{\circ}C$		
	Time at different temperatures (s)					Time at different shear rates (s)		
	160°C	180°C	200°C	220°C	230°C	13s ⁻¹	14s ⁻¹	17~18s ⁻¹
#1	232	189	288	98	828.8			
#2	230	200	246	276	1,050			
#3						159	400	750

The experimental data was fitted with the first two models as described earlier. Significant deviations were found perhaps because of a long shearing time and thus large strains. However, the erosion rate of a PC drop can be described by the two-parameter model proposed by Kenley *et al.* (1987). Equation 3.6 was modified with the remaining volume (V_r , defined as V_t/V_0 , where V_t is the volume at time t and V_0 is the initial volume). The rate constant k_{app} can be calculated using least square regression of the decay of the relative volume:

$$\ln(V_r) = -k_{app} \times (t - t_{on}) \quad (3.7)$$

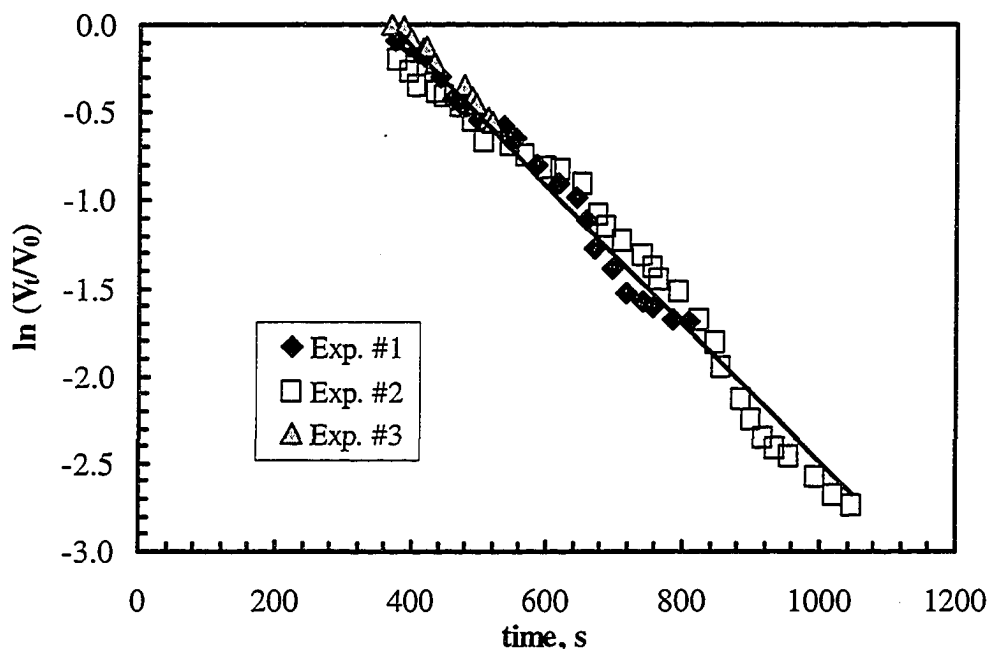


Figure 3.13 PE2/PC5 erosion profile – Semilogarithmic plot of volume remaining versus time for determination of the erosion rate.

Table 3.5 Kinetic constants for PE2/PC5 erosion at 230°C.

Exp. No.	$k_{app} \pm SD^a$ (s ⁻¹)	$t_{on} \pm SD^a$ (s)	R ^b
#1	0.0040 ± 0.0001	366 ± 7	0.992
#2	0.0039 ± 0.0001	363 ± 12	0.986
#3	0.0039 ± 0.0001	373 ± 3	0.994
Mean ± SD	0.0039 ± 0.0001	368 ± 7	

a. SD stands for standard deviation.

b. From least-square linear regression of $\ln(V_r) = -k_{app}(t-t_{on})$

Figure 3.13 shows a plot of the model (Kenley *et al.*, 1987) fit to the data. Table 3.5 lists the determined model parameters for the three sets of experiments. The results suggest that the model fits the PC drop erosion well. The apparent decay rate for the experiments are the same ($k_{app} = 0.0039 \pm 0.0001$) for three different runs of PC5/PE2

performed at $T = 230^\circ\text{C}$ and $\dot{\gamma} \approx 17\text{ s}^{-1}$. The onset time is also found to be similar for the three experiments ($t_{on} = 368 \pm 7\text{ s}$), suggesting that a particular softening time is needed to initiate the surface erosion phenomenon.

3.3.2 Parallel Breakup

3.3.2.1 Visualization

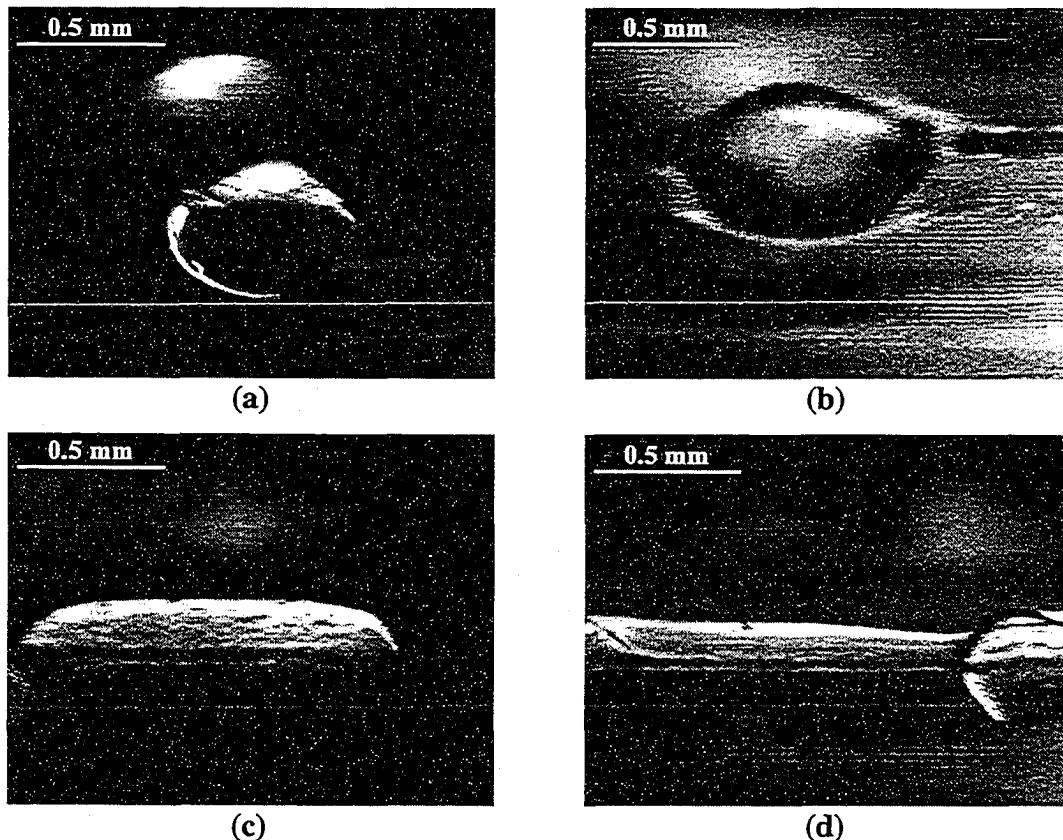


Figure 3.14 Drop deformation and breakup of a PC4 drop ($D_0=0.68\text{mm}$) in a PE2 matrix at 220°C subject to stepwise shear rate increase. Time and conditions for each figure: (a) initial drop: $t=0\text{s}$, $\dot{\gamma}=1.2\text{s}^{-1}$, $\eta_r=5.8$; (b) erosion of small droplets from the surface of mother drop: $t=421\text{s}$, $\dot{\gamma}=16.1\text{s}^{-1}$, $\eta_r=6.5$; (c) drop stretches into a sheet: $t=882\text{s}$, $\dot{\gamma}=32.4\text{s}^{-1}$, $\eta_r=6.4$; (d) breakup of the sheet: $t=883\text{s}$, $\dot{\gamma}=32.3\text{s}^{-1}$, $\eta_r=6.4$. Note scale bar. For the micrographs, the flow direction is horizontal and the vorticity direction is vertical.

Figure 3.14 shows typical images of a PC4 drop with an initial diameter of 0.68 mm deforming and breaking up in a PE2 matrix at 220°C for different shear rates. The viscosity ratio (η_r) of the system is approximately 6. At the beginning of the run, although the shear rate is low ($\dot{\gamma} = 1.2 \text{ s}^{-1}$), the spherical “mother” drop is already deformed (Figure 3.14a) to an elliptical shape. The mother drop deforms to a diamond-like shape when the shear rate is increased to about 9 s^{-1} , with small streams of droplets peeling off. When the shear rate is further increased to 16 s^{-1} , erosion occurs at the surface of the mother drop (Figure 3.14b). When the shear rate reaches 32 s^{-1} , the drop is stretched into a thin sheet (Figure 3.14c), and the sheet breaks up into two pieces within a second (Figure 3.14d). Figures 3.14c and 3.14d show a distinct breakup mode, which was termed “parallel breakup”, when the drop abruptly stretches into a thin sheet.

3.3.2.2 Parallel Breakup Mechanism

Figure 3.15 illustrates images of parallel breakup for a PE2/PC5 system at 230°C. Figure 3.15a shows the PC5 drop with an initial diameter of 0.51 mm. At a shear rate of 17 s^{-1} , erosion occurs at the surface of the drop. When the shear rate is increased to 30 s^{-1} , the mother drop maintains a diamond shape with few droplets peeling off (Figure 3.15b). The stretching and breaking up of the drop by the parallel breakup mechanism can be seen in Figures 3.15c–3.15g.

Figure 3.16 shows how drop volume changes with time based on geometric assumptions. The drop at t_0 (arbitrary zero time chosen for Figure 3.16, defined in the caption of Figure 3.15b) has an equivalent diameter D_0 of 0.48 mm. If the drop keeps an elliptical shape or an elliptical and cylindrical shape, its volume increases with time

sharply when the time is larger than 18 s. This suggests that the drop shape assumptions are inappropriate. It is appropriate to model the drop as a thin sheet for later stages of the breakup.

Figure 3.17 plots the reduced dimensions of the drop as a function of time. The dimensions of the drop are: length a in the flow direction, length b in the vorticity direction and length c in the velocity gradient direction. Length c of the drop is determined by assuming a drop shape and that the volume of the drop is conserved. If the drop has an elliptical shape when $t < t_0 + 18$ s (e.g., Figure 3.15b), c can be estimated as:

$$c = \frac{D_0^3}{ab} \quad (3.8)$$

However, if the drop is not rotating in the PE melt, but is stretching continuously when $t \geq t_0 + 18$ s (e.g., Figure 3.15c), c can be estimated as:

$$c = \frac{\pi D_0^3}{6A} \quad (3.9)$$

where A is the cross sectional area of the drop shown on the screen. The length data shown for each time in Figure 3.17 are averages of drop sizes obtained from 15 frames before and 15 frames after the time instant plotted. The last point is averaged over data from only 9 frames because the drop breaks up at this time already.

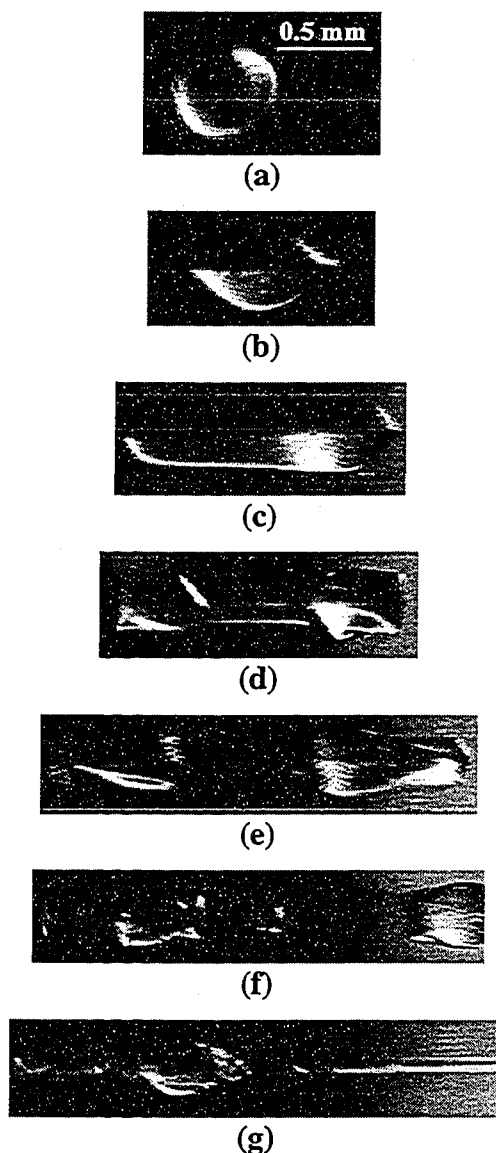


Figure 3.15 Deformation and breakup of a PC5 drop (initial diameter 0.51mm) in a PE2 matrix at 230°C subject to stepwise shear rate increase. Time and conditions for each figure: (a) initial drop: $t=50\text{s}$, $\dot{\gamma}=7.2\text{s}^{-1}$, $\eta_r=8.7$; (b) elliptical drop: $t=t_0=2348\text{s}$, $\dot{\gamma}=30.3\text{s}^{-1}$, $\eta_r=8.6$; (c) drop stretches into a sheet: $t=2368\text{s}$, $\dot{\gamma}=30.3\text{s}^{-1}$, $\eta_r=8.6$; (d) continues stretching: $t=2370\text{s}$, $\dot{\gamma}=30.5\text{s}^{-1}$, $\eta_r=8.6$; (e) drop rupture begins: $t=2370\text{s}$, $\dot{\gamma}=30.5\text{s}^{-1}$, $\eta_r=8.6$; (f) drop has ruptured: $t=2371\text{s}$, $\dot{\gamma}=30.2\text{s}^{-1}$, $\eta_r=8.6$; (g) daughter droplet that results from breakup: $t=2375\text{s}$, $\dot{\gamma}=30.6\text{s}^{-1}$, $\eta_r=8.6$. Note scale bar. For the micrographs, the flow direction is horizontal and the vorticity direction is vertical.

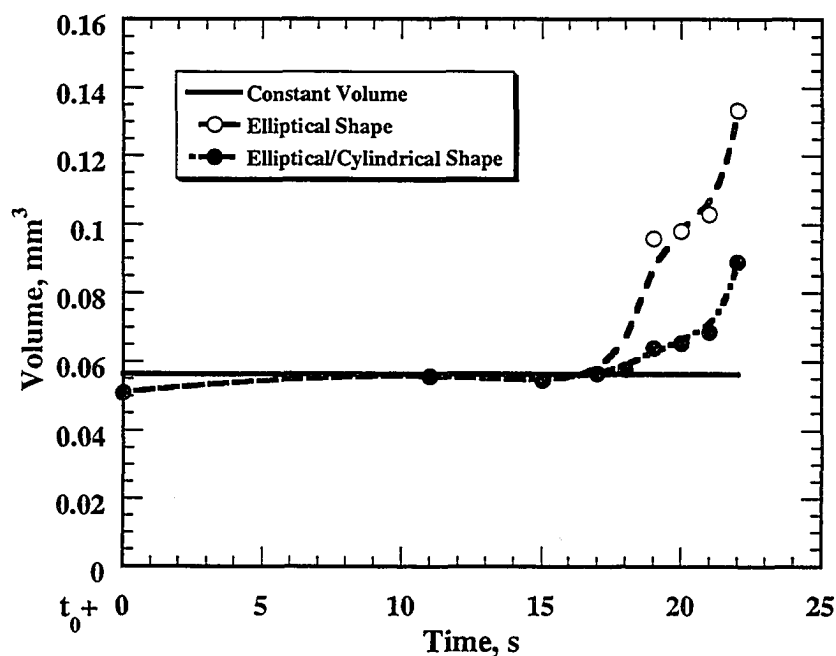


Figure 3.16 Drop volume changes with time if the drop keeps an elliptical shape or elliptical/cylindrical shape. The time, t_0 , corresponding to the time indicated in Figure 3.15b.

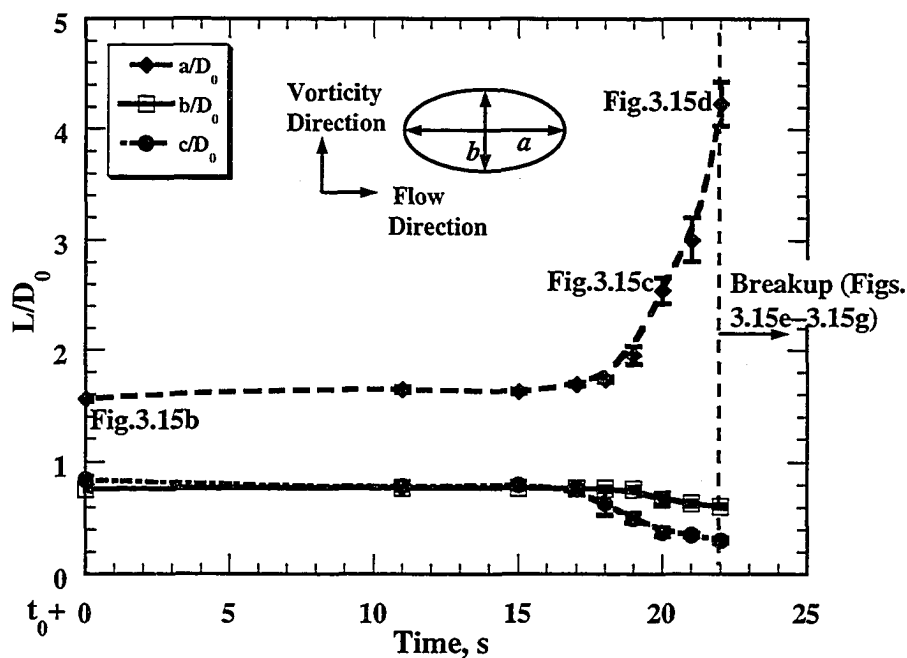


Figure 3.17 Reduced lengths a , b and c plotted versus time for a PC5 drop from Figure 3.15. The drop has an equivalent diameter $D_0 = 0.48 \text{ mm}$ at time t_0 , corresponding to the time indicated in Figure 3.15b.

The shear rate in the experiment shown in Figures 3.15b–3.15g is approximately 30s^{-1} , and the corresponding viscosity ratio (η_r) of the system is about 9. The length, a , of the mother drop is elongated in the flow direction at the beginning of the breakup process. The drop grows into a flat elliptical shape, which is quickly transformed into a flat sheet with triangular ends pointing outward (Figure 3.15c). Figure 3.15d shows that the drop has two thick triangular ends with tips pointing inward. In Figure 3.16, the length, a , of the drop has increased threefold from Figure 3.15b to Figure 3.15d and the width, c , of the drop has decreased by 64%.

Figure 3.15e shows that the two thick ends separate from each other and are connected by a very thin sheet (0.07 mm in thickness). The thin sheet weakens and ruptures (Figure 3.15f). The drop then breaks into two large irregular-shaped daughter droplets (Figure 3.15e). Smaller satellite droplets resulting from the breakup of the thin ligament that was connecting the drops are shown in Figure 3.15f. Figure 3.15g shows that one of the large daughter droplets soon obtains a diamond-like shape and behaves like the original mother drop, not only in its shape, but also in the mode of its deformation and breakup. For example, streams of small droplets and ribbons erode off continuously into the PE melt from one of the large daughter droplets. Such behavior was observed and discussed for a mother drop earlier.

3.3.2.3 Stress Analysis

As has been shown earlier in Chapter 2, the formation of sheets observed in polymer drop breakup experiments is different from the formation of cylinders in Newtonian systems. The polymer drop used has a diameter in the order of 1 mm and thus

the interfacial stress ($2\Gamma/D$, where D is drop diameter and Γ is interfacial tension) between polymer systems, for example, PE/PC and PE/PS, is in the order of 10 N/m^2 . This interfacial stress is small when compared with either the viscous stress ($\tau = \eta_m \dot{\gamma}$) or the normal stress $N_1(\dot{\gamma}) = T_{11}(\dot{\gamma}) - T_{22}(\dot{\gamma})$ ($N_1 \approx 2G'$ at low shear rate or frequency), which are in the order of 100 N/m^2 or greater. As a result, in polymer systems when the drop has a diameter of 1 mm, the interfacial stress is not strong enough to pull in an extended drop into a cylindrical shape. Instead, a sheet is formed. It is also found that the rate of decrease of length b is less than the rate of decrease of length c (Figure 3.17). This may be attributed to the fact that the drop is more elastic than the matrix (see G' data in Figure 2.2b), which elongates the drop in the vorticity direction (Mighri and Huneault, 2001a) and therefore, retards the decrease in length b .

Table 3.6 lists the critical conditions for drop breakup. In Newtonian systems, the critical condition for drop breakup is correlated using Capillary number (Ca) and viscosity ratio (η_r). However, one finds no such correlation as far as Capillary number (Ca) and viscosity ratio (η_r) are concerned for the critical condition of the parallel breakup (Figure 3.18). Therefore, viscous stresses may not be sufficient to describe the breakup phenomenon and normal stresses in polymers may be important in drop deformation and breakup. Since the breakup stresses acting on the drop are the viscous stress and normal stress from the matrix phase, and the restoring stresses are interfacial stress and normal stress in the drop, one can apply the stress ratio to describe the drop breakup critical condition (Sundararaj *et al.*, 1995; Ghodgaonkar and Sundararaj, 1996; Lin *et al.*, 2003a; see also Chapter 2):

Table 3.6 Critical conditions for parallel breakup experiments.

System: Matrix/ Drop	Test Temp. (°C)	Initial Drop Diam. (mm)	Critical Shear Rate ($\dot{\gamma}$, s ⁻¹)	Viscosity Ratio (η_r)	Elastic Modulus (G', Pa)		Capillary Number (Ca)	Deborah Number (De)
					Drop	Matrix		
PE2/PC4	220	0.67	32.3	6.4	48,300	6,700	404	3.14
PE2/PC4	220	0.68	32.3	6.4	48,300	6,700	410	3.14
PE2/PC4	220	0.68	23.9	6.3	35,300	4,900	316	2.32
PE2/PC4	230	0.66	21.6	3.9	12,200	3,900	284	1.11
PE2/PC5	230	0.51	30.3	8.6	63,800	5,700	273	2.94
PE1/PC1	220	0.60	6.8	6.4	1,170	430	41	0.34
PE2/PC1	220	0.58	1.8	2.4	120	270	27	0.09
PE2/PC1	220	0.40	5.5	2.6	770	910	54	0.28
PE2/PC3	220	0.59	1.9	2.8	210	290	29	0.09
PE1/PS	190	0.52	3.8	9.1	7,640	190	85	3.80
PE2/PS	190	0.45	2.7	3.3	5,610	670	160	2.70

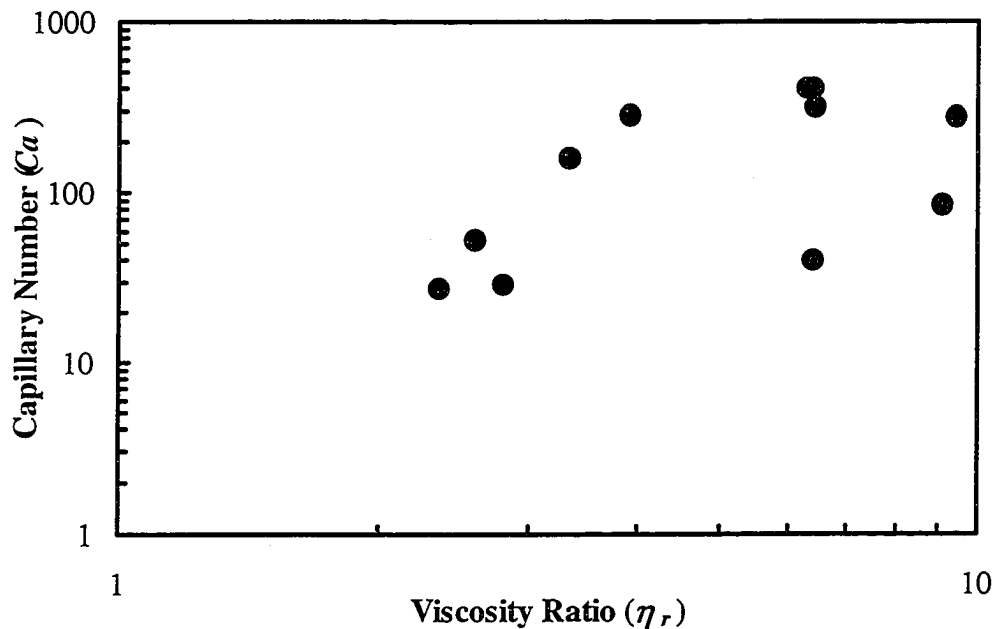


Figure 3.18 Capillary number versus viscosity ratio when parallel breakup occurs. No relationship emerges.

$$S_r = \frac{\text{Breakup Stress}}{\text{Restoring Stress}} = \frac{\eta_m \dot{\gamma} + 2G'_m}{\Gamma/R + 2G'_d} \quad (3.10)$$

where the subscripts d stands for the drop phase and m , the matrix phase.

Figure 3.19 shows a plot of stress ratio at the critical breakup point versus Deborah number for the parallel breakup of the drop. The stress ratio decreases as Deborah number increases. This is due to a faster increase in elasticity of the drop over that of the matrix. The drop forms parallel sheets more easily at higher De , where the drop behaves like a solid. The stress ratio can be correlated with Deborah number using a power law equation with the power law index equals to -0.9 . Figure 3.19 also suggests that, at a particular Deborah number, the drop will not break up below a critical stress ratio.

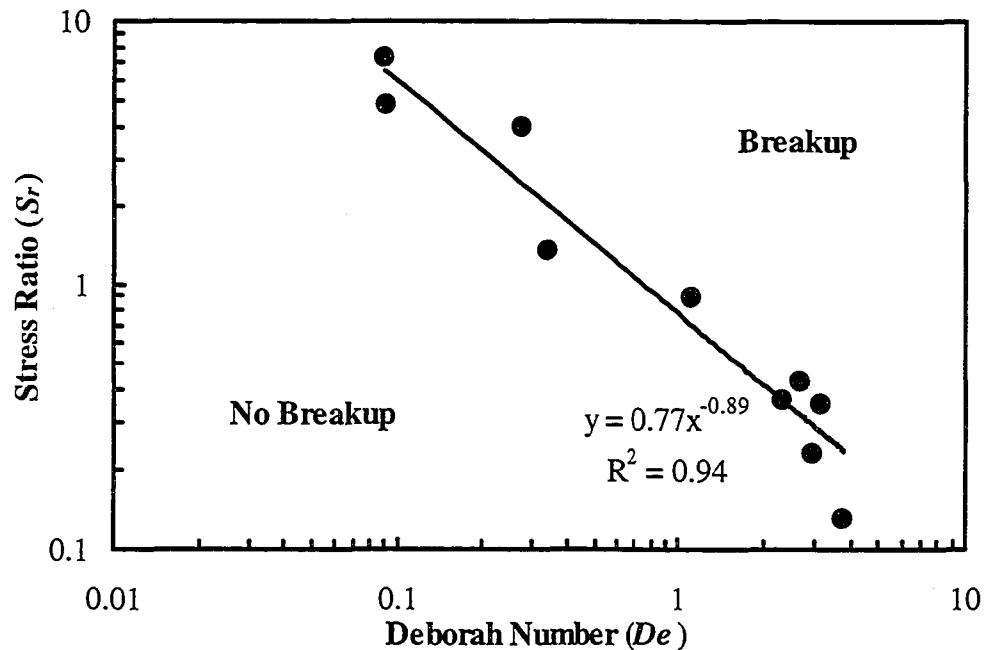


Figure 3.19 Stress ratio versus Deborah number when parallel breakup occurs.

3.3.3 Vorticity Alignment and Breakup

3.3.3.1 Visualization

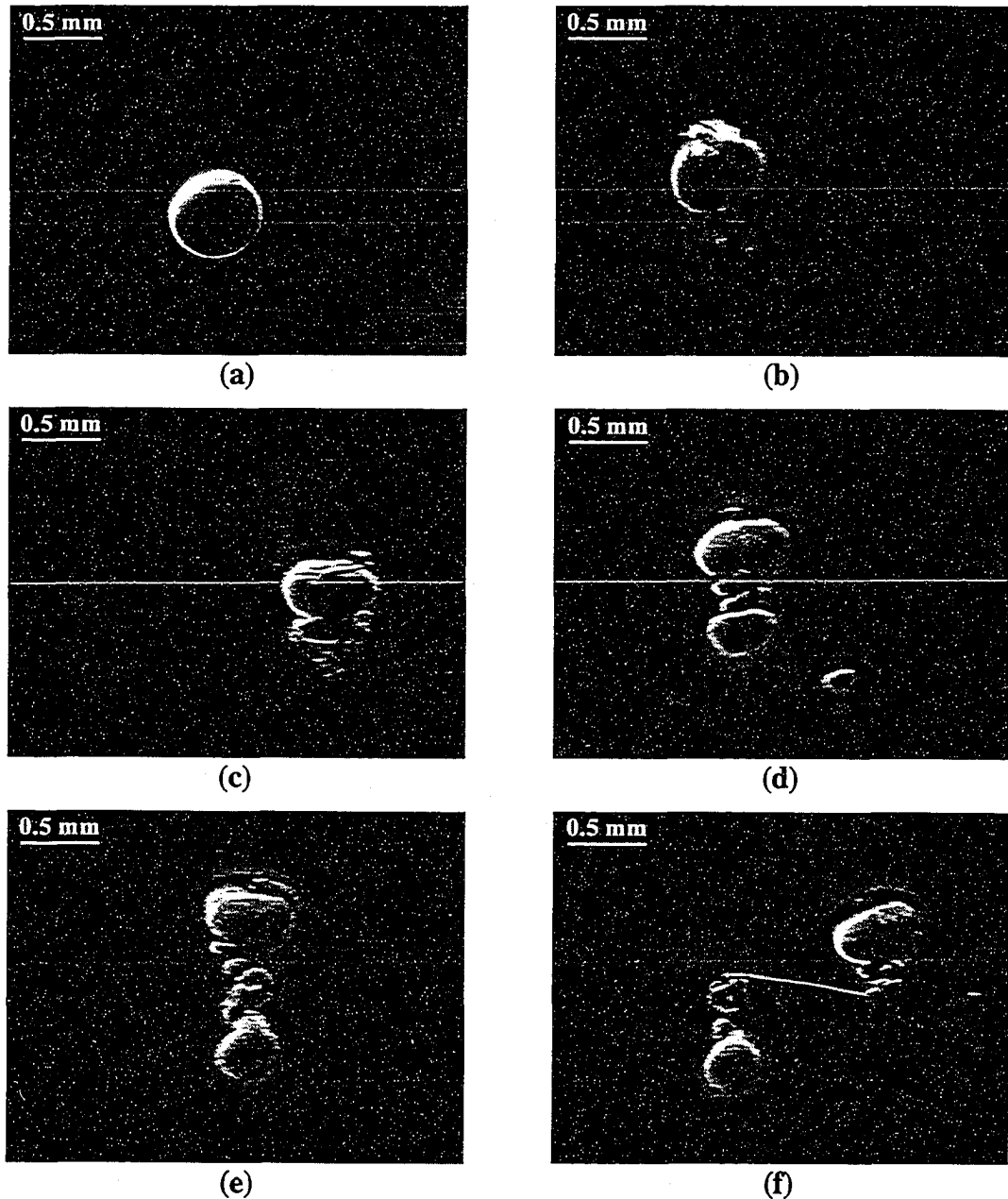


Figure 3.20 Deformation and breakup of a PC3 drop ($D_0 = 0.60$ mm) in a PE1 matrix at 220°C subject to a stepwise shear rate increase. Time and conditions for each figure: (a) $t=72\text{s}$, $\dot{\gamma}=5.4\text{s}^{-1}$, $\eta_r=7.4$; (b) $t=461\text{s}$, $\dot{\gamma}=7.9\text{s}^{-1}$, $\eta_r=7.6$; (c) $t=653\text{s}$, $\dot{\gamma}=7.8\text{s}^{-1}$, $\eta_r=7.6$; (d) $t=874\text{s}$, $\dot{\gamma}=8.6\text{s}^{-1}$, $\eta_r=7.6$; (e) $t=941\text{s}$, $\dot{\gamma}=8.3\text{s}^{-1}$, $\eta_r=7.6$; (f) $t=950\text{s}$, $\dot{\gamma}=8.3\text{s}^{-1}$, $\eta_r=7.6$. Note scale bar. For the micrographs, the flow direction is horizontal and the vorticity direction is vertical.

Figure 3.20 shows a series of images for a PC3 drop ($D_0 = 0.60$ mm) during deformation and breakup in PE1 matrix at 220°C subject to a stepwise shear rate increase. At the shear rates studied, the system has an almost constant viscosity ratio of 8. Figure 3.20a shows that the drop has a nearly spherical shape at a shear rate of 5s^{-1} . As the shear rate is increased to 8s^{-1} , the drop is slightly deformed and twisted, looking like a “heart” as shown in Figure 3.20b (236s at 8s^{-1}). The drop is surrounded by a thin layer of small droplets and small streams of droplets are released from the bottom of the drop and rapidly dispersed into the PE1 matrix. Figure 3.20c (428s at 8s^{-1}) illustrates that the mother drop is slightly stretched along the vorticity direction. A narrow waist develops in the mid-section of the drop, leading to a thin thread at the mid-section of the elongated drop, which is undergoing helicoidal rotation. This thread continues to elongate. Figure 3.20d illustrates that the drop elongates in the vorticity direction and a small droplet can be seen breaking off from the bottom of the mother drop. Figures 3.20e and 3.20f show that the mother drop continuously elongates in the vorticity direction at a shear rate of 8s^{-1} , and finally breaks at the thinnest portion of the elongated thread in the vorticity direction.

The drop is deformed to a shape that is inhomogeneous along the vorticity axis in Figure 3.20. Another kind of vorticity alignment and breakup occurs when the drop stretches to a cylinder in the vorticity direction before breaking up. Figure 3.21 shows an example of a PS cylinder in a PE1 matrix at 190°C . The PS drop is initially deformed to an elliptical shape aligned in the vorticity direction, and it continues to elongate in the vorticity direction to form a cylinder (Figure 3.21a). It then breaks up into two or more smaller cylinders (Figure 3.21b). The broken daughter cylinder is able to break up in the

same way as the mother drop to very small droplets. The small strings seen in Figure 3.9 are undergoing the same type of breakup except that the strings or cylinders in Figure 3.9 are much smaller. It is evident that system properties affect the size scale as this breakup occurs.

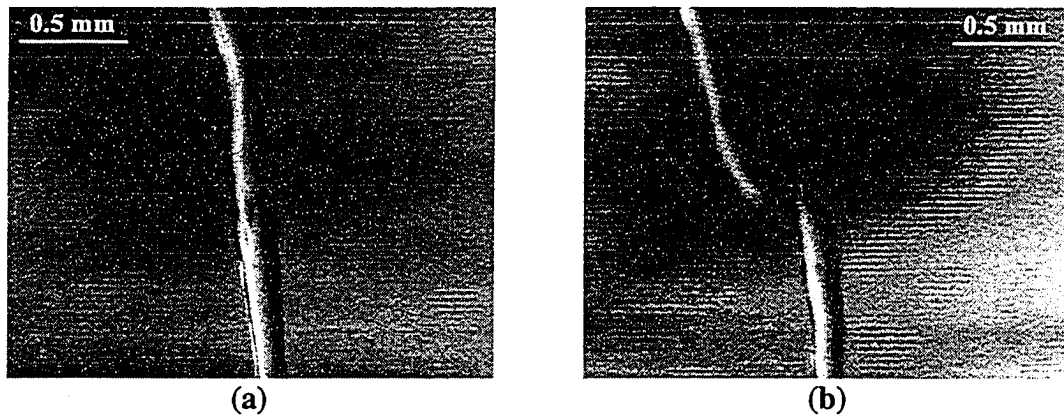


Figure 3.21 Deformation and breakup of a PS drop ($D_0 = 0.59$ mm) in a PE1 matrix at 190°C subject to a stepwise shear rate increase. Time and conditions for each figure: (a) $t=1270\text{s}$, $\dot{\gamma}=6.2\text{s}^{-1}$, $\eta_r=7.8$; (b) $t=1458\text{s}$, $\dot{\gamma}=6.4\text{s}^{-1}$, $\eta_r=7.7$.

3.3.3.2 Discussion

The drop aligns in the vorticity axis and elongates in the same axis and subsequently breaks up. This phenomenon is referred as “vorticity alignment and breakup”. Table 3.7 lists the critical conditions for drop vorticity breakup experiments. The elongation of the drop along the vorticity direction, like the rod climbing Weissenberg phenomenon, is caused by the normal stresses in both drop and matrix phases (Hobbie and Migler, 1999; Migler *et al.*, 1999; Mighri and Huneault, 2001a).

Table 3.7 Critical conditions for vorticity breakup experiments.

System: Matrix/ Drop	Test Temp. (°C)	Initial Drop Diam. (mm)	Critical Shear Rate ($\dot{\gamma}$, s ⁻¹)	Viscosity Ratio (η_r)	Elastic Modulus (G' , Pa)		Stress Ratio (S_r)	Deborah Number (De)
					Drop	Matrix		
PE1/PC3	220	0.60	8.3	7.6	2,390	540	0.80	0.39
PE1/PC3	220	0.66	6.1	7.5	1,450	370	0.97	0.29
PE1/PS	190	0.59	6.4	7.7	11,800	370	0.14	6.40
PE1/PSOX	190	0.51	4.7	12.1	13,800	250	0.09	6.43
PE2/PSOX	190	0.67	3.8	4.4	11,650	190	0.22	5.20

Figure 3.22 shows the shear stress and normal stress growth of PC3 after a sudden increase of shear rate to 1s⁻¹ and 3s⁻¹ at 220°C. The data were obtained in a Rheometrics RMS800 Rheometer with a 25 mm cone and plate fixture, where the cone angle was 0.1 radians and gap was 0.056 mm. The shear stress grows with time and reaches to a steady state value at less than 0.1 s, but the normal stress grows much more slowly, and reaches a steady state value at around 10 s. It is not able to obtain the stress growth at higher shear rate since the maximum shear rate attainable without losing material from the flow cell is 3s⁻¹. However, the stress data at low shear rate illustrate well the transient behavior of shear stress and normal stress at higher shear rate. The viscous force reaches its steady state value rapidly, and the normal forces generated by the drop and the matrix grow over a longer period of time, resulting in the drop growing along the vorticity axis at a later time followed by a continuous drop elongation along the vorticity direction (see Figures 3.20c-e).

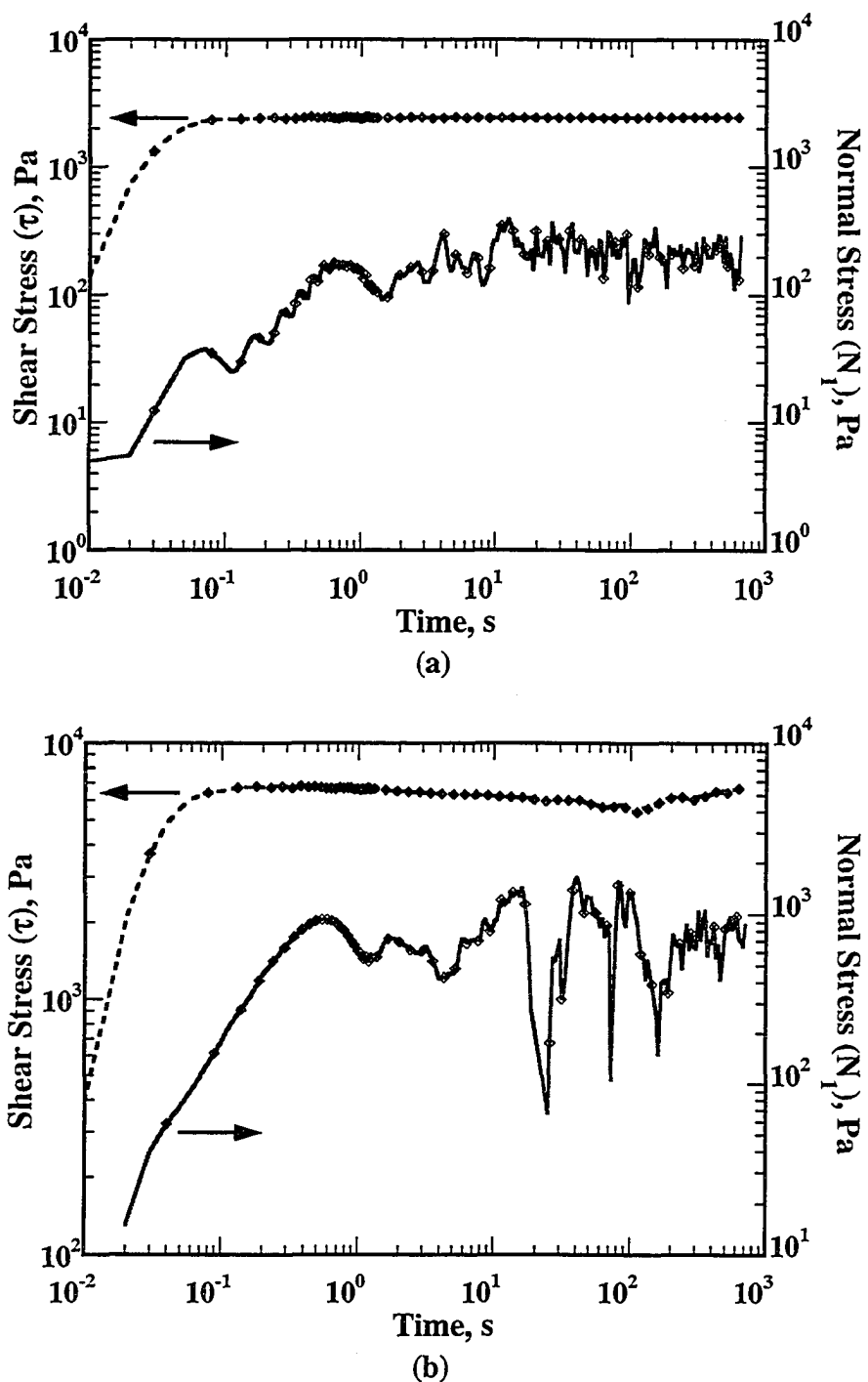


Figure 3.22 Stress growth of PC3 at 220°C and a shear rate of (a) 1s^{-1} and (b) 3s^{-1} .

The drop in Figure 3.20f breaks up at a shear rate of 8.2s^{-1} , where the viscous stress, $\eta_m \dot{\gamma}$, is 2780 N/m^2 , the interfacial stress, $2\Gamma/D$, is 60 N/m^2 , the drop normal

stress is approximate 4780 N/m^2 ($2G'_d$) and the matrix normal stress is around 1080 N/m^2 ($2G'_m$). The drop normal stress is 3.4 times larger than that of the matrix and 0.7 times higher than the viscous stress. The stress ratio, S_r , for this system is 0.80, which means that the drop normal stress overcomes the matrix normal stress and viscous stress. As a result, the drop grows in the vorticity direction. It is found that the drop vorticity alignment and breakup only occurs when S_r is less than 1 and the drop is more elastic than the matrix (see Table 3.7).

3.3.4 Tip Streaming

3.3.4.1 Visualization

Figure 3.23 presents a series of images on drop deformation and breakup in a lower viscosity ratio system, PC1/PE2. The drop has an initial diameter of 0.58 mm and the viscosity ratio, η_r , is approximately 2. Since the system has a low viscosity ratio, the drop is rapidly deformed into an elliptical shape even at a low shear rate of approximately 2s^{-1} (Figure 3.23a). Under the same shear rate, the drop continues to be stretched along the flow direction with small streams of droplets coming off its pointed ends, as shown in Figure 3.23b. This phenomenon, described as “tip streaming”, has been observed experimentally by several researchers for low viscosity ratio Newtonian systems with $\eta_r < 0.1$ (Taylor, 1934; Grace, 1982; Bartok and Mason, 1959; Rumscheidt and Mason, 1961; de Bruijn, 1993).

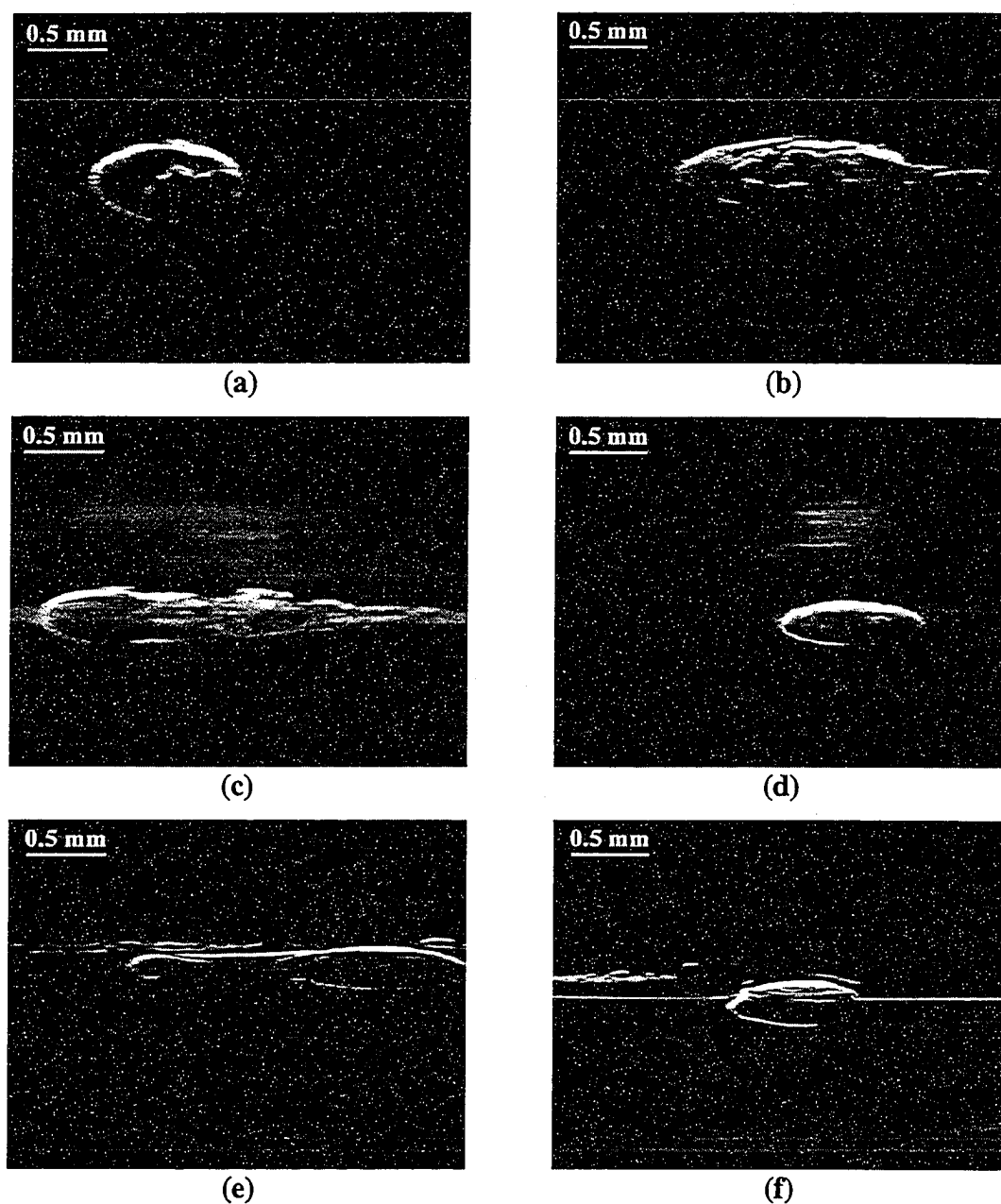


Figure 3.23 Deformation and breakup of a PC1 drop ($D_0 = 0.58$ mm) in a PE2 matrix at 220°C subject to a stepwise shear rate increase. Time and conditions for each figure: (a) $t=13\text{s}$, $\dot{\gamma}=1.8\text{s}^{-1}$, $\eta_r=2.4$; (b) $t=139\text{s}$, $\dot{\gamma}=1.8\text{s}^{-1}$, $\eta_r=2.4$; (c) $t=191\text{s}$, $\dot{\gamma}=1.8\text{s}^{-1}$, $\eta_r=2.4$; (d) $t=376\text{s}$, $\dot{\gamma}=1.8\text{s}^{-1}$, $\eta_r=2.4$; (e) $t=444\text{s}$, $\dot{\gamma}=5.5\text{s}^{-1}$, $\eta_r=2.6$; (f) $t=456\text{s}$, $\dot{\gamma}=5.6\text{s}^{-1}$, $\eta_r=2.6$. Note scale bar. For the micrographs, the flow direction is horizontal and the vorticity direction is vertical.

The deformed drop continues to release small droplets by “tip streaming” until the drop is stretched into a “flattened sausage” or a long slender sheet (Figure 3.23c). The “sausage” is then broken up parallel to the flow direction into smaller daughter droplets and satellites, which continue to be deformed and broken upon further increase in shear rate. Figures 3.23d and 3.23e show one of the daughter droplets undergoing further deformation and breakup. When the shear rate is increased to approximately 6s^{-1} , this elliptical daughter droplet is stretched along the flow direction to a slender sheet, which is subsequently broken along the flow direction again (Figure 3.23e). Figure 3.23f is one of the granddaughter droplets, showing “tip streaming” from its pointed ends. The drops break by “tip streaming” and “parallel breakup” several times until they become very small.

3.3.4.2 Discussion

Figure 3.23 shows that a combined breakup mode rapidly reduces the mother drop from millimeter to micrometer in size via several slender sheet breakups, and thousands of micron sized droplets are released via “tip streaming” from the pointed ends of larger drops. Table 3.8 lists the critical conditions for the occurrence of tip streaming for the polymer systems studied. The critical shear rate is approximately constant, $\sim 2\text{s}^{-1}$, which is lower than that for the other three kinds of breakup. Tip streaming is observed when the viscosity ratio was varied from 0.2 to 4, a ratio value much higher than that for Newtonian systems. This is probably due to viscoelasticity of both the drop and matrix phases.

Table 3.8 Critical conditions for tip streaming experiments.

System: Matrix/ Drop	Test Temp. (°C)	Initial Drop Diam. (mm)	Critical Shear Rate ($\dot{\gamma}$, s ⁻¹)	Viscosity Ratio (η_r)	Elastic Modulus (G', Pa)		Capillary Number (Ca)	Deborah Number (De)
					Drop	Matrix		
PE2/PC1	220	0.58	1.8	2.4	120	270	27	0.09
PE2/PC3	220	0.59	2.1	2.8	250	330	32	0.10
PE1/PS	190	0.52	3.0	9.7	6,220	130	68	3.00
PE2/PS	190	0.45	1.3	3.8	2,670	280	83	1.30
PE2/PA6	230	0.48	2.5	0.2	16	310	39	0.03
PE2/PA6	230	0.50	1.6	0.2	10	180	27	0.02
PE1/PBT	230	0.60	3.1	0.6	40	120	31	0.03

Figure 3.24 shows that stress ratio versus Deborah number for tip streaming. The stress ratio decreases as Deborah number increases and a power law correlation fits the experimental data well, with a power law index of -1.0 . This suggests that the drop elasticity drop promotes tip streaming. Milliken and Leal (1991, 1992) have also shown that the elasticity affects tip streaming in extensional flow fields, and tip streaming occurs even when $\eta_r > 0.5$ if the drop Deborah number is greater than 1. However, results presented in this thesis suggest that drop elasticity facilitates polymer drop tip streaming even in a simple shear flow field. Tip streaming occurs at viscosity ratios from 0.2 to 10, whereas tip streaming will not occur for a clean Newtonian drop at $\eta_r > 0.1$.

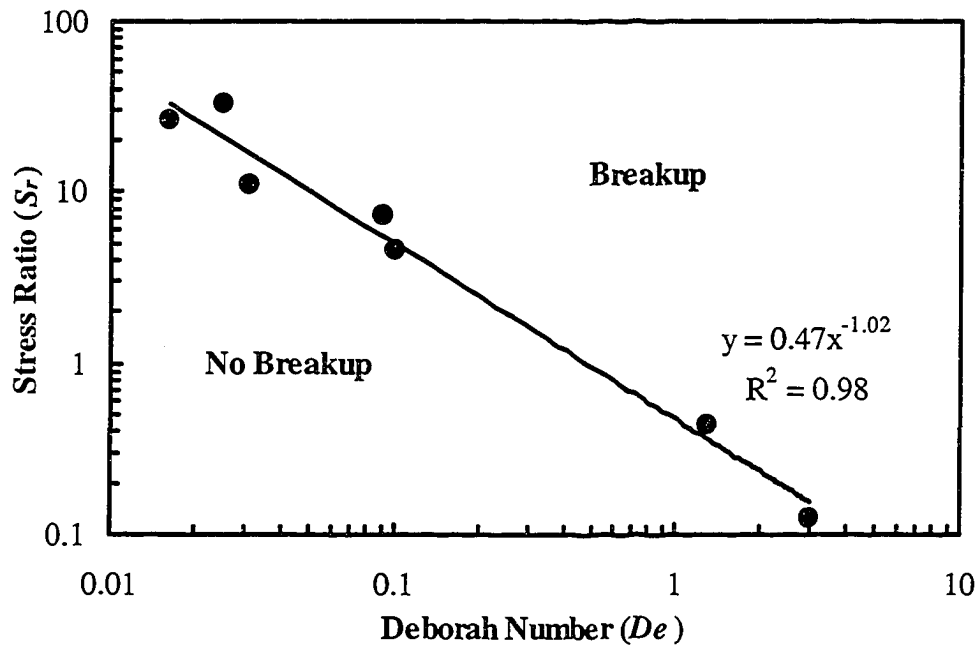


Figure 3.24 Stress ratio versus Deborah number when tip streaming occurs.

3.3.5 Summary on Drop Deformation and Breakup Mechanisms

Four kinds of breakup modes for polymer drops in a polymer matrix under simple shear have been shown: erosion (3.3.1), parallel breakup (3.3.2), vorticity alignment and breakup (3.3.3) and tip streaming (3.3.4). Figure 3.25 summarizes the breakup mechanisms observed for polymer drop in simple shear. Drop breakup occurs over the full range of viscosity ratio studied from 0.2 to 60, contrary to empirical correlations and theoretical predictions of drop breakup in Newtonian systems (Taylor, 1932, 1934; Grace, 1982).

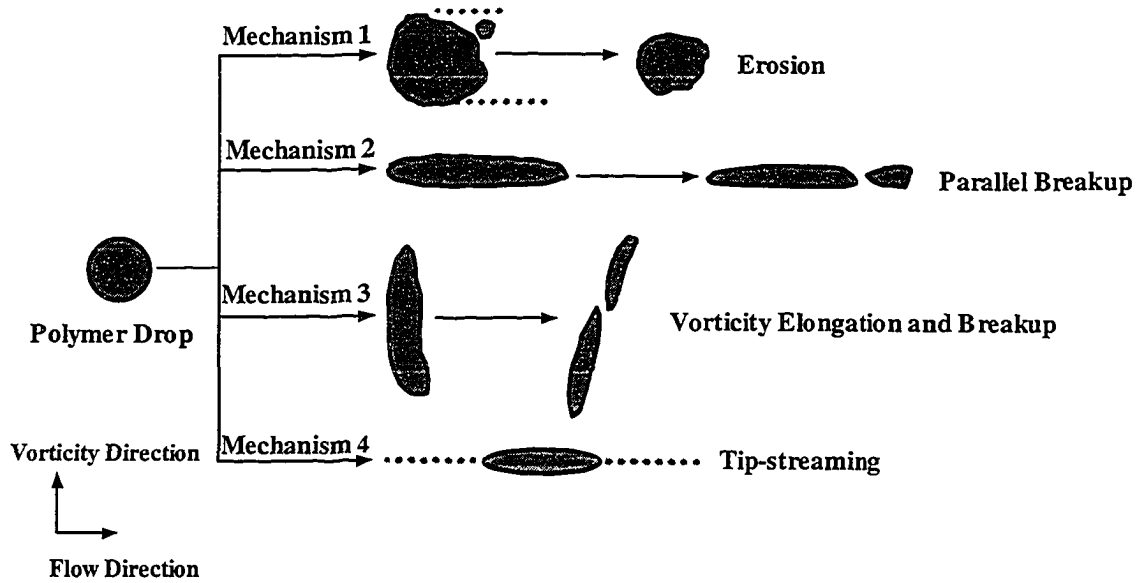


Figure 3.25 Polymer drop breakup mechanisms subject to simple shear flow.

Figure 3.26 shows a plot of critical Capillary number versus viscosity ratio for drop breakup in simple shear flow. The solid lines correspond to Grace's (1982) correlation for Newtonian drop breakup, and the data points are from the experiments on polymer drops. It is clear from this plot that a polymer drop breaks up at higher Capillary number than a Newtonian drop. Although tip streaming occurs at a lower Ca , Ca is still much higher than that for Newtonian drop tip streaming and drop fracture. The other important discovery is that a polymer drop breaks up at a viscosity ratio even higher than 3.5, which is impossible for a Newtonian system. In the literature, the Newtonian correlations have been extended to polymer systems; however, based on the results presented in this thesis, it is evident that the Newtonian results are not appropriate for polymer blends.

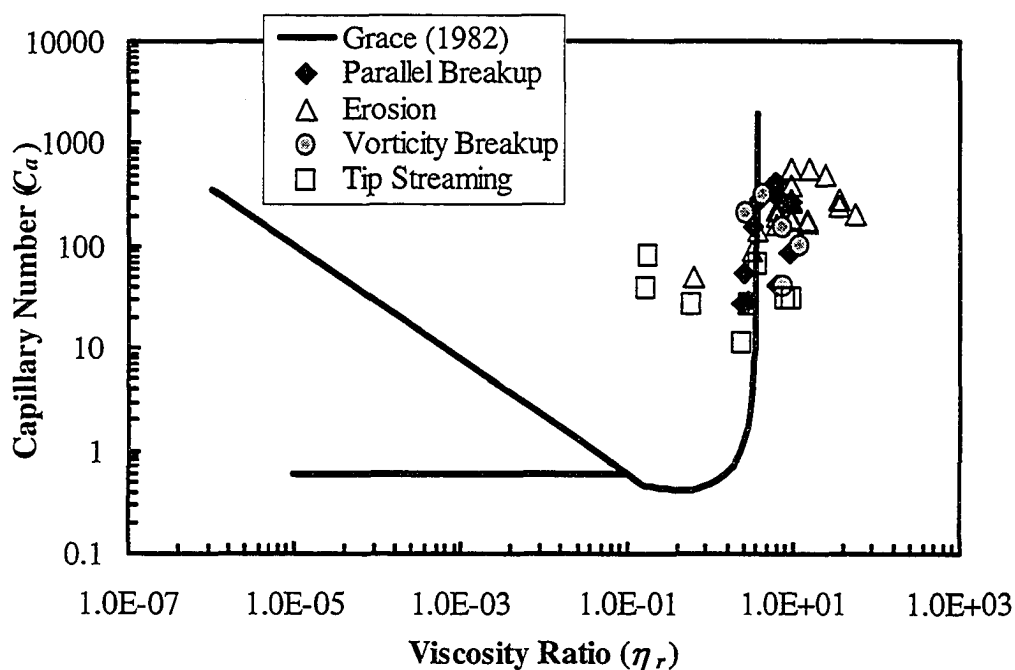


Figure 3.26 Capillary number versus viscosity ratio for drop breakup subject to simple shear flow. The solid lines are experimental correlations from Grace (1982) for Newtonian drops and the data points correspond to polymer drop breakup.

It has been shown that the critical shear rate of polymer drop erosion relates with viscosity ratio (3.3.1.3). During the experiments, when the shear rate is increased stepwise, different drop breakup occurs. Figure 3.27 shows the critical shear rate versus viscosity ratio for different drop breakup mechanisms under simple shear flow. Tip streaming occurs at a lowest shear rate, around $2\text{--}3\text{s}^{-1}$ at $0.2 < \eta_r < 10$. Erosion takes place for a wide viscosity ratio range of polymer systems ($0.5 < \eta_r < 60$). Parallel breakup happens at a lower shear rate than erosion when $\eta_r < 6$; the shear rate for parallel breakup increases sharply with viscosity ratio and at $6 < \eta_r < 10$, parallel breakup occurs at high shear rates; no parallel breakup observed when $\eta_r > 10$ since the highest shear rate achievable is 50s^{-1} for current Couette cell, which may be not high

enough to induce this kind of breakup at high viscosity ratios. Vorticity breakup occurs at $4 < \eta_r < 12$ and at a shear rate that is higher than that for tip streaming and lower than that for erosion.

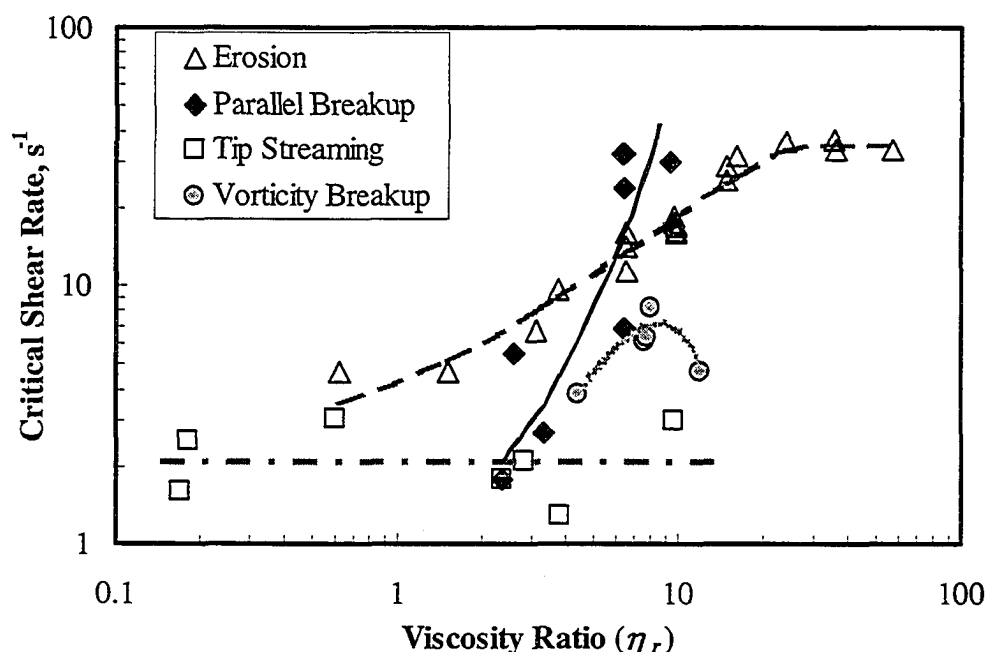


Figure 3.27 Critical shear rate for polymer drop breakups at different viscosity ratios subject to simple shear flow. The lines are guides to the eyes: parallel breakup —, erosion — —, vorticity breakup ·····, tip streaming - · - ·.

Polymer drop breakup mechanisms: erosion, parallel breakup and vorticity alignment, are unique. Though tip streaming has been observed in Newtonian systems, polymer drop breakup through tip streaming occurs even when the viscosity ratio is higher than 3.5. The different breakup phenomena observed for polymer systems may be due to several reasons including the shear-thinning characteristic of polymer melts, the existence of normal stresses in the drop and in the matrix, and the extremely high stresses in polymer systems due to the very high melt viscosity.

Normal stresses are found to play an important role in polymer drop deformation and breakup. The stress ratio (S_r) correlates well with Deborah number (De) for parallel breakup (3.3.2) and tip streaming (3.3.4). Drop vorticity alignment and breakup are also related to the normal stresses existing in polymers. It appears that even for erosion, normal stress may be important. This can be proved by a careful examination of erosion data (Figures 3.6 and 3.7): the drop deforms to a diamond shape and is later stretched in the vorticity direction. Therefore, the stress ratio and Deborah number may be important to characterize polymer drop breakup.

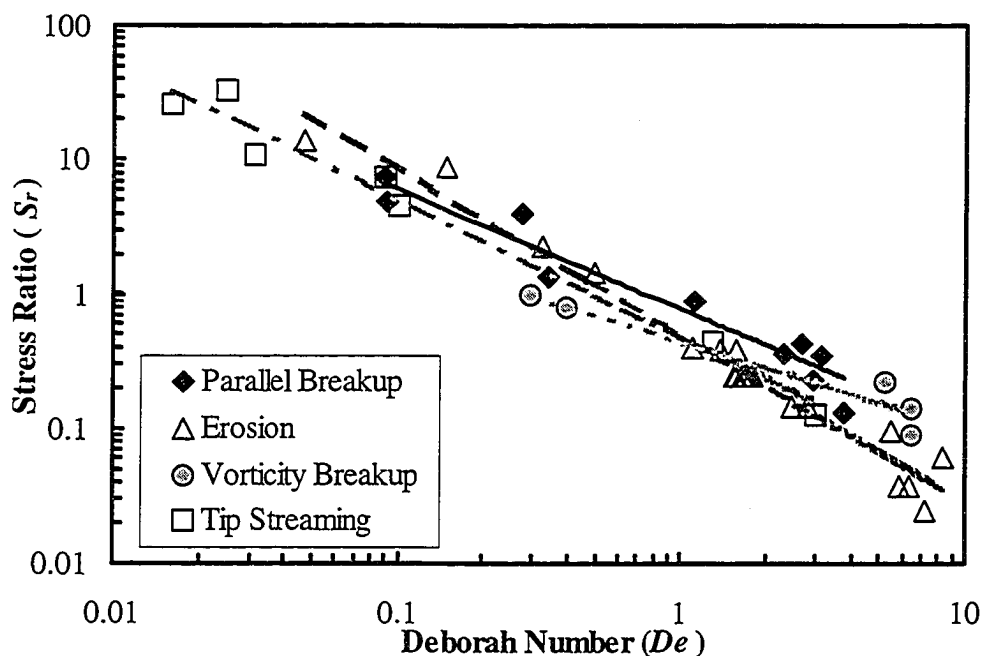


Figure 3.28 Stress ratio versus Deborah number for polymer drop breakup subject to simple shear flow. The lines drawn are the trends of breakups: parallel breakup —, erosion — —, vorticity breakup ·····, tip streaming - · - ·.

Figure 3.28 plots the experimental data for the four different breakups. For each breakup, a trend line is used. When $De < 0.2$, drop breakup sequence with the increase

of stress ratio is tip streaming and then erosion; when $0.2 < De < 1.0$, drop breakup starts with vorticity breakup, then tip streaming and erosion, and finally, parallel breakup; when $De > 1.0$, drop breaks up through tip streaming and erosion first, and then vorticity breakup, and last parallel breakup. Figure 3.28 also shows that at higher De , polymer drop breaks up at a lower S_r . That is, the drop elasticity promotes drop breakup and the matrix elasticity resists drop breakup.

3.4 CONCLUSIONS

Four breakup mechanisms were visualized for polymer drops in a polymer matrix undergoing simple shear flow generated by a transparent Couette device: (1) erosion – thin ribbons and streams of droplets peeled off from the mother drop surface; (2) parallel breakup – a drop abruptly stretched to a sheet or a flat sausage in the flow direction and subsequently broke up parallel to the flow direction; (3) vorticity alignment and breakup – a drop that aligned, elongated and broke up along the vorticity axis; and (4) tip streaming – streams of small droplets came off the pointed mother drop. This is the first time that drop breakup mechanisms (1), (2) and (3) have been visualized in polymer systems and they are unique to viscoelastic systems. Though tip streaming is also observed for Newtonian drops, it can occur in polymer systems at $\eta_r > 0.1$. Despite the fact there is an abundance of literature indicating that there is no drop breakup above $\eta_r > 3.5$, drop breakup was observed even at viscosity ratios as high as 60. The rule that no drop breaks up in simple shear flow at $\eta_r > 3.5$ does not hold for polymer systems.

Sheet formation was observed during drop deformation and breakup: sheets form at the surface of the mother drop at the beginning of the drop surface erosion and the

entire drop deforms into a sheet during parallel drop breakup. Sheet breakup provides an efficient and rapid reduction in the dimension of the drop size since the sheets are on the order of 1 μm thick, and when they break up, they create drops 1,000 times smaller than the initial drop size.

Surface erosion is one of the primary breakup mechanisms for polymer systems: the mother drop slowly shrinks by giving off streams of sheets, cylinders and daughter droplets. The daughter droplets are able to break up again until a size on the order of microns is achieved. Pseudo-first order decay kinetics was applied to describe the drop erosion phenomenon. The onset time and the apparent decay rate for PE2/PC5 system at 230°C show that the kinetic model is appropriate for PC drop erosion in PE matrix.

A polymer drop may break up through many mechanisms during shearing. In general, tip streaming occurs first at lower shear rate for systems with $0.2 < \eta_r < 10$ and $0.02 < De < 3$; erosion takes place at $0.6 < \eta_r < 60$ and $0.05 < De < 9$; parallel breakup is seen at $2 < \eta_r < 10$ and $0.09 < De < 4$, and it occurs normally at a higher shear rate than tip streaming and erosion; vorticity alignment and breakup occurs for $4 < \eta_r < 12$, $0.3 < De < 6.5$ and $S_r < 1$. It is important to note that the equipment was limited to a shear rate less than 50 s^{-1} , and therefore, it may not be able to reach a high enough shear rate to see parallel breakup in higher viscosity ratio systems. However, parallel breakup is expected at higher η_r also based on results from extrusion and batch mixing.

In all the breakup mechanisms, normal stress plays an important role. The stress ratio (S_r) between the breakup stress, which was made up of the viscous stress and matrix normal stress, and the restoring stress, which was made up of the interfacial stress and drop normal stress, decreases with the increased drop Deborah number (De). The stress

ratio decreases with Deborah number, that is, the drop is easier to break up if it has a higher De .

3.5 REFERENCES

- Bentley, B.J. *PhD thesis*, California Institute of Technology, 1985.
- Bentley, B.J.; Leal, L.G. *J. Fluid Mech.* **1986**, *167*, 219-240.
- Briscoe, B.J.; Lawrence, C.J.; Mietus, W.G.P. *Adv. Colloid Interface Sci.* **1999**, *81*, 1-17.
- Chapleau, N.; Favis, B.D.; Carreau, P.J. *Polymer* **2000**, *41*, 6695-6698.
- Chen, H.; Nandakumar, K.; Sundararaj, U. *manuscript in preparation*, 2004a.
- Chen, H.; Nandakumar, K.; Sundararaj, U. *Polym. Eng. Sci.* **2004b**, *44*, 1258-1266.
- de Bruijn, R.A. *Chem. Eng. Sci.* **1993**, *48*, 277-284.
- Elemans, P.H.M.; Janssen, J.M.H; Meijer, H.E.H. *J. Rheol.* **1990**, *34*, 1311-1325.
- Elmendorp, J.J.; Van der Vegt A.K. In *Two Phase Polymer Systems*; Utracki, L.A. Ed.; Hanser Publishers: New York, 1991, p.166-184.
- Favis, B.D.; Chalifoux, J.P. *Polym. Eng. Sci.* **1987**, *27*, 1591-1600.
- Flumerfelt, R.W. *Ind. Eng. Chem. Fundam.* **1972**, *11*, 312-318.
- Grace, H.P. *Chem. Eng. Commun.* **1982**, *14*, 225-277.
- Hobbie, E.K.; Migler, K.B. *Phys. Rev. Lett.* **1999**, *82*, 5393-5396.
- Kao, S.V.; Mason, S.G. *Nature* **1975**, *253*, 619-621.
- Karam, H.J.; Bellinger, J.C. *I & EC Fundam.* **1968**, *7*, 576-581.
- Kenley, R.A.; Lee, M.O.; Mahoney, T.R.; Sanders, L.M. *Macromolecules* **1987**, *20*, 2398-2403.

- Levitt, L.; Macosko, C.W.; Pearson, S.D. *Polym. Eng. Sci.* **1996**, *36*, 1647-1655.
- Lin, B.; Mighri, F.; Huneault, M.A.; Sundararaj, U. *Macromol. Rapid Commun.* **2003a**, *24*, 783-788.
- Lin, B.; Sundararaj, U.; Mighri, F.; Huneault, M.A. *Polym. Eng. Sci.* **2003b**, *43*, 891-904.
- Lin, B.; Sundararaj, U. *Polymer* **2004**, *45*, 7605-7613.
- Lindt, J.T.; Ghosh, A.K. *Polym. Eng. Sci.* **1992**, *32*, 1802-1813.
- Macosko, C.W. *Rheology: Principles, Measurements, and Applications*; Wiley: New York, 1993; p189.
- Mighri, F.; Carreau, P.J.; Ajji, A. *J. Rheol.* **1998**, *42*, 1477-1490.
- Mighri, F.; Huneault, M.A. *J. Rheol.* **2001a**, *45*, 783-797.
- Mighri, F.; Huneault, M.A. *3rd Pacific Rim Conference on Rheology*, Paper No. 005, 2001b.
- Migler, K.B.; Hobbie, E.K.; Qiao, F. *Polym. Eng. Sci.* **1999**, *39*, 2282-2291.
- Migler, K.B. *J. Rheol.* **2000**, *44*, 277-290.
- Milliken, W.J.; Leal, L.G. *J. Non-Newtonian Fluid Mech.* **1991**, *40*, 355-379.
- Milliken, W.J.; Leal, L.G. *J. Non-Newtonian Fluid Mech.* **1992**, *42*, 231-239.
- Milliken W.J.; Stone H.A.; Leal L.G. *Phys. Fluids A* **1993**, *5*, 69-79.
- Milliken W.J.; Leal L.G. *J. Colloid Interface Sci.* **1994**, *166*, 275-285.
- Potente, H.; Bastian, M.; Bergemann, K.; Senge, M.; Scheel, G.; Winkelmann, Th. *Polym. Eng. Sci.* **2001**, *41*, 222-231.
- Powell, R.L.; Mason, S.G. *AIChE J.* **1982**, *28*, 286-293.
- Rallison, J.M. *Annu. Rev. Fluid Mech.* **1984**, *16*, 45-66.

- Ramaswamy, S.; Leal, L.G. *J. Non-Newtonian Fluid Mech.* **1999**, *85*, 127-163.
- Rumscheidt, F.D.; Mason, S.G. *J. Colloid Interface Sci.* **1961**, *16*, 238-261.
- Rwei, S.P.; Manas-Zloczower, I.; Feke, D.L. *Polym. Eng. Sci.* **1990**, *30*, 701-706.
- Rwei, S.P.; Manas-Zloczower, I.; Feke, D.L. *Polym. Eng. Sci.* **1991**, *31*, 558-562.
- Scott, C.E.; Macosko, C.W. *Polym. Bull.* **1991**, *26*, 341-348.
- Scott, C.E.; Macosko, C.W. *Polymer* **1995**, *36*, 461-470.
- Stone, H.A. *Annu. Rev. Fluid Mech.* **1994**, *26*, 65-102.
- Sundararaj, U.; Macosko, C.W.; Rolando, R.J.; Chan, H.T. *Polym. Eng. Sci.* **1992**, *32*, 1814-1823.
- Sundararaj, U.; Dori, Y.; Macosko, C.W. *SPE ANTEC Tech. Papers* **1994**, *52*, 2448-2451.
- Sundararaj, U.; Dori, Y.; Macosko, C.W. *Polymer* **1995**, *36*, 1957-1968.
- Taylor, G.I. *Proc. R. Soc. London, Ser. A* **1932**, *138*, 41-48.
- Taylor, G.I. *Proc. R. Soc. London, Ser. A* **1934**, *146*, 501-523.
- Torza, S.; Cox, R.G.; Mason, S.G. *J. Colloid Interface Sci.* **1972**, *38*, 395-411.
- Tretheway, D.C.; Leal, L.G. *AIChE Journal* **1999**, *45*, 929-937.
- Utracki, L.A.; Shi, Z.H. *Polym. Eng. Sci.* **1992**, *32*, 1824-1833.
- van Krevelen, D.W. *Properties of Polymers*, 2nd ed.; Elsevier Scientific Company: Amsterdam, 1976.
- Vanoene, H. *J. Colloid Interface Sci.* **1972**, *40*, 448-467.
- Varanasi, P.P.; Ryan, M.E.; Stroeve, P. *Ind. Eng. Chem. Res.* **1994**, *33*, 1858-1866.

Willemse, R.C.; Ramaker, E.J.U.; van Dam, J.; de Boer, A.P. *Polymer* **1999**, *40*, 6651-6659.

Wu, S.H. *Polym. Eng. Sci.* **1987**, *27*, 335-343.

Wu, S.H. In *Polymer Handbook*; Brandrup, J.; Immergut, E.H. Eds., 3rd ed.; John Wiley & Sons: New York, 1989, p.411-434.

Chapter 4

Effect of Pre-made Compatibilizer and in-situ Compatibilization on Polymer Drop Deformation and Breakup Mechanisms in Couette Cell

4.1 INTRODUCTION

Polymer blends are composed of at least two polymers. Blends provide an effective and economical way to create new materials (Elmendorp and Van der Vegt, 1991; Utracki and Shi, 1992). Most polymer pairs are immiscible, and they need to be compatibilized (Utracki, 2002). Compatibilization is a process that modifies the interfacial properties of immiscible blends and stabilizes the desired morphology; therefore, it can affect the final properties of the blends. There are two basic compatibilization methods: one way is addition of a third component, a pre-made compatibilizer, into a polymer blend; another method is reactive compatibilization, or in-situ compatibilization, by chemical reaction between two polymeric components during blending (Utracki, 2002).

Studies on how compatibilizer affects drop deformation and breakup are scarce in the literature. Levitt and Macosko (1999) sheared polypropylene (PP) drops and poly(methyl methacrylate) (PMMA) drops inside polystyrene (PS) matrix with a counter-rotating parallel plate device and found that drop cross-sectional area increased when a block copolymer (10 wt% based on the drop phase) was added. They attributed this increase to either a reduction in interfacial tension or a reduction in slip. It might also be due to a combination of these two effects and a gradient in interfacial tension. van Puyvelde *et al.* (2002) studied model blends composed of 1% polyisobutene (PIB) in

polydimethylsiloxane (PDMS) with PIB-PDMS diblock copolymer in a shearing cell. They observed that the PIB drop with 2% copolymer showed pointed ends in the flow direction during shearing and ascribed this to the accumulation of block copolymer at the drop tips. They suggested that this accumulation resulted in a lower local interfacial tension giving a higher local curvature to balance the pressure jump across the interface. This is consistent with rheological results (Velankar *et al.*, 2004). van Puyvelde *et al.* (2002) also found that the PIB drop with 10% copolymer had almost no deformation. They explained that this was due to the strong Marangoni stress, which immobilized the interface at high surface coverage. More recently, Jeon and Macosko (2003) visualized block copolymer distribution on a sheared polymer drop by using a fluorescent labeled poly(styrene-*b*-methacrylate) (NBD-PS-*b*-PMMA). They observed higher block copolymer concentrations at the drop edges and tips, which was thought to be due to convection of block copolymer induced by shear flow.

It has been thought that the role of the compatibilizers (or surfactants in emulsions) (Milliken *et al.*, 1993; Milliken and Leal, 1994; Tretheway and Leal, 1999) is to lower the interfacial tension and therefore, to facilitate drop breakup. For Newtonian systems, in the presence of compatibilizers or surfactants, drop deformation increased at a given Capillary number (Ca , the ratio of the viscous stress to the interfacial stress). With compatibilizer, the critical Capillary number for drop deformation and breakup decreased, and tip streaming was observed. Tip streaming is a phenomenon where streams of small droplets are released in the flow direction from the tips of a pointed drop (Chapter 3). However, some other studies (Sundararaj and Macosko, 1995; Hu *et al.*, 2000; Velankar *et al.*, 2001) showed that the compatibilized drops were more stable

against breakup and coalescence. Therefore, the effects of compatibilizers on drop breakup are still not well understood.

An important parameter often used when characterizing drop breakup is the viscosity ratio. Viscosity ratio, η_r , is a ratio of the drop phase viscosity to the matrix phase viscosity. It has been shown (Lin *et al.*, 2002, 2003a, 2003b, 2003c; Lin and Sundararaj, 2004) that polymer drops can break up at a viscosity ratio higher than 3.5, a phenomenon impossible in Newtonian systems. Four kinds of breakup mechanisms have been observed in polymer systems, namely:

1. “Erosion” – surface erosion (Potente *et al.*, 2001; Lin *et al.*, 2002, 2003b) from the drop in the form of thin ribbons and streams of small droplets (Lin *et al.*, 2002, 2003b);
2. “Parallel breakup” – the drop breaks after being stretched into a thin sheet (Scott and Macosko, 1991, 1995; Lindt and Ghosh, 1992; Sundararaj *et al.*, 1992, 1994, 1995, 1996; Lin *et al.* 2003a, 2003c) or a flat sausage (Lin *et al.* 2003c) parallel to the flow direction (Lin *et al.* 2003a, 2003c);
3. “Vorticity elongation and breakup” – the drop breaks after being elongated in the vorticity direction (Hobbie and Migler, 1999; Migler *et al.*, 1999; Migler, 2000; Mighri and Huneault, 2001; Lin *et al.*, 2003c);
4. “Tip streaming” (Lin *et al.*, 2003c) – a well-known breakup mechanism even in Newtonian systems.

It should be mentioned that only “tip streaming” is observed in Newtonian systems (Taylor, 1934; Bartok and Mason, 1959; Rumscheidt and Mason, 1961; Grace, 1982; de Bruijn, 1993; Milliken *et al.*, 1993; Milliken and Leal, 1991, 1992, 1994; Tretheway and

Leal, 1999). All of the other three mechanisms are unique to viscoelastic systems. In this chapter, the effects of pre-made compatibilizer and in-situ reactive compatibilization on polymer drop deformation and breakup in simple shear flow under quasi-equilibrium conditions are reported. The polymer drops used have a diameter of 0.5 ~ 1.0 mm.

4.2 EXPERIMENT

4.2.1 Materials and Preparation

The polymer systems consisted of drops of polystyrene (PS), polystyrene oxazoline (PSOX) and Nylon 6 (PA6) inside a polyethylene (PE) matrix. Two grades of PE were used, PE1 and PE2. Diblock copolymer, polystyrene-block-polyethylene (P(S-b-E)) was used as compatibilizer for the PE/PS system. For the PE/PSOX and PE/PA6 systems, polyethylene maleic anhydride (PEMA) was added into PE matrix to generate reactive systems. Figure 4.1 shows the reaction between PSOX and PEMA and also between PA6 and PEMA. The P(S-b-E) copolymer came in powder form and was synthesized by researchers at University of Minnesota. It is a symmetric block copolymer with a molecular weight (M_n) of 100,000-100,000 g/mol (Lyu *et al.*, 2002).

All the other polymers were obtained in pellet form from commercial sources. Table 4.1 lists some properties and sources of the homopolymers used. Dynamic rheological characterizations were performed using a Rheometrics RMS800 Rheometer with a 25 mm parallel plate fixture operated at 10% strain. The complex viscosity and elastic modulus for PS, PSOX, PA6 and PE were shown in Figures 3.2c and 3.2d. The PS and PA6 spherical drops were specially prepared in silicone oil. The detailed procedure can be found in Lin *et al.* (2003b; see also Chapter 2). To avoid reaction of the oxazoline

group during the heating process of spherical drop preparation, the PSOX was added to the Couette cell as non-spherical chunks directly after cutting the pellets. The interfacial tension between PE and PS at 190°C is 4.9 mN/m (Elemans *et al.*, 1990) and between PE and PA6 at 230°C is 15.2 mN/m (Chapleau *et al.*, 2000).

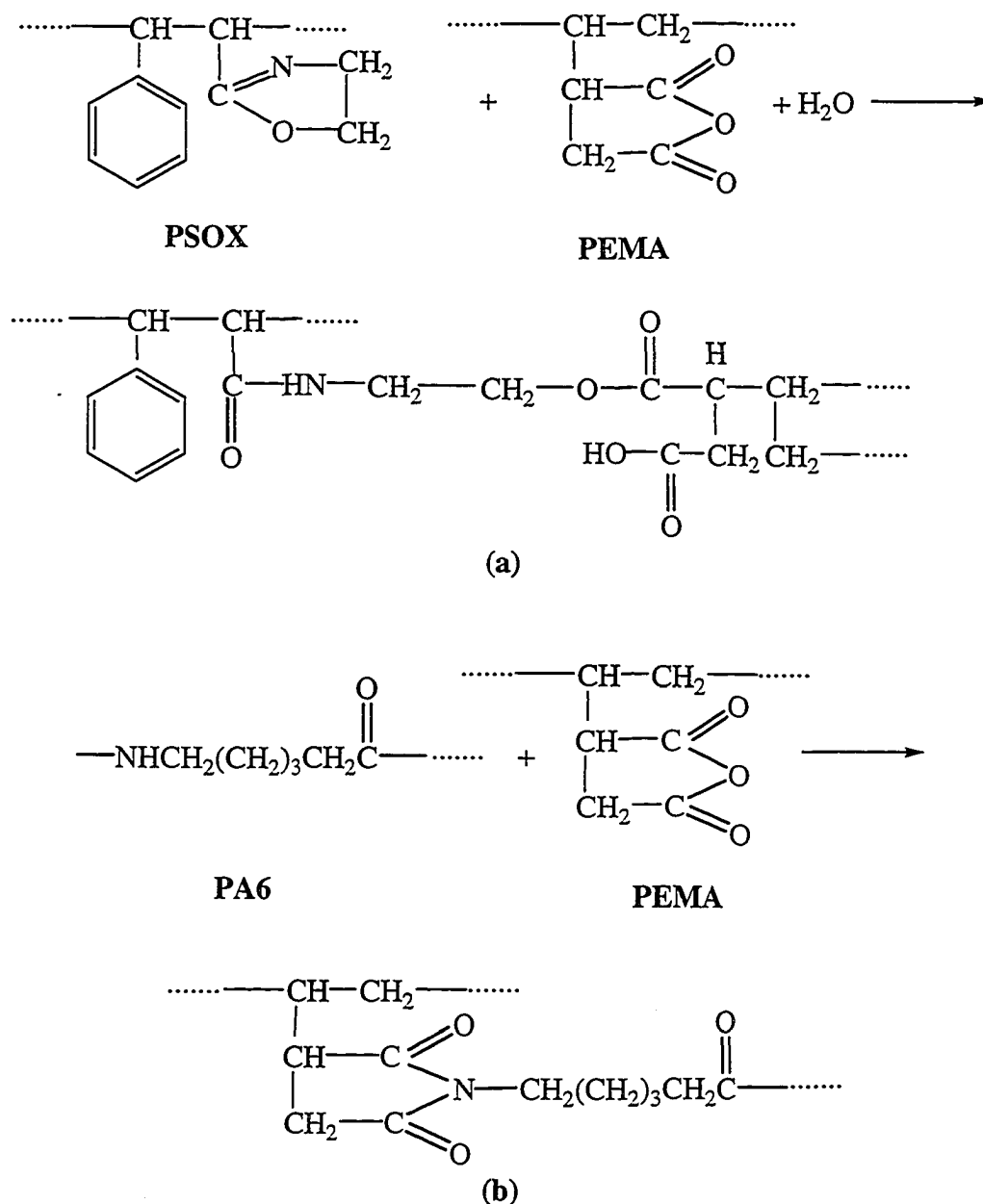


Figure 4.1 (a) Cross-linking reaction between PSOX and PEMA; (b) Graft reaction between PA6 and PEMA.

Table 4.1 Properties of homopolymers used.

Polymer (Abbreviation)	Source (Commercial Name)	Molecular Weight (M_w , g/mol)	Viscosity at $\dot{\gamma}=1s^{-1}$ (Pa·s)	Elastic Modulus at $\dot{\gamma}=1s^{-1}$ (Pa)	Function-ality ^a
Polystyrene (PS)	Dow (Styron 666D)	160,000	4,500 (190°C)	1,300 (190°C)	
Polystyrene Oxazoline (PSOX)	Dow	160,000	8,300 (190°C)	3,370 (190°C)	1% Oxazoline
Nylon 6 (PA6)	Scientific Polymer Products	10,000	170 (230°C)	7 (230°C)	
Polyethylene (PE1)	Petromont (DMDA-8920)	53,400	450 (190°C) 370 (230°C)	30 (190°C) 20 (230°C)	
Polyethylene (PE2)	Petromont (DMDB-8907)	68,900	1,400 (190°C) 1080 (230°C)	210 (190°C) 160 (230°C)	
Polyethylene Maleic Anhydride (PEMA)	DuPont (Fusabond MB265D)	48,400	650 (190°C) 510 (230°C)	60 (190°C) 70 (230°C)	1% MAH

a. Provided by supplier.

4.2.2 Experimental Setup

The specially designed transparent Couette flow cell consists of two counter-rotating concentric cylinders. A detailed description of the setup can be found elsewhere (Mighri and Huneault, 2001; Chapter 3). In the present Couette setup, the visualization plane is the plane containing the flow direction and the vorticity axis.

4.2.3 Experimental Procedure

At the beginning of each run, the Couette cell was preheated to 125°C. The gap of the Couette cell was then filled with PE pellets premixed with a small amount of thermal stabilizer (Irganox 1076), from Ciba Chemicals, and 4 to 6 PS or PA6 spheres or PSOX chunks were inserted carefully into the PE matrix. The drops with copolymer, P(S-b-E), were prepared in two ways. One method was to premix 1 wt% or 5 wt% P(S-b-E) with PS in an APAM miniature mixer (Breuer *et al.*, 2004) at 190°C and 50 rpm, and then spherical drops were made in heated silicone oil. The other method was to insert a PS drop dry coated with P(S-b-E) into a PE pellet. The maximum or saturation interfacial coverage, Σ_{\max} , for 100,000-100,000 g/mol P(S-b-E) is estimated to be 0.15 molecule/nm², based on $\Sigma_{\max} = 0.25$ molecule/nm² for 20,000-20,000 g/mol P(S-b-E) (Lyu *et al.*, 2002) and the scaling rule $\Sigma_{\max} \sim M_n^{-1/3}$ (Bates and Fredrickson, 1999). This saturation interfacial coverage corresponds to only 0.06 wt% of copolymer for a 0.5 mm diameter PS drop if all the copolymer distributes at the drop surface without micelle formation. When PEMA was used, the drop phase was inserted into a PEMA pellet first before it was added to the Couette apparatus.

Complex viscosity and elastic modulus were also measured for PS+1%P(S-b-E) and PS+5% P(S-b-E). The results for PS+1%P(S-b-E), PS+5% P(S-b-E) and PS are shown in Figure 4.2. It should be noted that both the viscosity and elastic modulus of PS+5% P(S-b-E) are lower than those of PS (Figure 4.2), but the viscosity and elastic modulus of PS+1% P(S-b-E) are greater than those of PS. According to Jones *et al.* (1999), a possible reason for the viscosity increase or decrease is the extent of penetration

of the homopolymer matrix into the copolymer micelles. If the micelles act as inert spheres where the micellar corona behaves as a dry brush, the viscosity increases. On the other hand, if the micelles work as plasticizers where the corona becomes “wet”, the viscosity decreases. In this chapter, the measured rheology data is used for PS premixed with P(S-b-E) and the data of PS coated with P(S-b-E) is estimated by PS data.

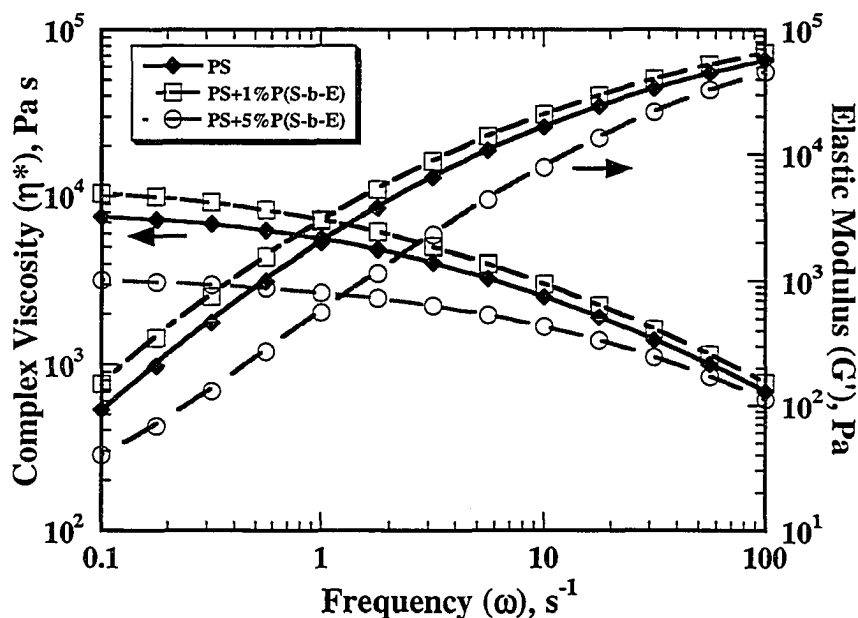


Figure 4.2 Complex viscosity and elastic modulus for PS, PS+1%P(S-b-E) and PS+5%P(S-b-E) at 190°C.

Experiments were performed by increasing shear rate stepwise at a constant temperature of 190°C for PE/PS and PE/PSOX, and 230°C for PE/PA6. The drop deformation and breakup were recorded at a well-controlled shear rate. The recording was analyzed separately using Adobe Photoshop software. Drop images at given deformation times were grabbed and their dimensions were measured based on prior calibration.

4.3 RESULTS AND DISCUSSION

4.3.1 Effect of Pre-made Compatibilizer

Figure 4.3 shows a series of micrographs of an uncompatibilized PS drop ($D_0 = 0.52$ mm) deforming and breaking up in a PEI matrix. Initially the PS drop is quite spherical (Figure 4.3a). Tip streaming occurs when the shear rate is increased to 3s^{-1} and small droplets come off the mother drop in the flow direction. At this point, the viscosity ratio is 10. When the shear rate is further increased to 4s^{-1} , the drop is first stretched to a sausage shape (Figure 4.3b), and then breaks up into two daughter droplets (Figure 4.3c); that is, it breaks up via parallel breakup (Lin *et al.*, 2003a, 2003c). Following the daughter droplet on the left side of the image in Figure 3c ($D \approx 0.35$ mm), it is seen that the droplet elongates continuously in the vorticity direction. The vorticity alignment and elongation (Chapter 3), similar to the rod-climbing Weissenberg phenomenon, is attributed to the high normal stress in polymers (Mighri and Huneault, 2001; Hobbie and Migler, 1999; Migler *et al.*, 1999; Migler, 2000; Chapter 3). No breakup occurs even when the shear rate is increased to 8s^{-1} (Figure 4.3d).

Figure 4.4 shows micrographs of the deformation and breakup of a PS drop premixed with 5% P(S-b-E). The drop, with a diameter of 0.58 mm, has already begun to deform at the beginning of the recording (Figure 4.4a). Tip streaming (Lin *et al.*, 2003c) is observed at $\dot{\gamma} \approx 3\text{s}^{-1}$, and then, the drop begins to elongate in the vorticity direction. When the shear rate is increased to 4s^{-1} , less tip streaming is observed (Figure 4.4b), but the drop still grows in the vorticity direction. After about 360 s at this shear rate (4s^{-1}), the drop breaks up into two daughter droplets via vorticity elongation (Figure 4.4c).

Breakup occurs at lower shear rates for the diblock compatibilized system. When the lower daughter droplet ($D \approx 0.35$ mm) in Figure 4.4c that had a tiny elastic cylindrical tip at the top of the droplet is followed, it is found that the tip breaks off from the droplet at a shear rate of 7s^{-1} (Figure 4.4d). An elastic tip extending from the drop is also observed for PS premixed with 1% P(S-b-E) drop (see Figure V.1 in Appendix V).

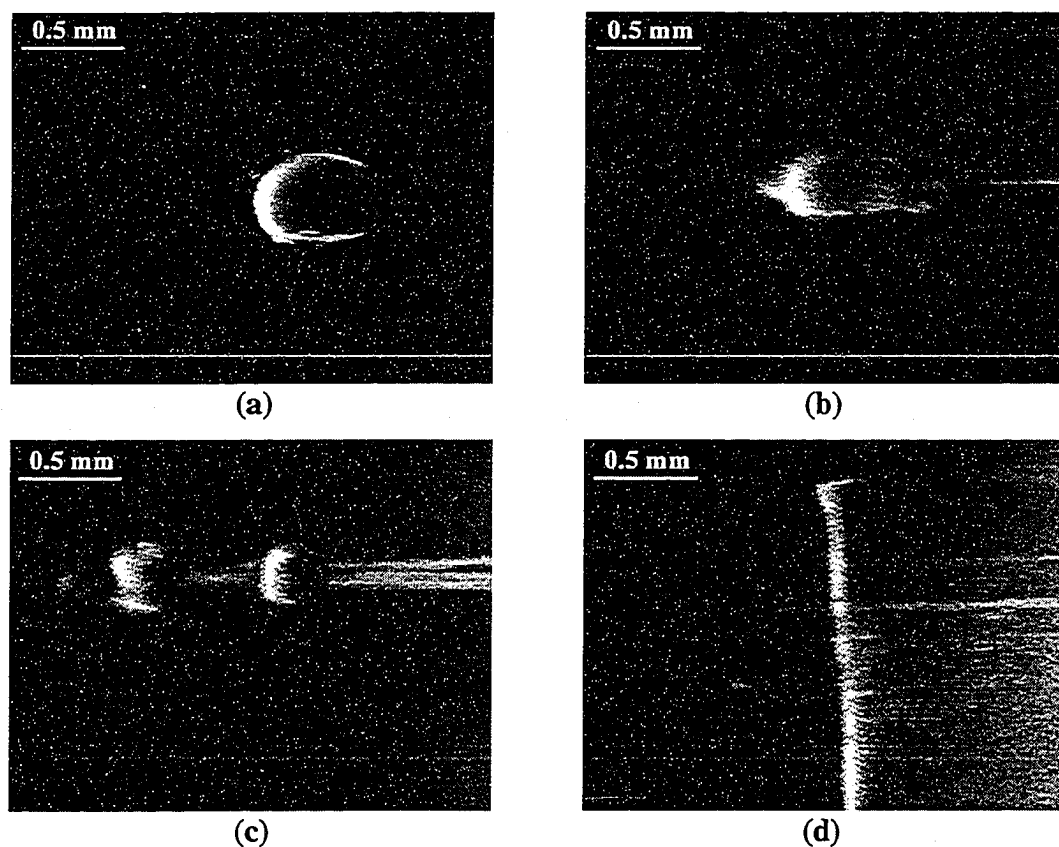


Figure 4.3 Deformation and breakup of a PS drop ($D_0=0.52\text{mm}$) in a PE1 matrix at 190°C subject to a stepwise shear rate increase. Time and conditions for each figure: (a) $t=5\text{s}$, $\dot{\gamma}=0.3\text{s}^{-1}$, $\eta_r=15.0$; (b) $t=535\text{s}$, $\dot{\gamma}=4.4\text{s}^{-1}$, $\eta_r=8.7$; (c) $t=541\text{s}$, $\dot{\gamma}=4.0\text{s}^{-1}$, $\eta_r=9.0$; (d) $t=1547\text{s}$, $\dot{\gamma}=8.4\text{s}^{-1}$, $\eta_r=7.0$. Note scale bar. For the micrographs, the flow direction is horizontal and the vorticity direction is vertical.

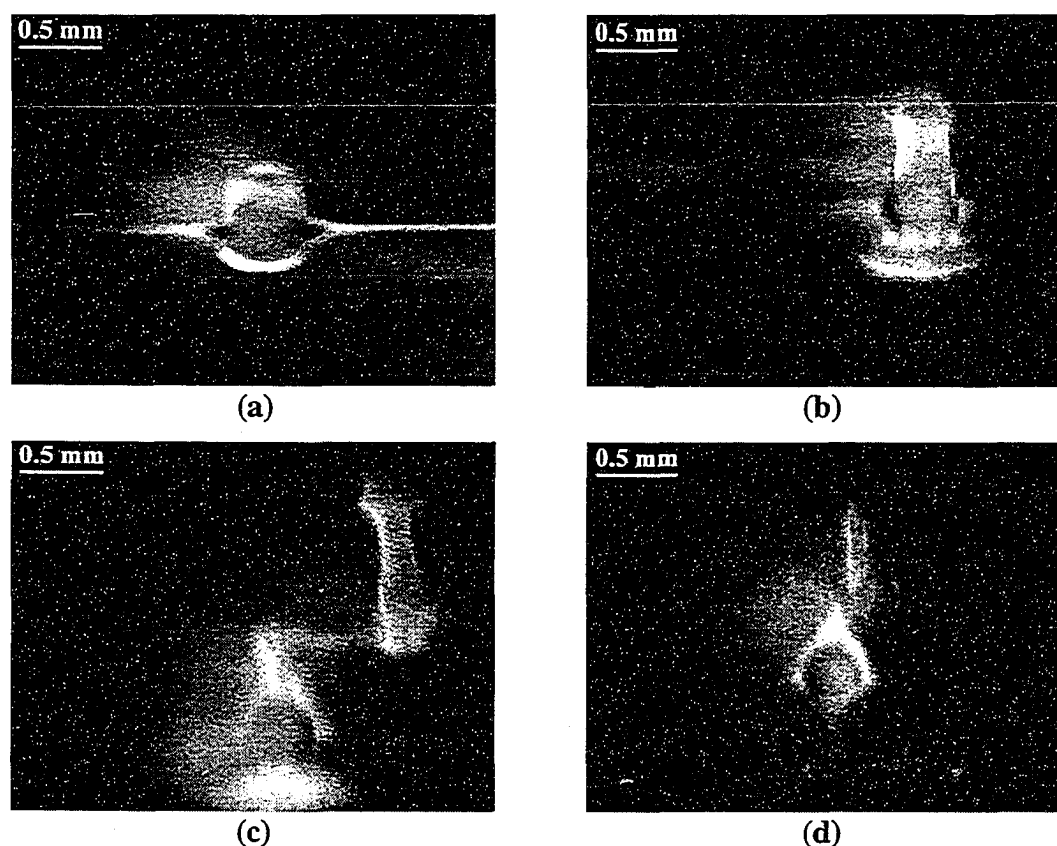


Figure 4.4 Pre-made copolymer. Deformation and breakup of a PS+5%P(S-b-E) drop ($D_0=0.58\text{mm}$) in a PE1 matrix at 190°C subject to a stepwise shear rate increase. Time and conditions for each figure: (a) $t=0\text{s}$, $\dot{\gamma}=3.0\text{s}^{-1}$, $\eta_r=5.3$; (b) $t=126\text{s}$, $\dot{\gamma}=3.6\text{s}^{-1}$, $\eta_r=5.2$; (c) $t=480\text{s}$, $\dot{\gamma}=3.8\text{s}^{-1}$, $\eta_r=5.2$; (d) $t=669\text{s}$, $\dot{\gamma}=6.6\text{s}^{-1}$, $\eta_r=4.7$. Note scale bar. For the micrographs, the flow direction is horizontal and the vorticity direction is vertical.

The tiny elastic cylindrical tip found during drop deformation and breakup (Figures 4.4c-4.4d) is somewhat similar to what was observed by van Puyvelde *et al.* (2002). However, the tip in the work by van Puyvelde *et al.* (2002) was in the flow direction while the tip in this work was in the vorticity direction. van Puyvelde *et al.* (2002) showed that a drop composed of PIB premixed with 2% PIB-PDMS copolymer exhibited pointed ends in the flow direction when the drop was sheared inside PDMS. In their experiments, the viscosity ratio was close to 1, both drop and matrix phases were

nearly Newtonian without noticeable elasticity, and the drop had a diameter in the order of micron. Therefore, shear stress and interfacial stress are the two important factors in their case. In this thesis, the tiny tip was developed in the vorticity direction. The possible reasons are that both PS drops and PE matrix have high viscosities and elastic moduli (see Figures 3.2 and 4.2). The drop phase has much higher viscosity and elastic modulus than those of the matrix phase, with both viscosity ratio and elastic ratio (G_d'/G_m') higher than 5, and the drop diameter is on the order of a millimeter. As a result, besides shear stress and interfacial stress, normal stresses are also important, and phenomena such as drop alignment and elongation in vorticity axis are observed.

To compare the importance of convection and diffusion of the copolymer along the drop interface, the surface Peclet number is normally used:

$$Pe_s = \dot{\gamma}R^2 / D_s \quad (4.1)$$

where R is the drop radius and D_s is the surface diffusivity of the surfactant molecule. At large Pe_s ($\gg 1$), convection prevails and at low Pe_s ($\ll 1$), diffusion becomes important. The copolymer diffusivity can be estimated by using the PS data having the same molecular weight (200,000 g/mol) in a PE matrix. The diffusivity is calculated (van Krevelen, 1976) to be around 4.2×10^{-13} cm²/s at a shear rate of 4s^{-1} and 190°C (see Appendix III). Therefore, the Pelect number is $\sim 10^9 \gg 1$, which indicates that convection of the copolymer induced by shear flow is much more important (van Puyvelde *et al.*, 2002; Jeon and Macosko, 2003). When the copolymer accumulates at the drop tip, it increases the local curvature. The interfacial tension is reduced locally and the interfacial

tension gradient increases across the drop, thus increasing the drop Marangoni or interfacial stress substantially (Velankar *et al.*, 2004). The drop is resistant (Lin *et al.*, 2003a; Chapters 2 and 3) to deformation and breakup; therefore, the tiny tip is easier to break up when compared to the drop itself. In other words, the presence of the tiny tip stabilizes the drop.

Figure 4.5 shows the deformation and breakup of a PS drop with a diameter of 0.53 mm dry-coated with P(S-b-E). For compatibilized drop prepared in this way, it is not able to weigh the exact copolymer added. According to the group contribution method (van Krevelen, 1976), the densities of PS and PE at 190°C are 990 kg/m³ and 860 kg/m³, respectively. The weight of the copolymer at the drop surface is estimated by using the arithmetic average density of PS and PE. Since all the copolymer is added at the drop surface and the average thickness of the copolymer powder added at the drop surface is probably close to 0.1 mm, the drop surface copolymer concentration will be around 5 wt% based on the drop, much greater than the maximum coverage concentration (0.06 wt%). Though it is difficult to tell whether the interface between the drop and the matrix phase is saturated with copolymer or not, enough copolymer was added to saturate the drop surface if all the copolymer powders stay at the interface and no micelles are formed.

Tip streaming is observed at a shear rate of 2s⁻¹ (Figure 4.5a). After approximately 800 s, the drop interface becomes obscure (Figure 4.5b) and the drop appears to be larger with its 2D cross-sectional area around 1.2 times that of the initial drop. This may be because the drop has flattened in the direction perpendicular to the

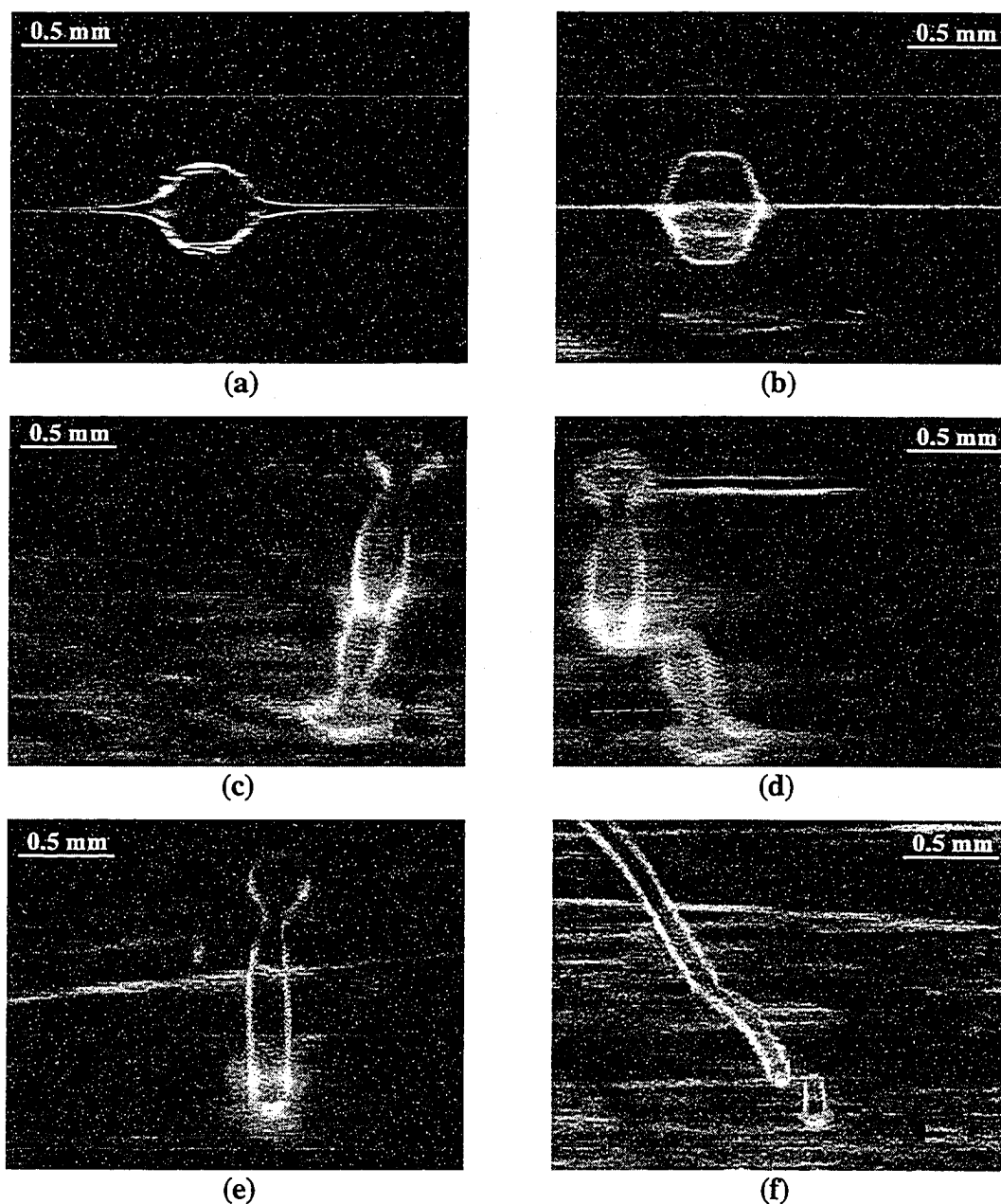


Figure 4.5 Pre-made copolymer. Deformation and breakup of a PS drop ($D_0=0.53\text{mm}$) coated with P(S-b-E) in a PE1 matrix at 190°C subject to a stepwise shear rate increase. Time and conditions for each figure: (a) $t=114\text{s}$, $\dot{\gamma}=2.3\text{s}^{-1}$, $\eta_r \approx 10.5$; (b) $t=801\text{s}$, $\dot{\gamma}=2.3\text{s}^{-1}$, $\eta_r \approx 10.5$; (c) $t=1124\text{s}$, $\dot{\gamma}=2.3\text{s}^{-1}$, $\eta_r \approx 10.5$; (d) $t=1158\text{s}$, $\dot{\gamma}=3.4\text{s}^{-1}$, $\eta_r \approx 9.3$; (e) $t=1291\text{s}$, $\dot{\gamma}=6.0\text{s}^{-1}$, $\eta_r \approx 7.8$; (f) $t=1665\text{s}$, $\dot{\gamma}=7.4\text{s}^{-1}$, $\eta_r \approx 7.4$. Note scale bar. The viscosity ratio is obtained by using PS data for drop phase viscosity. For the micrographs, the flow direction is horizontal and the vorticity direction is vertical.

viewing plane. Figure 4.5c shows that the drop elongates in the vorticity direction continuously. It breaks up into two daughter droplets at $\dot{\gamma} \approx 3\text{s}^{-1}$ as shown in Figure 4.5d. Again, it is evident that addition of compatibilizer allows the drop to break up at a lower shear rate than the uncompatibilized case. The daughter droplet at the top of the image in Figure 4.5d ($D \approx 0.42\text{ mm}$), like the mother drop, aligns and elongates in the vorticity direction when the shear rate is increased to 6s^{-1} (Figure 4.5e). Much more elongation is observed when the shear rate is increased to 7s^{-1} . Figure 4.5f shows the breakup of the daughter droplet (see bottom of Figure 4.5f).

The increase in drop cross-sectional area with copolymer present at the interface has also been observed by Levitt and Macosko (1999). In their experiments, the drop was generated by breaking up a polymer fiber with 10% block copolymer, used as the drop phase, sandwiched between two another polymer disks, used as the matrix phase. The sandwiched sample was put into the parallel plate device at the experimental temperature for one hour before the motors started to rotate. The drop obtained by this method had most of the copolymers distributed evenly at the drop surface before shearing (Jeon and Macosko, 2003). In this thesis, when the copolymer is added evenly at the drop surface at the beginning of the experiment, the PS drop interface has an almost uniform P(S-b-E) layer and the interfacial concentration is much greater (~ 80 times) than the concentration required for saturation of the drop surface before shearing. There is less concentration gradient for this case and the interface may be sufficiently saturated so that the interfacial stress around the drop is homogeneous. The copolymer at the interface of the PS drop and PE matrix may also suppress interfacial slip (Zhao and Macosko, 2002). As a consequence, a drop will be stretched more and thus have a larger cross-sectional area in

the viewing plane. The drop can break up at a lower shear rate because the interfacial tension is lowered by the copolymer at the interface.

Tip streaming is observed in Newtonian systems with (de Bruijn, 1993; Milliken *et al.*, 1993; Milliken and Leal, 1994; Tretheway and Leal, 1999; Hu *et al.*, 2000) or without (Taylor, 1934; Bartok and Mason, 1959; Rumscheidt and Mason, 1961; Grace, 1982; de Bruijn, 1993) surfactants in simple shear flow. It occurs at viscosity ratios less than 0.1 and breakup occurs at a lower critical Capillary number than that for drop fracture (Taylor, 1934; Bartok and Mason, 1959; Rumscheidt and Mason, 1961; Grace, 1982; de Bruijn, 1993). Tip streaming is observed in PE/PS system with or without copolymer even when the viscosity ratio is greater than 3.5, a region where breakup is impossible for Newtonian systems in a simple shear flow field.

It has been shown (Milliken and Leal, 1991, 1992) that the drop elasticity affects tip streaming in extensional flow fields, and tip streaming occurs even when $\eta_r > 0.5$ if the drop Deborah number, De , is greater than 1. The Deborah number is defined as:

$$De = \lambda \dot{\gamma} \quad (4.2)$$

where $\dot{\gamma}$ is the applied shear rate and λ is the relaxation time. For polymers studied, λ is obtained from the complex viscosity versus frequency data. The intersection of the line representing the zero shear viscosity limit at low frequency and the line representing the power law viscosity at high frequency was determined to be the critical frequency, ω_c , and $\lambda = 1/\omega_c$. In PE1/PS system, tip streaming is observed for $De = 3$ and $\eta_r = 10$. This suggests that drop elasticity facilitates polymer drop tip streaming even in a simple shear

flow field. Furthermore, tip streaming can occur at $\eta_r > 3.5$, something that is impossible for Newtonian drops.

All tip streaming occurs at a low shear rate of 2~3 s^{-1} , which is consistent with other systems studied in Chapter 3. Tip streaming is more prevalent when copolymer is present. When shear is imposed on a PS drop, the copolymer, P(S-b-E), will redistribute its concentration at the interface, with higher concentration at the drop ends and tips (Jeon and Macosko, 2003). This copolymer concentration gradient results in an interfacial tension gradient along the drop, therefore the tips are easier to deform and break up as “tip streaming” and release small droplets into the matrix.

Table 4.2 summarizes the observations on PS drop deformation and breakup in PE matrix without and with the block copolymer. For PE1/PS, the PS drop exhibits tip streaming, parallel breakup and vorticity alignment, but no vorticity breakup is observed even when the shear rate is increased to 8 s^{-1} . For PE1/PS+1%P(S-b-E), the viscosity ratio of the system is higher than that of the uncompatibilized system, and the drop breaks up in the vorticity direction at a shear rate of around 7 s^{-1} . For PE1/PS+5%P(S-b-E), the viscosity ratio is lower than the uncompatibilized system and the drop breaks up at a lower critical shear rate. The lower viscosity ratio may also account for the observed differences between the two copolymer systems, but in both cases, vorticity breakup is observed whereas it is not seen in the uncompatibilized system.

The drops with premixed copolymer show a higher critical shear rate for breakup than that seen for the drop dry-coated with copolymer. This may be due to the lower interfacial block copolymer concentration and higher concentration gradient for the premixed drop as compared to the dry-coated drop. For a premixed drop with 1%

copolymer, a tiny tip is first developed from the mother drop (Table 4.2) since the interfacial concentration is below the saturation interfacial coverage (see Chapter 5). For a premixed drop with 5% copolymer, the interfacial coverage is calculated to be 0.16 chains/nm² (Chapter 5), which is the saturation interfacial coverage estimated from Lyu *et al.* (2002) and Bates and Fredrickson (1999). The mother drop with 5% P(S-b-E) is first broken up in the vorticity direction and then a tiny tip is observed in a daughter droplet. Since interfacial area increases upon breakup, interfacial copolymer concentration may be insufficient to saturate the surface of this smaller droplet. In the experiments done in the Couette cell, the drop was put into the Couette device at 125°C and then the temperature was increased to 190°C directly in around fifteen minutes. Once the temperature reached 190°C, the experiment started. Therefore, the copolymer may not have had sufficient time to distribute itself over the surface at the drop. For drop premixed with copolymer, before the experiments, some of the copolymer may still stay inside the drop and the copolymer will most likely be distributed throughout the drop. When the drop is sheared inside the matrix, interfacial concentration gradient arises due to the shear-induced convection. After the first drop breakup, some of the daughter droplets may not have enough interfacial coverage of copolymer and concentration gradient exists. Therefore, a small tiny cylindrical tip develops and stabilizes the drop.

However, for a dry-coated PS drop, all the copolymers are at the drop interface before shearing and the interfacial concentration is around 80 times that of the saturation coverage before shearing. Though not all the block copolymer will stay at the interface during the experiment, the high initial concentration seems to help keep a significant amount of copolymer at the interface. Due to the high interfacial copolymer

concentration, the drop interface is obscured and the drop cross-sectional area is increased (Figure 4.5b). After the first breakup, the daughter droplets, like their mother drop, may still have sufficient copolymer and less concentration gradient at the interface, and therefore, break up in the vorticity direction easily.

Table 4.2 Summary on PS drop deformation and breakup in PE matrix without and with block copolymer P(S-b-E)

Matrix/Drop	Drop Diam. (mm)	Shear Rate ($\dot{\gamma}$, s ⁻¹)	Breakup Mode	Notes
PE1/PS	0.52	3.0 ($\eta_r=10$)	Tip streaming	
	0.52	4.0 ($\eta_r=9$)	Parallel breakup	
	0.36	8.4 ($\eta_r=7$)	Vorticity alignment	No Breakup at this shear rate
PE1/PS+1%P(S-b-E)	0.51	4.4 ($\eta_r=11$)	Tiny cylindrical tip breaks off	Cylindrical tip along the vorticity axis develops at 4.4s ⁻¹
	0.51	6.5 ($\eta_r=9$)	Vorticity breakup	
PE1/PS+5%P(S-b-E)	0.58	3.0 ($\eta_r=5$)	Tip streaming	
	0.58	3.8 ($\eta_r=5$)	Vorticity breakup	
	0.35	6.6 ($\eta_r=5$)	Tiny cylindrical tip breaks off	Cylindrical tip along the vorticity axis develops at 3.8s ⁻¹
PE1/PS+P(S-b-E) (dry-coated)	0.53	2.3 ($\eta_r\approx 10$)	Tip streaming	The viscosity of the drop phase is estimated from PS
	0.53	3.4 ($\eta_r\approx 9$)	Vorticity breakup	
	0.42	7.4 ($\eta_r\approx 7$)	Vorticity breakup	

In general, the effect of block copolymer on drop deformation and breakup is complex. It may stabilize the drop by forming a tiny elastic cylindrical tip if there is a copolymer concentration gradient and insufficient interfacial coverage at the interface. In this case, the convection of the copolymer dominates when a shear field is applied, and the copolymer stabilizes the drop against deformation and breakup because of interfacial tension gradient, as shown in Figure 4.4. It may also help drop area generation and drop breakup if copolymer is saturated and distributes homogeneously across the interface, which is shown for the case of the PS drop coated with P(S-b-E) shown in Figure 4.5. The stretching of the drop surface may be attributed to the reduction of interfacial slip and/or the decrease of the interfacial tension.

4.3.2 Effect of Reactive Compatibilization

4.3.2.1 Cross-Linking Reaction

Figure 4.6 shows the deformation and breakup of a PSOX chunk (~ 0.67 mm in diameter) inside a PE2 matrix. Figures 4.6b, d, f and h are the corresponding schematics for Figures 4.6a, c, e and g. The schematics are shown to clarify the drop interface. This is a non-reactive system since PE has no reactive functionality. This run was performed to check the effect of the oxazoline group on breakup without any in-situ reaction. The PSOX chunk aligns in the vorticity direction (Figure 4.6a) and surface erosion (Lin *et al.*, 2003b) occurs for the elongated drop, with streams of droplets peeling off the mother drop. The PSOX drop subsequently breaks into three droplets at a shear rate of 4s^{-1} (Figure 4.6b). The center daughter droplet elongates in the vorticity direction (Figure 4.6c) and breaks up into five droplets (Figure 4.6d) at a higher shear rate of 6s^{-1} . The

PSOX drop may break up at a lower shear rate than the PS drop (see Figure 4.2) because the PSOX drop is larger and the viscosity ratio is lower for this system than for the PE1/PS system. Similar results were obtained when a PSOX chunk was sheared inside a PE1 matrix.

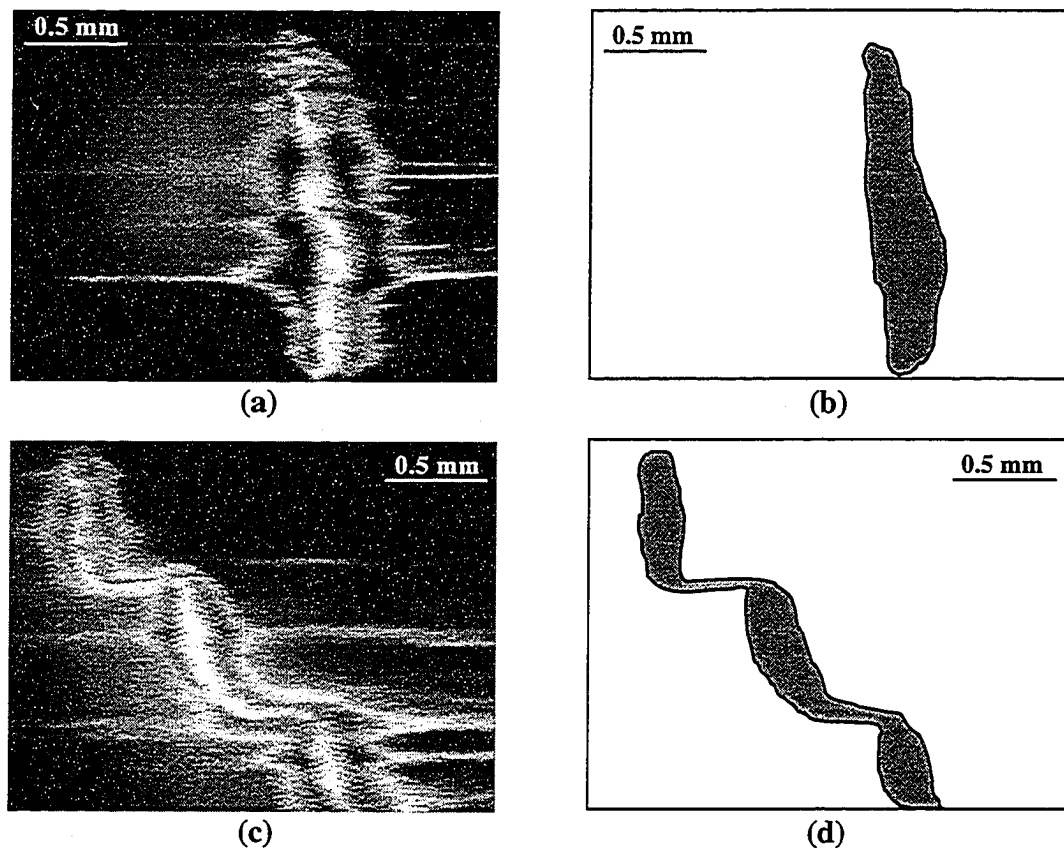


Figure 4.6 Deformation and breakup of a PSOX chunk ($D_0 \approx 0.67$ mm) in a PE2 matrix at 190°C subject to a stepwise shear rate increase. Time and conditions for each figure: (a) $t=0$ s, $\dot{\gamma}=2.3\text{ s}^{-1}$, $\eta_r=5.0$; (c) $t=358$ s, $\dot{\gamma}=3.8\text{ s}^{-1}$, $\eta_r=4.4$; (e) $t=378$ s, $\dot{\gamma}=3.6\text{ s}^{-1}$, $\eta_r=4.5$; (g) $t=723$ s, $\dot{\gamma}=6.0\text{ s}^{-1}$, $\eta_r=3.9$. Figures (b), (d), (f) and (h) are schematics for (a), (c), (e) and (g). Note scale bar. For the micrographs, the flow direction is horizontal and the vorticity direction is vertical.

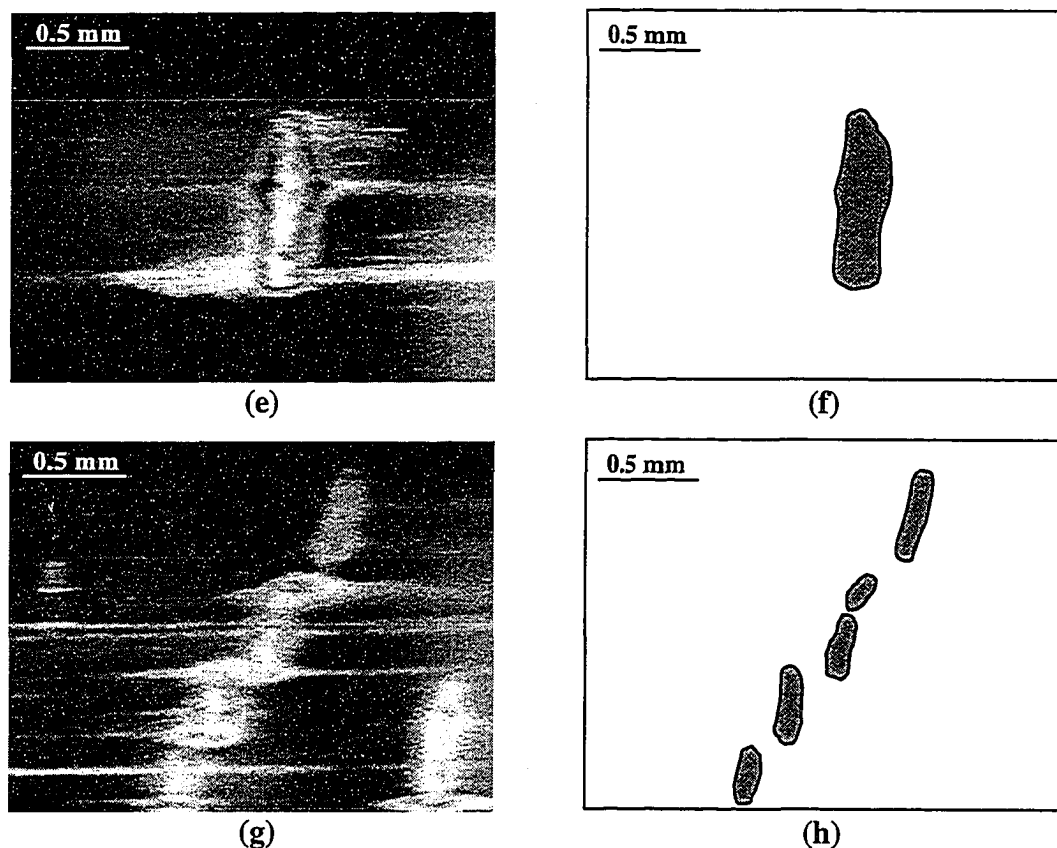


Figure 4.6 (Continued).

When the PSOX chunk is inserted inside a PEMA pellet and then put into the PE2 matrix, a very different breakup behavior is observed (see Figure 4.7). The drop viscosity is estimated by PSOX viscosity and the matrix viscosity by PE viscosity. The PSOX chunk (Figure 4.7a, $D \approx 0.60$ mm) initially aligns and elongates in the vorticity direction (Figure 4.7b). No surface erosion is observed at shear rates less than 4s^{-1} (Figures 4.6a-4.7c). A thin tip forms at the bottom of the drop, elongates, and then breaks up at $\dot{\gamma} \approx 4\text{s}^{-1}$ (Figure 4.7c). Erosion fully develops when the shear rate is increased to 9s^{-1} (Figure 4.7d). The drop breaks up at $\dot{\gamma} \approx 10\text{s}^{-1}$ (Figure 4.7e), a shear rate higher than that for the case without reaction (Figure 4.6). Similar results were obtained when a PSOX chunk was sheared inside PE1.

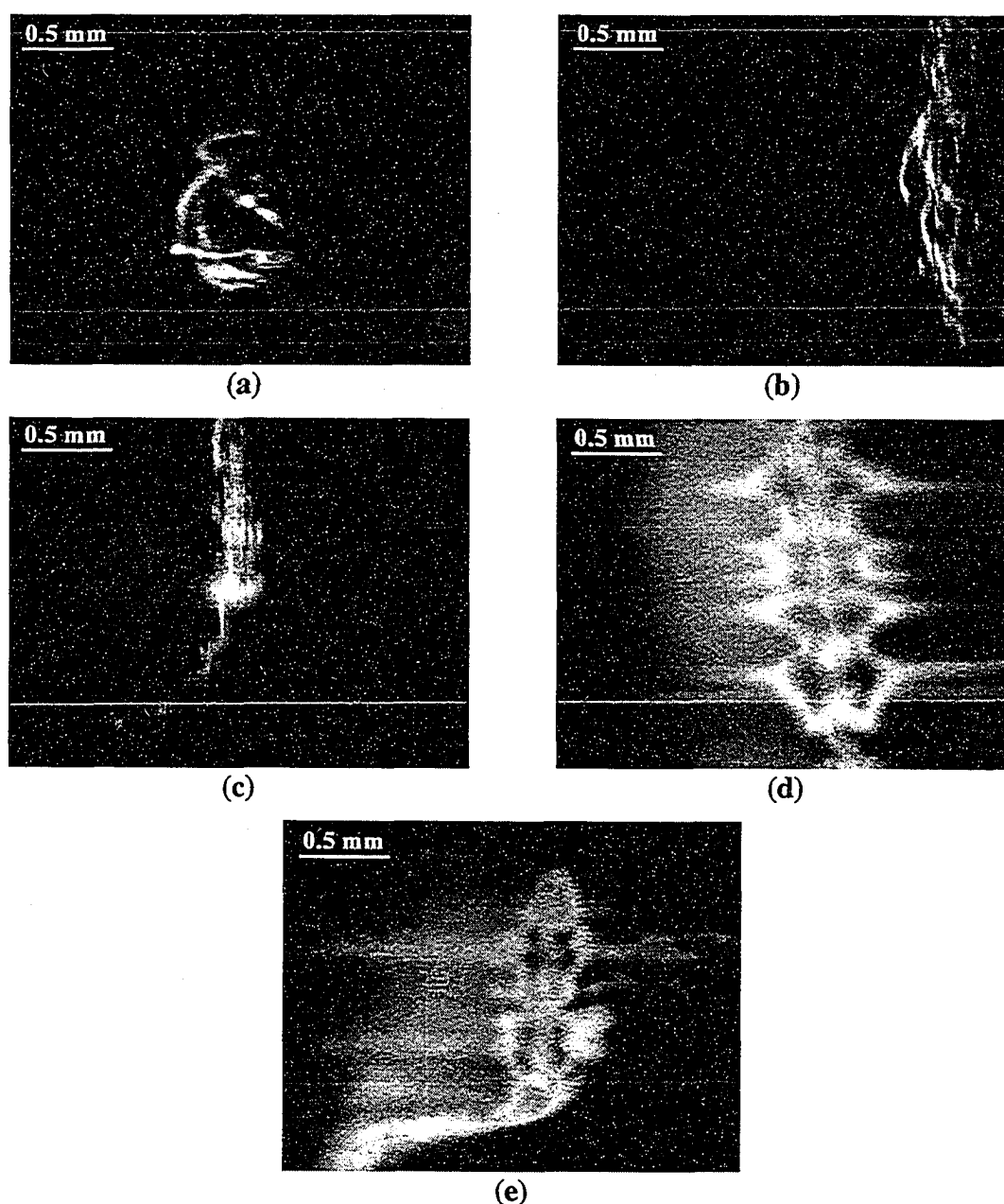


Figure 4.7 Reactive system. Deformation and breakup of a PSOX chunk ($D_0 \approx 0.60 \text{ mm}$) inserted inside a PEMA pellet then in a PE2 matrix at 190°C subject to a stepwise shear rate increase. Time and conditions for each figure: (a) $t=0\text{s}$, $\dot{\gamma}=0.6\text{s}^{-1}$, $\eta_r \approx 6.4$; (b) $t=145\text{s}$, $\dot{\gamma}=1.9\text{s}^{-1}$, $\eta_r \approx 5.2$; (c) $t=734\text{s}$, $\dot{\gamma}=4.1\text{s}^{-1}$, $\eta_r \approx 4.3$; (d) $t=1159\text{s}$, $\dot{\gamma}=8.9\text{s}^{-1}$, $\eta_r \approx 3.4$; (e) $t=1445\text{s}$, $\dot{\gamma}=9.7\text{s}^{-1}$, $\eta_r \approx 3.3$. Note scale bar. The viscosity ratio is obtained by using PSOX data for drop phase viscosity. For the micrographs, the flow direction is horizontal and the vorticity direction is vertical.

**Table 4.3 Summary on PSOX drop deformation and breakup in PE matrix
without and with cross-link reaction**

Matrix/Drop	Drop Diam. (mm)	Shear Rate ($\dot{\gamma}$, s ⁻¹)	Breakup Mode	Notes
PE1/PSOX	0.52	1.1 ($\eta_r=18$)	Erosion	The images appear hazy
	0.52	4.7 ($\eta_r=12$)	Vorticity breakup	
PE1+PEMA/PSOX	0.63	5.6 ($\eta_r=11$)	Tiny cylindrical tip breaks off	Cylindrical tip along the vorticity axis develops at 1.4s ⁻¹
	0.63	7.5 ($\eta_r=10$)	Erosion	
	0.63	10.5 ($\eta_r=9$)	Vorticity breakup	The viscosity of the drop phase is estimated from PSOX
PE2/PSOX	0.66	2.3 ($\eta_r=5$)	Erosion	
	0.66	3.8 ($\eta_r=4$)	Vorticity breakup	
	0.39	5.5 ($\eta_r=4$)	Vorticity breakup	
PE2+PEMA/PSOX	0.60	4.1 ($\eta_r=4$)	Tiny cylindrical tip breaks off	Cylindrical tip along the vorticity axis develops at 1.9s ⁻¹
	0.60	6.4 ($\eta_r=4$)	Erosion	
	0.60	9.7 ($\eta_r=3$)	Vorticity breakup	The viscosity of the drop phase is estimated from PSOX

Table 4.3 compares the breakup mechanisms for non-reactive (PE/PSOX) and reactive (PE+PEMA/PSOX) systems. Erosion and vorticity alignment and breakup occur at a lower shear rate for PE/PSOX systems. With PEMA, a tiny cylindrical tip is extended from the mother drop and aligns in the vorticity direction. This tiny tip is

similar to that observed for PE/PS premixed with copolymer. The oxazoline in PSOX undergoes a ring opening reaction with the maleic anhydride (Liu *et al.*, 1990; Figure 4.1a) in PEMA and leads to cross-linking at the interface. The newly cross-linked PS-PE material may act as a copolymer initially. The copolymer is swept by shear flow to the drop tip by convection and, as a result, a tiny cylindrical tip develops. This tiny tip stabilizes the drop and the drop breaks up at a much higher shear rate than that for the non-reactive system. The cross-linked interface may also reduce or completely restrict erosion from the drop surface until the shear rate is increased further.

4.3.2.2 Graft Reaction

Figure 4.8 shows a PA6 drop shearing in a PE1 matrix at 230°C. The drop has an initial diameter of 0.58 mm. The viscosity ratio of the system is 0.5. No obvious drop deformation is observed when the shear rate is increased up to 13s⁻¹.

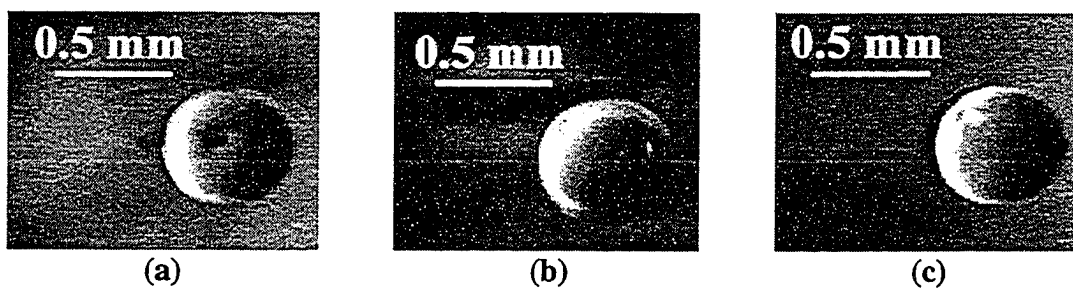


Figure 4.8 Deformation and breakup of a PA6 drop ($D_0=0.58\text{mm}$) in a PE1 matrix at 230°C subject to a stepwise shear rate increase. Time and conditions for each figure: (a) $t=17\text{s}$, $\dot{\gamma}=1.3\text{s}^{-1}$, $\eta_r=0.46$; (b) $t=169\text{s}$, $\dot{\gamma}=2.2\text{s}^{-1}$, $\eta_r=0.48$; (c) $t=961\text{s}$, $\dot{\gamma}=13.3\text{s}^{-1}$, $\eta_r=0.56$. Note scale bar. For the micrographs, the flow direction is horizontal and the vorticity direction is vertical.

Figure 4.9 is the deformation and breakup micrographs of a PA6 drop embedded in a PEMA pellet sheared inside a PE1 matrix at 230°C. Figure 4.9a is the spherical PA6

drop after shearing at 2s^{-1} for 13 s. Figure 4.9b shows that a thin layer of sheet is tearing out of the mother drop after 40 s of shearing at 2s^{-1} . The sheet is rapidly and continuously pulling off at a time of 55 s (Figure 4.9c). In another 25 s, the sheet is stretched so much that it is all around the Couette gap (Figure 4.9d). The sheet thickness can be estimated by taking 0.2 mm as the sheet width (Figure 4.9d), 355 mm as the sheet length (based on that the average diameter of the Couette is 113 mm), and assuming that the drop volume conserves. Then, the thickness of the sheet is calculated to be $0.8\ \mu\text{m}$. No drop or sheet is discernable after Figure 4.9d. This is because the thin sheet is ruptured to many micron sized daughter droplets around the Couette gap. At this point, it is unable to capture the droplets clearly.

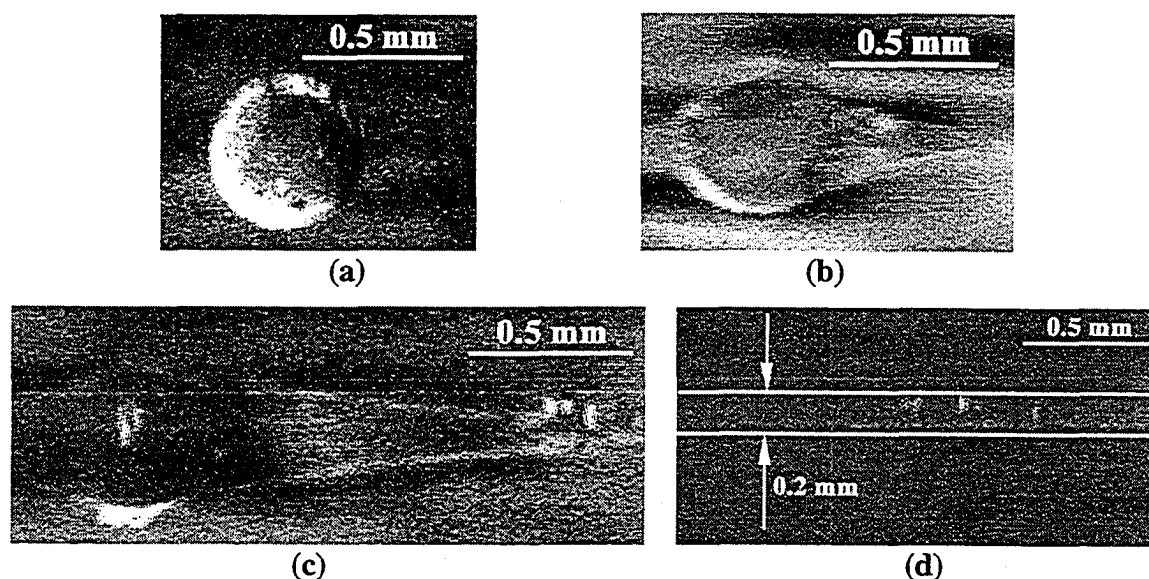


Figure 4.9 Reactive system. Deformation and breakup of a PA6 ($D_0=0.48\text{mm}$) inserted inside a PEMA pellet then in a PE1 matrix at 230°C subject to a stepwise shear rate increase. Time and conditions for each figure: (a) $t=13\text{s}$, $\dot{\gamma}=1.9\text{s}^{-1}$, $\eta_r \approx 0.48$; (b) $t=40\text{s}$, $\dot{\gamma}=1.8\text{s}^{-1}$, $\eta_r \approx 0.48$; (c) $t=55\text{s}$, $\dot{\gamma}=1.9\text{s}^{-1}$, $\eta_r \approx 0.48$; (d) $t=80\text{s}$, $\dot{\gamma}=1.9\text{s}^{-1}$, $\eta_r \approx 0.48$. Two lines are drawn in (d) to show the width of the sheet. Note scale bar. The viscosity ratio is obtained by using PA6 data for drop phase viscosity. For the micrographs, the flow direction is horizontal and the vorticity direction is vertical.

The observations on a PA6 drop without and with PEMA deforming and breaking up inside a PE matrix are very different. This may be due to the fast graft reaction between PA6 and PEMA (Figure 4.1b). The interfacial reaction takes place in less than 2 min. The interfacial reaction may suppress the interface slip (Zhao and Macosko, 2002), therefore a sheet is easily tearing off. The formation of the very thin sheet provides an efficient way to achieve rapid size decrease (Sundararaj *et al.*, 1995; Willemse *et al.*, 1999).

4.4 CONCLUSIONS

The effects of pre-made compatibilizer and in-situ reactive compatibilization on polymer drop deformation and breakup were studied in a specially designed transparent Couette mixer. Figure 4.10 summarizes the effect of diblock copolymer and in-situ reaction on polymer drop deformation and breakup in simple shear. It is found that the effect of pre-made copolymer on the drop deformation and breakup is complex. It may help drop breakup if the copolymer at the interface is sufficient and has a uniform interfacial concentration (Figure 4.10a), and it may resist drop breakup if the copolymer at the interface is insufficient and has an interfacial concentration gradient (Figure 4.10b). Initially, the rapid interfacial graft reaction promotes drop breakup (Figure 4.10c), but as the grafted amount increases, the interfacial cross-linking stabilizes polymer drop (Figure 4.10d).

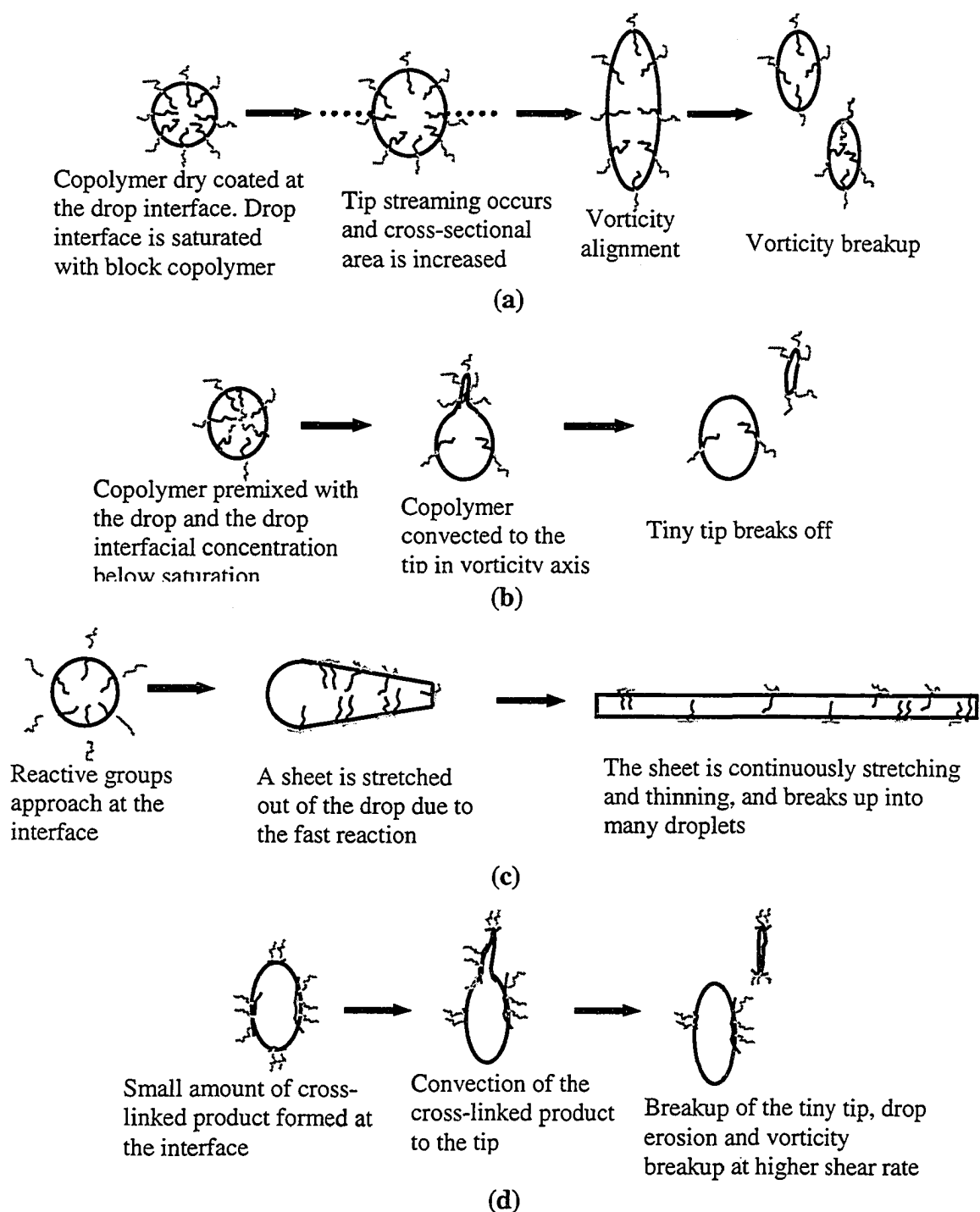


Figure 4.10 Schematics of effect of copolymer and in-situ reaction on polymer drop breakup. (a) Copolymer is dry coated evenly at the drop surface and the drop surface is saturated with block copolymer; (b) Copolymer is premixed with the drop phase and the drop interfacial concentration is lower than the saturation coverage; (c) Fast graft reaction occurs at the interface; (d) Cross-linking reaction takes place gradually and small amount of cross-linked product forms at the interface. For all schematics, the flow direction is horizontal and the vorticity direction is vertical.

PS drops with or without compatibilizer sheared in a PE matrix align and elongate in the vorticity direction. When pre-made compatibilizer (P(S-b-E)) is added inside the drop phase (PS), if the interfacial copolymer concentration is below saturation, an elastic thin cylindrical tip develops in the vorticity direction and then ruptures from the elongated mother drop. For the case of a PS drop dry coated with P(S-b-E) and the drop interface is saturated with the block copolymer, the drop interface is obscured and the drop breaks up more easily than the pure drop. An uncertainty arises for polymer blends with pre-made copolymer experiments since it is hard to determine if the copolymer is at the interface or forms micelles. Therefore, only qualitative study of pre-made copolymer effect is presented.

For a reactive system, when a PSOX drop is sheared in a PEMA phase, the breakup occurs at a higher shear rate. This may be due to the cross-linking reaction between PSOX and PEMA at the interface, producing a cross-linked copolymer that forms a tiny cylindrical tip and prevents drop breakup. All compatibilized cases, except drops coated with copolymer, showed a tiny cylindrical tip and the formation of this tiny tip stabilized the mother drop. However, when a PA6 drop is sheared in a PEMA phase, the drop deforms and breaks up much more easily, and even breaks up at a shear rate as low as 2s^{-1} within 1 min. The rapid interfacial reaction between PA6 and PEMA may help suppress interfacial slip and a very thin sheet is pulled out of the mother drop, which subsequently breaks up rapidly into many tiny droplets.

4.5 REFERENCES

- Bartok, W.; Mason, S.G. *J. Colloid Interface Sci.* **1959**, *14*, 13-26.
- Bates, F.S.; Fredrickson, G.H. *Phys. Today* **1999**, *52*, 32-38.
- Breuer, O.; Sundararaj, U.; Toogood, R.W. *Polym. Eng. Sci.* **2004**, *44*, 868-879.
- Chapleau, N.; Favis, B.D.; Carreau, P.J. *Polymer* **2000**, *41*, 6695-6698.
- de Bruijn, R.A. *Chem. Eng. Sci.* **1993**, *48*, 277-284.
- Elemans, P.H.M.; Janssen, J.M.H; Meijer, H.E.H. *J. Rheol.* **1990**, *34*, 1311-1325.
- Elmendorp, J.J.; Van der Vegt, A.K. In *Two Phase Polymer Systems*, Utracki, L.A. Ed.; Hanser Publishers: New York, 1991; p.166-184.
- Grace, H.P. *Chem. Eng. Commun.* **1982**, *14*, 225-277.
- Hobbie, E.K.; Migler, K.B. *Phys. Rev. Lett.* **1999**, *82*, 5393-5396.
- Hu, Y.T.; Pine, D.J.; Leal, L.G. *Phys. Fluids* **2000**, *12*, 484-489.
- Jeon, H.K.; Macosko, C.W. *Polymer* **2003**, *44*, 5381-5386.
- Jones, T.D.; Bates, F.S.; Macosko, C.W. *Polym. Prepr. Am. Chem. Soc.* **1999**, *40*, 1097-1098.
- Levitt, L.; Macosko, C.W. *Macromolecules* **1999**, *32*, 6270-6277.
- Lin, B.; Sundararaj, U.; Mighri F.; Huneault, M.A. *SPE ANTEC Tech. Papers* **2002**.
- Lin, B.; Mighri F.; Huneault, M.A.; Sundararaj, U. *Macromol. Rapid Commun.* **2003a**, *24*, 783-788.
- Lin, B.; Sundararaj, U.; Mighri F.; Huneault, M.A. *Polym. Eng. Sci.* **2003b**, *43*, 891-904.
- Lin, B.; Sundararaj, U.; Mighri F.; Huneault, M.A. *SPE ANTEC Tech. Papers* **2003c**.
- Lin, B.; Sundararaj, U. *Polymer* **2004**, *45*, 7605-7613.
- Lindt, J.T.; Ghosh, A.K. *Polym. Eng. Sci.* **1992**, *32*, 1802-1813.

- Liu, N.C.; Baker, W.E.; Russell, K.E. *J. Appl. Polym. Sci.* **1990**, *41*, 2285-2300.
- Lyu, S.; Jones, T.D.; Bates, F.S.; Macosko, C.W. *Macromolecules* **2002**, *35*, 7845-7855.
- Milliken, W.J.; Leal, L.G. *J. Non-Newtonian Fluid Mech.* **1991**, *40*, 355-379.
- Milliken, W.J.; Leal, L.G. *J. Non-Newtonian Fluid Mech.* **1992**, *42*, 231-239.
- Milliken W.J.; Stone H.A.; Leal L.G. *Phys. Fluids A* **1993**, *5*, 69-79.
- Milliken W.J.; Leal L.G. *J. Colloid Interface Sci.* **1994**, *166*, 275-285.
- Mighri, F.; Huneault, M.A. *J. Rheol.* **2001**, *45*, 783-797.
- Migler, K.B.; Hobbie E.K.; Qiao, F. *Polym. Eng. Sci.* **1999**, *39*, 2282-2291.
- Migler, K.B. *J. Rheol.* **2000**, *44*, 277-290.
- Potente, H.; Bastian, M.; Bergemann, K.; Senge, M.; Scheel, G.; Winkelmann, Th.
Polym. Eng. Sci. **2001**, 222-231.
- Rumscheidt, F.D.; Mason, S.G. *J. Colloid Interface Sci.* **1961**, *16*, 238-261.
- Scott, C.E.; Macosko, C.W. *Polym. Bull.* **1991**, *26*, 341-348.
- Scott, C.E.; Macosko, C.W. *Polymer* **1995**, *36*, 461-470.
- Sundararaj, U.; Macosko, C.W.; Rolando, R.J.; Chan, H.T. *Polym. Eng. Sci.* **1992**, *32*,
1814-1823.
- Sundararaj, U.; Dori, Y.; Macosko, C.W. *SPE ANTEC Tech. Papers* **1994**, *52*, 2448-
2451.
- Sundararaj, U.; Dori, Y.; Macosko, C.W. *Polymer* **1995**, *36*, 1957-1968.
- Sundararaj, U.; Macosko, C.W. *Macromolecules* **1995**, *28*, 2647-2657.
- Sundararaj, U.; Macosko, C.W.; Shih, C.K. *Polym. Eng. Sci.* **1996**, *36*, 1769-1781.
- Taylor, G.I. *Proc. R. Soc. London, Ser. A* **1934**, *146*, 501-523.

- Tretheway, D.C.; Leal, L.G. *AIChE Journal* **1999**, *45*, 929-937.
- Utracki, L.A.; Shi, Z.H. *Polym. Eng. Sci.* **1992**, *32*, 1824-1833.
- Utracki, L.A. *Can. J. of Chem. Eng.* **2002**, *80*, 1008-1016.
- van Krevelen, D.W. *Properties of Polymers*, 2nd ed.; Elsevier Scientific Company: Amsterdam, 1976.
- van Puyvelde, P.; Velankar, S.; Mewis, J.; Moldenaers, P. *Polym. Eng. Sci.* **2002**, *42*, 1956-1964.
- Velankar, S.; van Puyvelde, P.; Mewis, J.; Moldenaers, P. *J. Rheol.* **2001**, *45*, 1007-1019.
- Velankar, S.; van Puyvelde, P.; Mewis, J.; Moldenaers, P. *J. Rheol.* **2004**, *48*, 725-744.
- Willemse, R.C.; Ramaker, E.J.U.; van Dam, J.; de Boer, A.P. *Polymer* **1999**, *40*, 6651-6659.
- Zhao, R.; Macosko, C.W. *J. Rheol.* **2002**, *46*, 145-167.

Chapter 5

Morphology Development of Polymer Blends in a Miniature Mixer

5.1 INTRODUCTION

Melt blending of homopolymers is an efficient route to create new materials. However, most polymer blends are immiscible and the interface between the phases is sharp. Therefore, immiscible blends usually exhibit inferior mechanical properties to either of its component homopolymers, owing to the lack of entanglements between phases. Compatibilizers are often added to immiscible polymer blends to improve interfacial adhesion (Liu *et al.*, 1993; Creton *et al.*, 2001; Eastwood and Dadmun, 2002; Benkoski *et al.*, 2003) and to achieve the desired morphology (Anastasiadis *et al.*, 1989; Favis and Chalifoux, 1987; Lepers and Favis, 1999; Leper *et al.*, 1999; Liang *et al.*, 1999; Potschke *et al.*, 2000; Lyu *et al.*, 2002; Utracki, 2002), and thus, to improve the mechanical properties. Two methods are involved in introducing compatibilizers to polymer blends: one is to add a pre-made compatibilizer; and the other one is in-situ compatibilization, where chemical reaction between two polymeric components is taking place during blending (Utracki, 2002).

Though batch mixers and extruders are widely used in industry for polymer blending, the minimum amount of material needed to use even in a laboratory batch mixer is around 50 g. Since new copolymers are obtained in small quantity, a minimixer, Alberta Polymer Asymmetric Minimixer (APAM) (Breuer *et al.*, 2004), is used for most of the polymer blends studied in this chapter. The advantages of using this miniature mixer are that it requires a small quantity of materials (< 2 g); it has the ability to

generate both shear and extensional flow; and it has good mixing efficiency similar to that of a batch mixer (Breuer *et al.*, 2004).

Melt blending is complicated because it involves time and temperature dependent non-Newtonian materials, and also the flow field is a combination of shear and extensional flow. During the blending process, melting and mixing are the most important and basic processing steps because melting affects the process rate and mixing determines the morphology (Grulke, 1994). In Chapters 2-4, the initial morphology development is studied by visualizing a single polymer drop deformation and breakup subject to shear flow generated by parallel plates (Chapter 2) and simple shear generated by Couette apparatus (Chapters 3-4). It was found that polymer drops can break up at a viscosity ratio greater than 3.5 in simple shear flow, which is impossible for Newtonian drops that have been widely studied in the literature (e.g., Taylor, 1932, 1934; Grace, 1982). Polymers are viscoelastic and shear thinning materials. Different deformation and breakup mechanisms are observed, such as erosion, parallel breakup and vorticity alignment and breakup. Sheets are formed when a polymer drop is sheared in either a parallel plate or a Couette device. Sheet formation is a key part of the initial polymer morphology development. Besides drop breakup, drop coalescence is another important aspect to affect the final size of the dispersed drop (Utracki and Shi, 1992; Sundararaj and Macosko, 1995; Fortelny, 2000).

Two equations are frequently used by polymer blending researchers to estimate the final dispersed particle size of the blends. One is the Taylor limit (Taylor, 1932, 1934) and the other is Wu's correlation (Wu, 1987). Taylor (1932, 1934) studied a single Newtonian drop in another Newtonian liquid subject to simple shear flow. By balancing

the interfacial force and the shear force, he predicted the maximum drop size that would be stable for small deformations in Newtonian fluids:

$$D = \frac{4\Gamma(\eta_r + 1)}{\dot{\gamma}\eta_m\left(\frac{19}{4}\eta_r + 4\right)} \quad \eta_r < 2.5 \quad (5.1)$$

where D is the drop diameter, $\dot{\gamma}$ is shear rate, Γ is interfacial tension, η_m is the viscosity of the matrix or major phase, η_d is the viscosity of the drop or the minor phase, and $\eta_r = \eta_d / \eta_m$ is the viscosity ratio. This relation is valid for small deformations in Newtonian fluids when $\eta_r < 2.5$. Taylor (1932) predicted that no drop breakup will occur when $\eta_r > 2.5$.

Wu's correlation (Wu, 1987) is based on the final particle diameter of extruded polymer blends where the minor phase had a concentration of 15 wt%:

$$D = \frac{4\Gamma\eta_r^{\pm 0.84}}{\dot{\gamma}\eta_m} \quad (5.2)$$

where the plus (+) sign in the exponent applies for $\eta_r > 1$ and the minus (-) sign applies for $\eta_r < 1$. Therefore, there is a minimum particle size at $\eta_r = 1$. It is important to note that this is an empirical correlation and has no theoretical basis, however, it provides a good first estimation of particle size for polymer blends.

In this chapter, the visualization results on how a single drop deforms and breaks up in the APAM are presented first. Then, the effects of the interfacial compatibilization on polymer blend morphology are discussed. The effects of feeding sequences, pre-made compatibilizer and in-situ reactive compatibilization will also be discussed.

5.2 EXPERIMENT

5.2.1 Materials

The fluid systems used for visualization were composed of corn syrup (lily white, from Best Foods Canada Inc.) and PDMS (polydimethylsiloxane) or silicone fluid (DMS-T35, from Gelest Inc.). Table 5.1 lists some properties of the corn syrup and silicone oil used. The viscosity and the interfacial tension were obtained at room temperature (22°C).

Table 5.1 Properties of corn syrup and silicone oil used.

	Density ^a (kg/m ³)	Viscosity ^b (Pa·s)	Refractive Index ^a	Interfacial Tension ^b (mN/m)	Viscosity Ratio
Corn Syrup	1,420	5.4	1.49	35.53	1.08
Silicone Oil	971	5.0	1.40		

a. Provided by the supplier, at 25°C.

b. Measured at room temperature, 22°C.

The corn syrup viscosity was measured with a Haake Viscometer VT550 having concentric cylinder geometry, and the silicone oil viscosity was obtained with Rheometric RMS 800 by using a 50 mm parallel plate fixture at 100% strain. The interfacial tension between the syrup and the oil was measured in a Tensiometer (Kruss K12) with ring method. The refractive index for the syrup is 1.49 and 1.40 for the oil.

The difference is 0.09, which is sufficient to visualize the syrup drop inside the oil directly.

Tables 5.2 and 5.3 list the polymers used in this study. The homopolymers: polystyrene (PS), Styron 666D and polystyrene oxazoline (PSOX) with 1% oxazoline, were kindly provided by Dow Chemical Co.; polyethylene (PE) was donated by Petromont; poly(methyl methacrylate) (PMMA) was from Rohm and Haas; and polyethylene maleic anhydride (PEMA) with 1% MAH was kindly supplied by DuPont Canada. Dynamic rheological characterizations were performed on a Rheometrics RMS800 Rheometer with a 25 mm parallel plate fixture at 10% strain. The interfacial tension between PS and PE at 190°C is 4.9 mN/m (Elemans *et al.*, 1990), and between PS and PMMA at 190°C is 1.5 mN/m (Sundararaj *et al.*, 1995a). The symmetric diblock copolymers were polystyrene-block-polyethylene (P(S-b-E)) (Lyu *et al.*, 2002) synthesized by researchers at University of Minnesota and polystyrene-block-poly(methyl methacrylate) (P(S-b-MMA)) provided by French National Center for Scientific Research (CNRS, France). The homopolymers came in pellet form and the copolymers, in powder form. All the polymers used in the experiments were dried in a vacuum oven overnight at 90°C. For systems with copolymer, the blend has a composition of 90:10 wt%, and the copolymer is 10 wt% of the dispersed phase unless otherwise specified.

Table 5.2 Properties of homopolymers used.

Polymer (Abbreviation)	Source (Commercial Name)	Molecular Weight (M_w , g/mol)	Density (kg/m^3)	Glass Transition Temp. (T_g , °C) ^a	Viscosity at $\dot{\gamma}=65\text{s}^{-1}$ & 190°C (Pa·s)	Elastic Modulus at $\dot{\gamma}=65\text{s}^{-1}$ & 190°C (Pa)
Polystyrene (PS)	Dow (Styron 666D)	160,000	1050 (25°C) ^a 990 (190°C) ^b	100	900	44,300
Polystyrene Oxazoline (PSOX, 1% oxazoline)	Dow	160,000		105	1,240	64,100
Poly(methyl methacrylate) (PMMA)	Rohm & Haas	110,000	1170 (25°C) ^a 1000 (190°C) ^b	114	5,070	269,400
Polyethylene (PE)	Petromont (DMDA-8920)	53,400	954 (25°C) ^a 860 (190°C) ^b		300	6,070
Polyethylene Maleic Anhydride (PEMA, 1% MAH)	DuPont (Fusabond MB265D)	48,400	950 (25°C) ^a		400	8,850

a. Provided by supplier.

b. Calculated according to van Krevelen (1976).

Table 5.3 Properties of copolymers used.

Polymer (Abbreviation)	Source	Molecular Weight (M_n , g/mol) ^a
Polystyrene-block-polyethylene (P(S-b-E))	University of Minnesota (Lyu <i>et al.</i> , 2002)	100,000-100,000
Polystyrene-block-poly(methyl methacrylate) (P(S-b-MMA))	CNRS, France	25,000-25,000
		50,000-50,000
		80,000-80,000

a. Provided by supplier.

5.2.2 Experimental Setup

The Couette apparatus used for visualization is specially designed and constructed (see Appendix I). Both cylinders are made of quartz. The inner cylinder has a diameter of 102 mm and the gap between the cylinders is 4 mm. The visualization plane consists of flow direction ($x_1: \theta$) and the velocity gradient direction ($x_2: r$).

The APAM is a miniature batch mixer composed of an asymmetric rotor and a cylindrical chamber (Breuer *et al.*, 2004, see Figure 5.1). The stainless steel chamber ($D_i \times H$: 13 mm \times 31 mm) is heated with a band heater. A Teflon ring is used between the rotor and the chamber to avoid direct metal contact. A detailed description of the mixer is given in Breuer *et al.* (2004). The total volume of the mixer is 2.2 mL. A DC motor (KBMD-240D from KB Electronics, Inc.) is used to control the rotational speed of the upper disk. When visualizing the drop deformation and breakup process, the stainless chamber can be replaced with a transparent cast acrylic chamber. A Pulnix CCD camera [TMC-7DSP] with zoom attachment mounted onto a X-Y-Z positioning movement (from Edmund Industrial Optics) is put in front of the transparent chamber. The visualization plane through the chamber consists of the axes $x_1: \theta$ and $x_2: z$.

The larger batch mixer used is a Haake Rheomix series 600 batch mixer as shown schematically in Figure 5.2. The mixer is connected to a Rheocord90 control panel. Before blending, the mixer is preheated to the required barrel temperature and the rotors are set to the desired rotation rate.

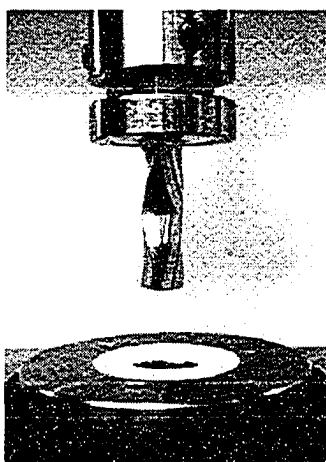


Figure 5.1 Photograph of the APAM setup. The diameter of the stainless chamber is 13 mm. For more details, refer to Breuer *et al.* (2004).

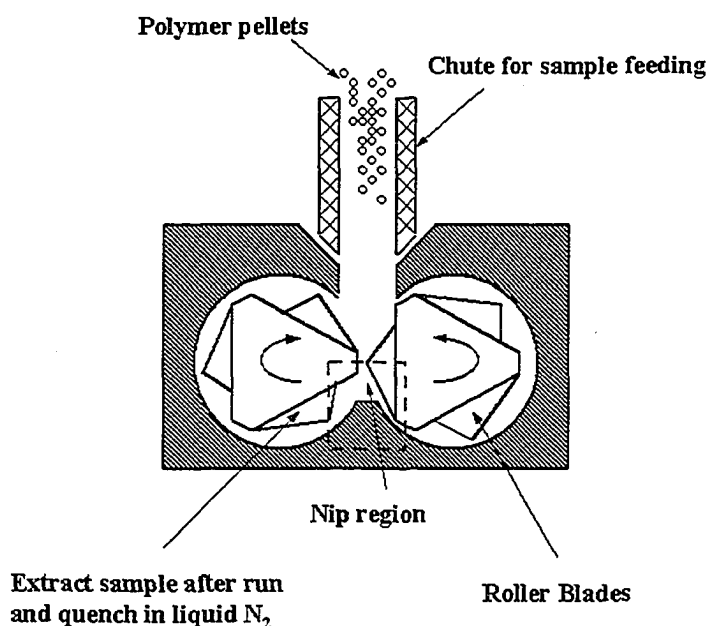


Figure 5.2 Batch mixer cross-sectional view.

5.2.3 Experimental Procedure

Before each run, the mixer temperature was preheated to 190°C, except for the visualization experiments, which were carried out at room temperature. The materials were fed into the chamber when the temperature reached the set point. The rotational

speed was 50 rpm (rotations per minute) except when otherwise specified. A value of 50 rpm corresponds to a maximum shear rate of 65s^{-1} in the minimum gap of the batch mixer. The shear rate distribution in the APAM has a wider range based on recent simulation results by Bai *et al.* (2004). The maximum shear rate is around 100s^{-1} , the average is 33s^{-1} and 6% of the APAM's shear rate is equal to or greater than 65s^{-1} . The complex viscosity and elastic modulus of the homopolymers at 65s^{-1} are listed in Table 5.2. The viscosity ratios of polymer blends presented in this chapter are calculated at a shear rate of 65s^{-1} unless specified. After each run, the sample was quickly quenched in liquid nitrogen.

5.2.4 Scanning Electron Microscopy (SEM) and Image Analysis

The morphology of the fractured surface of the blend sample was analyzed using a Hitachi S2700 scanning electron microscope (SEM) with Princeton Gamma Tech (PGT) Imix imaging software. The fractured surfaces of the samples were initially sputter coated with carbon black and gold before imaging. SEM micrographs were taken at 20 kV accelerating voltage.

The particle size of the dispersed phase was measured with SigmaScan Pro (version 4.01) software. The area (A) of each particle was determined and the equivalent diameter was obtained by assuming that the particle cross-section was circular in shape, i.e.:

$$D_{eq} = \sqrt{\frac{4A}{\pi}} \quad (5.3)$$

This equivalent diameter (D_{eq}) was used to obtain the number average diameter (D_n) and volume average diameter (D_v):

$$D_n = \frac{\sum_{i=1}^n D_{eq,i}}{n} \quad (5.4)$$

$$D_v = \frac{\sum_{i=1}^n D_{eq,i}^4}{\sum_{i=1}^n D_{eq,i}^3} \quad (5.5)$$

where n is the number of particles. Several SEM micrographs (> 200 particles) were used to determine the average diameter of each sample. The polydispersity of particles was determined as D_v/D_n . The particle size correction was neglected for the data presented because the difference between the measured average particle size and the corrected particle size with Cruz-Orive method was less than 10% (Sundararaj and Macosko, 1995).

The shape factor of the particles was also calculated. It was obtained from $4\pi \times A/P^2$, where A is drop area and P is drop perimeter. A perfect circle has a shape factor of 1.00 and a line has a shape factor approaching 0.00. The shape factor for the dispersed particles obtained from the SEM micrographs was 0.91 ± 0.01 , suggesting that the particles were close to spherical shape.

5.2.5 Transmission Electron Microscopy (TEM)

Some of the quenched blends were microtomed at room temperature. The morphology of the cross section of the blends with a thickness ~ 70 nm was analyzed using a Hitachi H-7000 transmission electron microscope (TEM) at 75 kV operating voltage. TEM was used to examine micelles in the samples.

5.3 RESULTS

5.3.1 Visualization

Figure 5.3 shows a corn syrup drop deforming and breaking up inside silicone oil at room temperature subject to stepwise shear rate increase generated by a Couette apparatus (see Appendix D). The viscosity ratio of the system is around 1. The initial drop diameter is 0.84 mm. The spherical drop is deformed to an elliptical shape at a shear rate of 3s^{-1} (Figure 5.3a). If the time for the image in Figure 5.3a is taken as t_0 and the shear rate is increased to 8s^{-1} (Figures 5.3b-e), the drop stretches continuously in the flow direction symmetrically and it breaks up into three daughter droplets after 50 s, with a smaller one in the middle and two bigger ones at the ends.

When the corn syrup drop is mixed with silicone oil inside the APAM (Figure 5.4), the drop deforms and breaks up in a different way from those shown in Figure 5.3. The rotation speed is 10 rpm and the average shear rate is around 7s^{-1} . The initial drop shown in Figure 5.4 has a diameter of 0.89 mm. Figure 5.4a shows the elliptical drop and the corresponding time is taken as t_0 . As the rotor rotates in a counter-rotating direction if viewing from the top of the chamber, the drop is stretched into an asymmetric shape, with a tapering tail on the left (Figure 5.4b). The tail narrows (Figure 5.4c) and the drop looks

like a tadpole. The drop then breaks up into three daughter droplets, with the biggest one at the right end, and the smallest at the left end (Figure 5.4d).

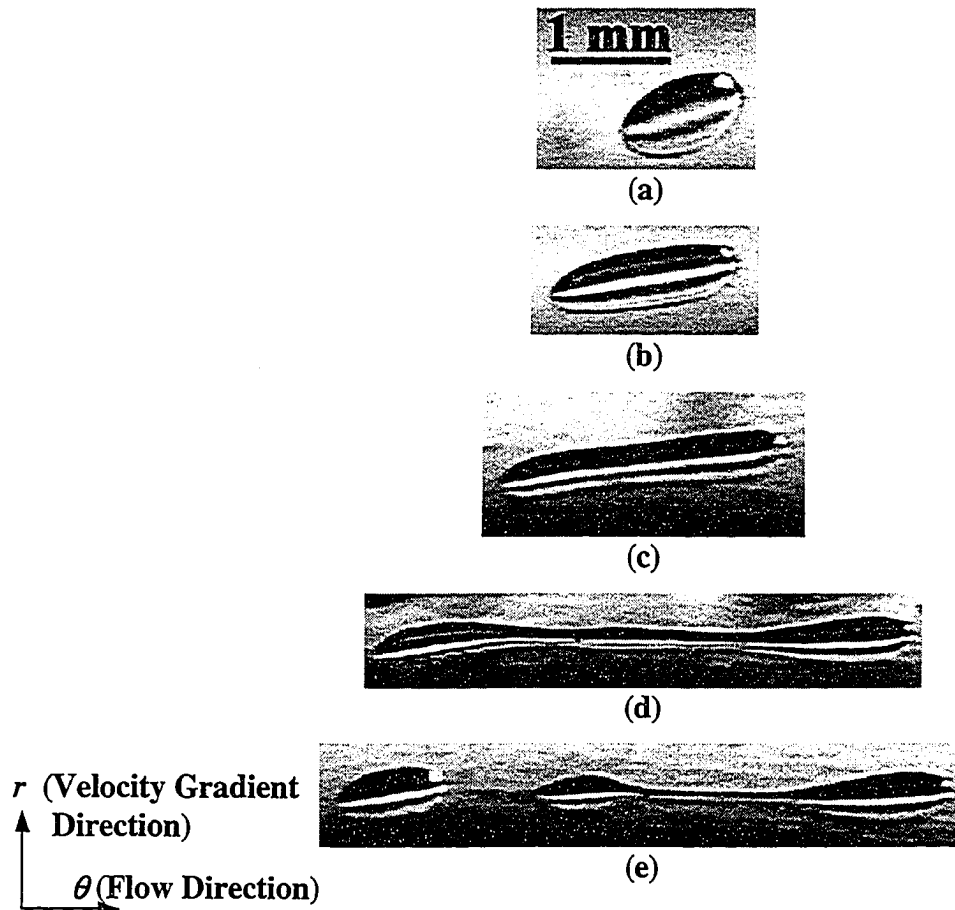


Figure 5.3 Deformation and breakup of a corn syrup drop ($D_0=0.84$ mm) in silicone oil at room temperature subject to a stepwise shear rate increase generated by a Couette apparatus. The viscosity ratio is 1.08. Time and conditions for each figure: (a) $t=153s=t_0$, $\dot{\gamma}=3.4s^{-1}$; (b) $t=t_0+39s$, $\dot{\gamma}=7.8s^{-1}$; (c) $t=t_0+45s$, $\dot{\gamma}=7.8s^{-1}$; (d) $t=t_0+48s$, $\dot{\gamma}=7.9s^{-1}$; (e) $t=t_0+49s$, $\dot{\gamma}=7.9s^{-1}$. Note scale bar.

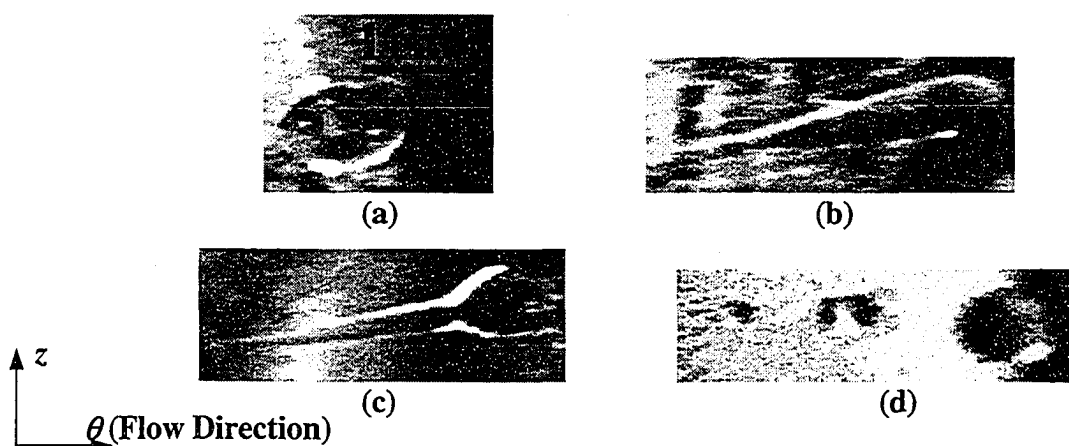


Figure 5.4 Deformation and breakup of a corn syrup drop ($D_0=0.89$ mm) in silicone oil at room temperature and 10 rpm in the APAM. The viscosity ratio is 1.08. Time and conditions for each figure: (a) $t=100s=t_0$; (b) $t=t_0+2s$; (c) $t=t_0+3s$; (d) $t=t_0+8s$. Note scale bar.

The behavior of the corn syrup drop in the Couette apparatus is different from that observed in the APAM due to the different flow fields that the drop experienced. The flow field in the APAM, unlike the Couette, consists not only of shear flow, but also extensional flow. The rotation of the asymmetric rotor generates a velocity, v_θ , which is a function of both r and z . The flow field inside the APAM resembles that of a twin rotor batch mixer or a twin-screw extruder. Figures 5.3 and 5.4 suggest that the results obtained from shear flow field cannot be simply applied into the real industry case. However, visualization of one polymer drop deformation and breakup helps to gain insight into how the basic process occurs and to understand the more complicated case. Figure 5.3 presents a corn syrup rupturing into three almost evenly-sized daughter droplets because the shear rate is only a function of r direction and it is homogeneous across the drop. Figure 5.4 shows that the corn syrup breaks up into three daughter droplets of different sizes since v_θ is a function of both r and z and it varies with the drop positions. Therefore, it stretches the drop into an asymmetric shape, with a big head at a

higher z and a tapering body titling to lower z . The drop also breaks up in a shorter time due to the existence of extensional flow, which is a stronger flow field (Grace, 1982).

The morphology development of polymer blends involves dynamic equilibrium between drop breakup and coalescence. In this thesis, only the drop breakup process is considered. Drop coalescence is another important aspect that must be taken into account for the final particle distribution. Figure 5.5 shows two syrup drops coalescing inside the silicone oil in the APAM at 10 rpm. The left drop has an initial diameter of 1.04 mm and the right one, 0.94 mm at t_0 (Figure 5.5a). The two drops approach together after 9 s as the rotor turns (Figure 5.5b). At a time of 14 s, the left drop squeezes on the top of the right drop (Figure 5.5c). Within another 1 s, the two drops merge together (Figure 5.5d) and become one drop with a diameter of around 1.21 mm (Figure 5.5e).

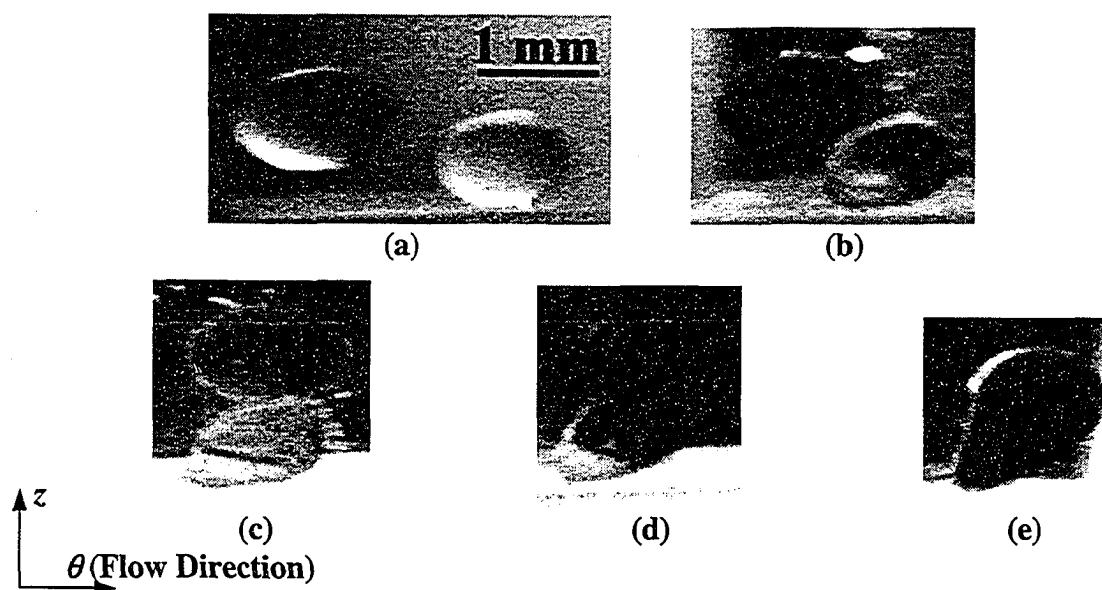


Figure 5.5 Coalescence of two corn syrup drops ($D_{0,L}=1.04$ mm; $D_{0,R}=0.94$ mm) in silicone oil at room temperature and 10 rpm in the APAM. The viscosity ratio is 1.08. Time and conditions for each figure: (a) $t=1277s=t_0$; (b) $t=1286s=t_0+9s$; (c) $t=1291=t_0+14s$; (d) $t=1292=t_0+15s$; (e) $t=1294=t_0+17s$. Note scale bar.

5.3.2 Polymer Blends

5.3.2.1 Blends from Batch Mixer and APAM

The morphology of polymer blends depends on material physical and chemical properties, and processing conditions. During polymer blending process, drop deformation, breakup and coalescence take place inside the mixer simultaneously and the dynamic equilibrium of drop breakup and coalescence determines the final particle distribution. Compatibilized blends are much more complicated due to either the addition of a third component or reaction of polymer components. In the following sections, the effects of pre-made compatibilizer and in-situ reactive compatibilization on blend morphology are studied.

Figure 5.6 compares the number average diameter and polydispersity of the dispersed particle size obtained from the batch mixer and the APAM at 190°C. Blends prepared in the APAM show similar number average particle size as those obtained from the batch mixer (Breuer *et al.*, 2004). Though the polydispersity of the dispersed particle show a wider particle distribution from the APAM, the results are still very satisfactory for blending small quantity materials. The data obtained from the APAM are used in the rest of this chapter.

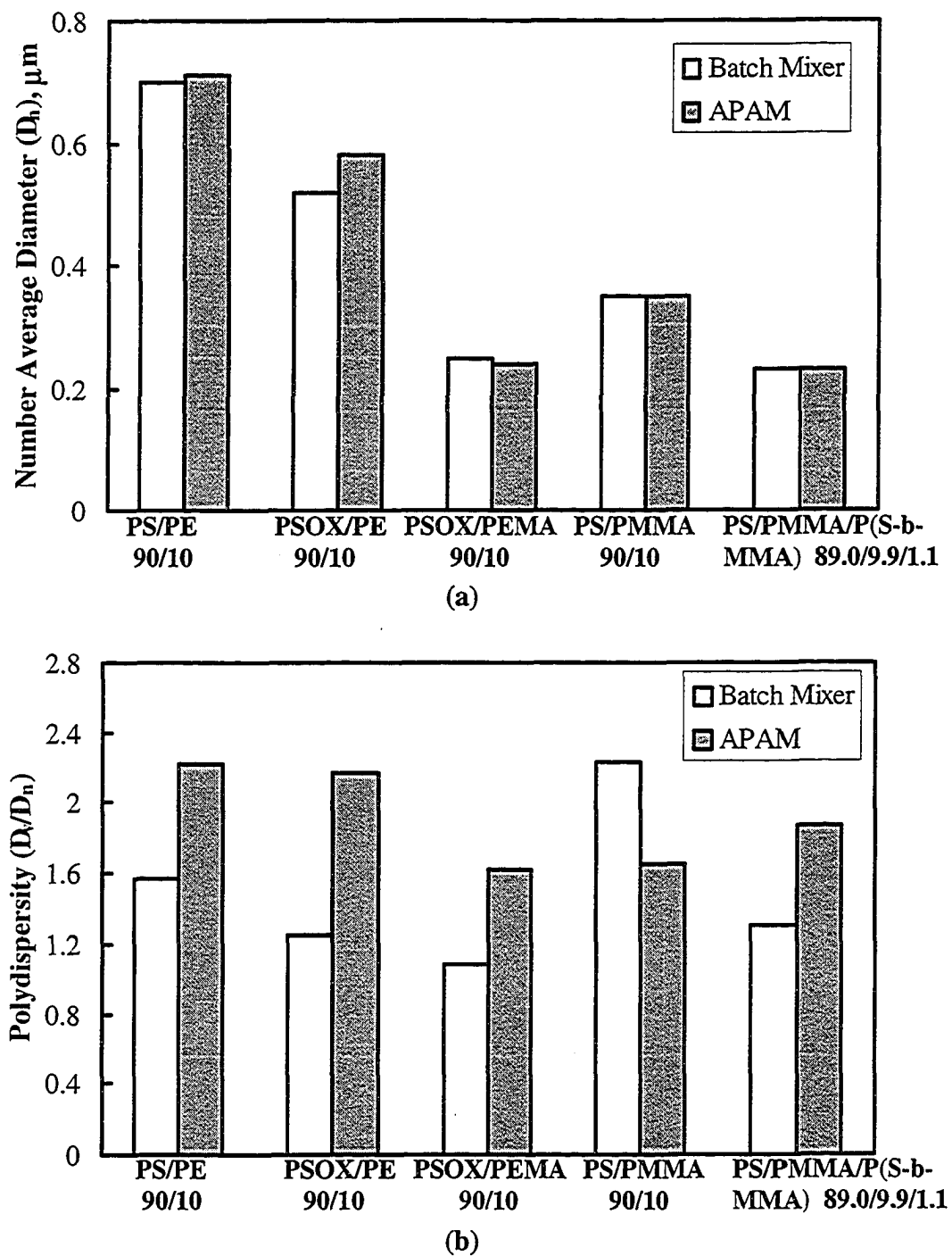


Figure 5.6 (a) Number average diameter and (b) Polydispersity of dispersed particle size obtained from batch mixer and the APAM. The block copolymer P(S-b-MMA) used has a molecular weight of 80,000-80,000 g/mol.

5.3.2.2 Pre-made Copolymer

5.3.2.2.1 Copolymer Composition

The emulsification curve, which relates the minor phase particle size to the amount of interfacial agent added to the classical emulsions, has been shown to be able to apply to polymer blends (e.g., Matos *et al.*, 1995; Cigana *et al.*, 1996). Figure 5.7 shows the emulsification curve for PS/PE (90/10) after addition of diblock copolymer P(S-b-E). The number and volume average diameters of PE decrease with increasing copolymer content sharply when the weight percentage of the copolymer is less than 5% of the dispersed phase. An equilibrium size ($d_v = 0.80 \pm 0.05 \mu\text{m}$ and $d_n = 0.47 \pm 0.03 \mu\text{m}$) is achieved when the copolymer amount is greater than 5%. The decrease in particle size is due to the interfacial tension reduction (Taylor, 1932, 1934; Anastasiadis *et al.*, 1989; Favis and Chalifoux, 1987; Lepers and Favis, 1999; Leper *et al.*, 1999; Liang *et al.*, 1999; Potschke *et al.*, 2000; Lyu *et al.*, 2002; Utracki, 2002) after a copolymer is added into an immiscible blend. The decrease is also due to the coalescence suppression (Sundararaj and Macosko, 1995; Lepers and Favis, 1999; Leper *et al.*, 1999; Lyu *et al.*, 2002) of the blend in the presence of the copolymer. The leveling off of the dispersed drop size at a higher copolymer concentration indicates a saturation of copolymer at the interface and formation of micelles in the homopolymer phases.

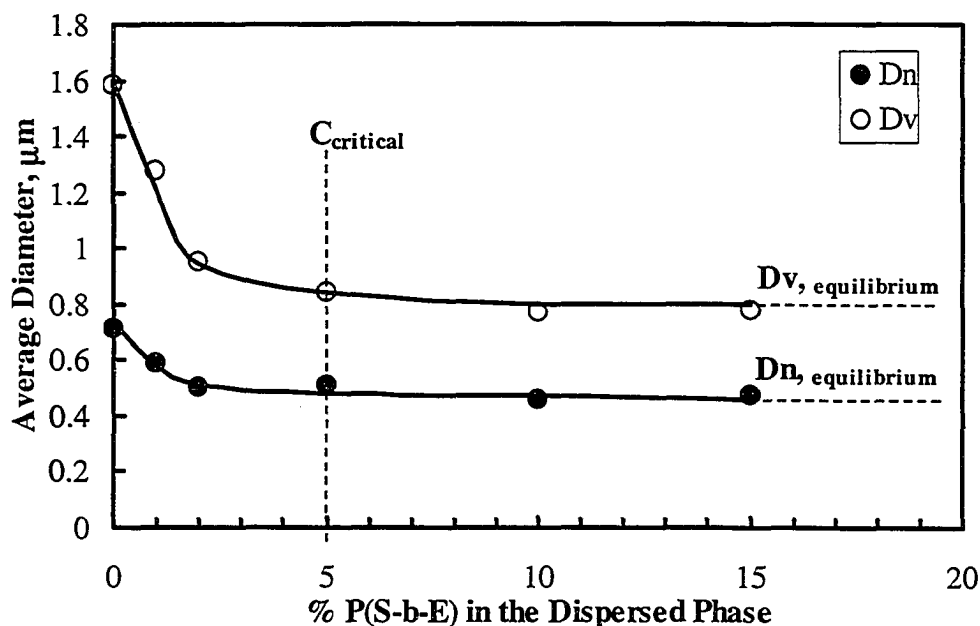


Figure 5.7 Dependence of the dispersed phase size for PS/PE (90/10) blend as a function of the weight percentage of P(S-b-E).

If the critical concentration from the emulsification curve is taken as 5%, the number of molecules required to saturate the interface is 6.3 nm^2 per molecule according to Matos *et al.* (1995, see also Appendix IV for calculation details). It suggests that the saturation concentration for P(S-b-E) with $M_n = 100,000$ – $100,000 \text{ g/mol}$ at the interface is $0.16 \text{ molecule/nm}^2$. This is comparable to the estimation of the maximum interfacial coverage based on Lyu *et al.* (2002), which is $0.15 \text{ molecule/nm}^2$ (see Chapter 4). The interfacial tension at an interfacial coverage of $0.15 \text{ molecule/nm}^2$ is 80% of the uncompatibilized blend, that is, 3.9 mN/m (Lyu *et al.*, 2002) for the compatibilized blends with copolymer composition no less than 5%. According to Taylor's equation (5.1), the particle size is proportional to the interfacial tension and its reduction resulting from interfacial tension should be 20%, i.e., the number average particle size should decrease from 0.71 μm to 0.57 μm if only the interfacial tension contribution is

accounted. However, the number average particle size is less than 0.57 μm when the addition of the copolymer is equal or more than 5%. Therefore, the further reduction comes from coalescence suppression (Sundararaj and Macosko, 1995; Lepers and Favis, 1999).

5.3.2.2.2 Copolymer Molecular Weight

Figure 5.8 shows the effect of molecular weight of a symmetric diblock copolymer P(S-b-MMA) on the dispersed drop size of blend PS/PMMA (90/10). The viscosity ratio of the blend at a shear rate of 65s^{-1} is 5.6, where Taylor's theory predicts no breakup. As M_n increases, the number and volume average particle diameters decrease first and then levels off when $M_n \geq 50,000 - 50,000$ g/mol (Figure 5.8). The entanglement molecular weight for PS is 13,000 g/mol (Fetters *et al.*, 1994) and for PMMA is 7,000 g/mol (Fuchs *et al.*, 1996). All the copolymers used have a molecular weight above entanglement molecular weight, which is required for good interfacial adhesion (Creton *et al.*, 2001; Eastwood and Dadmun, 2002; Benkoski *et al.*, 2003). The lower molecular weight copolymer (e.g., 25,000-25,000 g/mol) is able to diffuse to the interface quickly and to prevent dynamic coalescence, but it may be not so efficient to provide static stability (Macosko *et al.*, 1996). The high molecular weight diblock copolymer (e.g., 80,000-80,000 g/mol) can provide static stability, but is not very efficient since its mobility is reduced significantly (Macosko *et al.*, 1996).

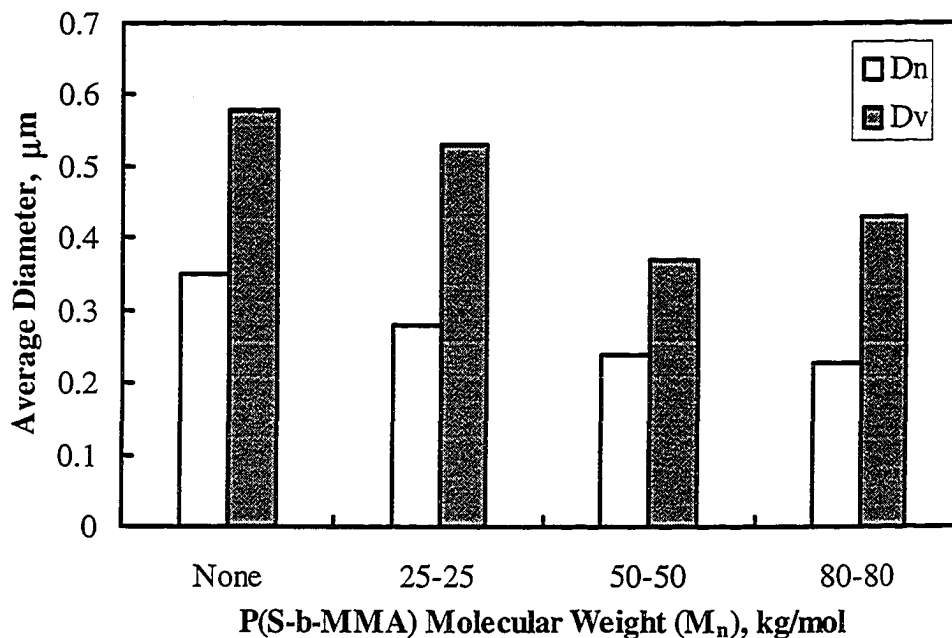


Figure 5.8 Dependence of the dispersed phase size for PS/PMMA (90/10) blend as a function of copolymer P(S-b-MMA) molecular weight. The amount of copolymer is 10% of PMMA.

Recently, Galloway *et al.* (2004) studied the effect of molecular weight of diblock copolymer (P(S-b-E)) on polymer blend (PS/PE 50/50) morphology. They showed that there is an optimum molecular weight of copolymer, which is efficient in reducing the final dispersed particle size and stabilizing the morphology during annealing. Though the current chapter of this thesis did not show the optimum diblock molecular weight for the PS/PMMA blend since only three different molecular weight of P(S-b-MMA) were studied, results suggest that the copolymer with a molecular weight of 80,000-80,000 g/mol may be too high for blend PS/PMMA. The effects of the diblock molecular weight on final morphology will be further discussed in Section 5.3.2.2.3.

5.3.2.2.3 Blending Sequences

The morphology of polymer blends depends on how the polymers incorporate with each other. Therefore, the blending sequence is important. Two systems, PS/PE/P(S-b-E) and PS/PMMA/P(S-b-MMA), are used to study the effect of blending sequence on morphology. The experiments can be classified according to melting and mixing sequences: premelting, first mixing and second mixing. Premelting is a process that the polymers stay inside the mixer at the set temperature without rotating the rotor. First mixing is that some part or all of the polymers are mixed together for the first time. Second mixing is that polymers are mixed again after some of them have been mixed earlier.

Table 5.4 shows the number and volume average particle size of the final dispersed drop for PS/PE/P(S-b-E) blend after different blending conditions. Premelting does not affect the blend final particle size (D_n or D_v). However, for the cases when PS is melted (softened) or mixed with copolymer first, especially for the premixed case, the final particle size of the blend decreases. For the case when PE is first mixed with copolymer in a master batch and then mixed with PS in a second batch, the final particle size increases. A possible reason for these observations may be due to the fact that the block copolymer, P(S-b-E), prefers PE phase (Lyu *et al.*, 2002). Therefore, if the copolymer is first melted or mixed with PS, it migrates to PE phase when it later mixes with PE, resulting in less micelles formed and better distribution at the interface. If the copolymer is first mixed with PE, most of the copolymer stays in PE phase as micelles,

Table 5.4 Effect of blending sequences on particle size**Blend: PS/PE (90/10) with 10% P(S-b-E)**

Feeding Sequences			D_n (μm)	D_v (μm)	D_w/D_n	Comments
Premelt	First Mix	Second Mix				
No	All mixed together for 10 min	No	0.46	0.77	1.67	Premelt has no effect
All polymers for 5 min	Mixed for 10 min	No	0.46	0.65	1.41	
All polymers for 10 min	Mixed for 10 min	No	0.46	0.72	1.57	
No	PS+P(S-b-E) mixed for 10 min	PE added and mixed for 10 min	0.41	0.54	1.32	Premelt or premix block copolymer with PS results in finer particle distribution
PS+P(S-b-E) for 10 min	Mixed with PE for 10 min	No	0.35	0.53	1.51	
No	PS+P(S-b-E) mixed for 10 min, then took out samples	Premixed sample with PE mixed for 10 min	0.42	0.65	1.55	PE premixed with block copolymer in a master batch increase the final particle size
No	PE+P(S-b-E) mixed for 10 min	PS added and mixed for 10 min	0.42	0.74	1.76	
PE+P(S-b-E) for 10 min	Mixed with PS for 10 min	No	0.44	0.99	2.25	
No	PE+P(S-b-E) mixed for 10 min, then took out samples	Premixed sample with PS mixed for 10 min	0.50	0.78	1.56	

and does not move to the blend interface efficiently, leading to a slight increase in the final particle size. Additionally, the block copolymer has a high molecular weight (100,000-100,000 g/mol), well above the entanglement molecular weight of PE, 800 g/mol (Fetter *et al.*, 1994) and PS, 13,000 g/mol (Fetter *et al.*, 1994). Such a high molecular weight may inhibit the mobility of the block copolymer to the interface

(Sundararaj and Macosko, 1995; Macosko *et al.*, 1996; Galloway *et al.*, 2004; see also Section 5.3.2.2.2). So, if both PS and PE together with P(S-b-E) are melted together, the high molecular weight diblock may stay in homopolymer phases, and does not affect the final morphology. As a result, premelting shows no effect when all the polymers are added together.

Tables 5.5-5.7 show the particle size of PS/PMMA/P(S-b-MMA) blend obtained from different blending sequences. The molecular weights of the diblock copolymer used are 25,000-25,000 g/mol in Table 5.5, 50,000-50,000g/mol in Table 5.6 and 80,000-80,000 g/mol in Table 5.7. Without the copolymer, the dispersed phase of the pure blend has a number and a volume average diameter of 0.35 μm and 0.58 μm , respectively. With the lower molecular weight (25,000-25,000 g/mol) block copolymer (Tables 5.5), the minor phase particle size decreases if premelting or premixing is applied before blending all materials together. With the higher molecular weight (50,000-50,000 g/mol) block copolymer (Table 5.6), the particle size does not change much. However, with the highest molecular weight (80,000-80,000 g/mol) block copolymer (Table 5.7), the particle size increases significantly if either premelting or premixing is used during the blending. The dispersed phase of some blends in Table 5.7 has a number and a volume average diameter close to or slightly greater than that of the pure blend and the particles show a wider distribution. This suggests that the high molecular weight diblock copolymer fails to function at the interface, owing to the steric effects that reduce the mobility of the copolymer to the interface (Sundararaj and Macosko, 1995; Macosko *et al.*, 1996) and formation of micelles in the homopolymer phase. However, a lower molecular weight P(S-b-MMA), <80,000-80,000 g/mol, is more efficient in obtaining a

fine morphology since the diblock has better mobility and less micelles are formed, which allows it to reach the interface to inhibit drop coalescence.

The formation of micelles can be confirmed with TEM micrographs (Figures 5.9 and 5.10). For PS/PMMA blends studied, PMMA is the minor phase and the white particles in the micrographs is the PMMA phase; PS is the major phase and the darker continuous phase is the PS phase. Therefore, the diblock copolymer appears to be a mixture of white and dark in the micrographs. If the copolymer forms micelle in PMMA phase, it appears to be darker; if it forms micelle in PS phase, it appears to be lighter.

Table 5.5 Effect of blending sequences on particle size

Blend: PS/PMMA (90/10) with 10% P(S-b-MMA) (25,000-25,000 g/mol)

Feeding Sequences		D_n (μm)	D_v (μm)	D_v/D_n
First Mix	Second Mix			
No copolymer. PS+PMMA mixed for 10 min	No	0.35	0.58	1.66
All mixed together for 10 min	No	0.28	0.53	1.89
Premelt all for 10 min and then mixed for 10 min	No	0.25	0.51	2.04
PMMA+P(S-b-MMA) mixed for 10 min	PS added and mixed for 10 min	0.20	0.24	1.20
PMMA+P(S-b-MMA) mixed for 10 min, then took out the sample	Premixed sample together with PS mixed for 10 min	0.24	0.53	2.21
PS+P(S-b-MMA) mixed for 10 min	PMMA added and mixed for 10 min	0.23	0.32	1.39
PS+P(S-b-MMA) mixed for 10 min, then took out the sample	Premixed sample together with PMMA mixed for 10 min	0.22	0.30	1.36

Table 5.6 Effect of blending sequences on particle size**Blend: PS/PMMA (90/10) with 10% P(S-b-MMA) (50,000-50,000 g/mol)**

Feeding Sequences		D_n (μm)	D_v (μm)	D_v/D_n
First Mix	Second Mix			
No copolymer. PS+PMMA mixed for 10 min	No	0.35	0.58	1.66
All mixed together for 10 min	No	0.24	0.37	1.54
Premelt all for 10 min and then mixed for 10 min	No	0.22	0.44	2.00
PMMA+P(S-b-MMA) mixed for 10 min	PS added and mixed for 10 min	0.22	0.29	1.32
PMMA+P(S-b-MMA) mixed for 10 min, then took out the sample	Premixed sample together with PS mixed for 10 min	0.22	0.31	1.41
PS+P(S-b-MMA) mixed for 10 min	PMMA added and mixed for 10 min	0.24	0.45	1.88
PS+P(S-b-MMA) mixed for 10 min, then took out the sample	Premixed sample together with PMMA mixed for 10 min	0.24	0.32	1.33

Table 5.7 Effect of blending sequences on particle size**Blend: PS/PMMA (90/10) with 10% P(S-b-MMA) (80,000-80,000 g/mol)**

Feeding Sequences		D_n (μm)	D_v (μm)	D_v/D_n
First Mix	Second Mix			
No copolymer. PS+PMMA mixed for 10 min	No	0.35	0.58	1.66
All mixed together for 10 min	No	0.23	0.43	1.87
Premelt all for 10 min and then mixed for 10 min	No	0.30	0.69	2.30
PMMA+P(S-b-MMA) mixed for 10 min	PS added and mixed for 10 min	0.26	0.54	2.08
PMMA+P(S-b-MMA) mixed for 10 min, then took out the sample	Premixed sample together with PS mixed for 10 min	0.38	0.73	1.92
PS+P(S-b-MMA) mixed for 10 min	PMMA added and mixed for 10 min	0.33	0.90	2.73
PS+P(S-b-MMA) mixed for 10 min, then took out the sample	Premixed sample together with PMMA mixed for 10 min	0.36	0.71	1.97

In Figure 5.9, samples were prepared in the following sequences: PS and P(S-b-MMA) were first mixed for 10 min, and then PMMA was added and mixed together for 10 min. In Figure 5.10, PS and P(S-b-MMA) were first mixed for 10 min in a master batch, and later mixed together with PMMA in a new batch for 10 min. Two different molecular weight diblock copolymers were used. One has a lower molecular weight, 25,000-25,000 g/mol (Figures 5.9a and 5.10a) and the other, higher molecular weight, 80,000-80,000 g/mol (Figures 5.9b, 5.10b and 5.10c). With a smaller molecular weight copolymer, the polymer blend morphology is finer. With a higher molecular weight copolymer, the dispersed phase particle size is bigger. More micelles are observed when the blend with a higher molecule weight diblock. The copolymer micelles are formed not only inside the white PMMA particles (Figures 5.9b and 5.10b), but also in the PS matrix (Figure 5.10c).

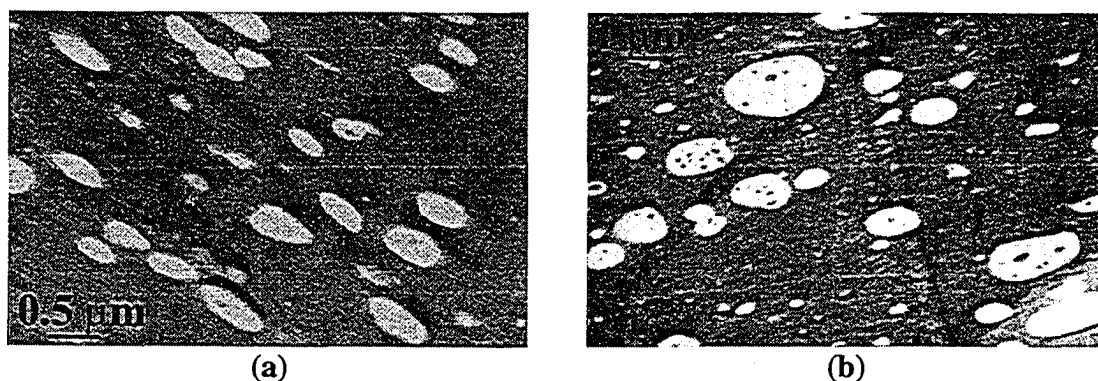


Figure 5.9 TEM micrographs of PS/PMMA/P(S-b-MMA) (89.0/9.9/1.1 wt%) blends. PS and P(S-b-MMA) were first mixed at 190°C for 10 min, and PMMA was then added and mixed for 10 min. The molecular weight of P(S-b-MMA) for each figure: (a) 25,000-25,000 g/mol, (b) 80,000-80,000 g/mol. Note scale bars.

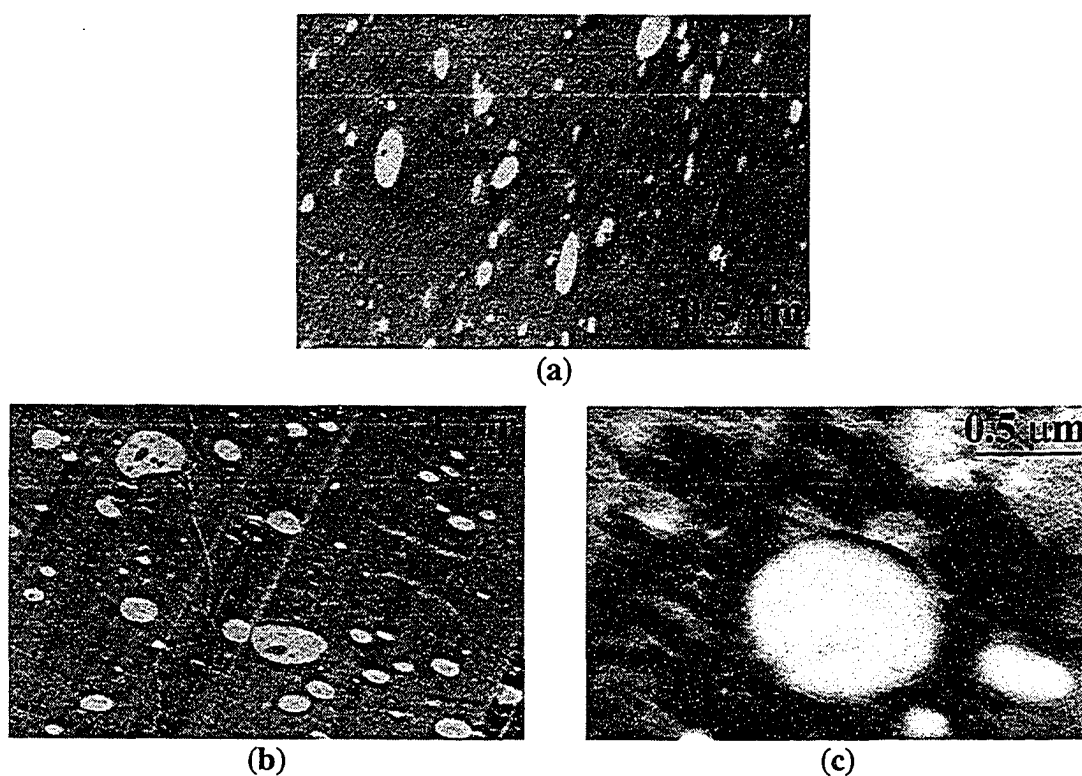


Figure 5.10 TEM micrographs of PS/PMMA/P(S-b-MMA) (89.0/9.9/1.1 wt%) blends. PS and P(S-b-MMA) were first mixed at 190°C for 10 min in a master batch and then mixed with PMMA in a new batch for 10 min. The molecular weight of P(S-b-MMA) for each figure: (a) 25,000-25,000 g/mol; (b) and (c) 80,000-80,000 g/mol. Note scale bars.

5.3.2.3 In-situ Reactive Compatibilization

5.3.2.3.1 Blend Composition

The oxazoline group in PSOX and the maleic anhydride group in PEMA undergo a cross-linking reaction when PSOX is melt blended with PEMA (Liu *et al.*, 1990; Figure 4.1a). Figures 5.11 and 5.12 show SEM micrographs for PSOX/PE/PEMA blends at several different compositions. Table 5.8 summarizes the average particle size and lists the particle size obtained from Taylor's limit and Wu's correlation for comparison.

When PSOX is 90% as the major phase and PE is the minor phase as shown in Figures 5.11a, the viscosity ratio of the system is 0.24, less than 1, and the number and

volume average diameters of the dispersed particles are $0.58\ \mu\text{m}$ and $1.26\ \mu\text{m}$. When the minor phase PE is changed to PEMA, the viscosity ratio of the system is 0.32, similar to the non-reactive blend. However, the number and volume average particle diameters are decreased to $0.24\ \mu\text{m}$ and $0.39\ \mu\text{m}$, which correspond to a 59% decrease in number average drop size and a 69% reduction in volume average drop size compared to the non-reactive blend. The particle distribution is also narrower as shown in Figure 5.11b, owing to the reaction.

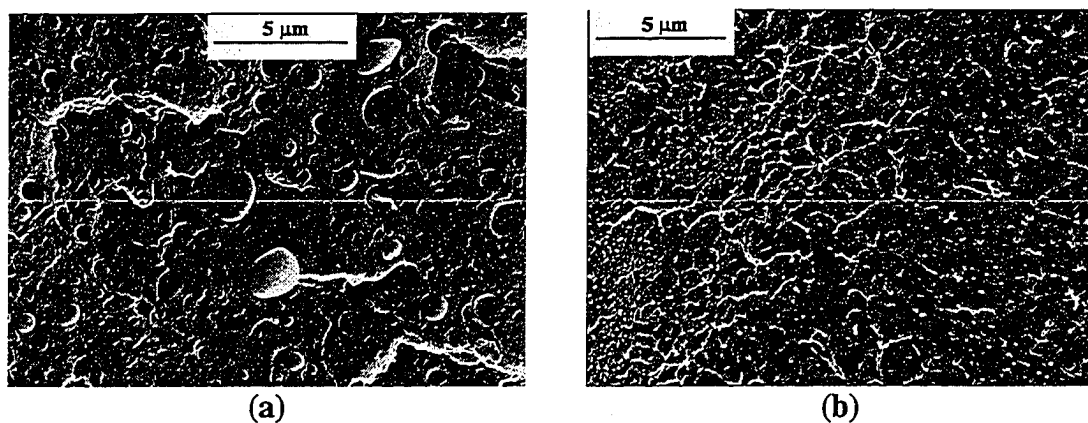


Figure 5.11 SEM micrographs of PSOX/PE/PEMA blends with a composition of (a) 90/10/0; (b) 90/0/10. Note scale bars.

When PSOX/PE/PEMA blend has 10% PSOX as the minor phase and the composition of PE and PEMA varies, the drop size decreases if PEMA content increases (Figures 5.12a-d and Table 5.8) because more PSOX reacts with PEMA. When PEMA is 10% of the blend, the micrograph shows that the dispersed phase is a mixture of particles and flat spherical domains. The flat spherical domains may be the cross-linked product. After PEMA exceeds 15% of the blend, no particle is discernable in SEM micrographs

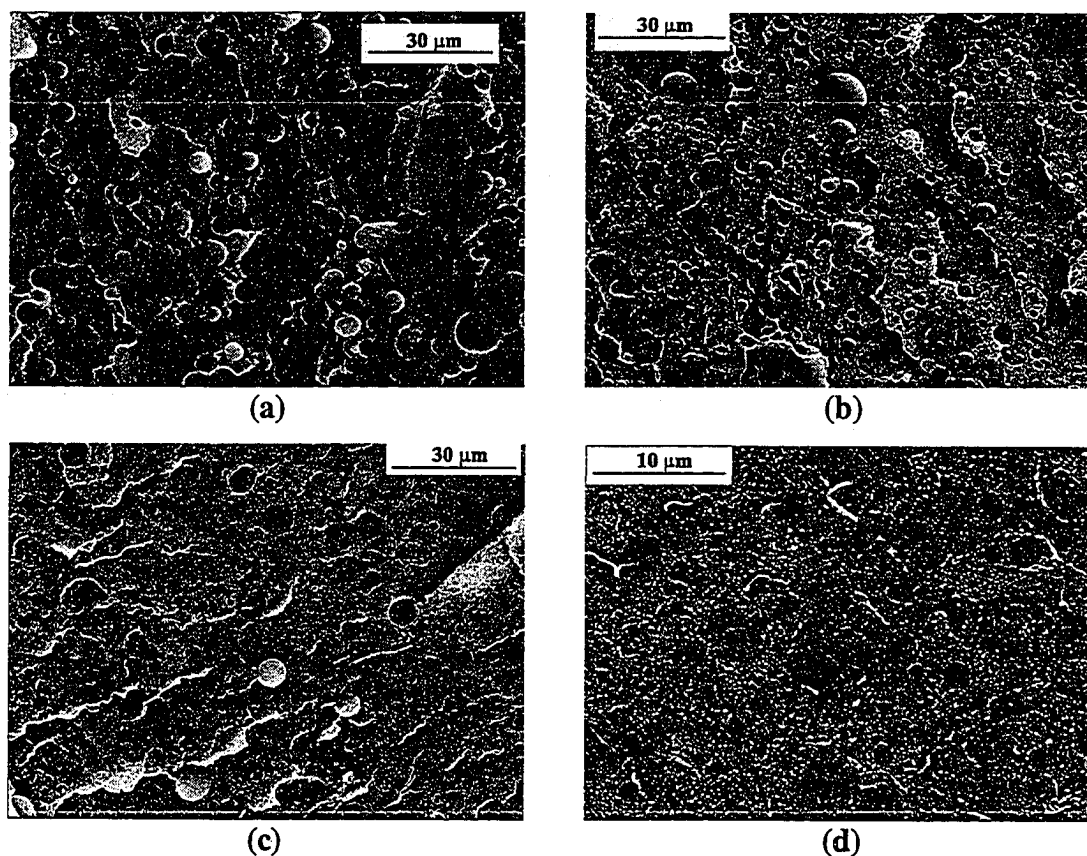


Figure 5.12 SEM micrographs of PSOX/PE/PEMA blends with a composition of (a) 10/90/0; (b) 10/85/5; (c) 10/80/10; (d) 10/75/15. Note scale bars.

Table 5.8 Effect of blend composition on particle size

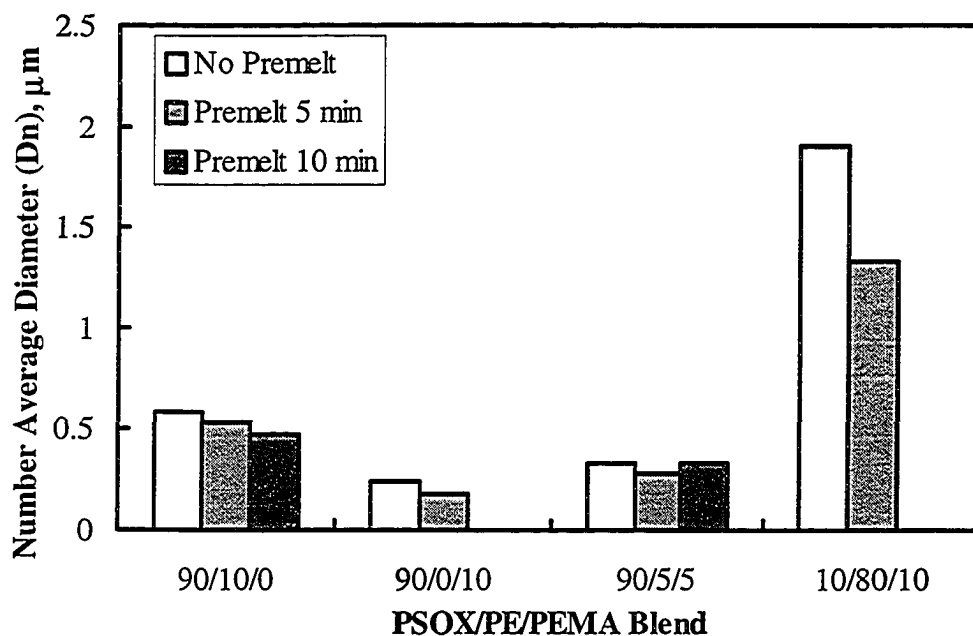
PSOX/PE/PEMA	η_r at 65s^{-1}	D_n (μm)	D_v (μm)	Taylor Limit (μm)	Wu's Correlation (μm)
90/10/00	0.24	0.58	1.26	0.06	0.80
90/5/5		0.33	0.49		
90/00/10	0.32	0.24	0.39	0.06	0.63
10/90/00	4.13	3.63	5.14		3.31
10/85/5		2.32	4.82		
10/80/10		2.17	3.61		
10/75/15		No particle discernable, only spherical domains ($D_n=1.33\ \mu\text{m}$ and $D_v=2.05\ \mu\text{m}$) embedded inside the matrix			

(Figure 5.12d), but flat spherical domains, adhering closely to the matrix, are clearly seen embedded inside the matrix. The domains appear to be smaller, having an average diameter: $D_n=1.3 \mu\text{m}$.

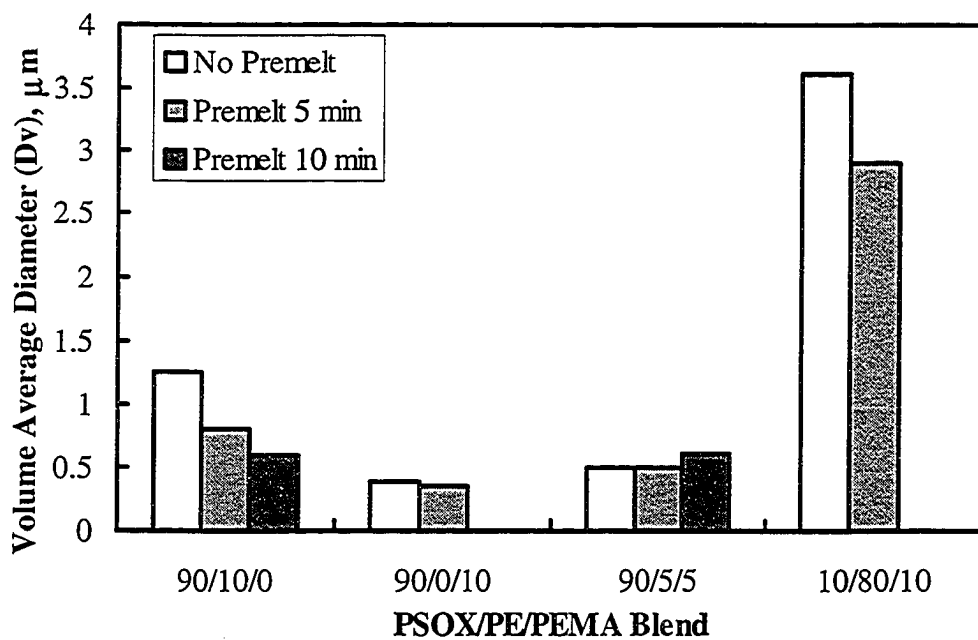
5.3.2.3.2 Premelting

Figure 5.13 shows the effect of premelting on the dispersed particle size of PSOX/PE/PEMA blends. It is found that for PSOX/PE system, keeping the polymers inside the APAM for either 5 min or 10 min before mixing decreases the final drop size. During the premelting process, the oxazoline group in PSOX may undergo decomposition, resulting in a lower interfacial viscosity (Favis and Chalifoux, 1987), and therefore, a finer morphology is observed when the polymers are melted inside the chamber first.

When PEMA is fed together with PSOX during the melting process, a cross-linking reaction takes place, leading to a layer of protective shell between the phases. The protective shell stabilizes the interface and suppresses drop coalescence (Sundararaj and Macosko, 1995), however, as more and more newly formed products accumulate at the interface, drop breakup becomes difficult (see Chapter 4). Therefore, at a premelting time of 5 min, there is a slight decrease in particle size; as the premelting time is increased to 10 min, the drop size is increased. This can be seen in PSOX/PE/PEMA 90/5/5 blend. For a blend composed of 10/80/10 PSOX/PE/PEMA, the particles can be clearly seen if polymers are blended immediately as they are fed in. However, if the polymers are



(a)



(b)

Figure 5.13 Dependence of the dispersed phase (a) number average diameter and (b) volume average diameter for PSOX/PE/PEMA blend as a function of premelting time. All polymers are added together. For the 10/80/10 blend, premelt 5 min, few particles are discernable, and spherical domains are averaged.

premelted for 5 min before mixing, almost no particles exist. Instead, only spherical domains as shown in Figure 5.12d are observed, which shows evidence that the reaction occurs during the melting process.

5.4 DISCUSSION

When a corn syrup drop is sheared inside silicone oil in the Couette apparatus and the APAM miniature mixer, different drop deformation and breakup phenomena occur owing to the different flow fields that the Couette cell and the APAM generated. The APAM can generate both shear and extension flow fields, like a batch mixer or an extruder. The syrup drop inside the APAM undergoes not only breakup, but also coalescence, a situation similar to the real case in industry. The visualization results indicate that the morphology development in polymer blends will be even more complicated in industry owing to the viscoelastic and shear-thinning properties of polymers combined with complex flow fields. In Chapters 3, it has been shown that a polymer drop experiences different kinds of breakup mechanisms even when it experiences only simple shear. If extensional flow coexists with shear flow, the breakup modes will be altered.

Polymer blends from the APAM showed similar number average dispersed phase particle size as those obtained from the batch mixer. This shows that the APAM is successful in effectively blending small amounts of polymer blends (Breuer *et al.*, 2004), which is useful for lab scale work and especially for materials that are available in small quantities and are expensive.

The effects of pre-made copolymer and in-situ reactive compatibilization on morphology development are studied inside the APAM. Generally, adding diblock copolymer or using in-situ reactive blends decreases dispersed phase drop size, due to the suppression of drop coalescence and the decrease in interfacial tension. The particle size decreases with the amount of copolymer added and it levels off at a certain amount, 5% for PS/PE blend. This suggests that there is a saturation or maximum concentration of the block copolymer at the interface, which is calculated to be $0.15 \text{ molecule/nm}^2$ (Matos *et al.*, 1995; Lyu *et al.*, 2002) for P(S-b-E) with a molecular weight of 100,000-100,000 g/mol.

Adding copolymer is not so efficient as in-situ reactive compatibilization since much of the copolymer tends to form micelles rather than migrate to the interface. The in-situ reactive blend, PSOX/PE/PEMA, shows a finer morphology and a better interfacial adhesion, for example, a reactive blend composed with 90% PSOX and 10% PEMA versus a non-reactive blend with 90% PSOX and 10% PE. When PSOX is the minor phase at 10% total concentration and the composition of the other two components PE and PEMA varies, it is found that the drop size decreases significantly as PEMA content increases due to the increased reaction between PSOX and PEMA. At 15% PEMA, no distinct particle is seen. Instead, small spherical domains are embedded inside the matrix. This indicates that the cross-linking reaction between the oxazoline group in PSOX and maleic anhydride group in PEMA reduces the dispersed phase size and increases the interfacial adhesion sufficiently so that the fracture surface is different. In this case, the cross-linked product acts as a protective shell around the dispersed particle, which stabilizes the drop (Chapter 4) and suppresses drop coalescence (Sundararaj *et al.*,

1995b). Additionally, the cross-linked product connects the minor phase with the major phase by chemical bonding and the interfacial adhesion is greatly improved and this will enhance the blend's mechanical properties. Therefore, interfacial reaction is a more efficient method in compatibilizing immiscible blends by creating smaller particle size and better interfacial adhesion.

Melting and mixing processes are important for polymer blends (Scott and Macosko, 1991, 1995; Lindt and Ghosh, 1992; Sundararaj *et al.*, 1992, 1995b). During the initial stages of polymer blending, polymer pellets softened or melt and deformed into lamellar structures or sheets (Lindt and Ghosh, 1992; Scott and Macosko, 1991, 1995; Sundararaj *et al.*, 1992, 1995b). The formation of a sheet is an effective way to achieve quick reduction in particle dimension (Sundararaj *et al.*, 1995b; Willemse *et al.*, 1999; Potente *et al.*, 2001; Lin *et al.*, 2003; Chapter 1). The effects of melting and mixing on compatibilized systems are complex and different results are obtained in different systems.

For PS/PE/P(S-b-E) blends, where the diblock copolymer has a molecular weight of 100,000-100,000 g/mol, if all the polymers are added together, premelting has no effect; if the copolymer is fed together with PS first, premelting or premixing decreases the final particle size; and if copolymer is added together with PE first, premelting or premixing increases the dispersed phase size slightly. In other words, premelting and premixing affect the final PE phase size in different ways depending on how the polymers are added. This may be due to the fact that P(S-b-E) prefers PE phase (Lyu *et al.*, 2002) and consequently, it likes to move to the interface if it is premelted or premixed

with PS and it dislikes the interface if it is first melted or mixed with PE. However, since the diblock has a high molecular weight, the steric effect should also be considered.

If the diblock copolymer molecular weight is too low, lower or close to the entanglement molecular weight, it suppresses dynamic coalescence, but may not be able to achieve static stability and to improve interfacial adhesion (Creton *et al.*, 2001; Eastwood and Dadmun, 2002; Benkoski *et al.*, 2003). If the copolymer molecular weight is too high, though the interfacial adhesion is improved, the steric effect reduces the copolymer mobility (Sundararaj and Macosko, 1995; Macosko *et al.*, 1996) and thus the ability to suppress dynamic coalescence. Therefore, an intermediate molecular weight diblock molecular weight is preferred to obtain a fine morphology. For the copolymer P(S-b-MMA) studied, the molecular weight is well above the entanglement molecular weight, or in other words, the molecular weight of P(S-b-MMA) is from intermediate to high. The particle size of PS/PMMA/P(S-b-MMA) blend decreases as the copolymer molecular weight increases from 25,000-25,000 g/mol to 50,000-50,000 g/mol, but it levels off as diblock molecular weight is increased to 80,000-80,000 g/mol.

The steric effect of copolymer on the final morphology can also be clearly seen by using different molecular weight P(S-b-MMA) for PS/PMMA blends. The molecular weights for the diblock copolymer are 25,000-25,000 g/mol, 50,000-50,000 g/mol and 80,000-80,000 g/mol. For the lower molecular weight diblock (25,000-25,000 g/mol), the blends show a finer particle size and distribution when either premelting or premixing process is used during the blending. For the higher molecular weight diblock (50,000-50,000 g/mol), the blends show a similar morphology when either premelting or premixing process is used. For the highest molecular weight diblock (80,000-80,000

g/mol), a coarsen morphology is obtained when either premelting or premixing is applied prior to blending. This once again underlines the importance of the mobility of the copolymer to the interface. It also suggests that melting process is crucial for morphology development in compatibilized systems. A finer morphology can be obtained when premelting is applied and the copolymer has an intermediate molecular weight.

Premelting also affects the morphology of a reactive system. For example, PSOX/PE/PEMA blends, when premelted for 5 min, a finer morphology is observed. However, when premelted for a longer time, e.g. 10 min, a coarser morphology is observed. Though PSOX experiences decomposition during the premelting process, the cross-linking reaction during the melting process may be more important in determining the final morphology. The reaction between PSOX and PEMA creates a new substance, acting as a copolymer at the interface. This newly formed product stabilizes the drop. At a short time of melting, it helps drop breakup and coalescence suppression. At a longer time of melting, it delays drop breakup as shown in Chapter 4.

5.5 CONCLUSIONS

The morphology of polymer blends using pre-made compatibilizer and in-situ compatibilizer is studied in a custom-built miniature mixer – the APAM. Visualization results show that polymers inside the APAM experience both shear and extensional flow, and drop deformation and breakup in the APAM are complex. The samples obtained from the APAM show a similar dispersed particle size to those obtained from a larger laboratory batch mixer. The APAM exhibits itself as a useful mixer for blending small quantities of expensive materials (Breuer *et al.*, 2004).

The compatibilized systems, either with pre-made copolymer, or in-situ reaction, show a finer morphology when compared with the uncompatibilized blends. The emulsification curve suggests that there exists a saturation interfacial concentration for block copolymer. Adding copolymer into an immiscible blend decreases interfacial tension and suppresses drop coalescence. It is found that coalescence suppression depends on the molecular weight of the interfacial agent and requires an intermediate molecular weight, which is able to provide both dynamic and static coalescence suppression. In-situ reaction is more efficient in generating fine particles and better interface adhesion.

Melting and mixing are proven to be important in compatibilized systems, though the effects differ from blend to blend. However, there are other factors, such as the preference of copolymer to a particular phase, diblock molecular weight and reactive functional group of polymers, which determine the interfacial distribution of compatibilizer and thus, influence the final morphology.

5.6 REFERENCES

- Anastasiadis, S.H.; Gancarz, I.; Koberstein, J.T. *Macromolecules* **1989**, *22*, 1449-1453.
- Bai, Y.; Sundararaj, U.; Nandakumar, K. *Polymer Processing Society 20th Annual Meeting*, Paper No. 240, **2004**.
- Benkoski, J.J.; Flores, P.; Kramer, E.J. *Macromolecules* **2003**, *36*, 3289-3302.
- Breuer, O.; Sundararaj, U.; Toogood, R.W. *Polym. Eng. Sci.* **2004**, *44*, 868-879.
- Cigana, P.; Favis, B.D.; Jerome, R. *J. Polym. Sci., B, Polym. Phys.* **1996**, *34*, 1691-1700.
- Creton, C.; Kramer, E.J.; Brown, H.R.; Hui, C.-Y. *Adv. Polym. Sci.* **2001**, *156*, 56-136.

- Eastwood, E.A.; Dadmun, M.D. *Macromolecules* **2002**, *35*, 5069-5077.
- Elemans, P.H.M.; Janssen, J.M.H.; Meijer, H.E.H. *J. Rheol.* **1990**, *34*, 1311-1325.
- Favis, B.D.; Chalifoux, J.P. *Polym. Eng. Sci.* **1987**, *27*, 1591-1600.
- Fetters, L.J.; Lohse, D.J.; Richter, D.; Witten, T.A.; Zirkel, A. *Macromolecules* **1994**, *27*, 4639-4647.
- Fuchs, K.; Friedrich, Chr.; Weese, J. *Macromolecules* **1996**, *29*, 5893-5901.
- Fortelny, I. *J. Macromol. Sci.-Phys.* **2000**, *B39*, 67-78.
- Galloway, J.A.; Jeon, H.K.; Bell, J.R.; Macosko, C.W. *submitted to Polymer* **2004**.
- Grace, H.P. *Chem. Eng. Commun.* **1982**, *14*, 225-277.
- Grulke, E.A. *Polymer Processing Engineering*; Prentice-Hall: New Jersey, 1994.
- Lepers, J.-C.; Favis, B.D. *AIChE J.* **1999**, *45*, 887-895.
- Lepers, J.-C.; Favis, B.D.; Lacroix, C. *J. Polym. Sci., B, Polym. Phys.* **1999**, *37*, 939-951.
- Liang, H.; Favis, B.D.; Yu, Y.S.; Eisenberg, A. *Macromolecules* **1999**, *32*, 1637-1642.
- Lin, B.; Sundararaj, U.; Mighri, F.; Huneault, M.A. *Polym. Eng. Sci.* **2003**, *43*, 891-904.
- Lindt, J.T.; Ghosh, A.K. *Polym. Eng. Sci.* **1992**, *32*, 1802-1813.
- Liu, N.C.; Baker, W.E.; Russell, K.E. *J. Appl. Polym. Sci.* **1990**, *41*, 2285-2300.
- Liu, T.M.; Xie, H.Q.; O'Callaghan, K.J.; Rudin, A.; Baker, W.E. *J. Polym. Sci., B, Polym. Phys.* **1993**, *31*, 1347-1362.
- Lyu, S.; Jones, T.D.; Bates, F.S.; Macosko, C.W. *Macromolecules* **2002**, *35*, 7845-7855.
- Macosko, C.W.; Guegan, P.; Khandpur, A.K.; Nakayama, A.; Marechal, P.; Inoue, T. *Macromolecules* **1996**, *29*, 5590-5598.
- Matos, M.; Favis, B.D.; Lomellini, P. *Polymer* **1995**, *36*, 3899-3907.

- Potente, H.; Bastian, M.; Bergemann, K.; Senge, M.; Scheel, G.; Winkelmann, Th.
Polym. Eng. Sci. **2001**, *41*, 222-231.
- Potschke, P.; Malz, H.; Pionteck J. *Macromol. Symp.* **2000**, *149*, 231-236.
- Scott, C.E.; Macosko, C.W. *Polym. Bull.* **1991**, *26*, 341-348.
- Scott, C.E.; Macosko, C.W. *Polymer* **1995**, *36*, 461-470.
- Sundararaj, U.; Macosko, C.W.; Rolando, R.J.; Chan, H.T. *Polym. Eng. Sci.* **1992**, *32*,
1814-1823.
- Sundararaj, U.; Macosko, C.W. *Macromolecules* **1995**, *28*, 2647-2657.
- Sundararaj, U.; Macosko, C.W.; Nakayama, A.; Inoue, T. *Polym. Eng. Sci.* **1995a**, *35*,
100-114.
- Sundararaj, U.; Dori, Y.; Macosko, C.W. *Polymer* **1995b**, *36*, 1957-1968.
- Taylor, G.I. *Proc. R. Soc. London, Ser. A* **1932**, *138*, 41-48.
- Taylor, G.I. *Proc. R. Soc. London, Ser. A* **1934**, *146*, 501-523.
- Utracki, L.A.; Shi, Z.H. *Polym. Eng. Sci.* **1992**, *32*, 1824-1833.
- Utracki, L.A. *Can. J. of Chem. Eng.* **2002**, *80*, 1008-1016.
- van Krevelen, D.W. *Properties of Polymers*, 2nd ed.; Elsevier Scientific Company:
Amsterdam, 1976 (chapter 4).
- Willemse, R.C.; Ramaker, E.J.U.; van Dam, J.; de Boer, A.P. *Polymer* **1999**, *40*, 6651-
6659.
- Wu, S.H. *Polym. Eng. Sci.* **1987**, *27*, 335-343.

Chapter 6

Conclusions and Future Work

6.1 GENERAL DISCUSSION AND CONCLUSIONS

In this thesis, the fundamental case — one polymer drop melting, deforming and breaking up in a second polymer melt subject to shear flow — is visualized and results are discussed. Most of the previous research has been done on Newtonian fluids at room temperature. Polymer systems are quite different from Newtonian systems because they are viscoelastic and shear thinning, and usually require high temperatures for processing. Two different kinds of apparatuses were used in this thesis to study the initial morphology development in shear flow. One is a custom built parallel plate device which was used to visualize the deformation and breakup of a single viscoelastic polymer drop (drop phase or minor phase), sandwiched between polymer disks which is composed of another kind of polymer (matrix phase or major phase), at high temperature and low shear rates (Chapter 2). The other apparatus is a specially-designed, transparent, heated Couette mixer used to study the deformation and breakup of a single polymer drop with and without compatibilizer (pre-made and in-situ compatibilization) inside a viscoelastic polymer matrix at high temperatures subject to simple shear (Chapter 3 and Chapter 4). The drops used in Chapters 2, 3 and 4 have a diameter of 0.5~1.0 mm.

When a polycarbonate (PC) drop was sheared inside a polyethylene (PE) matrix in a transparent rotating parallel plate device at 220°C and shear rates less than $2s^{-1}$, sheet formation was observed during the initial shearing of the drop. The drop then broke up via two different modes: either stretching into a thin thread (Type A) or extending into a

sheet with a thin cylindrical tip (Type B). The formation of the sheet was characterized by a critical strain, a normalized time defined as $\dot{\gamma}t_c$, where $\dot{\gamma}$ is shear rate and t_c is a critical time. At the critical strain or time, the drop length is stretched continuously in the flow direction (θ), somewhat decreased in the vorticity direction (r) and significantly decreased in the velocity gradient direction (z). The critical strain was related to viscosity ratio (η_r), stress ratio (S_r) and drop Deborah number (De). The viscosity ratio is a ratio of the drop phase viscosity to the matrix phase viscosity:

$$\eta_r = \eta_d / \eta_m \quad (6.1)$$

The stress ratio (Ghodgaonkar and Sundararaj, 1996; Lin *et al.*, 2003a; Lin and Sundararaj, 2004), which incorporates both drop and matrix normal stresses, is defined as:

$$S_r = \frac{\text{Breakup Stress}}{\text{Restoring Stress}} = \frac{\eta_m \dot{\gamma} + 2G'_m}{\Gamma/R + 2G'_d} \quad (6.2)$$

where G' is elastic modulus, Γ is interfacial tension and R is drop radius. The subscripts d stands for the drop phase and m for the matrix phase. Deborah number (De) is a ratio of the characteristic material relaxation time (λ) to the characteristic process time. Here t_c is used as the processing time:

$$De = \frac{\lambda}{t_c} \quad (6.3)$$

For Newtonian systems, drop breakup can be well characterized with the critical Capillary number (Ca) and the viscosity ratio (Taylor, 1932, 1934; Grace, 1982). The Capillary number is a ratio of shear stress to interfacial stress:

$$Ca = \eta_m \dot{\gamma} R / \Gamma \quad (6.4)$$

However, in polymer systems, a poor correlation is found between Ca and η_r . Instead, correlations using S_r and De described the breakup better.

For the systems studied in the parallel plate apparatus, the drop was easier to break up at a higher S_r . When S_r was less than 3, the normalized critical time for the drop to form a sheet was fairly constant and the drop was broken up through Type B breakup. When the stress ratio was higher than 3, the drop Deborah number was increased with increasing S_r , resulting in a delay in sheet formation and the drop broke up via Type A.

When the polymer drop was sheared in a counter-rotating Couette cell, four kinds of breakup mechanisms were observed in polymer systems without compatibilizer: (1) “erosion” – surface erosion from the drop in the form of thin ribbons and streams of small droplets; (2) “parallel breakup” – the drop broke abruptly after being stretched into a thin sheet or flat sausage parallel to the flow direction; (3) “vorticity alignment and breakup” – the drop broke after being elongated in the vorticity direction; (4) “tip streaming” – streams of small droplets were released from the tips of a pointed drop in the flow

direction.

Surface erosion is one of the primary breakup mechanisms for polymer systems: the mother drop slowly shrunk through erosion in the form of streams of sheets, cylinders and daughter droplets. The daughter droplets were able to break up again until a size on the order of microns is achieved. Pseudo-first order decay kinetics was used to describe the drop erosion phenomena.

In the presence of diblock copolymer, the polystyrene (PS) drop aligned in the vorticity axis in a PE matrix and subsequently broke up at a lower shear rate than that required for the uncompatibilized system in simple shear. If the copolymer distributed at the interface homogeneously, the drop cross sectional area was increased and the interface was obscured. If the copolymer distributed at the interface unevenly, a thin cylindrical tip stretched and ruptured from the mother drop in the vorticity axis due to shear-induced convection. The appearance of this tiny tip stabilized the drop. Consequently, the drop broke up at a higher shear rate than the case where the copolymer was evenly distributed at the interface.

Rapid in-situ reaction accelerated drop breakup. When reaction took place quickly, the drop was stretched into a very thin sheet due to the suppression of interfacial slip. However, the gradual interfacial reaction created new product, which accumulated at the drop interface, and a tiny cylindrical tip was developed which stabilized the drop, and the drop broke up at a higher shear rate.

The breakup modes of polymer drops are different from those observed in Newtonian systems. Drop breakup occurs over a wide range of viscosity ratio from 0.2 to 60, contrary to empirical correlations and theoretical predictions of drop breakup in

Newtonian systems (e.g., Taylor, 1932, 1934; Grace, 1982). It is observed that a polymer drop breaks up in simple shear even when the viscosity ratio is higher than 3.5, which has been proven to be impossible for Newtonian systems in simple shear flows. The different breakup phenomena observed for polymer systems may be due to (1) the shear-thinning characteristic of polymer melts; (2) the existence of normal stresses in the drop and in the matrix phases; (3) the extremely high stresses in polymer systems because of the very high melt viscosity.

Polymer drop breakup in simple shear can be described by two characteristic parameters: S_r and De , where the characteristic process time is the inverse of the critical shear rate where drop breakup occurs, that is,

$$De = \lambda \dot{\gamma} \quad (6.5)$$

It is found that S_r decreases with increased De , which suggests that the drop elasticity promotes drop breakup and the matrix elasticity resists drop breakup.

A polymer drop may break up through several mechanisms during shearing. In general, tip streaming occurs first at a lower shear rate for systems with lower viscosity ratio and Deborah number; erosion takes place at a wider viscosity ratio and Deborah number; parallel breakup happens at a viscosity ratio between 2 and 10 and a Deborah number between 0.09 and 4; vorticity breakup occurs when $S_r < 1$. Parallel breakup is not observed in systems with viscosity ratio greater than 10, since the maximum shear rate achievable is 50s^{-1} .

Polymer drop breakup mechanisms closely follow industrial observations. Drop erosion has been observed in scanning electron microscopy (SEM) micrographs of polypropylene/nylon 6 (PP/PA6) blend obtained from the melting section of a twin-screw extruder (TSE) (Potente *et al.*, 2001), though the authors did not identify this breakup as erosion. Potente *et al.* (2001) and Potente and Bastian (2001) have shown that in the melting section of TSE different breakup mechanisms take place in parallel, namely, quasi-steady drop breakup, folding, end pinching and tip streaming. These studies suggest that the observation of tip streaming in Couette cell, and drop stretching and folding and tumbling in parallel plates do exist in polymer blending process.

Drop vorticity alignment and breakup have been visualized in PE/PS systems with an optical slit die, which is positioned at the exit of a twin-screw extruder (Migler *et al.*, 1999; Hobbie and Migler, 1999). The flow inside the slit die is pressure driven and the shear rate is a function of the distance from one of the walls. The alignment and elongation of the drop in the vorticity direction resemble the Weissenberg rod climbing phenomenon, which is an indication of high normal stresses existing in polymers.

The sheeting mechanism has been observed in polymer blend initial morphology development in a batch mixer (Scott and Macosko, 1991, 1995), a twin-screw extruder (Sundararaj *et al.*, 1992, 1995) and a single screw extruder (Lindt and Ghosh, 1992). Sheet formation was observed for a number of times during the visualization studies of this thesis on drop deformation and breakup (Chapters 2-4). In Chapter 2, a polymer drop was stretched to a sheet when it was sheared in parallel plates initially. In Chapter 3, sheets were observed in two circumstances. One was at the surface of the mother drop at the beginning of the drop surface erosion, and the other was that the entire drop deformed

into a sheet before the drop broke up in the flow direction. In Chapter 4, a sheet was seen pulling out of a fast reactive drop. The sheets subsequently broke up to generate thousands of micron-sized droplets. Since the thickness of the sheets was on the order of 1 μm , when the sheets broke up, they created drops 1,000 times smaller than the initial drop size.

Polymer blending is fast and involves many different and complex steps. Although it is difficult to understand how one polymer phase disperses into another phase, the similarities between the lab results and the industrial polymer processing indicate that visualization is a useful and reliable tool to look through the basic phenomena involved in blending.

Studies on morphology development of polymer blends in the APAM (Chapter 5) show that melting and mixing are crucial steps. During the melting stage, polymers are melted or softened, and the dispersed phase may experience drop breakup and coalescence (Potente *et al.*, 2001; Potente and Bastian, 2001). Tip streaming, erosion and sheeting of the drop may occur simultaneously, while parallel and vorticity breakups occur at a high shear rate, most likely during the initial mixing process.

The compatibilized systems, either with pre-made copolymer, or in-situ reaction, show finer blend morphology than that of the uncompatibilized blends if all polymers are mixed together. It is found that the desired final particle distribution can be controlled by the feeding sequence of polymers. Premelting and premixing may help drop breakup during the initial blending process. However, they may also coarsen the final morphology depending on the reactivity of functionalized polymers or the molecular weight of a copolymer, and the preference of the copolymer to one of the homopolymer phases. Fast

interfacial reaction is an efficient way to achieve a fine morphology, while a slower reaction may actually coarsen the morphology. This is because a slow reaction, in particular, cross-linking reactions, will build up newly formed product at the drop interface unevenly, which stabilizes the drop (see Chapter 4). In this case, drop breakup and coalescence become more difficult compared with a non-reactive drop.

6.2 FUTURE WORK

Polymer drops showed different deformation and breakup mechanisms from Newtonian drops. In simple shear, polymer drops can break up at viscosity ratios higher than 3.5, which has been proven to be impossible for Newtonian drops. These findings are exciting. However, there are still a lot of puzzles needing resolution. In this section, some potential future work is listed and the list is broken up according to the experimental devices used.

6.2.1 Couette Cell

6.2.1.1 Effect of Interfacial Modifier on Drop Breakup

The effect of block copolymer and in-situ reaction on drop deformation and breakup has been studied qualitatively (Chapter 4). In the future, a quantitative study will be important to understand the effect of compatibilization on drop breakup in more details. Some potential work includes: (1) effect of copolymer interfacial concentration; (2) effect of copolymer molecular weight; (3) effect of reactive interfacial concentration.

For (1), the interfacial concentration can be changed by coating a drop with different amounts of copolymer solutions. The solutions can be prepared by varying

concentrations of the copolymer in a solvent. A drop with certain amount of copolymer is obtained after the solvent is evaporated.

For (2), the molecular weight of a copolymer can be varied from low to high, for example, for polystyrene-block-polyethylene (P(S-b-E)), a range of molecular weight from 3,000-3,000 g/mol to 200,000-200,000 g/mol would be a good selection since the entanglement molecular weight for PS is 13,000 g/mol (Fetters *et al.*, 1994). It has been found that an intermediate molecular weight copolymer suppresses drop coalescence efficiently (Macosko *et al.*, 1996; see also Chapter 5) since both dynamic and static coalescence can be suppressed. A recent study by Galloway *et al.* (2004) also suggests that there is an optimal diblock copolymer molecular weight in reducing the dispersed phase particle size and stabilizing the final morphology. The optimum molecular weight of P(S-b-E) for a PS/PE (50/50) blend is found to be 20,000-20,000 g/mol, which is above the entanglement molecular weight, but well below the molecular weight (100,000-100,000 g/mol) used in this thesis. So far, the effect of copolymer molecular weight on drop breakup has not been studied thoroughly.

For (3), in interfacial reactive polymer pairs, it is possible to change the concentration of the reactive groups and do a quantitative study. For example, for a polyethylene maleic anhydride/polystyrene oxazoline (PEMA/PSOX) system, the functional group concentration can be changed easily if PSOX is diluted with PS. A drop can be made out of the mixture in heated silicone oil (Lin *et al.*, 2003b; Chapter 2).

6.2.1.2 Effect of Drop Phase Concentration

In the experiments performed in the Couette cell, 4-6 drops were put inside the gap for each run. It is found that the drops tended to align along a line in the flow direction as they were sheared inside the Couette cell. This observation is similar to a recent study by Pathak *et al.* (2002). Pathak *et al.* (2002) found that polydimethylsiloxane (PDMS) droplets, varied from 1wt% to 35wt%, aligned into discrete layers when the droplets were sheared inside polyisobutene (PIB) between parallel plates at room temperature. However, this thesis considers only dilute drop concentration. The drops are isolated from each other, and thus, drop interaction is excluded. By increasing the drop phase concentration, for example, from 0.1% to 10%, the drop behavior will be more complicated. Drop collision and coalescence occur simultaneously with drop breakup, and drops aligning along the flow direction will be more obvious. Therefore, a study on drop phase concentration will give further insight into the final blend morphology development.

6.2.1.3 Three Dimension Visualization on Drop Deformation and Breakup

A Couette setup (see Appendix I) has been built in Dr. Sundararaj group's lab. The setup is able to visualize drop deformation and breakup in two different viewing planes and thus, to reconstruct drop images in three dimensions (3D). The 3D image will be helpful in understanding drop deformation and breakup in more detail. According to a recent 3D computational flow dynamics simulation study by Chen *et al.* (2004), an eroding drop showed a flattened profile in the velocity gradient direction (a non-viewing

direction in the present study). In this thesis, it has been assumed that the drop is stretched into a sheet before it broke up along the flow direction. The simulation result and the assumption can be verified by 3D experimental observation. The 3D visualization will give more valuable results on drop deformation, breakup and coalescence.

6.2.2 Parallel Plates

6.2.2.1 Radial and End/Wall Effects

In Chapter 2 (see also Lin and Sundararaj, 2004), drop deformation and breakup inside parallel plates were studied. The apparatus has a small diameter, 25 mm. The gap used is 2 mm. During the experiments, the drop size is ranged from 0.5 mm to 1.0 mm. The end or wall effect of the plates may not be negligible. A bigger device has been constructed, where the upper plate has a diameter of 102 mm and the lower plate is the outer cylinder of the Couette mixer (see Appendix I). Both plates can rotate simultaneously during the experiments. The drop can be viewed by adjusting the relative speed of the plates while the camera can be kept in a fixed position. The gap between the plates can be varied, and a bigger gap, such as 4 mm, can be easily obtained.

In the small parallel plates, the drop shifted to the radial edges when sheared for a longer time, normally > 20 min. This suggests that there is a radial migration effect during the experiment. The bigger plates will help in studying radial migration effect on drop deformation and breakup.

6.2.2.2 Cone-and-Plate Device

Unlike parallel plates, the flow field generated by a cone-and-plate device is pure simple shear. A cone plate with an angle of 5° and a diameter of 102 mm (Appendix I) has been constructed, using the same outer cylinder of the Couette mixer as the lower plate. Since the outer cylinder is like a cup outside, which is able to delay edge failure (Lyu *et al.*, 2002). Both Couette and cone-and-plate are good apparatuses to generate simple shear flow. Polymer sample loading will be easier for the cone-and-plate and a 3D view of drop makes future drop visualization promising.

6.3 REFERENCES

- Chen, H.; Nandakumar, K.; Sundararaj, U. *manuscript in preparation*, 2004.
- Fetters, L.J.; Lohse, D.J.; Richter, D.; Witten, T.A.; Zirkel, A. *Macromolecules* **1994**, *27*, 4639-4647.
- Galloway, J.A.; Jeon, H.K.; Bell, J.R.; Macosko, C.W. *submitted to Polymer*, 2004.
- Ghodgaonkar, P.G.; Sundararaj, U. *Polym. Eng. Sci.* **1996**, *36*, 1656-1665.
- Grace, H.P. *Chem. Eng. Commun.* **1982**, *14*, 225-277.
- Levitt, L.; Macosko, C.W. *Macromolecules* **1999**, *32*, 6270-6277.
- Lin, B.; Mighri, F.; Huneault, M.A.; Sundararaj, U. *Macromol. Rapid Commun.* **2003a**, *24*, 783-788.
- Lin, B.; Sundararaj, U.; Mighri, F.; Huneault, M.A. *Polym. Eng. Sci.* **2003b**, *43*, 891-904.
- Lin, B.; Sundararaj, U. *Polymer* **2004**, *45*, 7605-7613.

- Lindt, J.T.; Ghosh, A.K. *Polym. Eng. Sci.* **1992**, *32*, 1802-1813.
- Lyu, S.; Jones, T.D.; Bates, F.S.; Macosko, C.W. *Macromolecules* **2002**, *35*, 7845-7855.
- Macosko, C.W.; Guegan, P.; Khandpur, A.K.; Nakayama, A.; Marechal, P.; Inoue, T. *Macromolecules* **1996**, *29*, 5590-5598.
- Migler, K.B.; Hobbie, E.K.; Qiao, F. *Polym. Eng. Sci.* **1999**, *39*, 2282-2291.
- Hobbie, E.K.; Migler, K.B. *Phys. Rev. Lett.* **1999**, *82*, 5393-5396.
- Pathak, J.A.; Davis, M.C.; Hudson, S.D.; Migler, K.B. *J. Colloid Interface Sci.* **2002**, *255*, 391-402.
- Potente, H.; Bastian, M.; Bergemann, K.; Senge, M.; Scheel, G.; Winkelmann, Th. *Polym. Eng. Sci.* **2001**, *41*, 222-231.
- Potente, H.; Bastian, M. *Int. Polym. Proc.* **2001**, *1*, 14-30.
- Scott, C.E.; Macosko, C.W. *Polym. Bull.* **1991**, *26*, 341-348.
- Scott, C.E.; Macosko, C.W. *Polymer* **1995**, *36*, 461-470.
- Sundararaj, U.; Macosko, C.W.; Rolando, R.J.; Chan, H.T. *Polym. Eng. Sci.* **1992**, *32*, 1814-1823.
- Sundararaj, U.; Dori, Y.; Macosko, C.W. *Polymer* **1995**, *36*, 1957-1968.
- Taylor, G.I. *Proc. R. Soc. London, Ser. A* **1932**, *138*, 41-48.
- Taylor, G.I. *Proc. R. Soc. London, Ser. A* **1934**, *146*, 501-523.

Appendix I

New Mixing Device Design and Construction

Some common devices have been used in studying drop deformation and breakup since Taylor's pioneering work. Taylor (1934) built a parallel band apparatus composed of cinema film, which was stretched between two rollers. The apparatus was immersed into a glass sided box containing concentrated sugar syrup. A drop of Newtonian fluid was introduced into the syrup by means of a pipette and sheared by moving the bands in opposite directions. This idea was also utilized by Flumerfelt (1972). However, there are some experimental difficulties, especially since the belts did not ride completely flat on the guide plates, even when it was stretched very tightly. This caused an immeasurable variance in the gap between the belts, and consequently a high uncertainty in the results.

The computer controlled four-roll mill of Bentley and Leal (Bentley, 1985; Bentley and Leal, 1986) made a great contribution to the study of drop deformation and breakup. The four-roll mill is flexible in generating all types of linear 2-D flows. The shear rate at the center of the device was found to be directly proportional to the faster pair of diagonal rollers. In this device, the position of the center of a drop can be controlled by scanning each pixel in the field 60 times per second, and recognizing the frame, i.e. the boundaries of the drop. Then the immediate position of the center of mass was calculated and roller speed was adjusted. Computerized position control requires a sharp image of the drop, and no other drops in the field of view. With good control it is possible to hold a drop in view at higher shear rates. However, the four roll mill does not work well for highly viscoelastic fluids because the shear stresses generated by rotating

rollers may be too weak to overcome the large extensional stresses generated by the fluids; therefore, the fluid may not enter the compartment in between the rollers.

An opposed jets device designed by Janssen *et al.* (1993) can generate a similar flow field as the four-mill roll in the central region. In the opposed jets device, the position of a drop can be controlled by the ratio of the exit flow rates. The major improvement of this device is that it can be used to study viscoelastic fluids. The major disadvantage is that the device can only be used at room temperature, which limits its application to most polymers.

The Couette cell is the most popular device used for generating simple shear flow as have been shown in Chapters 3 and 4. The two cylinders can be counter-rotating or one of them is rotating. In most of the devices, the drop was viewed through a window above or below the gap between the cylinders. Therefore, the viewing plane includes the flow direction (x_1) and the velocity gradient direction (x_2) of the deforming drop. The Couette cell in Chapters 3 and 4 is from Industrial Materials Institute, National Research Council Canada (IMI, NRC, Mighri and Huneault, 2001) and it is different from the other designs in that: the viewing plane contains the flow direction (x_1) and the vorticity direction (x_3), and it can be easily heated up – the outer transparent cylinder can be heated with infrared heaters and the inner metal cylinder can be heated uniformly by six cartridge heaters.

Parallel plate devices using rotating transparent plates or cone-and-plate are also good for observing the deforming polymer drop (Chapter 2). Though the flow field generated by rotating the parallel plates is not homogenous, the parallel plates allow us to study very viscous polymers, which is the limitation of the Couette cell. The cone-and-

plate can generate a one-dimensional simple shear, but is more difficult to build and to align.

The study on one type of polymer pellet sheared inside another type of polymer in a parallel plate device was first studied by Sundararaj *et al.* (1994, see also Chapter 2). In their original parallel plates, they used two glass plates and the upper plate was controlled with a DC motor and the lower plate was stationary. To capture the images of the drop, one has to rotate the camera manually. This parallel plate device was later modified to counter-rotating plates by Levitt *et al.* (1996), where the lower plate was controlled with a rotary stage. The heating system was also redesigned by using a heating chamber, where the samples inside the parallel plates can be heated by a stream of hot air or hot nitrogen. Parallel plates were also used to observe three dimensional (3D) drop deformation by Guido and Villone (1998) and Yamane *et al.* (1998). However, all the 3D studies to date are limited to model fluids and room temperature.

A new mixing device has been designed and constructed in Dr. Sundararaj research group's laboratory to continue studying polymer systems. The enhanced features of the mixer are:

(1) It is able to capture the drop image in two planes including x_1 and x_3 in one plane and x_1 and x_2 in another plane; therefore, it can be used to recreate a 3D image of the drop.

(2) It can heat the polymers to high temperatures. Thus, high temperature polymers can be studied.

(3) It includes different devices: counter-rotating Couette cylinders, parallel plates and cone-and-plate.

(4) It allows quantitative on-line morphology analysis.

Figure I.1 illustrates the Couette cell setup. A drill press is used for mixer alignment. Both cylinders are made out of one piece of quartz. All quartz parts are custom built at Technical Glass Products. Figure I.2 shows the detailed dimensions of the cylinders. The outer cylinder (Figure I.2a) has a diameter of 110 mm and the inner cylinder (Figure I.2b), 102 mm. There is a cone shaped coated silver inside the inner cylinder in order to enhance lighting during the experiment. The inner cylinder of the Couette device can be changed to either a quartz plate (Figure I.2c) or a cone quartz plate (Figure I.2d) to generate a parallel plates or a cone-and-plate device.

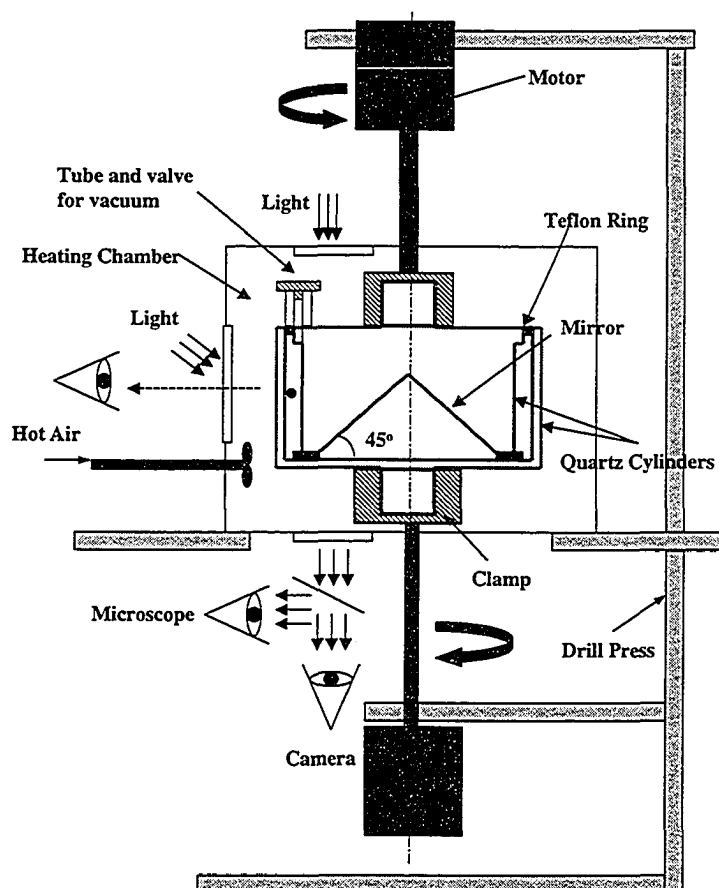


Figure I.1 Couette apparatus cross-sectional illustration.

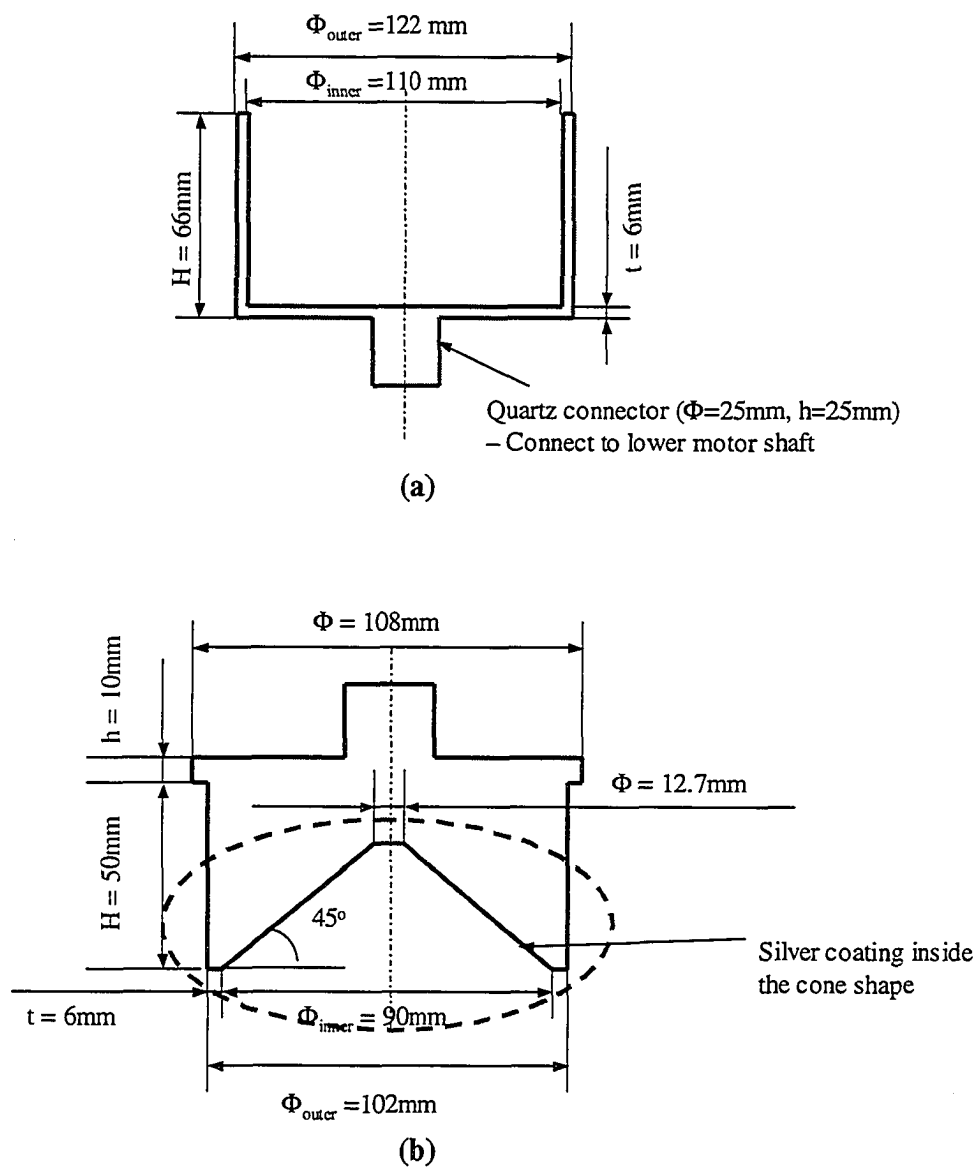


Figure I.2 Cross-sectional illustration of (a) Outer quartz cylinder; (b) Inner quartz cylinder; (c) Assembly of cylinders; (d) Inner quartz plate; (e) Inner quartz cone.

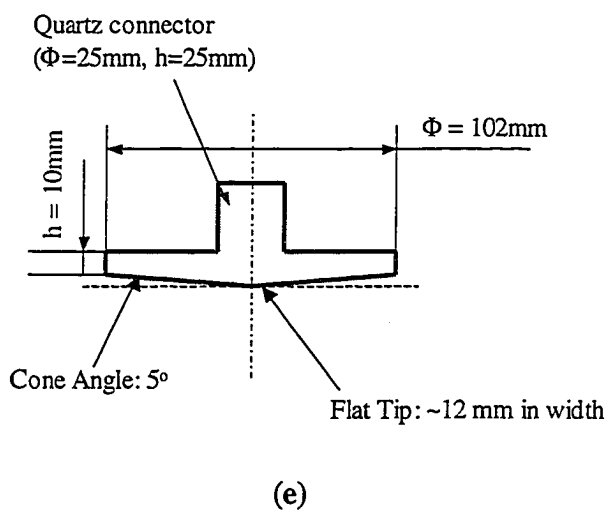
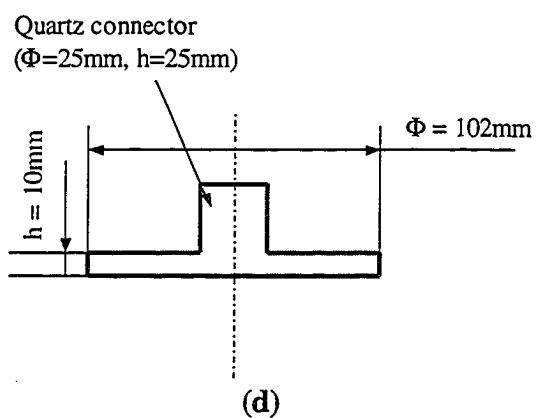
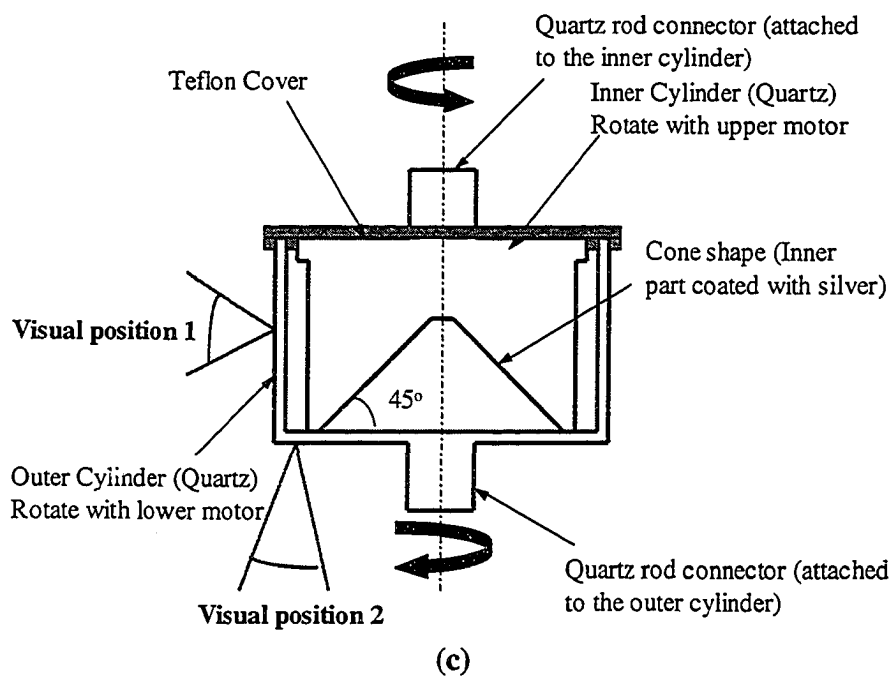


Figure I.2 (Continued).

During the designing and constructing the device, there are some challenges:

(1) The alignment of the equipment needs to be precise because any eccentricity will cause deviation from simple shear flow for Couette mixer and cone-and-plate device, and may cause equipment damage.

(2) Heating is important because we need to melt the polymer pellets. Therefore, a heating chamber is used. The outer shell of the chamber is made of stainless steel and the inner part is filled with ceramic. It can be heated with hot air or hot nitrogen.

(3) A tight seal is necessary to pull a vacuum and get rid of bubbles inside the melt and a Teflon cover is used as shown in Figure I.2c.

(4) Good lighting is essential to get good images. Three glass windows for lighting and camera are designed, and a cone shaped mirror is applied inside the inner quartz cylinder.

(5) The working distance of the camera cannot be too short (needs to be > 100 mm); otherwise, it will be not able to view the drop.

(6) In order to trace the drop during the experiments easily, one x - y - z positioning movement from Edmund Industrial Optics is placed for side view and one x - z positioning movement is mounted on the drill press plate to control the camera viewing from the bottom.

(7) A screen splitter (model: 613GS), from Colorado Video Inc., is connected with the cameras to get the images simultaneously.

(8) The experimental data is output from Labview.

REFERENCES

Bentley, B.J. *PhD thesis*, California Institute of Technology, 1985.

Bentley, B.J.; Leal, L.G. *J. Fluid Mech.* **1986**, *167*, 219-240.

Flumerfelt, R.W. *Ind. Eng. Chem. Fundam.* **1972**, *11*, 312-318.

Janssen, J.M.H.; Peters, G.W.M.; Meijer, H.E.H. *Chem. Eng. Sci.* **1993**, *48*, 255-265.

Mighri, F.; Huneault, M.A. *J. Rheol.* **2001**, *45*, 783-797.

Sundararaj, U.; Dori, Y.; Macosko, C.W. *SPE ANTEC Tech. Papers* **1994**, *52*, 2448-2451.

Taylor, G.I. *Proc. R. Soc. London, Ser. A* **1934**, *146*, 501-523.

Appendix II

Average Shear Rate in Couette Cell

Equations (3.1a) and (3.1b) are obtained for a power law fluid:

$$\eta = m|\dot{\gamma}|^{n-1} \quad (\text{II.1})$$

where η is the viscosity, $\dot{\gamma}$ is shear rate, m and n are constants. Therefore, the shear stress, τ , can be expressed as:

$$\tau = \eta\dot{\gamma} = m|\dot{\gamma}|^n \quad (\text{II.2})$$

Assumptions made for obtaining the shear rate in the cylindrical coordinates are: (1) steady state; (2) incompressible fluids; (3) isothermal; (4) velocity only θ dependent, that is, $v_r = 0$, $v_z = 0$, and no variation along z -axis; (5) no end and wall effects; (6) non-slip conditions. Therefore, the continuity and momentum equations can be written as follows:

$$\text{Continuity: } \frac{\partial \rho}{\partial t} + \frac{1}{r} \frac{\partial}{\partial r} (\rho r v_r) + \frac{1}{r} \frac{\partial}{\partial \theta} (\rho v_\theta) + \frac{\partial}{\partial z} (\rho v_z) = 0 \quad (\text{II.3})$$

and thus,

$$\frac{\partial v_\theta}{\partial \theta} = 0 \quad (\text{II.4})$$

This suggests that v_θ is not a function of θ . Since the velocity along z -axis is constant, v_θ is only a function of r .

Momentum:

r -component:

$$\rho \left(\frac{\partial v_r}{\partial t} + v_r \frac{\partial v_r}{\partial r} + \frac{v_\theta}{r} \frac{\partial v_r}{\partial \theta} - \frac{v_\theta^2}{r} + v_z \frac{\partial v_r}{\partial z} \right) = -\frac{\partial P}{\partial r} - \left[\frac{1}{r} \frac{\partial}{\partial r} (r \tau_{rr}) + \frac{1}{r} \frac{\partial \tau_{r\theta}}{\partial \theta} - \frac{\tau_{\theta\theta}}{r} + \frac{\partial \tau_{rz}}{\partial z} \right] + \rho g_r \quad (\text{II.5})$$

therefore,

$$\rho \frac{v_\theta^2}{r} = \frac{\partial P}{\partial r} \quad (\text{II.6})$$

z -component:

$$\rho \left(\frac{\partial v_z}{\partial t} + v_r \frac{\partial v_z}{\partial r} + \frac{v_\theta}{r} \frac{\partial v_z}{\partial \theta} + v_z \frac{\partial v_z}{\partial z} \right) = -\frac{\partial P}{\partial z} - \left[\frac{1}{r} \frac{\partial}{\partial r} (r \tau_{rz}) + \frac{1}{r} \frac{\partial \tau_{r\theta}}{\partial \theta} + \frac{\partial \tau_{zz}}{\partial z} \right] + \rho g_z \quad (\text{II.7})$$

and thus,

$$\frac{\partial P}{\partial z} = \rho g_z \quad (\text{II.8})$$

θ -component:

$$\rho \left(\frac{\partial v_\theta}{\partial t} + v_r \frac{\partial v_\theta}{\partial r} + \frac{v_\theta}{r} \frac{\partial v_\theta}{\partial \theta} + \frac{v_r v_\theta}{r} + v_\theta \frac{\partial v_\theta}{\partial z} \right) = -\frac{1}{r} \frac{\partial P}{\partial \theta} - \left[\frac{1}{r^2} \frac{\partial}{\partial r} (r^2 \tau_{r\theta}) + \frac{1}{r} \frac{\partial \tau_{\theta\theta}}{\partial \theta} + \frac{\partial \tau_{\theta z}}{\partial z} \right] + \rho g_\theta \quad (\text{II.9})$$

From equation (II.9),

$$0 = \frac{1}{r^2} \frac{\partial}{\partial r} (r^2 \tau_{r\theta}) \quad (\text{II.10})$$

therefore,

$$\tau_{r\theta} = \frac{C_1}{r^2} \quad (\text{II.11})$$

The shear stress, $\tau_{r\theta}$, also relates v_r as following:

$$\tau_{r\theta} = \tau_{\theta r} = -\mu \left[r \frac{\partial}{\partial r} \left(\frac{v_\theta}{r} \right) + \frac{1}{r} \frac{\partial v_r}{\partial \theta} \right] \quad (\text{II.12})$$

Now combine equation (II.11) with equations (II.2) and (II.12):

$$\frac{C_1}{r^2} = m \left[r \frac{\partial}{\partial r} \left(\frac{v_\theta}{r} \right) \right]^n \quad (\text{II.13})$$

Therefore, the velocity is solved:

~

$$v_{\theta} = -\frac{n}{2} \left(\frac{C_1}{m} \right)^{1/n} r^{-2/n+1} + C_2 r \quad (\text{II.14})$$

The boundary conditions are: (1) at the inner cylinder where $r=R_i$, $v_{\theta} = \Omega_i R_i$ and (2) at the outer cylinder where $r=R_o$, $v_{\theta} = \Omega_o R_o$. The subscripts i and o stand for inner and outer cylinders, respectively; Ω is the rotation speed. Substitute the boundary conditions into equation (II.14) and solve,

$$\begin{cases} C_1 = m \left[\frac{2(\Omega_o - \Omega_i)}{n} \frac{1}{R_i^{-2/n} - R_o^{-2/n}} \right]^n \\ C_2 = \Omega_i + \frac{\Omega_o - \Omega_i}{R_i^{-2/n} - R_o^{-2/n}} R_i^{-2/n} \end{cases} \quad (\text{II.15})$$

Therefore,

$$v_{\theta} = \left[\frac{\Omega_o - \Omega_i}{R_i^{-2/n} - R_o^{-2/n}} \right] (R_i^{-2/n} - r^{-2/n}) r + \Omega_i r \quad (\text{II.16})$$

and

$$\dot{\gamma} = r \frac{\partial}{\partial r} \left(\frac{v_{\theta}}{r} \right) = \frac{2}{n} \frac{\Omega_o - \Omega_i}{R_i^{-2/n} - R_o^{-2/n}} r^{-2/n} \quad (\text{II.17})$$

From equation (II.17),

$$\dot{\gamma}_i = \frac{2}{n} \frac{\Omega_o - \Omega_i}{R_i^{-2/n} - R_o^{-2/n}} R_i^{-2/n} \quad \text{at } R=R_i \quad (\text{II.18})$$

$$\dot{\gamma}_o = \frac{2}{n} \frac{\Omega_o - \Omega_i}{R_i^{-2/n} - R_o^{-2/n}} R_o^{-2/n} = \dot{\gamma}_i \left(\frac{R_o}{R_i} \right)^{-2/n} \quad \text{at } R=R_o \quad (\text{II.19})$$

Replace $\Omega_o - \Omega_i$ with Ω in equations (II.18) and (II.19), the equations (3.1a) and (3.1b)

in Chapter 3 are recovered:

$$\dot{\gamma}_i = \frac{2}{n} \left(\frac{R_i^{-2/n}}{R_i^{-2/n} - R_o^{-2/n}} \right) \cdot \Omega(t) \quad (3.1a)$$

$$\dot{\gamma}_o = \dot{\gamma}_i \left(\frac{R_o}{R_i} \right)^{-2/n} \quad (3.1b)$$

Appendix III

Diffusivity Calculation

The diffusivity is calculated according to van Krevelen (1976) equations (9.56) and (9.59):

$$D_s = k_D M_n^{-d} \quad (\text{III.1})$$

$$\log k_D \approx -7.1 + 6.5 \left(d - \frac{1}{2} \right) - \log \eta_m \quad (\text{III.2})$$

$$d = \frac{1}{3}(a+1) \quad (\text{III.3})$$

where M_n is the number average molecular weight, η_m is matrix viscosity, a , d and k_D are constants. The diffusivity of P(S-b-E) is estimated by using PS data with $M = 200,000$ g/mol in PE1 at 190°C and a shear rate of 4s⁻¹ with $\eta_m = 420$ N·s/m². The cohesive energy, E_{coh} , for PS and PE is 35610 J/mol and 8380 J/mol, and the molar volume, V , is 98.0 cm³/mol and 32.9 cm³/mol (Table 7.3 from van Krevelen, 1976). The solubility parameter for PS and PE is $\delta_{PS} = 19.06$ J^{1/2}/cm^{3/2} and $\delta_{PE} = 15.96$ J^{1/2}/cm^{3/2}, calculated from:

$$\delta = \left(\frac{E_{coh}}{V} \right)^{1/2} \quad (\text{III.4})$$

The difference between δ_{PS} and δ_{PE} is 3.1, greater than 3, and thus, $a = 0.5$. Combine equations (III.1), (III.2) and (III.3), the diffusivity is obtained: $D_s = 4.23 \times 10^{-13} \text{ cm}^2/\text{s}$.

REFERENCES

van Krevelen, D.W. *Properties of Polymers*, 2nd ed.; Elsevier Scientific Company: Amsterdam, 1976.

Appendix IV

Saturation Concentration

The saturation concentration of copolymer at interface is obtained from the critical concentration of emulsification curve (Matos *et al.*, 1995). The total area occupied by the dispersed phase is:

$$A = n \times 4\pi R^2 \quad (\text{IV.1})$$

$$n = \frac{\phi_d V_d}{\frac{4}{3}\pi R^3} \quad (\text{IV.2})$$

where ϕ_d is the volume fraction of the dispersed phase, V_d is the volume of the dispersed phase, R is the radius of dispersed phase. The number of molecules of the copolymer is calculated by:

$$N = mN_{Avo} / M_n \quad (\text{IV.3})$$

where m is the mass of copolymer used, N_{Avo} is the Avogadro number.

For PS/PE (90/10 wt%) blend, the critical concentration from emulsification curve is 5 wt%. At 190°C, the density of PS and PE is 0.99 g/cm³ and 0.86 g/cm³, respectively, according to group contribution method (van Krevelen, 1976). The density of P(S-b-E) is estimated by using the arithmetic average of PS and PE, 0.925 g/cm³. The

dispersed phase radius is 0.40 μm based on the average volume diameter. Therefore, the interfacial concentration occupied by P(S-b-E) with $M_n = 200,000$ g/mol is:

$$\frac{A}{N} = \frac{3\phi_d V_d M_n}{mRN_{Avo}} = 6.3 \text{ nm}^2/\text{molecule} \quad (\text{IV.4})$$

REFERENCES

Matos, M.; Favis, B.D.; Lomellini, P. *Polymer* **1995**, *36*, 3899-3907.

Appendix V

Movies on Drop Deformation and Breakup

Movie 1: Erosion

Surface erosion is seen for a PC5 (polycarbonate) drop ($D_0=0.83\text{mm}$) inside a PE2 (polyethylene) matrix at 230°C . The shear rate is around 17 s^{-1} . The erosion micrographs are shown in Figure 3.7. Interested readers can also refer to: Lin, B.; Sundararaj, U.; Mighri, F.; Huneault, M. A. *Polym. Eng. Sci.* **2003**, *43*, 891-904.

Movie 2: Parallel sheet breakup

A PC4 drop ($D_0=0.68\text{mm}$) is deforming and breaking up through a sheet in the flow direction in a PE2 matrix at 220°C . The shear rate is increased stepwise. The corresponding micrographs are shown in Figure 3.14. Interested readers can also refer to: Lin, B.; Mighri, F.; Huneault, M. A.; Sundararaj, U. *Macromol. Rapid Commun.* **2003**, *24*, 783-788.

Movie 3: Vorticity alignment and breakup

A PC3 drop ($D_0=0.60\text{ mm}$) is aligned in the vorticity direction and then elongating and breaking up in a PE1 matrix at 220°C subject to a stepwise shear rate increase. The corresponding micrographs are shown in Figure 3.20. Interested readers can also refer to: (1) Lin, B.; Mighri, F.; Huneault, M. A.; Sundararaj, U. *Soc. Plast. Eng. Tech. Papers*, **2003**, 2345-2349; (2) Chen, H.; Lin, B.; Sundararaj, U.; Nandakumar, K. *manuscript in preparation*.

Movie 4: Tip streaming

A PC1 drop ($D_0=0.58$ mm) is deforming and breaking up in a PE2 matrix at 220°C subject to a stepwise shear rate increase. The corresponding micrographs are shown in Figure 3.23. Interested readers can also refer to: Lin, B.; Mighri, F.; Huneault, M. A.; Sundararaj, U. *Soc. Plast. Eng. Tech. Papers*, **2003**, 2345-2349.

Movie 5: PS premixed with 1% P(S-b-E) drop

A PS+1%P(S-b-E) (polystyrene premixed with 1% polystyrene-block-polyethylene) drop ($D_0=0.51$ mm) is deforming and breaking up in a PE1 matrix at 190°C subject to a stepwise shear rate increase. Figure V.1 shows some micrographs from the video. Interested readers can also refer to: (1) Lin, B.; Mighri, F.; Huneault, M. A.; Sundararaj, U. *228th ACS National Meeting*, **2004**, 91, 825-826; (2) Lin, B.; Mighri, F.; Huneault, M. A.; Sundararaj, U. *Macromolecules*, submitted.

Movie 6: PS drop coated with P(S-b-E)

A PS drop ($D_0=0.53$ mm) coated with P(S-b-E) is deforming and breaking up in a PE1 matrix at 190°C subject to a stepwise shear rate increase. The corresponding micrographs are shown in Figure 4.5. Interested readers can also refer to: (1) Lin, B.; Mighri, F.; Huneault, M. A.; Sundararaj, U. *228th ACS National Meeting*, **2004**, 91, 825-826; (2) Lin, B.; Mighri, F.; Huneault, M. A.; Sundararaj, U. *Macromolecules*, submitted.

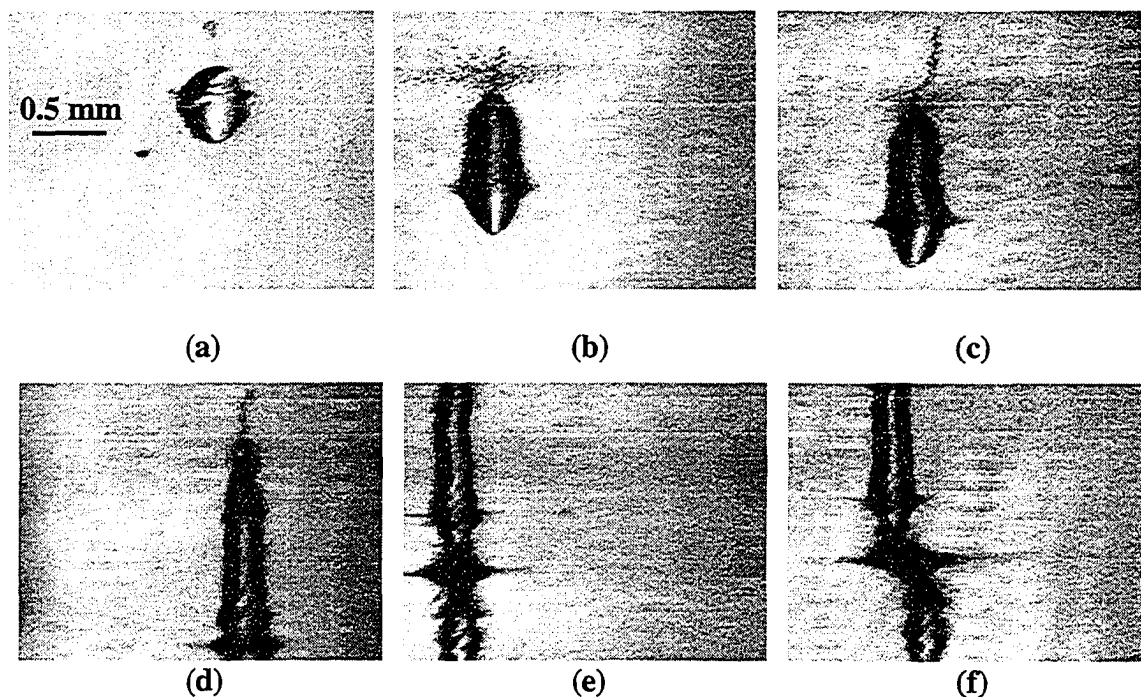


Figure V.1 Pre-made copolymer. Deformation and breakup of a PS+1%P(S-b-E) drop ($D_0=0.51\text{mm}$) in a PE1 matrix at 190°C subject to a stepwise shear rate increase. Time and conditions for each figure: (a) $t=2\text{s}$, $\dot{\gamma}=0.2\text{s}^{-1}$, $\eta_r=21$; (b) $t=396\text{s}$, $\dot{\gamma}=4.4\text{s}^{-1}$, $\eta_r=11$; (c) $t=505\text{s}$, $\dot{\gamma}=4.4\text{s}^{-1}$, $\eta_r=11$; (d) $t=719\text{s}$, $\dot{\gamma}=6.3\text{s}^{-1}$, $\eta_r=9$; (e) $t=814\text{s}$, $\dot{\gamma}=6.3\text{s}^{-1}$, $\eta_r=9$; (f) $t=816\text{s}$, $\dot{\gamma}=6.5\text{s}^{-1}$, $\eta_r=9$. The scale bar for each figure is same as shown in figure (a). For the micrographs, the flow direction is horizontal and the vorticity direction is vertical.